

Development of a Micro-Feeder for Cohesive Pharmaceutical Powders

Peter Chung-Hsien Hou

Strathclyde Institute of Pharmacy and Biomedical Sciences
University of Strathclyde
Glasgow, UK

A thesis submitted in fulfilment of the requirements for the degree of
Doctor of Philosophy

Submission Date: June 06, 2024

This thesis is the result of the author's original research. It has been composed by the author and has not been previously submitted for examination which has led to the award of a degree.

The copyright of this thesis belongs to the author under the terms of the United Kingdom Copyright Acts as qualified by University of Strathclyde Regulation 3.50. Due acknowledgement must always be made of the use of any material contained in, or derived from, this thesis.

Signed:

A handwritten signature in black ink, appearing to read "Peter H. Jones". The signature is written in a cursive style with a large, sweeping initial "P".

Date:

01/August/2023

Abstract

In recent years, the pharmaceutical industry has been striving to improve drug manufacturing processes to enable the accurate production of small batches for precision medicine and small-scale clinical trial medicine manufacturing. This aims to reduce manufacturing costs, improve drug manufacturing effectiveness, and ultimately provide more affordable life-saving medicines to the public. An important step in the manufacturing route for oral medicines is the consistent feeding of powdered materials, as any variation in the feed stream directly affects the quality attributes of the final drug product. However, achieving consistent and accurate powder flow rates in micro-feeding has remained a challenge in the pharmaceutical and biopharmaceutical industries, and current technologies such as screw feeders and vibrating feeders have limitations in meeting the precision and flow rate requirements of the pharmaceutical industry, particularly for future precision medicine products.

This research aimed to develop a novel micro-feeder for pharmaceutical drug manufacturing that provides accurate and consistent powder feeding. In this research study, two novel micro-feeders were developed that could consistently and accurately feed typical pharmaceutical materials at rates below 10 g/h, regardless of their sticky or cohesive nature. To achieve this, the initial micro-feeder design utilised a pneumatic approach with adjustable inserts and a plug to maintain low air velocity, critical for entrainment energy control to ensure consistent and accurate powder feeding. The second micro-feeder design featured a feeding screw and double-screw agitator to regulate powder flow. The feeding screw was inclined to control powder flow variation, while the agitator prevented issues such as rat holes or arching. Achieving control over the flow rate and minimising flow rate variations can be accomplished by adjusting the speeds of the screw and agitator. This design also addressed the challenge of refilling, which commercial feeders commonly face.

In this study, five different materials were used to assess the performance of the developed micro-feeders. The results demonstrated that these micro-feeders could continuously and consistently feed cohesive materials at a flow rate as low as 1 g/h. Furthermore, the effect of process parameters on the performance of the developed micro-feeder was studied to gain a deeper understanding of the system and to optimise its performance. As a result of the innovative and promising nature of these micro-feeders, a patent was filed in May 2022. The developed technology holds significant potential for commercialisation in precision medicine and is expected to have a long-term impact on the pharmaceutical and healthcare industries.

Contents

Abstract	ii
Contents	iii
List of Figures.....	x
List of Table.....	xx
Nomenclature.....	xxii
Acknowledgements.....	xxiv
Research Outputs	xxv
1 Introduction	1
1.1 Motivation	1
1.2 Research objectives	3
1.3 Research structure	3
2 Literature review	5
2.1 Microfeeder requirement.....	5
2.2 Feeding economics in pharmaceuticals	5
2.3 Regulatory requirement.....	7
2.4 Definition of micro-feeder	7
2.5 Micro-feeders in the pharmaceutical manufacturing process	8
2.5.1 Feeding in primary processing	10
2.5.2 Feeding in secondary processing.....	10
2.6 Common feeders in pharmaceutical application	11
2.6.1 Volumetric and gravimetric feeders.....	11
2.6.2 Screw feeder.....	12
2.6.3 Vibratory tray feeder	13
2.6.4 Weigh-belt feeder.....	15
2.6.5 Rotary valve	16
2.6.6 Venturi feeder.....	17
2.6.7 Commercially available micro-feeders	18
2.6.8 Summary.....	20

2.7	Recent research activities in feeding technologies	24
2.7.1	Screw feeder	24
2.7.2	Vibratory feeder	25
2.7.3	Screw-brush feeder.....	27
2.7.4	Fluidised feeder	28
2.7.5	Powder pump	29
2.7.6	Slide feeder	31
2.7.7	Summary.....	31
2.8	Factors affecting feeder performance.....	35
2.8.1	Material properties: Particle properties and bulk properties	35
2.8.1.1	Adhesive and cohesive forces	36
2.8.1.2	Bulk density	36
2.8.1.3	Particle size and shape	36
2.8.1.4	Particle size distribution.....	37
2.8.1.5	Powder flowability	37
2.8.2	Process design and parameters: General rules for feeder design	38
2.8.3	Environmental conditions: Moisture content and relative humidity.....	39
2.8.4	Powder flow measurement techniques	40
2.8.4.1	Hausner ratio and Carr Index.....	40
2.8.4.2	Angle of repose.....	41
2.8.4.3	Critical orifice diameter	42
2.8.4.4	Carney and Hall flowmeters	43
2.8.4.5	Jenike's flow function.....	44
2.8.4.5.1	Uniaxial compression test	45
2.8.4.5.2	Shear testing	46
2.8.4.5.3	Ball indentation	48
2.8.4.6	Torque rheometers	49
2.8.4.7	Permeability	50
2.8.4.8	Geldart's classification.....	52

2.8.4.9	Die fill	54
2.9	Design Guides.....	57
2.9.1	Pneumatic Conveying.....	57
2.9.2	Gas-solid separation – Cyclone separator	60
2.9.3	Screw feeder design	63
2.9.3.1	Hopper Design.....	67
2.9.3.2	Screw design	70
2.9.3.2.1	Screw blade angle and pitch.....	71
2.9.3.2.2	Throughput prediction	72
2.9.3.2.3	Volumetric efficiency	73
2.9.3.2.4	Feed factor	74
2.10	Summary of gaps in literature	76
3	Material and Material Characterisations	78
3.1	Particles shape and particle size distribution measurement	78
3.2	Powder density.....	78
3.3	Flowability.....	79
3.3.1	Hausner ratio and Carr Index measurement.....	79
3.3.2	Flow function coefficient measurement.....	79
3.4	Materials and characterisation results	81
4	Definition of terms.....	85
5	Development and implementation of a pneumatic micro-feeder for poorly-flowing solid pharmaceutical materials.....	87
5.1	Chapter Summary	87
5.2	Materials and method.....	88
5.2.1	Materials.....	88
5.2.2	Pneumatic micro-feeder.....	88
5.2.3	Mathematic model of pneumatic micro-feeder	92
5.2.3.1	Modelling the relationship between piston speed and powder mass flow rate	92
5.2.3.2	Modelling the relationship between air flow rate and mass flow rate	93

5.2.4	Design Calculation	95
5.2.4.1	Fluidisation categorisation based on Geldart's classification	95
5.2.4.2	Classification of powder transfer phase	96
5.2.4.3	Estimate the minimum entrainment air pressure and volumetric flow rate	97
5.2.4.4	Estimate the piston speed	98
5.2.4.5	Cyclone separator	98
5.2.5	Methods	100
5.3	Results and discussions.....	101
5.3.1	Micro-feeder performance statistics	101
5.3.2	Micro-feeding process analysis	102
5.3.3	The influence of equipment configurations and process parameters	103
5.3.3.1	Piston speed	103
5.3.3.2	Air supply line and process line inserts	105
5.3.3.3	Plug position	107
5.3.3.4	Air pressure	107
5.3.3.5	Air flow rate	108
5.3.3.6	Equipment and operational guideline	110
5.3.4	Feeding performance of different materials	111
5.3.5	Segregation and particle degradation	114
5.3.6	Current limitations of the pneumatic micro-feeder	115
5.4	Conclusions	115
6	Design and development of the pneumatic micro-feeder: A systematic approach.....	117
6.1	Chapter Summary	117
6.2	Materials and method.....	117
6.2.1	Material	117
6.2.2	Pneumatic micro-feeder.....	117
6.3	Result and discussion	118
6.3.1	Relationship between powder flow rate and piston speed.....	118
6.3.2	Relationship between powder flow rate and air velocity.	120

6.3.3	Relationship between powder flow rate and air mass flow rate.....	121
6.3.4	Relationship between powder flow rate and air entrainment energy.....	122
6.4	Conclusion.....	124
7	A continuous micro-feeder for cohesive pharmaceutical materials.....	125
7.1	Chapter Summary	125
7.2	Materials and method.....	126
7.2.1	Material characterisation and material properties	126
7.2.2	Design Calculation	126
7.2.2.1	Hopper estimate	126
7.2.2.2	Screw blade angle design	127
7.2.2.3	Inclined screw flow rate estimate	127
7.2.3	Micro-feeder design	128
7.2.3.1	Feeding screw	129
7.2.3.2	Double-screw agitator.....	129
7.2.4	Operation	130
7.3	Results and discussions.....	131
7.3.1	Mass flow rate analysis.....	131
7.3.2	Refilling	134
7.3.3	Effect of equipment configuration and process parameters on feeding performance.....	137
7.3.3.1	Feeding screw pitch.....	137
7.3.3.2	Double-screw agitator speed.....	140
7.3.3.3	Feeding screw speed	143
7.3.4	Performance statistics	147
7.3.5	Volumetric efficiency, feed factor and feed rate analysis.....	152
7.4	Conclusions.....	157
8	Maximising performance and efficiency of inclined screw feeders	158
8.1	Chapter Summary	158
8.2	Material and methods.....	159

8.2.1	Material characterisation and material properties	159
8.2.2	Inclined micro-feeder and operation	159
8.3	Results and discussions.....	160
8.3.1	The effect of screw angles on the powder feeding performance	160
8.3.2	The effect of feeding screw flight configuration at various feeding screw speeds	165
8.3.3	Optimising powder feeding performance: A study on feeding screw flight configurations at various feed rates	171
8.3.4	The effect of on inner screw pitch of a double-screw agitator at various feeding screw speeds.....	177
8.3.5	Optimising powder feeding performance: A study on inner screw pitch of double-screw agitator at various feed rates	182
8.3.6	Analysis of improvement between the original design and the optimal design	187
8.3.7	An observational feeding performance between the commercial and inclined micro-feeders.....	188
8.4	Conclusions	191
9	Conclusions and future works	193
9.1	Conclusions	193
9.2	Future works.....	195
9.2.1	The optimisation of the inclined micro-feeder	195
9.2.1.1	Multi-screw agitator	196
9.2.1.2	Vertical micro-feeder	196
9.2.2	Integration of pneumatic micro-feeder and inclined micro-feeder feeder.....	197
9.2.3	Automation & sensors.....	198
9.2.3.1	Gain-In-Weight (GIW) control loop.....	198
9.2.3.2	Loss-In-Weight (LIW) control loop.....	199
9.2.3.3	Mass flow sensor control loop	200
9.2.3.4	Pressure drop sensor control loop	201
9.2.4	Blender.....	202

10	Appendix	205
10.1	Appendix for Chapter 5	205
10.1.1	Detail design of pneumatic micro-feeder.....	205
10.1.1.1	Photograph of the pneumatic micro-feeder.....	205
10.1.1.2	Powder pump and entrainment bed	205
10.1.1.3	Air supply line	206
10.1.1.4	Hardware control unit	207
10.1.2	Piston speed calibration.....	208
10.1.3	Pre-run	209
10.1.4	Piston speed estimation.....	210
10.1.5	Disturbances and limitations.....	211
10.1.5.1	Disturbance from compression	211
10.1.5.2	Limitation from the separator.....	211
10.2	Appendix for Chapter 7	215
10.2.1	Graphic user interface	215
10.2.2	The effect of feed height on measurement noise.....	215
10.2.3	Comparison of moving mean filter and Savitzky-Golay derivative filter	216
10.2.4	Feeder performance summary	218
10.2.5	The effect of different speed ratios between the agitator and feeding screw.....	221
10.3	Additional tasks and engagements during PhD period	224
11	References.....	225

List of Figures

Figure 2-1: Schematic diagram of generic pharmaceutical manufacturing processes where feeders are involved. The green boxes show where feeders are applied in the process— adapted from (K-Tron International, 2009; Yoon et al., 2018).	9
Figure 2-2: Coperion K-Tron feeder examples (a) volumetric feeder vs (b) gravimetric feeder (K-Tron Technologies Inc, 2012).	12
Figure 2-3: Schematics of screw feeders: (a) single screw feeder and (b) twin screw feeder.	13
Figure 2-4: Typical construction of a vibratory feeder with an electromagnetic drive (Aleksandar I. Ribić & Željko V. Despotović, 2010).	15
Figure 2-5: Schematic of a weigh-belt feeder (Wagner et al., 2014)	16
Figure 2-6: Schematic of a typical rotary valve feeder and common rotor geometries (Mills, 2016a)	17
Figure 2-7: Basic type of venturi feeder (Mills, 2016a)	18
Figure 2-8: a schematic of pulse-inertia force actuated feeder.	26
Figure 2-9: A schematic of a vibratory sieve chut system experimental set-up.	26
Figure 2-10: A schematic view of the screw-brush feeder: a) without gas flow, b) with the gas flow (Barati Dalenjan et al., 2015).	27
Figure 2-11: Illustration of fluidised bed feeder (Suri and Horio, 2009).	28
Figure 2-12: Resolution of particle feeder: a) developed by Wibberley & Phong-Anant (1986); b) developed by Burch <i>et al.</i> (1991); and c) modified by <i>Tang & Chen (1999)</i> . The figure is adapted from (Tang and Chen, 1999).	29
Figure 2-13: A schematic view of the powder pump setups (Besenhard et al., 2017).	30
Figure 2-14: A schematic view of the double-acting slide feeder (Pohořelý et al., 2004).	31
Figure 2-15: Interplay of particle and bulk properties and their combined influence on potential feeder development challenge (McGlinchey, 2009).	38
Figure 2-16: The apparatus of the angle of repose measurement by Carr, 1965 (McGlinchey, 2009).	42
Figure 2-17: Measurement of angle of repose: a) injection method; b) discharge method; c) tilting method (Higashitani et al., 2020).	42
Figure 2-18: A critical orifice diameter measurement device (Baserinia et al., 2016b).	43
Figure 2-19: Flowmeter used for flow rate measurement of powder material: a) Japanese Industrial Standard Z 2502 Hall flowmeter (Higashitani et al., 2020) and b) ASTM standard B417-22 of the Carney flow meter (ASTM standard, 2022).	44
Figure 2-20: Uniaxial compression test for measuring the flow function of a powder (Schulze, 2007).	46

Figure 2-21: Shear tester: a) translational shear tester (Jenike), b) annular (ring) shear tester, and torsional shear tester (Mehos, 2018).	46
Figure 2-22: An example of ring shear tester: a) Shear cell of the Schulze ring shear tester, b) Schematic of the cross-section of the sample during preshear and shear to failure, c) Example of stress and tie data, d) Measurement of a yield locus by preshear and shear to failure from a ring shear tester (Deshmukh et al., 2019).	48
Figure 2-23: Ball indentation: a) definition of variables for ball indentation, b) indentation curve (SI et al., 2022).	49
Figure 2-24: FT4 powder rheometer (Freeman Technology Ltd, 2016).	50
Figure 2-25: The measurement of permeability: a) permeability tester and b) determination of K from the test result (Mehos, 2018).	51
Figure 2-26: Geldart's classification of powder flowability in the aerated states (Geldart, 1973; McGlinchey, 2009).	53
Figure 2-27: Modified Geldart's classification using Archimedes' number versus modified Reynolds's number (McGlinchey, 2009).	54
Figure 2-28: Powder flow into a die: a) nose flow, b) bulk flow and c) intermittent flow (Schulze, 2007).	55
Figure 2-29: Flow patterns in horizontal pneumatic conveying (Rhodes, 2008).	58
Figure 2-30: Mechanism of aggregate entrainment: a) Illustration depicting the concept of powder entrainment from the surface of a powder layer and b) the entrainment process driven by bending and shearing stress of an aggregate within the powder layer (Matsusaka and Masuda, 1996).	59
Figure 2-31: Typical grade efficiency curves for gas-solid separators (Rhodes, 2008).	61
Figure 2-32: Illumination of a reverse flow cyclone separator (Mills, 2016).	61
Figure 2-33: Typical proportions of a cyclone separator (Mills, 2016).	62
Figure 2-34: Performance curves for typical cyclone separators (Mills, 2016).	63
Figure 2-35: The velocity diagram for particle (Wada et al., 1990).	65
Figure 2-36: Five boundary surfaces in a screw pocket (Dai and Grace, 2008).	66
Figure 2-37: Flow profiles: a) mass flow hopper and b) funnel flow hopper (Rhodes, 2008).	67
Figure 2-38: Flow promoting devices: a) pneumatic discharge aids, b) vibrating insert, c) rotary valve with vertical axis and agitator (Schulze, 2007).	70
Figure 2-39: Velocity and displacement for material in contact with the flight surface (Yu, 1997).	74
Figure 3-1: Flow function of investigated pharmaceutical powders measured using a PFT shear cell tester.	81
Figure 5-1: A process flow diagram for the proposed micro-feeder's conceptual design.	89

Figure 5-2: Prototype of the micro-feeder system with (a) overview, (b) powder pump, (c) entrainment bed half-section view, (d) cyclone separator, (e) air supply line and process lines insert types (side view and top-front-right view), (f) plug position to regulate air velocity in the chamber (side view).....	91
Figure 5-3: Schematic of the powder behaviour in the fluidised bed section.....	93
Figure 5-4: Geldard's classification of fluidisation behaviour for tested materials.	96
Figure 5-5: Overall dimensions of cyclone separator.....	99
Figure 5-6: MCC powder feeding process at a feed rate of 3 g/h. Process parameters: piston speed of 2 mm/min; air pressure of 25 kPa; air flow rate of 4 l/min.....	100
Figure 5-7: An example of MCC recorded powder weight at 8 mm/min of piston speed with a linear line fit (red line). The enlarged view depicts a close view from 10 to 11 min, demonstrating that the actual dispensed powder weight was close to the linear regression line. It implies consistent powder feeding.	101
Figure 5-8: Standard deviations as a function of applying time changes and moving mean windows for a powder feeding at 11 g/h.....	102
Figure 5-9: a) The relative standard deviation of APAP mass flow rate as a function of the cross-section area in the process line controlled by three different insert sizes at a fixed plug position (open position/highest level of the plug). 30 kPa and 9 l/min of air flow rate for the mean powder rate of APAP at 3.4 g/h, 25 kPa of air pressure and 6 l/min of air flow rate for the mean powder rate of MCC at 6.0 g/h; b) the MCC feeding trend using 1/10D cut insert; c) the MCC feeding trend at 1/4D cut insert.	106
Figure 5-10: The relative standard deviation of the MCC flow rate (6 g/h) and APAP flow rate (3.3 g/h) as a function of different plug positions in the entrainment bed using the same insert size (1/10D cut insert for APAP, 1/4D cut insert for MCC) at same air flow rate and pressure settings (30 kPa and 9 l/min of air flow rate for APAP, 25 kPa of air pressure and 6 l/min of air flow rate for MCC).....	107
Figure 5-11: The relative standard deviation of the APAP flow rate (3.5 g/h) and MCC flow rate (6 g/h) as a function of the air pressure at 9 l/min of air low rate. A plug position of 1/2D and an insert size of 1/10D cut was set for APAP, and a plug position of full chamber and an insert size of 1/2D cut for MCC.....	108
Figure 5-12: Feeding performance of MCC and APAP for a different setting. a) The effect of air flow rate on the MCC flow rate (6 g/h) and APAP flow rate (3.5 g/h) at a fixed piston speed and equipment setting. It shows the RSDs of MCC (■) and APAP (▲) powder flow rate as a function of the air flow rate at fixed air pressures (25 kPa and 30 kPa) and plug positions (full chamber and 1/2D) with the same insert size (1/2D cut and 1/10D cut); b) the effect of air flow	

rate on the MCC powder flow rate; c) the effect of air flow rate on the APAP powder flow rate.	109
Figure 5-13: The equipment and operational guideline.	111
Figure 5-14: Feeding performance of MCC using the pneumatic micro-feeder. The air pressure, P , was set at 25 kPa. The air flow rate, Q , was adjusted to stabilise the powder flow rate. The piston speed, S , was varied to adjust the average powder flow rate.	111
Figure 5-15: Average powder mass flow rate with standard deviations of three repeat experiments as a function of piston speed for four different materials. H represents the Hausner ratio.	112
Figure 5-16: Comparison of MCC and APAP at similar feed rates. The parameters of MCC were set to 4 mm/min of piston speed, 25 kPa of air pressure and 5 l/min of air flow rate. APAP was fed at 7 mm/min of piston speed, 50 kPa of air pressure and 10 l/min of air flow rate.	114
Figure 6-1: A photo of a pneumatic micro-feeder prototype.	118
Figure 6-2: Linear relationship between average powder flow rate (averaged over three repeat experiments) with standard deviations shown as error bars, and piston speed for four different materials (MCC, CCS, XPVP, and APAP). H represents the Hausner ratio.	119
Figure 6-3: Predicted powder flow rate as a function of piston speed for four materials (MCC, CCS, XPVP, and APAP) using Equation 5-19. H represents the Hausner ratio.	120
Figure 6-4: The relationship between air velocity and powder flow rate for four materials. The air velocity is calculated by the air volumetric flow rate divided by the insert's free cross-sectional area. For all materials, the effect of air velocity on powder flow rate is minimal, with slight variation observed in air velocity across changes in powder flow rate. VMD represents the volume median diameter.	121
Figure 6-5: Relationship between powder flow rate and air mass flow rate for four different materials.	122
Figure 6-6: Entrainment energy as a function of powder flow rate for four different materials.	123
Figure 7-1: Hopper dimensions.	127
Figure 7-2: An overview of a schematic inclined micro-feeder.	128
Figure 7-3: Schematic diagram of the feeding screws in four pitches: 7 mm, 10 mm, 15 mm and 25 mm.	129
Figure 7-4: Schematic diagram of the double-screw agitator.	130
Figure 7-5: Data acquisition and analysis of continuous CCS powder feeding at 6 rpm feeding screw speed and 5 rpm double speed agitator speed over 2 hours: a) experimental mass acquired at 1-second intervals from the catch scale; b) filtered mass flow rate using a 60-second moving mean window. The green dashed line represents the mean powder flow rate,	

while the upper and lower solid red lines denote the predetermined range of variation, set at $\pm 5\%$ for this particular experiment. 132

Figure 7-6: Effect of powder flow rate on RSD for automation and manual operation with 60-second window measurement, and APAP with lowest powder rate at 120-second window measurement. a) an illustration of APAP feeding conducted over a 30-minute duration, with manual measurements recorded at one-minute intervals, juxtaposed with automatic data acquisition utilising a 1-minute moving mean filter; b) a comprehensive summary of the results obtained from both manual and automatic measurements. Each measurement was done in triplicate ($n = 3$). 133

Figure 7-7: Illustrations depicting the impact of hopper fill level on the consistency of powder feeding. a) Feed factors plotted against hopper fill level for six iterations of spray-dried lactose ($H = 1.21$ – fair-flowing) in volumetric mode, utilising a 22 mm double concave screw (Janssen et al., 2022). b) Feeding of MgSt with hopper fill level variation (Bin#) using a GEA compact feeder equipped with a 20 mm concave screw (Tahir et al., 2020). c) Feed factor variations across six different materials – Colour codes: Starch1500 (blue), Methocel DC2 (red), NAP+SiO₂ (orange), MgSt (black) and NAP (purple) (Van Snick et al., 2017). d) Diverse feeders delivering M200 grade mannitol with a coarse concave screw at 50% screw speed – Colour codes: Coperion-KTron KT20 (blue), Compact feeder (yellow), Compact feeder with adapted hopper (purple), ZD12FB (orange), and Brabender MT-S (green) (Hörmann-Kincses et al., 2022). 135

Figure 7-8: Refilling every 20 mins in continuous feeding demonstrated in three different materials: a) Variation in feed factor over feeding time, b) Changes in powder flow rate with respect to feeding time. All experiments were performed in triplicates ($n = 3$). The blue line is the mean powder flow rate. The blue shadow represents the SD of three repeated experiments. The red shaded belt represents $\pm 5\%$ 136

Figure 7-9: Illustration depicting the effect of hopper refill on powder feeding performance. a) Feed factor profile for paracetamol during a single feeding period. b) Mass flow profile of paracetamol powder across 11 refills in a feeding period, highlighting observable refill overshoots after each refill (Bekaert et al., 2022). 136

Figure 7-10: Standard deviation as a function of screw pitches for CCS, MgSt and APAP. Each measurement was done in triplicate ($n = 3$). 137

Figure 7-11: Effect of P/D on η_v in different tested materials a) CCS, b) MgSt, c) APAP, and d) summary of volumetric efficiency of all tested material. The speed of the feeding screw is configured to 2.5 rpm, and the agitator operates at a speed of 2.5 rpm. 138

Figure 7-12: Effect of P/D Ratio on Feed Factor (FF) in a) CCS, b) MgSt, and c) APAP... 140

Figure 7-13: The effect of double-screw agitator speed on powder flow rate, SD and RSD. a) The mean powder flow rate from three repeated experiments ($n = 3$) is plotted in relation to

agitator speed for three different powder properties at a fixed feeding screw speed of 3.5 rpm.
b) SD is plotted in relation to agitator speed. c) RSD is plotted in relation to agitator speed.
..... 142

Figure 7-14: Feed factor as a function of agitator speed at a constant screw speed of 3.5 rpm.
..... 143

Figure 7-15: Effects of feeding screw speed on powder flow rate, SD and RSD for three distinct powder properties. a) CCS, b) MgSt, and c) APAP powder feeding at varying feeding screw speeds and a constant agitator speed of 2.5 rpm. The blue line is the mean powder flow rate. The blue shadow represents the SD of three repeated experiments..... 144

Figure 7-16: Effects of feeding screw speed on powder flow rate, SD and RSD for three distinct powder properties. a) Mean powder flow rate of three repeat experiments as a function of feeding screw speed for three different powder properties at a constant double-screw agitator speed of 2.5 rpm; b) standard deviation as a function of feeding screw speed at 2.5 rpm of double-screw agitator speed; c) relative standard deviation as a function of feeding screw speed at 2.5 rpm of double-screw agitator speed. 146

Figure 7-17: Feed factor as a function of screw speed at a constant agitator speed of 2.5 rpm.
..... 147

Figure 7-18: Consistent feeding of optimal ratios was observed in three repeat experiments without feedback control for (a) CCS, (b) MgSt, and (c) APAP. The blue line is the mean powder flow rate. The blue shadow represents the SD of three repeated experiments. 148

Figure 7-19: The summary statistics of the powder flow rates and RSDs for the three materials. RSDs as a function of powder flow rate at the equal and optimal ratio of screw and agitator speed: a) CCS; b) MgSt; c) APAP. Horizontal and vertical errors represent the SDs of the powder flow rates and RSDs of triplicate experiments. Each measurement was done in triplicate ($n = 3$). 150

Figure 7-20: Repeatability and stability at the optimal ratios were investigated for the three materials. a) repeatability and b) stability as a function of powder flow rate at the optimal ratio.
..... 151

Figure 7-21: The summary of the powder flow rate as a function of agitator speed for the three different materials at optimal ratios, demonstrating a linear relationship. Experiments were conducted in triplicate ($n = 3$). 152

Figure 7-22: Effect of screw speed/agitator speed on the volumetric efficiency: a) CCS with a 7 mm pitch screw, b) MgSt with a 25 mm pitch screw, and c) APAP with a 25 mm pitch screw. The predicted volumetric efficiency is indicated by the blue dashed line. 153

Figure 7-23: Effect of agitator speed on the feed factor. Different symbols depict data points for CCS (green), MgSt (blue), and APAP (red), and linear regression lines for each material type demonstrate varying slopes and intercepts..... 154

Figure 7-24: Comparative analysis of theoretical powder flow rates (depicted by lines) for a) CCS, b) MgSt, and c) APAP. In Equation 2-31, the inclination correction factor, C , is set at 0.55 for all tested materials, with loading ratios of 0.474 for CCS, 0.138 for MgSt, and 0.120 for APAP. The blank experiment at an agitator speed of 5 rpm determines loading ratios. 155

Figure 7-25: Comparison of the theoretical flow rate (Equation 2-31) and observed flow rate for a) CCS, b) MgSt, and c) APAP. 156

Figure 8-1: Optimising the inclined micro-feeder: A step-by-step process for enhancing feeding performance. 159

Figure 8-2: Inclined micro-feeder schematic: A double-screw agitator and feeding screw facilitate efficient powder transfer and delivery. 160

Figure 8-3: The effect of three distinct feeding screw angles: a) 30° inclination, b) 0° horizontal, and c) -30° declination. 160

Figure 8-4: SD as a function of powder flow rate at optimal ratios of a) CCS and b) APAP for three different screw feeder angles: 30° inclination, 0° horizontal, and -30° declination. 161

Figure 8-5: Effect of feeding screw angle on repeatability as a function of powder flow rate: (a) CCS and (b) APAP. The graph shows the repeatability of powder feeding for two materials (CCS and APAP) as a function of the powder flow rate for different feeding screw angles. The results suggest that the feeding screw angle can influence the repeatability of powder feeding for different materials, with varying influences on the powder flow rate. 162

Figure 8-6: Stability as a function of powder flow rate: a) CCS b) APAP. The results suggest that the 30° inclination of the feeding screw provides more consistent stability across varying powder flow rates for both materials. 163

Figure 8-7: Feed factor as a function of screw speed in the powder feeding process of a) CCS, b) APAP at inclination angles of 30°, 0°, and -30°. 165

Figure 8-8: Enhanced feeding efficiency with modified micro-feeder outlet and feeding screw flight configurations: (a) shows the modified inclined micro-feeder fitted with an angled outlet adaptor, while b) and c) display high and low pitch ends for non-flowing material and cohesive material, respectively. The compression ends of both designs help enhance feeding efficiency. 166

Figure 8-9: Influence of screw speed on CCS powder flow rate, standard deviation, repeatability, and Stability at a fixed agitator speed of 2.5 rpm. a) shows the powder flow rate as a function of screw speed, while b) illustrates the SD. c) and d) display the repeatability and stability, respectively, as a function of screw speed. All measurements were taken at a fixed agitator speed of 2.5 rpm. 167

Figure 8-10: Influence of screw speed on APAP powder flow rate, SD, repeatability, and Stability at a fixed agitator speed of 2.5 rpm. a) shows the powder flow rate as a function of screw speed, while b) illustrates the SD. c) and d) display the repeatability and stability,

respectively, as a function of screw speed. All measurements were taken at a fixed agitator speed of 2.5 rpm. 169

Figure 8-11: Variation of feed factor with screw speed at a constant agitator speed of 2.5 rpm in the powder feeding process for a) CCS and b) APAP, showcasing the influence of various screw flight configurations. 171

Figure 8-12: SD of powder flow rate across different feeding screw flight configurations for a) CCS and b) APAP. It shows that equal-pitch compression ends generally have a low SD, while the 25/25 compression screw exhibits a minor SD for APAP. For CCS, 7/7 non-compression and 15/7 non-compression exhibit a minor SD. 173

Figure 8-13: Repeatability as a function of powder flow rate: a) CCS b) APAP for four different feeding screw flight configurations. 174

Figure 8-14: Influence of four different feeding screw flight configurations on powder feeding stability for a) CCS and b) APAP. 175

Figure 8-15: Variation of feed factor at an optimal point across the agitator speed in the powder feeding process for a) CCS and b) APAP. 177

Figure 8-16: Three inner screw double-screw agitators, each featuring a unique screw pitch of 7 mm, 10 mm, and 15 mm, respectively, while maintaining a uniform outer screw configuration. It studies the effect of different inner screw pitches of the double-screw agitator on cohesive powder feeding performance under different feeding screw speeds. 178

Figure 8-17: The effect of different inner screw pitches of the double-screw agitator on cohesive powder feeding performance under different feeding screw speeds: a) the effect of inner screw pitch on CCS powder flow rate at different screw speeds, with a fixed agitator speed of 2.5 rpm. b) the variation in SD with screw speed at a fixed agitator speed of 2.5 rpm. c) the relationship between repeatability and screw speed, with a fixed agitator speed of 2.5 rpm. d) the effect of screw speed on stability at a fixed agitator speed of 2.5 rpm. 179

Figure 8-18: The effect of different inner screw pitches of the double-screw agitator on non-flowing powder feeding performance under different feeding screw speeds: a) the effect of inner screw pitch on APAP powder flow rate at different screw speeds, with a fixed agitator speed of 2.5 rpm. b) the variation in SD with screw speed at a fixed agitator speed of 2.5 rpm. c) the relationship between repeatability and screw speed, with a fixed agitator speed of 2.5 rpm. d) the effect of screw speed on stability at a fixed agitator speed of 2.5 rpm. 180

Figure 8-19: The feed factor as a function of screw speed at a constant agitator speed of 2.5 rpm, featuring various agitator inner screw pitches in its configuration. 182

Figure 8-20: Relationship between powder flow rate and SD for a) CCS and b) APAP, using a double-screw agitator with varying inner screw pitches. Results show that the changes in the inner screw pitch of the double-screw agitator have a significant influence on powder flow rate and SD. 183

Figure 8-21: The effect of different inner screw pitches of a double-screw agitator on the repeatability of powder feeding as a function of powder flow rate for (a) CCS and (b) APAP, demonstrating the effect of varying inner screw pitch on the repeatability of consistent powder feeding for the two different materials. 184

Figure 8-22: The effect of inner screw pitch on feeding stability for (a) CCS and (b) APAP as a function of powder flow rate, demonstrating the relationship between flow rate and the stability of powder feeding while varying the inner screw pitch for both cohesive and non-flowing materials. 185

Figure 8-23: Effect of agitator screw inner pitch on feed factors with respect to agitator speed at the optimal powder feeding point. 186

Figure 8-24: A comparative analysis between the equipment designs presented in Chapter 6 and the optimal designs proposed in this study for a) CCS and b) APAP. The SDs are plotted in relation to the powder flow rates for each design..... 188

Figure 8-25: A comparative assessment of the performance of an inclined micro-feeder and two commercial feeders in volumetric feeding: a) CCS, b) APAP. The motor speeds were pre-determined and remained unchanged throughout the feeding process. 190

Figure 8-26: A comparative analysis of experimental data and literature findings, showcasing feeding CCS at varying feed rates using a powder pump, both without control (Cal) and with control (FF). The red band indicates a $\pm 5\%$ variation, as observed in a study by Fathollahi et al. (2021). Additionally, our experimental data is presented for further examination (b)..... 191

Figure 9-1: The multi-screw agitator to homogenise the powder density to minimise the powder flow rate variation..... 196

Figure 9-2: The schematic drawing of a vertical micro-feeder..... 197

Figure 9-3: A schematic of the integration of the pneumatic micro-feeder with the inclined micro-feeder..... 198

Figure 9-4: GIW control loop using weight scale a) batch process; b) continuous process. 199

Figure 9-5: LIW feedback loop 200

Figure 9-6: The mass flow sensor control loop. a) batch process; b) continuous process. 201

Figure 9-7: Differential pressure sensor control loop for batch (a) and continuous (b) processes, which uses three pressure sensors to regulate the powder flow rate and maintain consistency in feeding. 202

Figure 9-8: Conversion of pneumatic micro-feeders into a blender through integration: A novel approach for uniform blending in pharmaceutical manufacturing. 203

Figure 9-9: Schematic illustration of the inclined micro-feeder used as a blending feeder. This novel 2-in-1 application offers the potential for improved efficiency and reduced equipment costs in various industries, including pharmaceutical and food manufacturing..... 204

Figure 10-1: Photograph of the pneumatic micro-feeder system with a validation balance.	205
Figure 10-2: Overall dimension of powder pump and entrainment bed.	206
Figure 10-3: Air supply line assembled with a fluidised section.	207
Figure 10-4: (a) the electrical wiring between the stepper motor and the Arduino Mega micro-controller, (b) Network architecture of the pneumatic micro-feeder.....	208
Figure 10-5: The piston speed change over motor speeds with a picture of the pusher block and scale ruler.	209
Figure 10-6: MCC powder feeding process at a feed rate of 3 g/h with no pre-run (grey line) compared to the powder feeding with pre-run (red line). Process parameters: piston speed of 2 mm/min; air pressure of 25 kPa; air flow rate of 4 l/min.....	210
Figure 10-7: Comparison between free-filling experiment and powder compressed experiments for MCC at the same parameter settings.	211
Figure 10-8: The APAP separation in different separator materials: a) acrylonitrile butadiene styrene (ABS); b) polylactic acid (PLA); and c) stainless steel (SS).....	212
Figure 10-9: The design of the separator cone influences the stability of MCC powder flow rate: a) cone with a flat edge; b) cone with a radiused edge; c) flared cone with a radiused edge.	213
Figure 10-10: APAP adhered on the rods and the stainless steel separator wall.	213
Figure 10-11: Comparison of vibration and no vibration on the separator for MCC feeding at the same parameter settings (4 mm/min of piston speed, 25 kPa of air pressure and 6 l/min of air flow rate).	214
Figure 10-12: The MATLAB Design app GUI was utilised to regulate the motors and record the measurements from the lab-scale balance.	215
Figure 10-13: A comparison of two different configurations of the equipment, with the feed outlet to the balance pan set at two different heights: 120 mm and 80 mm. The parameters in the experiment were also set at equal speeds (2.5 rpm screw and agitator speeds), and a 10 mm pitch screw was used.	216
Figure 10-14: Comparison of moving mean filter and Savitzky-Golay derivative filter applications on powder flow rate. a) Analysis of APAP powder feeding using moving mean filter (red) and Savitzky-Golay derivative filter (blue). b) Analysis of data using a moving mean filter. c) Analysis of data using the Savitzky-Golay derivative filter.....	217
Figure 10-15: Comparison of repeatability for the equal and optimal ratios between screw speed and agitator speed as a function of powder flow rate for three different materials - a) CCS, b) MgSt, and c) APAP.....	222
Figure 10-16: Comparison of stability as a function of powder flow rate for three different materials - a) CCS, b) MgSt, and c) APAP, while comparing the equal and optimal ratios.	223

List of Table

Table 2-1: Commercially available micro-feeder.	19
Table 2-2: Feeder capacity of commercially commonly used feeders in literature (Engisch and Muzzio, 2014; Coperion, 2013; Gericke, 2022; and Brabender, 2023a, 2023b).....	20
Table 2-3: Current pharmaceutical powder feeders on the commercial market.	22
Table 2-4: Current micro-feeders and their feeding principles in the literature. Adapted from (Besenhard et al., 2016).	33
Table 2-5: General variables that influence powder flowability.	35
Table 2-6: Flowability indicator prescribed by USP29-NF26, 2006 (McGlinchey, 2009).....	41
Table 2-7: A table of flow function coefficient and flowability of solid powder indicator, adapted from (McGlinchey, 2009)	45
Table 2-8: Common screw design (adapted from Conveyors Incorporated, 2023).....	71
Table 2-9: The correction factor for screw inclination (PowderProcess.net, 2022).	73
Table 2-10: the loading ratio of the screw according to the flow properties of the solid (PowderProcess.net, 2022).	73
Table 3-1: A table of flow function coefficient and flowability of solid powder indicator, adapted from (McGlinchey, 2009)	81
Table 3-2: Pharmaceutical material selection and its feed rate in literatures.	82
Table 3-3: Powder properties of materials investigated to assess the performance of the designed micro-feeders.	84
Table 5-1: Flow pattern identification through solid loading.	97
Table 5-2: A summary of phases I, II and III at various piston speeds for the different materials.	104
Table 5-3: Summary of the feeding performance of different powder flow rates. The definitions of all listed parameters can be found in section 5.3.2.....	113
Table 5-4: Particle size distribution along with the system for APAP. All experiments were conducted in triplicate.	115
Table 7-1: Screw blade angles	127
Table 7-2: the design parameters and design calculation.....	128
Table 8-1: A comparison of the inclined micro-feeder versus two Brabender feeders.....	189
Table 10-1: Summary of the CCS feeding performance at two ratios between the screw and agitator speeds: equal and optimal ratios.	218
Table 10-2: Summary of the MgSt feeding performance at two ratios between the screw and agitator speeds: equal and optimal ratios.	219
Table 10-3: Summary of the APAP feeding performance at two ratios between the screw and agitator speeds: equal and optimal ratios.	220

Abbreviations

ABS	Acrylonitrile Butadiene Styrene
APAP	Paracetamol
API	Active Pharmaceutical Ingredient
CAGR	Compound Annual Growth Rate
CDMOs	Contract Development and Manufacturing Organisations
CCS	Croscarmellose Sodium
cGMP	current Good Manufacturing Practice
CTM	Clinical Trial Material
ECVT	Electrical Capacitance Volume Tomography
FDA	Food and Drug Administration
FDM	Fused Deposition Modelling
GIW	Gain-In-Weight
GUI	Graphical User Interface
HME	Hot-Melt Extrusion
HPAPI	High-Potent Active Pharmaceutical Ingredient
MCC	Microcrystalline cellulose
MgSt	Magnesium Stearate
NIR	Near Infrared
LIW	Loss-In-Weight
PID	Proportional Integral Derivative
PLA	Poly(lactic acid)
PSD	Particle Size Distribution
PZT	Piezoelectric Transducer
RSD	Relative Standard Deviation
R&D	Research and Development
SD	Standard Deviation
SiO ₂	Silicon dioxide
SLA	Stereolithography
USP	United States Pharmacopoeia
VMD	Volume Median Diameter
XPVP	Crospovidone
μAPAP	Micronised paracetamol

Nomenclature

A_b	Cross-section area of the powder pump	mm ²
A_r	Archimedes numbers	-
C	Compressibility	%
c	Carr Index	-
D_{10}	10% of particles in the powders are smaller than this size	μm
D_{50}	50% of particles in the powders are smaller than this size	μm
D_{90}	90% of particles in the powders are smaller than this size	μm
D_s	Interanal diameter of separator	mm
d_p	Paricle diameter	μm
E_{air}	Air kinetic energy	mW
$E_{Entrainment}$	Entrainment energy	mW
ffc	Flow function coefficient	-
g	Gravitational acceleration (= 9.807 m/s ²)	m/s ²
H	Hausner ratio	-
$L_{c,actual}$	Compression length	mm
Δm	Powder mass accumulated	g
\dot{m}	Powder flow rate	g/h
\dot{m}_{air}	Air mass flow rate	g/h
\dot{m}_p	Powder flow rate	g/h
$\overline{\dot{m}_p}$	Average powder flow rate	g/h
$\dot{m}_{p,b}$	Powder feed rate of powder pump	g/h
n	Number of samples	-
P	Air pressure	kPa
P_s	Screw pitch	mm
Q	Air flow rate	l/min
Q_f	Air volumetric flow rate	m ³ /h
r	Repeatability	%
Re	Reynolds numbers	-
RSD	Relative standard deviation	%
\overline{RSD}	Average relative standard deviation	%
S	Piston speed	rpm
S_{50}	Sphericity below 50% of all particles contained	-
Δt	Time window/Time difference	s
t	Time	s
$t_{phase I}$	Average compression phase	min
$t_{phase II}$	Acceleration phase	min
$t_{phase III}$	Stable feeding phase	min
U_{air}	Air velocity	m/s
U_t	Terminal velocity of spheric particles	m/s
v	Air velocity	m/s
v_r	Reliability	%
V_0	Powder flow velocity	m/s

V_b	Volume of powder occupied in the graduated glass cylinder	cm^3
VMD	Volume median diameter	μm
V_p	Particle volume	cm^3
V_t	Volume where powder occupied after tapping	cm^3
W	Powder mass	g
W_p	Particle weight	g
σ	Standard deviation	g/h
$\bar{\sigma}$	Average standard deviation	g/h
σ_1	The major principal consolidation stress	kPa
σ_c	The unconfined yield strength	kPa
σ_{Lowest}	Lowest standard deviation	g/h
$\sigma_{Highest}$	Highest standard deviation	g/h
σ_{RSD}	Stability	%
ρ_{air}	Air density	g/cm^3
ρ_b	Bulk density	g/cm^3
ρ_p	True density	g/cm^3
ρ_t	Tapped density	g/cm^3
ω	Motor speed	rpm
ω_{ag}	Agitator speed	rpm
ω_s	Screw speed	rpm
μ_{air}	Air viscosity	$\text{Pa}\cdot\text{s}$

Acknowledgements

I am deeply grateful to my supervisor, Dr. Daniel Markl, for his unwavering support, guidance, and expertise throughout the entire process of completing this thesis. His dedication to my success, invaluable feedback, and constructive criticism have played a pivotal role in shaping my research and improving my work. I am truly grateful for his mentorship and encouragement. I would also like to thank Prof. Gavin Halbert, Dr. Mira Naftaly, and Dr. Maximilian Besenhard for their help and advice on my work and for their time invested in this project over the past four years. I wish to extend my special gratitude to Professor Jerry Heng, my MSc supervisor at Imperial College London, for his unwavering support and valuable guidance throughout my academic journey.

I am grateful to the University of Strathclyde and the Centre of Continuous Manufacturing and Advanced Crystallisation (CMAC) for providing financial and facilities support for this research project and to the Postgraduate Institute for Measurement Science (the PGI) for their encouragement, support, and training. I am especially thankful to Dr. Richard Burguete for his constant encouragement, Leah Chapman for providing me with training in marketing and communications skills, and Linden Fradet for her unwavering support throughout my PhD journey. I am also thankful to my CMAC and PGI colleagues for their interest in my project and for sharing their knowledge.

My deepest appreciation goes to my dad, mom, and sister for their endless love, encouragement, and understanding. Their unwavering support, motivation, and belief in my abilities have been a driving force behind my pursuit of higher education. Their sacrifices and encouragement have been invaluable to my success, and I am deeply grateful for their constant presence in my life.

Last but not least, I would like to express my deepest gratitude to my loving wife, Jamie, for her unwavering support both mentally and financially. She has been patient with me during times of high pressure from my research, always being a good listener and my biggest supporter. Thank her for financial support for my “high-tech” toys and for always being my first audience for every event I participated in. She has been my motivation and inspiration throughout this challenging journey. I am truly grateful for her unconditional love and unwavering support, which have been the cornerstone of my success.

In conclusion, I would like to express my heartfelt appreciation to my supervisors, collaborators, family, and my dear wife, Jamie, for their unwavering support, encouragement, and belief in my abilities throughout this thesis. Without their guidance, love, and support, this work would not have been possible.

Research Outputs

Journal papers

1. Naftaly, M., Tikhomirov, I., **Hou, P.**, and Markl, D. (2020) Measuring open porosity of porous materials using THz-TDS and an index-matching medium. *Sensors*. 20 (11). Available from: doi:10.3390/s20113120.
2. **Hou, P.**, Besenhard, M.O., Halbert, G., Naftaly, M., and Markl, D., (2023) Development and implementation of a pneumatic micro- feeder for poorly-flowing solid pharmaceutical materials. *International Journal of Pharmaceutics*. 122691. Available from: doi:10.1016/j.ijpharm.2023.122691.
3. **Hou, P.**, Besenhard, M.O., Halbert, G., Naftaly, M., and Markl, D., A continuous micro-feeder for cohesive pharmaceutical materials. *International Journal of Pharmaceutics*. (Submitted for peer review).
4. **Hou, P.**, Besenhard, M.O., Halbert, G., Naftaly, M., and Markl, D., Maximising Performance and Efficiency of Inclined Screw Feeders through Optimisation Techniques. *Powder Technology* (Under internal review).
5. **Hou, P.**, Besenhard, M.O., Halbert, G., Naftaly, M., and Markl, D., Design and development of the pneumatic micro-feeder: A systematic approach. *International Journal of Pharmaceutics* (Under internal review).

Poster Presentation

- 1 **Hou, P.**, Besenhard, M.O., Halbert, G., Naftaly, M., and Markl, D., Design of a Micro-Feeder for Solid Pharmaceuticals, EPSRC CMAC Virtual Open Day, 2020, Glasgow, Online.

Poster Presentation

- 2 **Hou, P.**, Besenhard, M.O., Halbert, G., Naftaly, M., and Markl, D., Design of a Micro-Feeder for Solid Pharmaceuticals, EPSRC CMAC Mini-symposia, 2021, Glasgow, Online.

One-to-one meeting presentation

- 3 **Hou, P.**, Besenhard, M.O., Halbert, G., Naftaly, M., and Markl, D., A Novel Micro-Feeder for Solid Pharmaceuticals, EPSRC CMAC Open Day, 2022, Glasgow.

Poster Presentation

- 4 **Hou, P.**, Besenhard, M.O., Halbert, G., Naftaly, M., and Markl, D., A Continuous Micro-Feeder for Solid Pharmaceuticals, EPSRC CMAC Summer School, 2022, Glasgow.

Poster Presentation

- 5 **Hou, P.**, Besenhard, M.O., Halbert, G., Naftaly, M., and Markl, D., Development and Implementation of a Micro-Feeder for Poorly-Flowing Solid Pharmaceutical Materials, APS PharmSci Annual Conference, 2022, London.

Poster Presentation

- 6 **Hou, P.**, Besenhard, M.O., Halbert, G., Naftaly, M., and Markl, D., Development and Implementation of a Micro-Feeder for Poorly-Flowing Solid Pharmaceutical Materials, NPL PGI research and career showcase, Nov. 2022, London.

Poster Presentation

- 7 **Hou, P.**, Besenhard, M.O., Halbert, G., Naftaly, M., and Markl, D., Will a Micro-Feeder be a Game Changer for Next Generation of Drug Manufacturing?, NPL PGI research and career showcase, Nov. 2022, London.

Invited Talk

- 8 **Hou, P.**, Besenhard, M.O., Halbert, G., Naftaly, M., and Markl, D., A Novel Micro-Feeder for Solid Pharmaceutical Materials for Precision Medicine Manufacturing, STEM for BRITAIN, Mar. 2023, London, UK.

Finalist of STEM for BRITAIN (Presented in House of Commons)

- 9 **Hou, P.**, Besenhard, M.O., Halbert, G., Naftaly, M., and Markl, D., Three Minutes Thesis competition, Research Development Programme, University of Strathclyde, May. 2023.

3MT Presentation Video

- 10 **Hou, P.**, Besenhard, M.O., Halbert, G., Naftaly, M., and Markl, D., Enhancing Powder Handling with a Continuous Micro-feeder for Pharmaceutical Materials, PGI 7th Annual Conference, June. 2023.

Poster Presentation

- 11 **Hou, P.**, Besenhard, M.O., Halbert, G., Naftaly, M., and Markl, D., Enhancing Powder Handling with a Continuous Micro-feeder for Pharmaceutical Materials, CMAC summer school, June. 2023.

Poster Presentation (3rd Place Prize)

Patents

- 1 **Hou, P.**, Halbert, G., and Markl, D. (2022), Apparatus For Supplying A Particulate Material, *PCT/GB2023/051291*, Intellectual Property Office, UK.

Prizes

- 1 Strathclyde University Commercialisation & IP Gate 1 award (£2,000), May 2021.

- 2 CMAC doctoral training prize winner, June 2022.
- 3 Stephen Young Entrepreneur Award (£75,000), July 2022.
- 4 SIPBS WIDE professional career development winner (£500), Nov 2022.
- 5 PGI outstanding contribution award, May 2023.
- 6 Finalist of STEM for BRITAIN, Mar 2023.
- 7 PGI Travel award for STEM for BRITAIN (£500), May 2023.
- 8 Semi-finalist of Converge KickStart, May 2023.
- 9 CMAC and Strathclyde IP & Commercialisation contributed to PCT application (£7,600).
- 10 CMAC 2023 Summer School Poster 3rd Place Prize
- 11 Highly recommended for IChemE Global Award – Pharma Award 2023.

1 Introduction

1.1 Motivation

In recent years, the pharmaceutical industry has shown increasing interest in the development of micro-factories and continuous manufacturing processes to improve the efficiency of drug manufacturing and drug development (Burcham et al., 2018; Plumb, 2005). The goal is to achieve more effective and cost-efficient drug manufacturing processes that reduce waste and costs, enabling the introduction of more affordable life-saving medicines to the public (Janssen et al., 2022).

Solid oral dosage forms, such as tablets and capsules, represent the most common drug delivery systems (Hickey, 2001), with approximately 80% of marketed drugs being in solid form (Couillaud et al., 2019). However, a significant challenge in powder-based manufacturing is the accurate feeding of poorly flowing raw materials at the required ratios for a given formulation. Furthermore, the demand for precise feeding has risen significantly due to the research on novel high-potency drugs and personalised medicines (Copot, 2022; Rajjada et al., 2021). Accurate feeding is crucial for optimising medicine effectiveness, yield, and safety of operation, as well as reducing operational costs and minimising material and energy losses. The feeding of active pharmaceutical ingredients (APIs) and excipients is a critical step in the production of any formulated drug, as it directly influences the content uniformity and weight uniformity of the final product. Therefore, the improvement of drug manufacturing processes heavily relies on the utilisation of highly accurate feeders in the pharmaceutical manufacturing process (F. Stauffer et al., 2019).

The demand for enhanced accuracy in low-dosing feeders has been steadily increasing, particularly in applications such as direct compression, direct capsulising, feeding small quantities for seeding in crystallisation (Brown et al., 2018; Genck et al., 2002), and filling compartmentalised 3D printed medicines (Wang et al., 2018b). Inaccurate or inconsistent dosing rates can result in inconsistent variability in composition and weight in subsequent process steps, leading to the production of out-of-specified dosage forms (Blackshields and Crean 2018). Refilling is also a challenge in continuous powder feeding. The refilling interrupts the continuity of powder feeding and leads to inconsistent and inaccurate powder feed rates (Bekaert et al., 2022; Hanson, 2018). Several studies focus on refilling and attempting to overcome this issue to achieve real accurate and consistent continuous powder feeding (Bekaert et al., 2022; Blackshields and Crean, 2018; Bostijn et al., 2019; De Souter et al., 2023; Engisch and Muzzio, 2015; Hanson, 2018; Johnson et al., 2022; Nowak, 2013).

Furthermore, Welsch (2003) highlighted the crucial significance of an ultra-low feed rate (e.g., 50 g/h) with high precision (less than 1 g) in the compounding processes for plastics, specifically in feeding filler powder. This is essential because it involves feeding various fillers with a diverse range of flow behaviours. In the early stages of pharmaceutical drug development, the available amount of active pharmaceutical ingredient (API) for testing is often constrained to a range of 0.2–1.0 kg due to factors such as material costs, availability, and safety concerns, as noted by Plumb (2005) and Wang et al. (2017a). Furthermore, Nowak (2013) pointed out that the typical powder feed rates for magnesium stearate vary from 0.2 to 2 kg/h, with micro-feeders allowing rates as low as 50 g/h. Many potential medicines have projected API requirements below 1500 kg/year. Hence, the production rate of 5-15 kg/day (0.2 to 0.6 kg/h) in laboratory fume hoods has gained interest (Nagy et al., 2020).

Crystal seeding is a widely employed technique in the pharmaceutical industry during crystallisation processes. It aims to control nucleation and enhance crystal growth by introducing either homogeneous or heterogeneous crystals into the crystallising solution. This addition facilitates the nucleation and/or growth of more crystals, making seeding a crucial step in optimising crystallisation behaviours, process efficiency, and product quality (Parambil and Heng, 2017; Zhang et al., 2021). The current seeding method involves suspending the seed in a solvent, which is then injected into the nucleation vessel. Alternatively, seed crystals can be directly added to the crystallisation process from an external source, typically obtained from milled crystals or previous batch products (Nagy et al., 2020; Brown et al., 2018; Zhang et al., 2021). Since seeding particles are typically in the range of 50 to 100 μm , they exhibit cohesive powder properties, resulting in poor flowability. In batch crystallisation, seed loading typically ranges from 0.5 to 5 wt% (Nagy et al., 2020). The accurate quantity of seeding can significantly influence the size of the product particles and, consequently, the overall product quality (Orehek et al., 2021; Parambil and Heng, 2017; Zhang et al., 2021).

The increasing demand for the production of high-potency active pharmaceutical ingredients (HPAPIs) has been notable over the past decade, particularly in preclinical or clinical trials for cancer treatment (Bormett, 2008; Sacher et al., 2021). However, due to the high toxicity of HPAPIs to patients, careful powder handling and precise powder fill become crucial. Controlling the amount of HPAPIs is of utmost importance (Chamberlain et al., 2022; O Oyewumi, 2015; Sacher et al., 2021, 2020). HPAPIs often exhibit high cohesion and poor flowability, posing challenges in their handling and processing (Jones-Salkey et al., 2023; Sacher et al., 2021).

These industrial challenges emphasise the need for an accurate, consistent and continuous powder feeder to handle cohesive materials in small quantities. However, only a few

commercial feeders have successfully been deployed, such as micro-feeding via an auger method (Coperion, 2013; Amouzegar et al., 2000), vibratory channels (Tardos and Lu, 1996), micro-dosing (MG2, 2023; Besenhard et al., 2016), a pneumatic method (DEC Group, 2023; Bellon et al., 2013) or a rotor vane feeder (LCI Corporation, 2020). However, only a few commercial feeders (details of commercially available feeders are discussed in Section 2.6.7) can continuously feed the powder material at very low flow rates (<50 g/h) and these feeder are also challenged when handling the cohesive or non-flowing materials (Nowak, 2015; Kruisz et al., 2021; Jones-Salkey et al., 2023; Kerins et al., 2023).

In light of the demand for a highly consistent and continuous powder micro-feeder in the pharmaceutical industry, this research aims to develop a novel micro-feeder. The goal is to enable the continuous delivery of solid pharmaceutical cohesive materials with an accurate mass flow of below 10 g/h and a variation of under $\pm 5\%$ (CMAC, 2019; Enabling Technologies Consortium, 2020).

1.2 Research objectives

The primary objective of this research is to advance the knowledge on powder feeding in the pharmaceutical process by developing a new micro-feeder system that is characterised by high accuracy and reliability. The proposed work involves the design, fabrication, and systematic analysis of the micro-feeder, with the aim of achieving a target flow rate for feeding/dosing micrograms of powder (≤ 10 g/h) while minimising mass flow rate variation to less than 5%. The specific objectives are outlined as follows:

1. Develop, fabricate and demonstrate a new continuous micro-feeder designed to accurately feed small quantities of cohesive materials.
2. Examine the fundamental behaviours of the feeder to elucidate its core operating principles.
3. Investigate how design and processing parameters influence the performance of the feeder.
4. Establish the essential relationships needed to formulate operational guidelines for the feeder.

1.3 Research structure

To accomplish this research objective, a systematic approach was followed, comprising the following steps:

- Introducing the main objectives of this research including motivation and the thesis structure (Chapter 1).

- Conducting a comprehensive literature review of existing micro-feeder systems and summarising the current state of the art. This involves a thorough analysis of relevant literature to identify existing technologies, their advantages, limitations, and gaps in knowledge (Chapter 2).
- Elaborating on material selection and characterisation method (Chapter 3)
- Defining the key terms employed in this thesis (Chapter 4)
- Developing a concept of a novel batch micro-feeder system that is capable of providing a low feed rate with high accuracy and minimal fluctuations. This involves the design and fabrication of the micro-feeder, taking into consideration the characteristics of the pharmaceutical materials and the desired flow rate and accuracy (Chapter 5).
- Studying the influence of process parameters on the performance of the developed batch micro-feeder system. This involves conducting experimental investigations to understand how different process parameters, such as powder properties, feeder settings, and environmental conditions, affect the performance of the micro-feeder (Chapters 5 and 6).
- Developing a concept of a novel continuous micro-feeder which can consistently feed pharmaceutical powders. This involves the design and fabrication of the micro-feeder, and the study of the effect of process parameters on its performance (Chapter 7).
- Optimising the continuous micro-feeder system based on the findings from the experimental investigations. This involves refining the design and settings of the continuous micro-feeder to achieve the desired flow rate, accuracy, and minimal mass flow rate variation (Chapter 8).
- Summarising the conclusion and future work (Chapter 9).

The dissemination of the research findings through reputable academic journals will aim to enrich the existing body of knowledge in this field, fostering further understanding and application of micro-feeder systems in pharmaceutical manufacturing. Through the implementation of the proposed systematic approach, it is hoped that this research will make a meaningful contribution to the advancement of micro-feeder technology in the pharmaceutical industry, with the potential to enhance the efficiency and accuracy of powder-feeding processes.

2 Literature review

This chapter provides an extensive overview of micro-feeders in the pharmaceutical industry. It outlines the importance of feeders in the economics and regulatory requirement, the application of powder feeders, and current research.

2.1 Microfeeder requirement

2.2 Feeding economics in pharmaceuticals

The global pharmaceutical industry, with an estimated value of over \$1.4 trillion annually (Mikulic, 2022), incurs significant costs for drug manufacturing, which amounts to approximately \$150 billion, including a cost of goods ranging from 20% to 25% (Basu et al., 2008). In an effort to reduce manufacturing costs, minimise waste, and enhance efficiency in drug manufacturing, there has been a growing interest among pharmaceutical companies in adopting continuous processes for drug production (Brown et al., 2018). The shift from batch processes to continuous processes also offers advantages such as reduced development costs for new medicines and increased flexibility in producing smaller quantities of drug products for small patient populations (Burcham et al., 2018).

According to Evaluate Ltd. (2022) report, global pharmaceutical companies are projected to increase their spending on research and development (R&D) at a compound annual growth rate (CAGR) of 2.6% from 2021 to 2028. These companies are actively investing in improving their R&D efficiencies to reduce overall R&D costs. Azzaro-Pantel (2018) estimates that the pharmaceutical industry spends approximately \$2-3 billion per new drug. However, Evaluate Ltd. (2022) report also reports a decrease in the number of new drugs approved by the US Food and Drug Administration (FDA), with only 60 new drugs receiving FDA approval in 2021. Furthermore, Azzaro-Pantel (2018) indicates that the average drug development lifecycle, from discovery to marketing, spans approximately 10-18 years. These findings highlight the pressing need for enhancing the efficiency of new drug development.

DiMasi (2002) asserts that a reduction of 25% in the duration of various drug development phases could result in cost savings of up to 16% per drug, while a 50% reduction in time could lower costs by 29%. In pursuit of these goals, pharmaceutical scientists are exploring the use of micro-factories and continuous processes to expedite drug product development and manufacturing, which could potentially reduce R&D costs and industry failure rates. Accurate powder feeding plays a crucial role in enabling micro-factories and continuous processes (Byrn et al., 2015). As such, researchers are actively working on developing reliable and highly accurate micro-feeders for pharmaceutical applications.

The emergence of Industry 5.0, characterised by its focus on environmentally conscious, sustainable, human-centric, and resilient industries (Adel, 2022; Chourasia et al., 2023; Haleem and Javaid, 2019), has further emphasised the importance of precision and personalised medicine in the field of drug discovery and development. Precision and personalised medicine, particularly in the context of cancer treatment, has become a significant focus for global pharmaceutical companies (Evaluate Ltd., 2022). The principles of Industry 5.0, which prioritise personalised products, hold the potential to accelerate drug manufacturing efficiency, reduce waste in manufacturing processes, and make medicines more affordable and accessible to the public. The impact of the ongoing Covid-19 pandemic has also underscored the importance of expediting drug development and manufacturing processes to meet urgent global healthcare needs, leading to increased interest in continuous processes, including the development of reliable micro-feeders to ensure accuracy and quality in the production of drug products (Evaluate Ltd., 2022).

In addition to the broader implications for the pharmaceutical industry, micro-feeders hold particular relevance for three key service segments within the global pharmaceutical contract development and manufacturing organisations' (CDMOs) value chain.

- Small-scale clinical trial material (CTM) manufacturing involves the production of new chemical entities for early and late-phase clinical studies. The process development and manufacture to supply materials for clinical testing is costly, accounting for nearly 20% of the total R&D cost per successful drug (Farid et al., 2020). The global clinical trials market, valued at \$49.8 billion in 2022 (GVR, 2023), is also experiencing significant growth, with the UK ranking third globally for Phase I trials (APBI, 2019) and facing increasing competition from the Asia/Pacific region. The sub-segment of global clinical trial supply & logistics, valued at \$3.1 billion in 2020, is growing at a compound annual growth rate (CAGR) of 7.5% (GVR, 2023). This growth emphasises the urgent need for cost-effective technologies capable of supplying small batches for hundreds of patients.
- High-potency API (HPAPI) manufacturing involves the production of active pharmaceutical ingredients that elicit a biological response at very low doses. The high-potency product market, valued at \$30 billion, is projected to grow by 8.7% from 2020 to 2025. HPAPIs represent approximately 15% of all molecules in clinical research (Market Data Forecast, 2023).
- Personalised medicine manufacturing involves the production of on-demand medicine for small patient populations at sustainable costs. The personalised medicine market was valued at \$1.9 trillion in 2020 and is estimated to grow by 11.6% over the next 10 years (GLOBE NEWSWIRE, 2022).

These segments represent concrete use cases for micro-feeders, offering exciting opportunities for commercialisation and long-term impact in the pharmaceutical and healthcare industries. Specifically, micro-feeders can accelerate the shift towards agile medicines supply for varying patient demands, enable more sustainable drug product manufacture through reduced waste, footprint, and greater efficiency, boost the UK's CDMO competitiveness with cost-effective CTM/HPAPI manufacture, and result in cost savings for patients. Furthermore, micro-feeders can enable patient-centric healthcare, facilitating groundbreaking targeted therapies such as Zykadia® (Novartis, 2023) for specific lung cancers.

2.3 Regulatory requirement

In the food industry, the issue of overpacking or giving away excess product is often encountered in the packing of instant soup packets, as the weight of the powder cannot be precisely controlled (David J Smith, 2020). However, this practice results in increased operational costs and poor quality control. Unlike the food industry, the pharmaceutical industry faces strict limitations on overdosing, as it can lead to increased costs and potential side effects, while underdosing can compromise the effectiveness of treatment (Augsburger and Hoag, 2008).

To ensure accurate dosing, the packing of pharmaceutical products must adhere to regulations such as the European Pharmacopoeia, United States Pharmacopoeia (USP), and Japanese Pharmacopoeia, which dictate that dosage units must consistently fall within an acceptable range of the label claim. For instance, the USP<905> defines the uniformity of dosage as the degree of consistency in the amount of the drug substance among dosage units (U.S. Pharmacopoeial Convention, 2011). The US FDA also regulates content uniformity testing for pharmaceutical and medical items in accordance with the USP 788 guidelines (FDA USP 788, 2009). However, in 2013, the FDA withdrew its draft guidance on blend uniformity and weight uniformity due to concerns about its effectiveness, resulting in ongoing discussions on appropriate sampling methods (Nagy et al., 2020).

2.4 Definition of micro-feeder

In medicine manufacturing, the primary purpose is feed rate control to achieve consistently accurate proportioning of recipe components (API and excipients) for further downstream processing, e.g. tableting or capsule filling (Augsburger and Hoag, 2008; Hickey, 2001; Nagy et al., 2020). The feeder is required to produce a precise and controllable feed rate for the individual manufacturing steps. In the pharmaceutical industry, feeders can also operate in concert, and multiple feeders automatically adjust their respective feed rates to maintain the desired recipe proportions.

A micro-feeder is a module designed for a high-precision mass flow rate of ingredients such as APIs or excipients. Besenhard *et al.* (2017) defined a micro-feeder as being able to feed powder continuously below 360 g/h. Byrn *et al.* (2015) indicate that 48 g/h or less is required for precise and continuous drug manufacturing. Precision and personalised medicine are being pursued, and advanced accuracy and consistent micro-feeding at a low mass flow rate are required (Wang *et al.*, 2018b).

The Enabling Technologies Consortium (ETC™) is a platform where pharmaceutical and biotechnology companies discuss ideas, share information, and collaborate on the development of new enabling technologies. It highlights the need for a micro-feeder with specific requirements, including accurately feeding cohesive or poor-flowing materials with low mass flows (<10 g/h), such as magnesium stearate, sodium stearyl fumarate and silicon dioxide with the powder flow rate variation at <3% (Enabling Technologies Consortium, 2020).

2.5 Micro-feeders in the pharmaceutical manufacturing process

Solid dosage forms are the most popular final products in drug manufacturing (Hickey, 2001; Zhong *et al.*, 2018). More than 80% of medicines are in the form of solid dosages, such as tablets, capsules, powder, and sachets (Couillaud *et al.*, 2019). Generally, the pharmaceutical manufacturing process can be divided into two major stages: primary processing and secondary processing. The primary processing is a series of processes in the manufacturing of drug substances, e.g. API or excipient. For example, chemical synthesis or crystallisation are unit operations in primary processing. The secondary processing is the steps of conversion of the drug substances into products suitable for administration. For example, the secondary manufacturing for tablets consists of at least three unit operations: feeding, blending and compression. The manufacture of solid oral dosage forms begins with a feeding step and finishes with tableting or filling powder into a capsule (Burcham *et al.*, 2018; Yoon *et al.*, 2018). The feeding step can also include several different feeders, respectively, for API and excipients, where the accuracy of each feeder heavily influences the final product quality. Figure 2-1 shows a generic pharmaceutical manufacturing process. It also shows where the feeders (in green) play their roles in the manufacturing process.

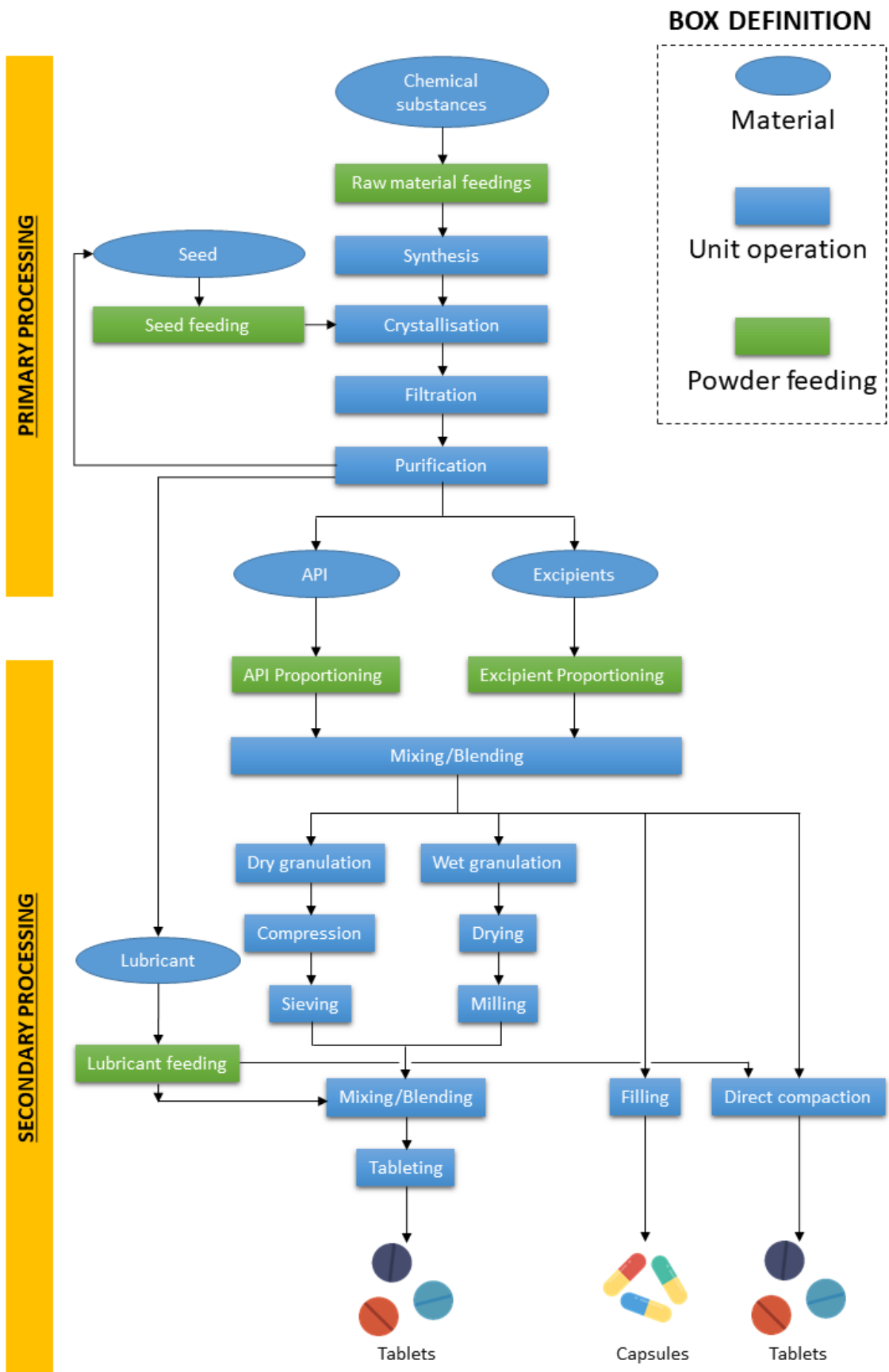


Figure 2-1: Schematic diagram of generic pharmaceutical manufacturing processes where feeders are involved. The green boxes show where feeders are applied in the process—adapted from (K-Tron International, 2009; Yoon et al., 2018).

2.5.1 Feeding in primary processing

As shown in Figure 2-1, a feeder is used for an initial step to feed the raw material (liquid and solid) to the process. It is also one of the vital operation units in the crystallisation process (Ramachandran et al., 2017). It is utilised to consistently feed the raw material or nuclei to the API production reactor or crystalliser. Crystal seeding is one of the crystallisation methods in the pharmaceutical process. It is the process of adding homogeneous or heterogeneous crystals to a crystallising solution to nucleate and grow more crystals. Seeding has emerged as one of the most critical steps in the crystallisation process optimisation. Seeding is a technique employed in large-scale operations to establish optimal conditions for crystal growth. The utilisation of seeding enables the mitigation of the difficulties associated with the control of nucleation (Besenhard et al., 2015; Nagy and Braatz, 2012). The mass and seed surface area are the main factors in the performance of the crystallisation process. The seed loading/feeding influences the kinetics of crystal growth and, thereby, product quality. Thus, accurate and consistent seed loading/feeding becomes a critical operation during crystallisation. In recent years, the development of continuous crystallisers has gained interest in order to provide an efficient and high throughput process (Brown et al., 2018). This requires accurate control of feeders to provide a precise mass of seeding per unit time into the reactor/crystalliser (Ramachandran et al., 2017). For these reasons discussed above, a feeder with a precise control feed rate is highly demanded in the development of the crystallisation process.

2.5.2 Feeding in secondary processing

In secondary processes, the materials fed in this stage usually are solid-state. Secondary processes are a series of processes to further modify the output (products) of primary processes in order to enhance the drug's properties. The powder feeders are highly applied in secondary processing, and their accuracy influences product quality and manufacturing cost. Four main processes - dry granulation, wet granulation, direct dosing, and direct compaction - are usually used for drug manufacturing.

Granulation is a size enlargement process utilised predominantly for the preparation of powders intended for tableting. In the realm of solid dosage forms, two principal granulation methods exist: dry granulation and wet granulation (Clayton, 2019). Dry granulation is a technique employed to create granules devoid of the incorporation of any liquid, whereas wet granulation involves the use of a binding liquid such as water or ethanol to facilitate the formation of granules. Among the two granulation methods, wet granulation is commonly employed as a preparatory technique to enhance the flowability, homogeneity, and compressibility of the powder mixture before its conversion into tablet form. However, granulation requires a blend of the drug substance and excipients in their required proportions.

In the blending stage, the accuracy and uniformity of the feed affect the quality of the blending, which indirectly affects the product quality during the granulation process. Dhenge *et al.* (2011) demonstrate that the powder feed rate has a significant influence on the particle properties of the transition and final states.

In recent years, the economic, technical and regulatory challenges associated with current drug manufacturing methods have prompted the industry to invest in more efficient and reliable product manufacturing technologies to help shorten development time, save costs and improve drug quality (Moghtadernejad *et al.*, 2018). Direct dosing and direct compaction are the techniques which are anticipated to achieve this target. Direct compaction is a technique to manufacture tablets by directly compacting powder blends of API with the excipients (Figure 2-1). Direct dosing is a technique of directly feeding API or a blend in a capsule (Stranzinger, 2018). Both techniques are the most straightforward and economical drug product processes (Engisch and Muzzio, 2014; Van Snick *et al.*, 2017). The challenge for both techniques is that they require high-performance feeders that can feed a small quantity of solids accurately and uniformly.

2.6 Common feeders in pharmaceutical application

2.6.1 Volumetric and gravimetric feeders

In general, powder feeders are divided into volumetric and gravimetric feeders. Both types of feeders are widely used for many bulk solid manufacturing processes. The choice of feeder type depends on the nature of the material and process. Both are available in many techniques, from the rotary valve, screw feeder, vibratory feeders to venturi feeders (Nagy *et al.*, 2020).

Volumetric feeders, as depicted in Figure 2-2a, are characterised as open-loop feeders dependent on a constant supply of material from a storage bin with a uniform bulk density to operate effectively. Volumetric feeders refer to the mechanism of dispensing a specified volume of material at a predetermined rate for a specific duration. The feed rate, expressed in grams per hour, is determined by multiplying the desired volumetric feed rate, typically denoted in litres per hour, by the bulk density of the material, measured in grams per litre. They are often deployed where the feed accuracy is not critical. The feed rate of a volumetric feeder is dictated by material properties such as bulk density and flowability. Therefore, a volumetric feeder is not suitable for applications that handle adhesive or cohesive powder. Such open-loop feeders do not use a monitoring and feedback system. Therefore, it cannot automatically compensate for any fluctuations that eventually affect product quality. In addition, a volumetric feeder requires regular manual recalibration.

In contrast, a gravimetric feeder (Figure 2-2b) is a closed-loop control feeder system that self-calibrates the flow rate and minimises variations based on bulk density. A gravimetric feeder generally consists of a volumetric feeder, a weighing platform and a gravimetric controller. Its self-adjusting ability provides good control over the product quality and reduces the waste of materials. Gravimetric feeders are usually used in handling materials whose physical characteristics vary. The Loss-in-Weight (LIW) feeder is one of the most common types in the pharmaceutical industry (Nowak, 2015). The LIW feeder is generally mounted on a load cell, which measures the reduced weight over time. The motor speed is transmitted to a multiplier to control the mass flow rate. The multiplier compares the reading with the setpoint and calculates a discrepancy to adjust the motor speed. However, vibrations and other disturbances can affect the accuracy of the gravimetric feeder. Second, a real-time control loop remains a challenge for gravimetric feeder design (Nowak, 2016).

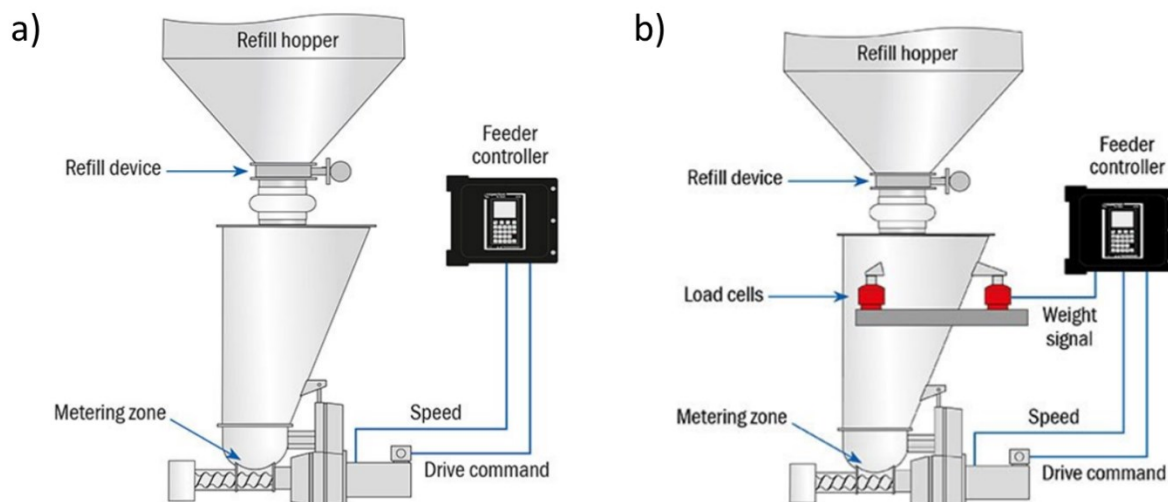


Figure 2-2: Coperion K-Tron feeder examples (a) volumetric feeder vs (b) gravimetric feeder (K-Tron Technologies Inc, 2012).

2.6.2 Screw feeder

A screw feeder is a type of positive displacement device that utilises a helical screw to transfer material. It is composed of a hopper and a helical screw (McGlinchey, 2009; Nagy et al., 2020). The flow rate is regulated by the motor speed, and a basic form of screw feeding is illustrated in Figure 2-3. The screw feeder has the advantage of providing an almost linear relationship between screw speed and discharge rate. For easy-flowing materials, a single screw is suitable, while cohesive or non-flowing materials are typically fed using a twin screw feeder. Both single and twin screw feeders can be configured as volumetric or gravimetric devices. By modifying the screw pitch, they can also be used for high-pressure duties. The screw feeder's operational capacity is typically restricted to negative-pressure environments due to the influence of differential pressure on the discharge rate (Mills, 2016a).

When handling cohesive or non-flowing materials, a screw feeder is usually integrated with a flexible wall hopper (Wagner et al., 2014). The flexible wall hopper is constructed from a rubbery material and equipped with external paddles that massage the wall; alternatively, an internal agitator may be installed in the hopper that rotates either vertically or horizontally to promote material flow. Both these devices are used to prevent the formation of bridges or ratholes in cohesive or non-flowing materials.

Despite its widespread use, the screw feeder still poses several challenges. For instance, powders may become compressed or caked during feeding through the screw, which is more apparent in twin-screw feeders (Blackshields and Crean, 2018). Other issues include the influence of refilling on the bulk density in the hopper, which can result in out-of-specification flow rates (De Souter et al., 2023; Engisch and Muzzio, 2015; Johnson et al., 2022; Peterwitz et al., 2022). Scientists are striving to enhance the screw feeder's accuracy and consistency by optimising its feedback control (Hanson, 2018; Johnson et al., 2022) and screw design (Fernandez et al., 2011; Li et al., 2020; Minglani et al., 2020).

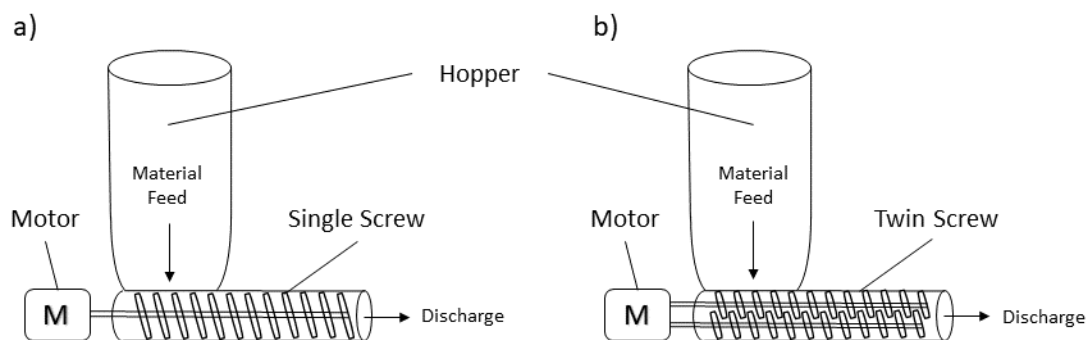


Figure 2-3: Schematics of screw feeders: (a) single screw feeder and (b) twin screw feeder.

2.6.3 Vibratory tray feeder

Vibratory feeders are widely applied in various industries, such as pharmaceuticals, food processing, mining, and chemicals (Chandravanshi and Mukhopadhyay, 2017). Vibrating feeders are often chosen when handling fine powder or granular materials or where moving parts such as screws can damage the granules (Yang and Evans, 2007). A vibratory feeder commonly consists of a hopper, a vibratory drive unit that could be piezoelectric, electromagnetic, or pneumatic motors, and a transporting trough.

The operational principle of the vibratory feeder is based on the principles of vibration and gravity. The powder or granular material moves in a series of small hops as the feed tray vibrates, resulting in continuous motion. The vibration frequency determines the flow rate. The vibratory feeder can be categorised based on the drive unit of applying vibration to the trough. There are three common types of vibrating techniques:

Electromagnetic vibratory feeders generate vibration through the back-and-forth motion of alternating electrical current in the coil (Figure 2-4). When the current flows in a specific direction, the coil attracts the magnet and generates tension in the springs. The magnet is then released as the current changes direction, and the stored potential energy in the springs propels the tray forward. By repeating this process at a high frequency, a continuous flow of powder feeding is achieved (Aleksandar I. Ribić & Željko V. Despotović, 2010; Vujović and Despotović, 2015).

Electromechanical vibratory feeders, also known as eccentric-mass mechanical feeders, use electric motors to rotate eccentric weights to generate vibration. Although a single rotating eccentric mass is a simple design, it is more common to use two counter-rotating masses whose axes of rotation lie in the same plane and rotate in synchronisation to produce the required oscillation (Chandravanshi and Mukhopadhyay, 2015; Singh and Chandravanshi, 2022).

Hydraulic and pneumatic vibratory feeders use pneumatic or hydraulic oscillating pistons to actuate the transporting through, offering the significant advantage of being suitable for use in hazardous areas. The motors that drive the pumping units can be placed in non-hazardous areas, negating the need for costly explosion-proof specifications (Mišljen et al., 2015).

A significant advantage of vibratory feeders is their lack of moving parts, such as screws, that could cause damage to the feed material (Wagner et al., 2014). Moreover, these feeders are capable of handling a broader range of flow rates than other feeders. However, the control of vibratory feeders is limited, and they are incapable of providing a linear feed rate. Additionally, the vibration of the feeder may cause material segregation (McGlinchey, 2009). The handling of cohesive or non-flowing materials is also a challenge for this technology, and it has poor repeatability. These issues must be addressed when considering the application of vibratory feeders. Therefore, numerous studies have been conducted to optimise the vibratory feeder's operation and address these challenges. Section 2.7.2 will discuss the relevant literature on this topic.

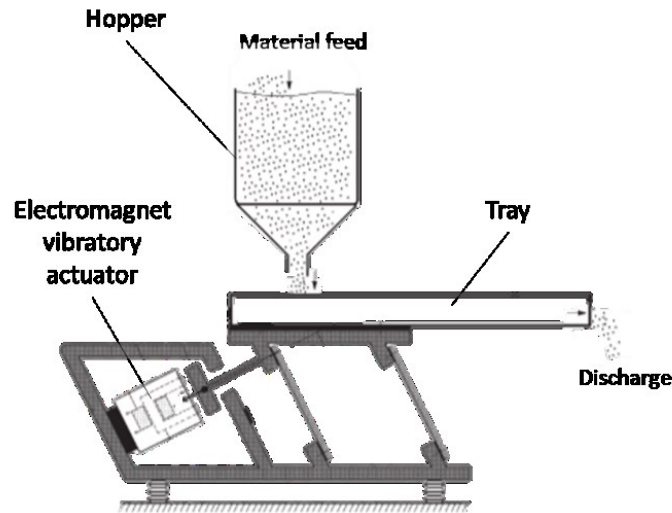


Figure 2-4: Typical construction of a vibratory feeder with an electromagnetic drive (Aleksandar I. Ribić & Željko V. Despotović, 2010).

2.6.4 Weigh-belt feeder

The weigh-belt feeder has found wide-ranging applications in diverse industries such as mineral, chemical, food, and pharmaceuticals (Cunningham et al., 2010; Mahajan et al., 2018). It is composed of a moving conveyor belt and a shear gate with a weighed section that facilitates a continuous supply of powdered material. The conveyor belt transports the material, while the shear gate ensures homogenisation of the powder profile, and the weighing section provides an accurate measurement of the feed weight. Regulating the belt speed enables the maintenance of the desired feed rate (Messmer, 2013; Wagner et al., 2014). Figure 2-5 illustrates the schematic of a weigh-belt feeder. This feeder is cost-effective, capable of handling a broad range of feed rates, and easy to maintain and clean (Wagner et al., 2014). Nevertheless, belt wearing or tearing can compromise the containment of the powdered material. Moreover, the accumulation of cohesive or adhesive materials on the belt restricts the use of weigh-belt feeder in applications that require high levels of accuracy and consistency (Mahajan et al., 2018, 2016; Zhao and Collins, 2003). To overcome these challenges, measures such as anti-static Teflon coating, a more polished surface, or a self-cleaning system may be employed. However, such measures entail increased investment and maintenance costs.

Overall, the weigh-belt feeder remains a critical piece of equipment in many industries, and ongoing research and development will likely continue to enhance its capabilities and overcome its limitations.

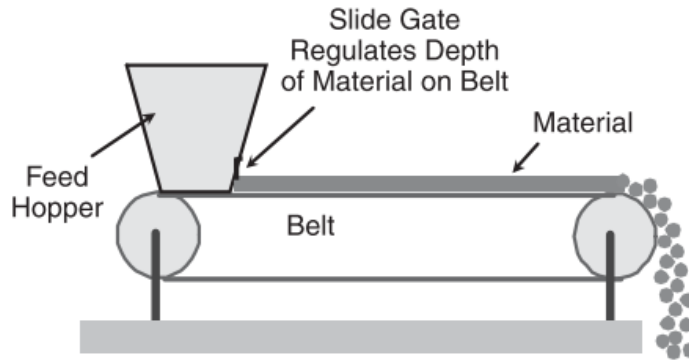


Figure 2-5: Schematic of a weigh-belt feeder (Wagner et al., 2014)

2.6.5 Rotary valve

Rotary valves have become a popular choice for powder flow rate control in solids handling processes due to their numerous advantages. The simplicity of their operation, easy adjustability, and broader range flow rate control make them ideal for use in various industries, including chemical, food, and pharmaceutical sectors (de Vasconcelos and Amarante Mesquit, 2011; Francis et al., 2006; Mills, 2016a; Moghtadernejad et al., 2018; Molerus, 1996).

The rotary valve is composed of two primary components: the rotor and the housing. The inlet port continuously fills with material, which is then transferred by the motor-driven rotor to the outlet port. The compact mechanical device operates under gravity flow, discharging and charging bulk powders. Its operation is controlled by adjusting the speed of the rotor, thereby regulating the powder flow rate. The design of rotary valves varies depending on the specific process requirements. There are numerous types and configurations of rotors available on the market (Gericke, 2023; Rotolok UK, 2023). Figure 2-6 shows an example of a typical rotary valve feeder and various rotor types and configurations.

The flowability of the material under gravity flow plays a critical role in the performance of the rotary valve. The device is susceptible to material properties, such as particle size and cohesion, which influence the flowability of the material. These lead to issues such as bridging and rathole. Therefore, the rotary valve is typically only used in feeding easy-flowing materials.

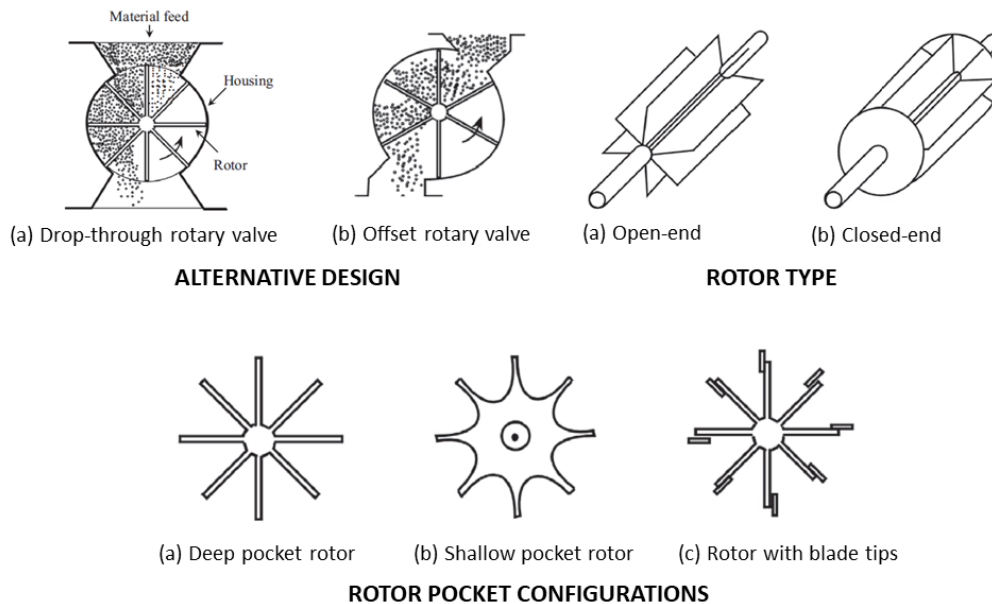


Figure 2-6: Schematic of a typical rotary valve feeder and common rotor geometries (Mills, 2016a)

2.6.6 Venturi feeder

The venturi feeder is a type of feeder that utilises the venturi effect to facilitate the transfer of powder (McGlinchey, 2009; Mills, 2016a). In this system, the material is conveyed from a hopper to a region where the cross-sectional area of the pipeline is reduced. The reduction in the cross-sectional area results in a pressure drop in the region, as per Bernoulli's principle. Consequently, the solid material is conveyed by the flow of air. The powder flow rate in the venturi feeder can be regulated by modulating the air flow rate. Figure 2-7 displays the fundamental configuration of the venturi feeder.

One significant advantage of venturi feeders is their simplicity. Unlike other feeding systems, such as screw or belt feeders, venturi feeders have no moving parts, which minimises the risk of mechanical failure and reduces maintenance costs. Additionally, their compact design means that they require less space and can be easily integrated into existing production lines, making them a cost-effective solution for many businesses.

However, the feed rate range may be limited due to the fixed design. The wear and particle degradation issues associated with venturi feeders can also be significant concerns in some applications. The high air velocity used to transport the powder can cause abrasive wear on the feeder, particularly on the throat and converging section. Additionally, the effect of the particles against the walls of the feeder can cause degradation, resulting in changes in particle size and shape that can affect the flow rate and consistency of the material.

Despite these challenges, venturi feeders remain a popular choice for many industries due to their cost-effectiveness, versatility, and ease of use. Advances in materials science and engineering may also help to address some of the wear and degradation issues associated

with this feeding system, making it an even more attractive option for businesses seeking efficient and reliable powder transfer solutions.

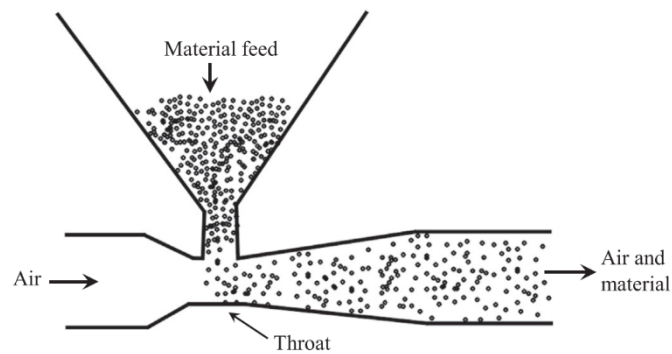


Figure 2-7: Basic type of venturi feeder (Mills, 2016a)

2.6.7 Commercially available micro-feeders

Table 2-1 provides an overview of different powder feeding and dosing systems and their specifications. The featured models, such as K-Tron MT-12, MG2 Microdose, Fill2weight_VF1, MD-120 and μ PTS, employ various operational principles like loss-in-weight systems, gravimetric vibratory feeding, loss-in-weight systems, piezo vibration feeding, rotating vane feeding, and pressure transfer system feeding, respectively. The feed capacities range from grams per hour to grams per minute, accommodating different production scales. These systems handle particle sizes spanning from micrometres to millimetres and cater to a broad spectrum of bulk density. Manufactured by industry leaders like Coperion, MG2, 3P Innovation, LCI and DEC group, these feeders find applications in processes such as tablet pressing, capsule filling, granulation, coating, mixing, blending, compounding, powder filling, inhalation, formulation, and API processing. The references provide links to manufacturers' websites for in-depth information, case studies, and resources related to each powder feeder model.

Table 2-1: Commercially available micro-feeder.

Model	Operation Principle	Mass flow rate (g/h)	Powder Properties	Application	Reference
K-Tron MT-12 & MT-20	Employing a tandem auger screw system to facilitate the seamless conveyance of material from a hopper, ultimately discharging it through the outlet.	32 - 3540	Semolina, Bulk density 0.783 kg/dm ³ MgSt, Bulk density 0.14 kg/dm ³ XPVP, Bulk density 0.33 kg/dm ³	Jet mill, continuous extrusion, continuous feeding	(Coperion, 2013), (Engisch and Muzzio, 2014), (Blackshields and Crean, 2018), (Sacher et al., 2021)
Apparatus for controlled delivery of powdered solid materials (US patent)	The use of an inclined auger screw to introduce powder into an air chamber, facilitating the generation of dry powder aerosols.	0.2-5 (20% to 30% variation)	particle size less than about 10 µm.	Dry powder aerosol generators for toxicity testing in pharmaceuticals	(Amouzegar et al., 2000)
MG2 Microdose	Employing the vibratory sieve for material transfer involves utilising the sieve's vibrating mechanism to facilitate the movement of the material.	0.36 - 0.54	90 – 160 µm, Bulk density: 0.67 - 0.74 kg/dm ³ , moderate flowing material	Continuous capsule filling	(MG2, 2023) (Besenhard et al., 2016)
3P innovation Vibratory feeder_Fill2weight_VF1	Employing piezo vibration to induce container vibration, utilising a stirrer to disrupt aggregation and promote powder movement, and employing a pin valve to regulate the flow rate.	3.6 - 1440	0.5 kg/dm ³ , moderate to free-flowing powders. magnesium stearate and paracetamol.	Continuous and on-demand filling (e.g. blenders, millers, biovessels)	(3P Innovation, 2022) (Llusa, 2014)
LCI Circle Feeder™_MD-120	Utilising a flat and rotating vane to transport the powder to the outlet hole.	>32	Micronised calcium carbonate or bulk density under 0.16 kg/dm ³	Continuous feeding in various industry	(LCI Corporation, 2020)
DEC µPTS	Employing the DEC PTS Transfer System®, where the process begins with a powder-first vacuum to transfer the material into a vessel. Subsequently, positive pressure is applied to pressurise the vessel, facilitating the discharge of the powder.	3.6-450	Very fine (<1 µm) and coarse powder, cohesive and wet material, or low MIE (<1 mJ), variations in bulk density	Filling lines or continuous processes for various industries (including reactors, dryers and centrifuges)	(DEC Group, 2023) (Bellon et al., 2013)
Vibra-flow feeder	Employing frequency control to achieve a consistent flow in the screw feeder, resulting in enhanced precision and a reduced standard deviation in the feed rate.	<3.6	Sand (1568 - 1518 kg/m ³), seed (363 kg/m ³), Fiber-glass (734 kg/m ³)	Mixing, granulation and crystallisation	(Tardos and Lu, 1996)

In addition, Table 2-2 presents information on the feeder capacity of various commercially widely used feeders from different suppliers, including Coperion, Gericke, Brabender, Retsch, Hosokawa, and FRITSCH. The data, sourced from Engisch and Muzzio (2014), Coperion (2013), Gericke (2022), and Brabender (2023a, 2023b), includes details such as supplier, model, volumetric throughput (measured in dm³/h), gravimetric throughput (in kg/h) for both low and high values, and hopper capacity (in kg).

Table 2-2: Feeder capacity of commercially commonly used feeders in literature (Engisch and Muzzio, 2014; Coperion, 2013; Gericke, 2022; and Brabender, 2023a, 2023b).

Supplier	Model	Volumetric throughput (dm ³ /h)		Gravimetric throughput (kg/h) ^a		Hopper capacity (kg) ^a
		Low	High	Low	High	
Coperion	K-Tron KT12*	0.031	5.89	0.032	3.0	1
Gericke	FEEDOS S	0.5	500	0.250	250	7.5
Brabender	FW20/0	1	75	0.500	37.5	2.5
Brabender	MiniTwin MT	1	5	0.500	2.5	0.25
Retsch	DR100/15		30		15	1.3
Hosokawa	MIKRO®	0.04	10	0.02	5	Various
FRITSCH	LABORETTE 24	0.12	180	0.06	90	0.5
	V-Channel					
Coperion	V100	1	500	0.5	250	5

*Minimum feed rate cannot be less than 32 g/h.

^aGravimetric throughput assumes a bulk density of 0.5 kg/dm³.

2.6.8 Summary

In numerous industrial processes, feeders are a critical component that significantly influences the quality of the final product (Blackshields and Crean, 2018). This is especially true in the pharmaceutical industry, where precision and accuracy are essential. With the advent of Industry 5.0, there has been a shift in focus towards personalised products (Adel, 2022; Chourasia et al., 2023; Haleem and Javaid, 2019); in pharmaceutical manufacturing, the need for precision and accuracy is paramount, and the use of micro-feeders can help to ensure that the final product meets the required standards. For example, micro-feeders can be used to precisely control the amount of highly-potent active pharmaceutical ingredients in a drug formulation, ensuring that the product is consistent and effective (M O Besenhard et al., 2015; Sacher et al., 2021). Additionally, micro-feeders can be used to create personalised formulations tailored to individual patient needs, further advancing the concept of personalised medicine.

In the preceding sections, a diverse range of commercial feeders was explored, and their operational methods, benefits, and drawbacks were evaluated. The selection of an appropriate feeder is a critical factor that varies depending on the material being fed and the process involved. Table 2-3 provides a comprehensive overview of the typical feeders employed in the pharmaceutical industry, their advantages, and the difficulties associated with their use.

Despite their usefulness, commercial feeders often fall short of meeting industrial requirements, and therefore, researchers are actively exploring the development of more advanced micro-feeders. In the following section, we will delve deeper into the current achievements in micro-feeder technology and their potential applications in the pharmaceutical industry.

Table 2-3: Current pharmaceutical powder feeders on the commercial market.

Feeder Type	Operation principle	Advantages	Limitations	Commercial examples
Single-screw feeder	Employing a motorised single screw that rotates to transport material from a hopper and release it into a production process.	<ol style="list-style-type: none"> 1. The broad range of feed screw configurations available facilitates the handling of a diverse array of materials and feed rates. 2. Flexibility in terms of customisation for installation or process requirements is a notable advantage. 	<ol style="list-style-type: none"> 1. The capability of handling a limited spectrum of materials is restricted to those that are relatively easy-flowing. 2. Adhesive and cohesive materials can accumulate within the feeder, impeding its operation. 3. Wearing of moving components is a potential concern. 4. The operational cost can be high. 	<ol style="list-style-type: none"> 1. K-Tron, KQx4 or Sxx/KSxx 2. Bradender, DSxx or DSRxxx series 3. Gericke, FEEDOS
Twin-screw feeder	Two parallelly rotating feed screws facilitate the conveyance of materials from a storage hopper and discharge them into a production line.	<ol style="list-style-type: none"> 1. It is well-suited for managing materials that are cohesive or have limited flowability. 2. It is characterised by a self-wiping action that facilitates the flow of sticky materials and minimises accumulation of materials in the discharge tube. 3. It features a linear flow rate. 	<ol style="list-style-type: none"> 1. Cleaning can be a challenging task. 2. The material may undergo compression during operation. 3. There is a risk of blockage in case of material accumulation within the discharge tube. 4. The initial investment cost and ongoing maintenance expenses can be considerable. 	<ol style="list-style-type: none"> 1. K-Tron, KT-12 – Twin auger screws 2. Brabender, DDSRxx & MiniTwin MT
Flexible wall hopper	A flexible hopper made of EPDM or other plastic materials, equipped with an agitating paddle that operates externally to massage the hopper wall. it is commonly utilised in conjunction with a single or twin screw feeder to handle materials that are either cohesive or non-flowing.	<ol style="list-style-type: none"> 1. The occurrence of bridging and ratholing can be reduced. 2. It enables the handling of diverse types of materials. 	<ol style="list-style-type: none"> 1. It is not capable of handling materials that have a tendency to pack tightly. 2. The operation cost and maintenance expenses are likely to rise. 	<ol style="list-style-type: none"> 1. Brabender, FlexWall®

Vibratory tray feeder	Material is conveyed by vibration. By adjusting the vibration amplitude and frequency, the feed rate can be controlled.	<ol style="list-style-type: none"> 1. Capable of accommodating a broader range of flow rates. 2. Characterised by a straightforward design and ease of operation. 3. The installation and maintenance costs are relatively low. 	<ol style="list-style-type: none"> 1. The feed rate is non-linear and not highly precise in replicating a given process. 2. Vibrations can cause segregation of materials. 3. Cohesive materials and fine powders tend to accumulate on the feeder tube/tray, making it unsuitable for their handling. 4. Flow rate control is suboptimal, and it is not capable of providing a linear feed rate. 5. The operation of this equipment is noisy. 	<ol style="list-style-type: none"> 1. K-Tron, K3 series 2. Brabender, DVT series 3. Gericke, GVD
Weigh-belt feeder	Employing a belt conveyor to transport the material. Load cells are integrated within the material bed to measure weight and ensure precision. A shear gate is installed to homogenise the powder profile. The belt speed is constantly regulated to maintain the desired feed rate	<ol style="list-style-type: none"> 1. Improved flexibility in handling materials. 2. Relatively simple design. 3. Easy to clean and maintain. 	<ol style="list-style-type: none"> 1. The belt's wear can pose containment challenges. 2. High flow rate variability may arise due to cohesive or adhesive materials accumulating on the belt. 3. The equipment generates dust during operation. 4. Regular maintenance is necessary to prevent belt slippage. 	<ol style="list-style-type: none"> 1. K-Tron, SWB-300 and SWB-600 2. Brabender, DBWxxx series
Rotary valve	Employing a motor-driven rotor with blades or vanes enclosed in the housing. As the rotor turns, material flows into the spaces between the blades and is discharged into the process.	<ol style="list-style-type: none"> 1. Efficient and cost-effective. 2. Occupies minimal space due to its compactness. 3. Dependable and consistent in operation. 	<ol style="list-style-type: none"> 1. Possesses high material handling capacity. 2. Abrasion may occur when material becomes trapped between the vane tip and the housing during rotation. 3. An airlock can result in significant flow rate fluctuations. 	<ol style="list-style-type: none"> 1. K-Tron, ZRD & ZXD 2. Gericke, Hypergienic rotary valve
Venturi feeder	Employing venturi effect to convey the powder flow. By changing the air flowrate to control the powder flow rate.	<ol style="list-style-type: none"> 1. No moving parts 2. Compact size with minimal space requirements. 3. Economical and affordable. 	<ol style="list-style-type: none"> 1. Potential wear and tear concerns. 2. Absence of a linear relationship between air flow and discharge flow. 3. Not suitable for regulating flow rate. 	<ol style="list-style-type: none"> 1. Fox Venturi eductors

2.7 Recent research activities in feeding technologies

While oral solid dosage medicines remain the most used medicinal forms, a consistent and continuous feed rate is regarded as one of the critical requirements of the overall process (Engisch and Muzzio, 2014). Due to industrial demand, many types of micro-feeders ranging from capillaries, vibratory sieve to screw feeding have been investigated recently to feed a small quantity of powder accurately. This section discusses the current research on screw feeders and some novel designs, such as brush screw feeders, particle feeders and powder pumps.

2.7.1 Screw feeder

The screw feeder is a highly versatile piece of equipment that's widely used in industrial settings to handle various types of bulk materials. However, despite its extensive use and development, there's still a considerable need to improve the performance of screw feeders in terms of high-precision feeding. To address this need, researchers have identified five key aspects for optimisation: hopper configuration, screw design, sensors, control strategies, and modelling and simulation.

Continuous and consistent powder feeding is required to achieve continuous drug manufacturing. However, the feed rate slowly decreases over time when the hopper fill level decreases during feeding (Blackshields and Crean, 2018; Janssen *et al.*, 2022). A periodic hopper refilling is needed, but this action can cause a disturbance of the feeding accuracy due to material density increase from compression by the refilling material. Engisch & Muzzio (2015) and De Souter *et al.* (2023) studied and suggested several methods to minimise the influence of refilling, such as maintaining an optimal range of hopper filling level, using discharge screens, and gently refilling the hopper to minimise feed rate deviations. Santos *et al.* (2018) and Beretta *et al.* (2023) also studied the influence of material properties on screw feeder performance, such as different hopper fills and screw speeds.

Similarly, optimising screw design aims to reduce compaction and influence on bulk density while selecting the appropriate screw type for various raw materials. M. Bortolamasi and J. Fottner (2001), Fernandez, Cleary & McBride (2011), Minglani *et al.* (2020) and Li *et al.* (2020) focused on the improvement of the screw design.

Developing reliable sensors for real-time monitoring of feeding has also emerged as a critical area for improvement. The incorporation of such sensors, as proposed by Singh *et al.* (2015), can significantly improve the accuracy of feeding and minimise errors. Several studies focus on developing a reliable powder mass flow sensor, such as the capacitance sensor developed by Alvarado-Hernández *et al.* (2020) and Martínez-Cartagena *et al.* (2021), and the electrical

capacitance volume tomography (ECVT) developed by Abrar *et al.* (2020) and Huang *et al.* (2021).

Control strategies are equally important for reducing variations in feeding. Studies by Kruisz *et al.* (2021) and Johnson *et al.* (2022) have explored various control strategies to minimise feeding variations. Finally, powder flow modelling and simulation can assist in predicting powder behaviour and aid in feeder design. Researchers have proposed techniques for developing accurate models of powder flow behaviour (Bekaert *et al.*, 2022; Fernandez *et al.*, 2011; Johnson *et al.*, 2022; Shier *et al.*, 2022).

In conclusion, while screw feeders have undergone significant development, there's still room for improvement in terms of precision feeding, especially in the micro-feeder development field. Ongoing optimisation efforts in hopper configuration, screw design, sensor development, control strategies, and modelling and simulation are likely to lead to improved performance and accuracy of the screw feeder in the coming years.

2.7.2 Vibratory feeder

According to Section 2.6.3, the vibratory feeder's simple design and easy operation make it a commonly used feeder in the pharmaceutical industry. However, it has some limitations that scientists are trying to overcome. For example, Singh & Chandravanshi (2022) studied the electromechanical vibratory feeder's performance by analysing the influence of different motor positions on the trough using dynamic analysis. Aleksandar I. Ribić & Željko V. Despotović (2010) improved the electromagnetic vibratory feeder by integrating the proportional integral derivative (PID) controller with a state observer to allow fast disturbance rejection and reference tracking in amplitude increase and decrease, showing promising improvements. Semenov *et al.* (2021), Kharitonov *et al.* (2022), and Bettega *et al.* (2023) used a mathematical model to predict powder behaviour in the vibratory feeder and optimise the control loop to improve its feed rate accuracy.

Other designs of vibratory feeders discussed in other literature include the pulse inertia force actuated feeder and vibratory sieve chute feeder. Wang *et al.* (2018b, 2018a) developed a pulse inertia force actuated feeder consisting of a piezoelectric transducer (PZT) stack actuator and a tapered glass capillary nozzle (Figure 2-8). The results showed that this feeder could accurately dose cohesive fine powder in a minimum mean dose of around 0.6 mg in a single pulse inertia force with below 5% variation. However, this feeder is limited to dosing and cannot be used for continuous feeding.

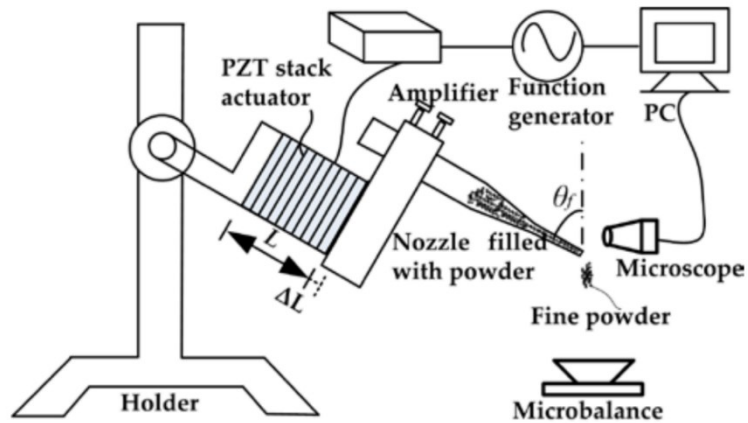


Figure 2-8: a schematic of pulse-inertia force actuated feeder.

Besenhard *et al.* (2015a, 2016) developed a vibratory sieve chut system (Figure 2-9) in which a vibratory sieve is mounted on top of a chut. The powder is discharged from the sieve to the chut and then to a catch scale, which reads and records the weight every second and transfers the data to a LabView program for data analysis. By regulating the frequencies and amplitudes, this feeder can achieve continuous feeding of pharmaceutical materials in the range of 1.5 to 100 mg/s with a variation below <1.5 mg/s. However, the powder's properties can significantly affect its feed rate consistency like other vibratory feeders, especially at high feed rates or when feeding times exceed 30 minutes. Sieving the powder is required to increase its consistency in high feed rate, making it a drawback of this system.

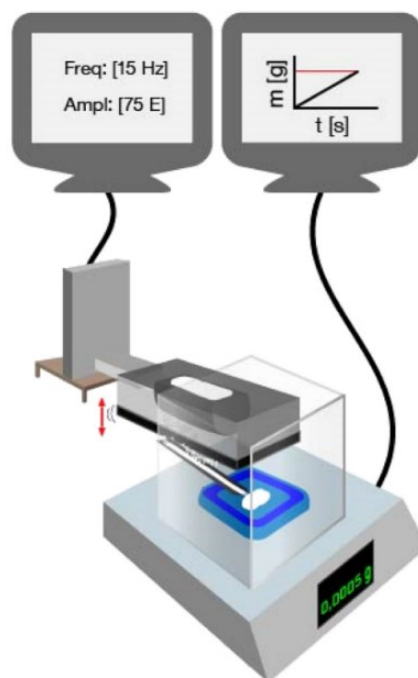


Figure 2-9: A schematic of a vibratory sieve chut system experimental set-up.

2.7.3 Screw-brush feeder

Screw feeders are a widely utilised type of powder feed system, and researchers Barati Dalenjan, Jamshidi & Ale Ebrahim (2015) developed a screw-brush feeding system by incorporating a brush conveyor following a single screw feeder (

Figure 2-10a). The brush conveyor acts as a secondary controller or stabiliser of the powder flow rate. The study demonstrates that introducing the brush section to the screw feeder led to a stabilised feeding of fine zinc oxide powder at a low flow rate of 72 – 630 g/hr. The authors also investigated the effect of air on this design (

Figure 2-10b) and examined the influence of introducing a minimum gas flow rate to the screw-brush feeder to facilitate the powder flow in order to achieve a homogeneous solid-gas flow.

The results indicated that the intervention of the gas flow rate could reduce the mean aggregate size of average particle size distribution and provide a homogenous gas-particle flow. However, this design has certain drawbacks, such as increased variation with rising flow rate, the need for consistent material properties, the potential for high shear stress that may cause particle grinding, and contamination (hygienic) concerns. Nonetheless, further study is required to evaluate its application on cohesive materials.

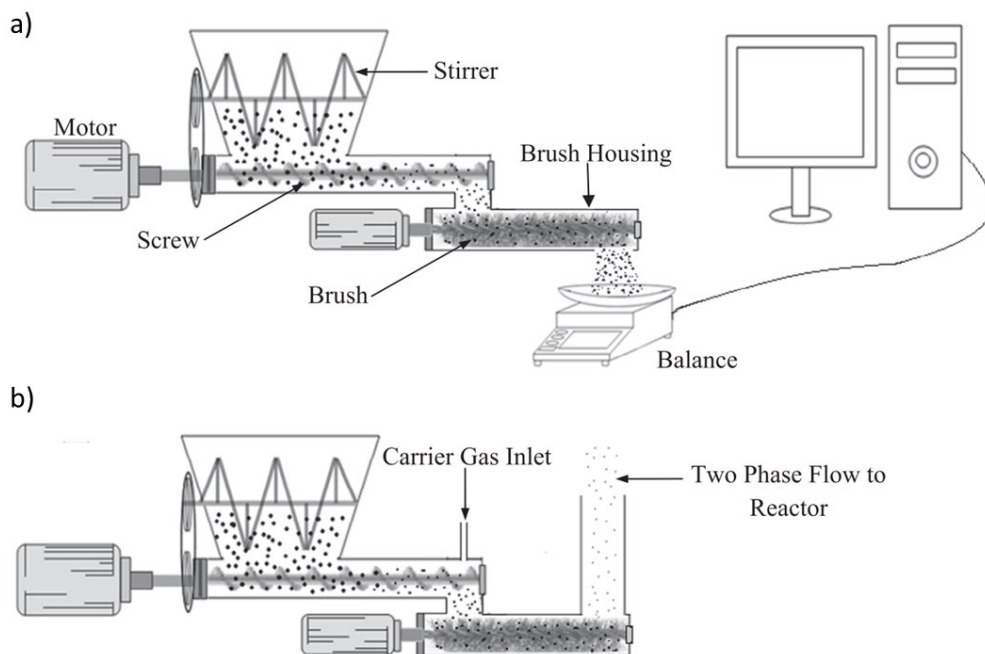


Figure 2-10: A schematic view of the screw-brush feeder: a) without gas flow, b) with the gas flow (Barati Dalenjan et al., 2015).

2.7.4 Fluidised feeder

In 1959, Wen & Simons developed a fluidised bed feeder (Figure 2-11a) utilising the principle of fluidisation to feed and fluidise powder within a bed, with efflux occurring through a tube in the bed wall. By regulating the pressure in the fluidiser and air flow rate, the powder flow rate could be controlled. Later, Annamalai *et al.* (1992) developed an off-take system (Figure 2-11b) which used compressed air to locally dilute and fluidise powder from the side wall rather than the bottom of the fluidised bed, resulting in a small locally fluidising feeder that could handle flow rates from 30 to 1800 g/h with good repeatability. This design demonstrated a counter-correction between the mass flow rate and dilute air flow rate.

Suri & Horio (2009) further improved this design by using a cartridge as the fluidised bed to fluidise powder from the cartridge bottom, which enabled the system to be a closed system. They then used secondary air to adjust the feed rate (Figure 2-11c), achieving a wide range of feed rates from 36 to 3853 g/h. This improved system eliminated the powder flow dependence on bed height. However, similar to other pneumatic feeders, it faced challenges such as segregation and solid-air separation, as well as requiring secondary air flow rate control which complicated the control.

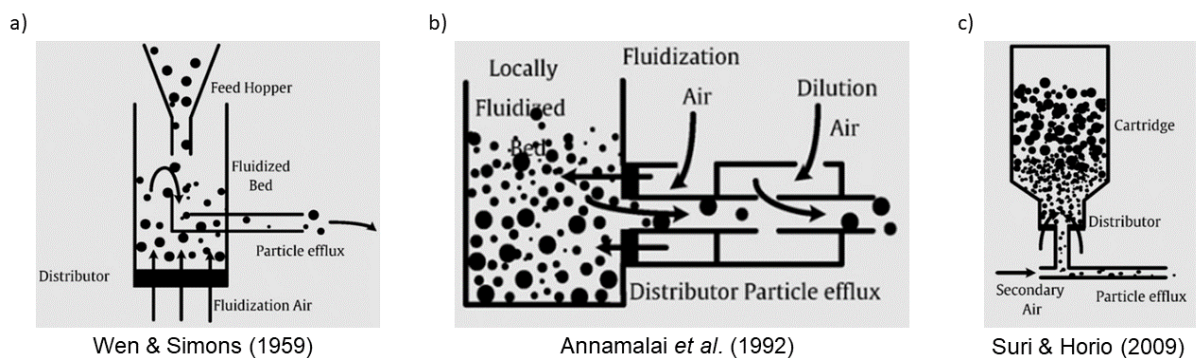


Figure 2-11: Illustration of fluidised bed feeder (Suri and Horio, 2009).

Wibberley & Phong-Anant (1986) developed a closed system with a syringe-type design that utilised a similar concept as mentioned above (Figure 2-12a). In this system, the powder was initially fed into the feed vial, which was fitted with a sintered distributor plate. A fluidised gas was introduced to fluidise the powder and prevent compaction, while a carrier gas was used to blank the powder and carry the powder. The powder was then forced out of the feed vial by pushing the vial upward, with the feed vial displacement rate controlling the powder flow rate. This system achieved between 2 and 100 g/h coal, but it was not easy to construct and operate.

Burch *et al.* (1991) optimised Wibberley & Phong-Anant's design and developed a particle feeder (Figure 2-12b), which was later modified by Tang & Chen (1999) for application on Geldard C particles, very cohesive particles with a size of 20 to 30 μm (Figure 2-12c). It utilises

controlled aerodynamic stripping of the powder surface by passing a carrier gas through a narrow gap between a cylindrical piston and the inner wall of the reservoir. The solid-gas flow then passes through a 1/8 inch stainless steel feed tube. When the reservoir is moved upward, the gas is compressed and carries the particles to the feed tube. The flow rate can be controlled by changing the gas flow and the movement of the reservoir. The principle of this method utilises Bernoulli's principle by changing the cross-sectional area to increase the gas velocity to "pick up" particles from the surface of the particle bed.

This particle feeder design demonstrated a powder flow rate ranging from 0.6 to 31.8 g/h, with short-term fluctuations up to 3% and long-term fluctuations up to 5% in feeding rates. The technique could handle particle sizes ranging from 20 to 250 μm . While this design demonstrated reasonable control of the powder flow rate, it is important to acknowledge its inherent limitations, including issues with segregation and compression resulting from air pressure. Moreover, the design is not suitable for continuous powder feeding as it lacks the capacity to refill. The control mechanism is also relatively complex, warranting further consideration.

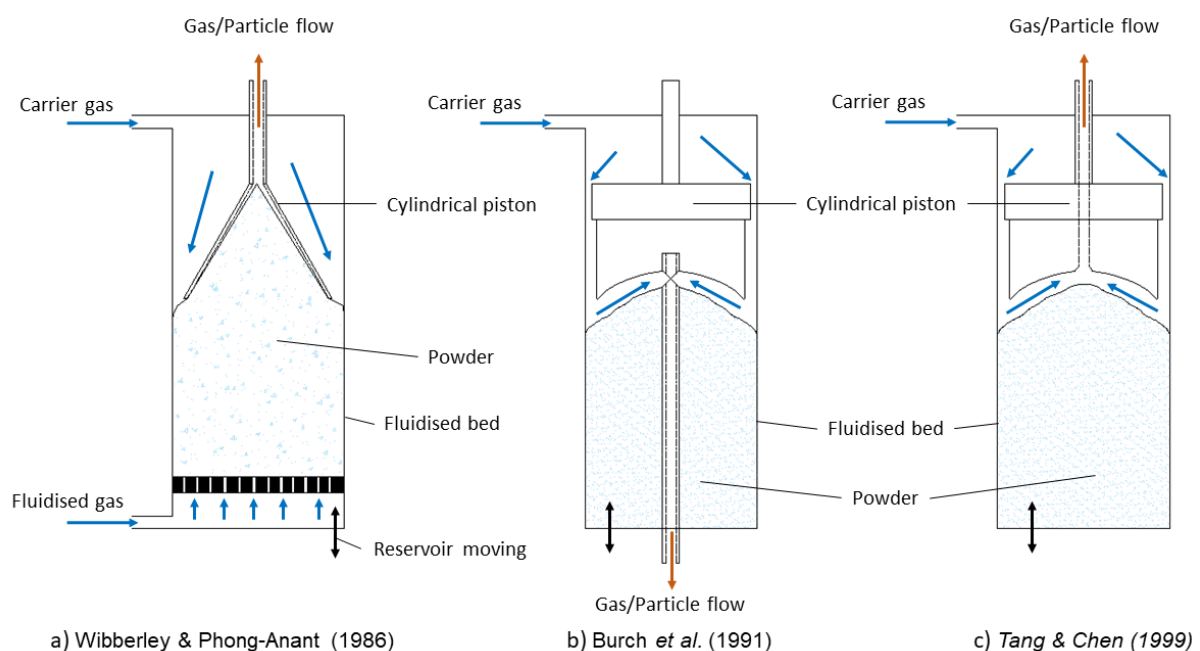


Figure 2-12: Resolution of particle feeder: a) developed by Wibberley & Phong-Anant (1986); b) developed by Burch *et al.* (1991); and c) modified by Tang & Chen (1999). The figure is adapted from (Tang and Chen, 1999).

2.7.5 Powder pump

Besenhard *et al.* (2017) developed a cylinder-piston feeder (also known as a powder pump) that offers volumetric control of the powder flow rate. The system comprises a cartridge, a motorised plunger, a scraper, and a chute, as shown in Figure 2-13. The powder is loaded into the cartridge and pushed by the motorised plunger into the top plate, where the scraper

sweeps the powder to the angled chute. The pump speed and scraper speed can be adjusted to control the powder flow rate, with the study demonstrating a powder flow rate of 5 g/h or less with reduced fluctuation. However, limitations of the design include dependence on powder compaction occurs in the cartridge section during upward plunger movement, which leads to feed rate variation and reduces repeatability. For handling a wider range of flow rates and materials, the system requires changes in piston size. Moreover, refilling and service time are limitations for continuous processing.

Fathollahi *et al.* (2020) conducted a study on density variation during processing by examining the displacement-feed factor curve for different particle sizes and flow properties, using this curve for calibration and prediction of feed rate. They also developed a two-stage feed control strategy in 2021 to minimise feed rate deviation, improve feeding accuracy and consistency, and reduce the influence of effective displacement density variation on the feed rate. Sacher *et al.* (2020) implemented the powder pump and a conventional loss-in-weight (LIW) feeder in hot-melt extrusion (HME) and evaluated their accuracy and reproducibility in high-potency active pharmaceutical ingredient (API) low feed rate performance. The powder pump dosed the API and the LIW feeder handled the polymer, with the results demonstrating good accuracy and reproducibility for short processing hours but inhomogeneous API feeding after a few hours of process time. Sacher, Fathollahi & Khinast (2021) compared the performance of the powder pump and conventional LIW feeder, finding similar performance but higher accuracy in the low feed rate for the powder pump. However, overcoming the requirement of pre-conditioning and the inability to refill make the powder pump unsuitable for continuous drug manufacturing, which is a requirement in the pharmaceutical industry.

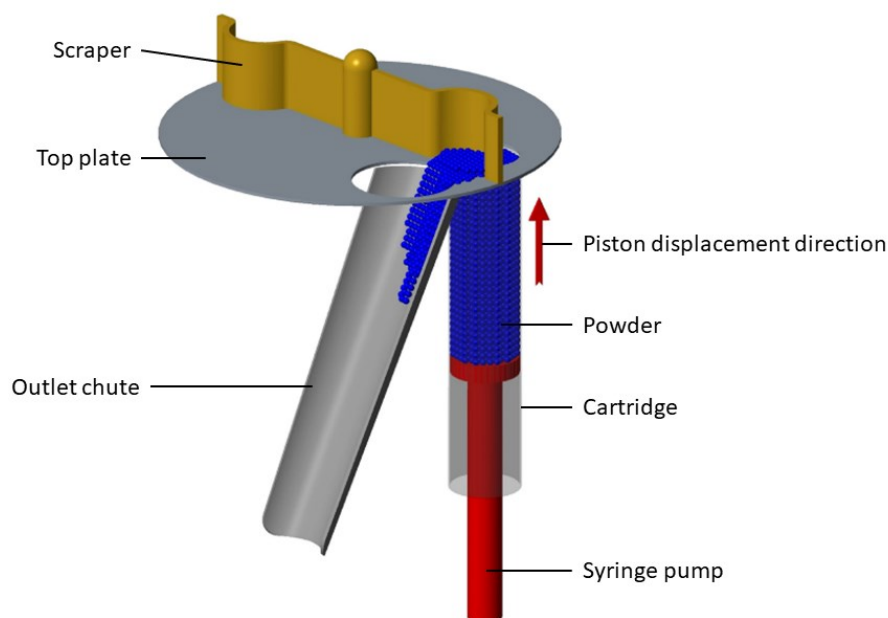


Figure 2-13: A schematic view of the powder pump setups (Besenhard *et al.*, 2017).

2.7.6 Slide feeder

In their 2004 publication, Michael Pohořelý et al. described the development of a double-acting air-driven slide feeder (Figure 2-14) that demonstrated operational reliability and reproducibility in feeding various particulate materials, including sand, γ -alumina, ceramsite, dried sewage, and shredded wood. The feeding process involves filling two containers with the powder at the outset of the experiment. Two pockets on the side plate are connected to the pneumatic transport pipe, with one pocket filling while the other dispenses the powder into the transport pipe. The powder then settles into the Tee section, where it is swept by constant pressure transport air to a collection pot and weighed. The system is capable of feeding the listed materials at rates ranging from 100 (shredded wood) to 1,800 g/h (sand), with average deviations ranging from 0.14% (for isometric and smooth particles of alumina and sand) to 15% (for fibrous dried sewage sludge and shredded wood). However, the design is unsuitable for low flow rates below 100 g/h, and further study is necessary to evaluate its feeding performance for cohesive materials. Its feed rate is not continuous but rather consists of pulse feeding. The pharmaceutical industry, in particular, may encounter segregation and solid-air separation challenges in drug manufacturing.

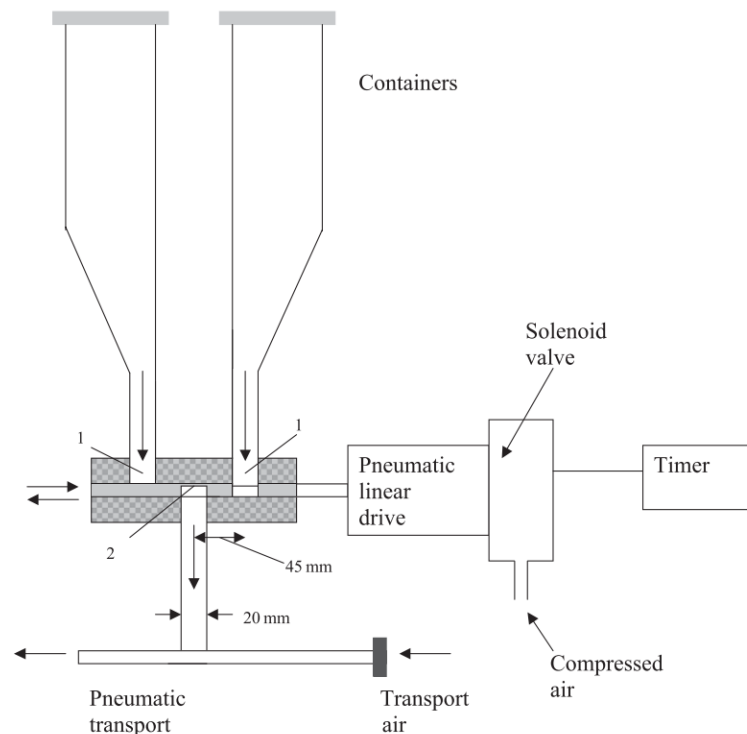


Figure 2-14: A schematic view of the double-acting slide feeder (Pohořelý et al., 2004).

2.7.7 Summary

Powder handling is a crucial aspect in a multitude of industries. In drug manufacturing, the accuracy, consistency, and continuous feeding of powder have become increasingly essential, particularly in the recent development of precision medicine and personalised medicine.

Section 2.7 provides a comprehensive overview of the current research in powder feeder development. Powder feeders generally employ one of three main feeding mechanisms: mechanical feeders, vibratory feeders, and pneumatic/fluidised feeders. Table 2-4 presents an overview of current studies investigating these novel feeder mechanisms and analysing their respective performances, advantages, and drawbacks.

The studies indicate several improvements in the design of screw feeders and vibratory feeders, including mechanism optimisation and control system development. Additionally, exciting novel feeding mechanisms, such as the powder pump, have accelerated the development of powder feeders and their application in drug manufacturing. However, developing a reliable and consistent feed rate feeder necessitates a thorough understanding of the factors that affect the design of a dependable powder feeder, from powder and material properties to process parameters and environmental conditions. Section 2.8 will delve into this topic in greater detail.

Table 2-4: Current micro-feeders and their feeding principles in the literature. Adapted from (Besenhard et al., 2016).

Publication year	Author	Investigated materials	Feed rates	Variation	Concept
Mechanical feeder					
2011	Fernandez,				Applying DEM to study flow behaviour in diverse screw designs can inform the development of an improved screw for powder feeding.
2020	Cleary & McBride,				
2020	Minglani <i>et al.</i> , Li <i>et al.</i>				
2015	Barati Dalenjan, Jamshidi & Ale Ebrahim	Zinc oxide	72 - 630 g/h	2 -14%	The screw-brush feeding system utilises a brush conveyor to stabilise the powder flow rate downstream of a single screw feeder.
2017 2020 2021	Besenhard <i>et al.</i> , Fathollahi <i>et al.</i> , Fathollahi <i>et al.</i>	α -lactose monohydrate powders, API and spray- dried intermediate	1 - 100 g/h	4 - 20%	Powder pump, a cylinder-piston feeder, loads powder into a cartridge and uses a motorised plunger and scraper to control the flow rate via adjustable speed settings.
Vibratory feeder					
2012	Chen, Seyfang & Steckel	Lactose Powder	3.6 - 36 g/h	<3%	Vibrating capillary - Through the employment of a vibrating capillary and modulation of both frequency and amplitude, the regulation of flow rate and variability was achieved.
2012 2014	Zainuddin <i>et al.</i> ; Horio, Yasuda & Matsusaka	Microcrystalline cellulose	86.4 - 306 g/h	3 - 5%	Vibration shear tube method - The study expelled powder through a narrow gap between a vibrating tube and a flat surface, subjecting each particle to high shear forces to overcome adhesion and friction. The powder flow rate was regulated by controlling the vibration amplitude.
2015 2016	Besenhard <i>et al.</i>	Inhalac 230 Respitose SV003	3.6 – 7.2 g/h	4.6 - 12%	Vibratory sieve chute system - to transfer powder from chute to receiver using vibration. The feeder achieved continuous feeding of pharmaceutical materials by regulating frequencies and amplitudes.
2018	Wang <i>et al.</i>	Respitose SV003 Granulac 230	1.4 - 1.8 g/h	<12%	The pulse inertia force was utilised to effectuate the vibration and transportation of the powder, with the flow rate of the powder being regulated by controlling the frequency of the applied force.

Pneumatic/Fluidised feeder

1986	Wibberley & Phong-Anant	Coal	2.0 - 97.2 g/h		The study employed a motorised screw jack to narrow the fluidised chamber, while carrier gas was used to fluidise the powder and prevent compaction. Top carrier gas was used to blank the gas-powder mixture.
1991	Burch <i>et al.</i>	Geldart A particles: coal and coal-derived char particles. Geldart C particles: coal-derived ashes and CaO powders	1.2 - 12 g/h	Short term: <12% Long Term: >15%	This method strips particles from the powder surface by passing a carrier gas through a narrow gap between a cylindrical piston and the reservoir wall, then carries them through a feed tube when the reservoir is elevated. The flow rate is adjustable through gas flow and reservoir motion.
1999	Tang & Chen	Geldart A particles: coal and coal-derived char particles. Geldart C particles: coal-derived ashes and CaO powders	0.6 - 31.8 g/h	Short term: <3% Long Term: >5%	Modified Burch <i>et al.</i> (1991)'s design
2004	Michael Pohořelý <i>et al</i>	Silica sand, g-alumina, ceramsite (fired claystone), digested and dried municipal sewage sludge, and shredded hard wood.	100 - 1800 g/h	0.14% - 15%	Slide feeder - filling two containers with powder and then using two pockets on the side plate to dispense and receive powder into the pneumatic transport pipe. The powder is then transported by constant pressure air.
2009	Suri & Horio	Charcoal, glass beads, Neo beads	36 - 3852 g/h		The study improved upon Wen & Simons (1959)'s work by using a cartridge as a closed fluidised bed for powder fluidisation from the bottom.

2.8 Factors affecting feeder performance

In the micro-feeder design, there are a number of factors that can affect feeder performance. This section discusses these factors encountered in the design of the micro feeder. These factors can be categorised into three main factor groups: material properties, process parameters and environmental conditions. The powder flow rate accuracy is a function of these factor groups. It can be written as below:

$$\text{Powder flow rate accuracy} = f(\text{material properties, process parameters, environmental conditions})$$

The equation shows that the powder flow rate accuracy is typically a non-linear function of the different variables (Clayton, 2019). Understanding these factors is critical for the development of a micro-feeder. Table 2-5 lists and groups the variables that influence feeder performance. In particular, we will review more details of the following factors in this section:

1. Material properties: Particle properties and bulk properties
2. Process parameters: General rules for feeder design
3. Environmental conditions: Moisture content and relative humidity

Table 2-5: General variables that influence powder flowability.

Material properties	Process parameters	Environmental conditions
Particle Properties	Pressure	Consolidation
Particle size and shape	Temperature	Aeration
Surface area	Vibration frequency	Humidity level
Bulk properties	Vibration amplitude	The extent of shear/strain
Bulk density	Screw speed	Excessive plant vibration
True density	Air flow rate	Environment temperature
Cohesion	Refill	Operation
Adhesion	Hopper design	Material storage
Elasticity	Feedback control	
Plasticity	Weight measurement method	
Porosity	Construction materials	
Electrostatic charge	Equipment surface finish	
Hardness/Friability		

2.8.1 Material properties: Particle properties and bulk properties

The flow behaviour of powders is determined by the material properties, which encompass both particle properties and bulk properties. These properties play a crucial role in feeder performance and design (Bostijn *et al.*, 2019). In order to design a reliable and consistent powder feeder, a comprehensive understanding of material properties is necessary. Particle properties, such as particle size distribution, particle shape, and particle density, are known to

significantly influence bulk properties and, subsequently, powder flow behaviour (Augsburger and Hoag, 2008).

2.8.1.1 Adhesive and cohesive forces

The existence of molecular forces gives rise to the inclination of solid particles to adhere either to each other or to other surfaces, a phenomenon commonly referred to as cohesion and adhesion. Cohesion refers to the attractive force between molecules of the same substance. Adhesive force is the attractive force between molecules and other surfaces. It is the force that causes dissimilar materials to stick together. This force is often responsible for phenomena such as adhesion, where two different materials cling to each other. These forces can be attributed to several molecular-level interactions, including Van der Waals forces, hydrogen bonding, electrostatic forces, mechanical lock and liquid bridge. Van der Waals forces arise from fluctuations in electron distribution around atoms and molecules. They can result in temporary dipoles, inducing a weak attraction between adjacent molecules. Hydrogen bonding is a specific type of dipole-dipole interaction where a hydrogen atom, bonded to a highly electronegative atom (such as oxygen, nitrogen, or fluorine), experiences attraction to another electronegative. Electrostatic forces occur between an ion and a polar molecule. The charged ion is attracted to the opposite partial charge on the polar molecule. Other forces such as surface tension and wetting are also the adhesive forces. The moisture can increase the adhesive and cohesive forces due to the liquid bridges and capillary pressure.

2.8.1.2 Bulk density

Bulk density is a measure of the powder mass divided by its bulk volume. It is often determined using methods that involve filling a known volume with the powder and measuring the mass. It is typically expressed in units such as grams per cubic centimetre (g/cm^3) or kilograms per litre (kg/l). Several factors, including particle size and shape, moisture content, and compaction during storage or handling, influence a powder's bulk density. It is an important characteristic because it can affect the flow properties, compressibility, and packaging of the powder.

2.8.1.3 Particle size and shape

Particle size and shape are closely related to adhesive and cohesive forces, which in turn affect bulk density. Both adhesive and cohesive forces can cause significant variations in bulk density, negatively affecting powder flow rate reduction. Specifically, as particle size decreases, the specific surface area increases, could result in increased Van der Waals forces, electrostatic forces, and surface tension forces, which contribute to higher interparticle forces and tensile strength between particles, ultimately leading to poor flow behaviour (Rhodes, 2008a; Shaikh et al., 2018). It is generally observed that powders with smaller

particle sizes exhibit reduced flowability. Van der Waals forces tend to dominate flowability in particles with diameters less than 10 μm . To mitigate cohesive forces, particle suspensions (fluidisation) using air or gas as flow agents are commonly employed to maintain adequate particle distances, granulation to increase the particle size or surface treatment such as coating (Rhodes, 2008a).

Particle shape, particularly irregular shape, has a similar influence as particle size on powder flow behaviour. Irregular shape increases particle surface area, leading to higher cohesive forces. Mechanical interlocking caused by irregular shapes is another contributing factor to bulk density variation. In general, manufacturers may consider modifying particle shape to a more rounded shape, if feasible, to reduce contact areas and friction forces, thus improving particle flow (Clayton, 2019).

2.8.1.4 Particle size distribution

Particle size distribution (PSD), which refers to the range of powder sizes in a given material, is another critical factor influencing bulk density and particle flow behaviour. In the manufacturing of powders for drug applications, variations in particle size are inevitable, resulting in either monomodal or polymodal distributions depending on the manufacturing process. Polymodal distribution occurs when combining two or more monomodal distributions to form a powder mix. The PSD also affects the porosity in bulk density, as fine particles can fill the void spaces between coarse particles in materials with broader PSD ranges, leading to either tightly packed powders or unfilled void spaces. These factors can significantly affect bulk density measurements, making the powder flow rate unpredictable.

2.8.1.5 Powder flowability

In addition to particle properties, external variables play a crucial role in powder behaviour. Factors such as consolidation, aeration, humidity level, the extent of shear, and equipment surface properties can significantly influence the flowability of powders (Clayton, 2019). Therefore, a comprehensive understanding of both particle properties and external variables is essential for designing or selecting reliable and effective powder feeders in industrial applications (Figure 2-15). Details regarding the measurement of powder flowability are addressed in Section 2.8.4.

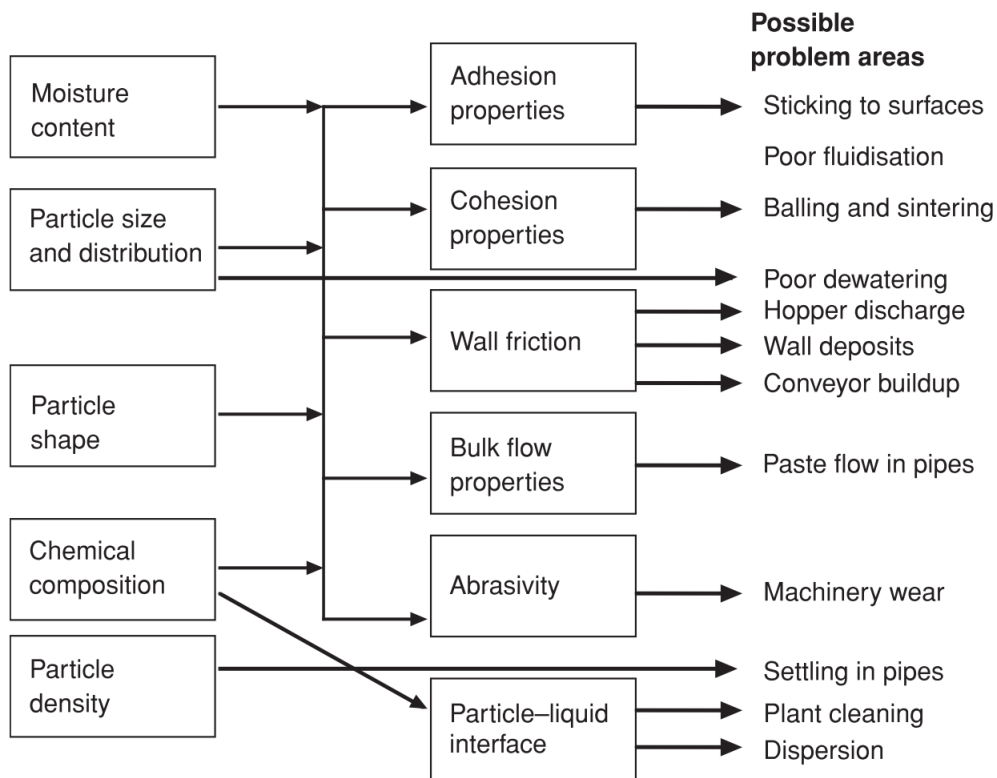


Figure 2-15: Interplay of particle and bulk properties and their combined influence on potential feeder development challenge (McGlinchey, 2009).

2.8.2 Process design and parameters: General rules for feeder design

In the design of powder feeders, the process parameters may vary depending on the specific feeder design. However, certain general rules can be previewed and applied during the design stage to ensure optimal performance. These rules, as identified by previous research, include:

- Avoiding the formation of stagnant zones, such as nonsufficient steep areas and gaps between process connections, which can hinder the flow of powder particles (Schulze, 2008).
- Preventing the formation of ratholes in the hopper design, which can disrupt the flow of powder particles. This can be achieved through measures such as reducing the hopper's material level, adding internal mechanical agitators or external vibrators, and enlarging the outlet opening (Burstein et al., 2020).
- Avoiding the use of construction materials that can generate electrostatic charges as the particles slide along the surface.
- Ensuring that the internal wall surface finish of the feeder does not trap powder particles, thus preventing clogging or blockages.
- Ensuring a pressure balance between the feeder and the subsequent process to avoid backpressure affecting the mass flow rate (Hanson, 2018).

- Addressing the refill process in the feeder design remains a significant research gap. This includes investigating the refill method, refill control algorithm, the reaction time of the refill device, and the size of the refill hopper (Engisch and Muzzio, 2015).
- Avoiding segregation occurrence by the feed mechanism, as highlighted by previous studies (Engisch and Muzzio, 2015).
- Considering other relevant process parameters such as operating pressure, temperature, air flow rate, motor speed, power consumption, and their effects on feeder performance.
- Taking into account the cleanability of the feeder, as it plays a crucial role in maintaining hygienic and efficient operation (Enabling Technologies Consortium, 2020; Wagner et al., 2014).

In order to comprehensively assess the concepts for a novel micro-feeder and understand the influence of all system parameters, it is essential to consider these general rules during the design process. This will help ensure that the feeder is designed to meet the desired performance requirements and can effectively deliver powder particles for the intended application. Further research and development in this area are warranted to advance the understanding and optimisation of powder feeder designs.

2.8.3 Environmental conditions: Moisture content and relative humidity

The environmental conditions in powder processing, including moisture content, storage conditions, environmental temperature, and vibration, play a crucial role in determining the quality and behaviour of powders. Among these factors, moisture content and relative humidity are of particular concern due to their significant influence on powder properties.

Moisture can accumulate between powder particles, resulting in the formation of liquid bridges, as highlighted by Schulze in 2007. These liquid bridges increase the cohesiveness between particles due to surface tension and negative capillary pressure, leading to changes in powder flowability and bulk density, ultimately affecting the powder flow rate. Additionally, the lubricating effect of water can cause the powder to compact, further influencing its behaviour. Moreover, moisture can alter the surface properties of particles, leading to softening or swelling (Rhodes, 2008a). The characterisation of these variables presents inherent complexities, thereby rendering the prediction of their influence on flow properties a challenging task with limited certainty.

As a result, careful control of the process environment is essential in the design of powder handling plants, including the regulation of temperature and humidity in the storage room. Moisture can enter the powder processing system from various sources, such as the process environment, process air supply, and even air leakage from process connections. Therefore,

in the development of micro-feeders, moisture content and humidity are critical factors that cannot be overlooked, as they significantly influence the performance and behaviour of powders in the processing system and also the quality of the final product (Nagy et al., 2020). Proper management of these environmental conditions is crucial to ensure the quality and stability of powder processing operations.

2.8.4 Powder flow measurement techniques

There are many different flowability assessment methods such as the Hausner ratio (Hausner, 1967) or Carr index (Carr, 1965), and Jenike flow function coefficient (Jenike, 1964). Flowability is typically classified into three major categories: easy-flowing, cohesive, and non-flowing materials. Easy-flowing materials, such as plastic pellets and flakes, flow easily by gravity and can be effectively fed using equipment such as vibrating feeders or screw feeders. Cohesive materials, such as titanium oxide and pigments, exhibit high surface energy and tend to aggregate into large masses, similar to snowballs. Cohesive materials still exhibit some level of flowability, but bridging and rathole formation can present challenges in feeding. Non-flowing materials, such as silicon dioxide and rubber particles, possess higher cohesion and adhesion forces due to factors such as irregular particle shape, static attraction, or moisture absorption. These materials exhibit extremely sticky behaviour, making them particularly challenging to feed. Powder flowability is particularly important in drug manufacturing as it affects the accuracy of powder feeding, dosing, and uniformity of blending, eventually affecting the final product quality.

2.8.4.1 Hausner ratio and Carr Index

Hausner ratio and Carr Index are frequently used in pharmaceuticals as an indication of the powder flowability. Both approaches offer economical and straightforward techniques for measuring powder flowability. The Hausner ratio (H) is a ratio of the tapped density (ρ_t) to bulk density (ρ_b) or aerated density to identify the flowability of a powder indirectly:

$$H = \frac{\rho_t}{\rho_b}, \quad \text{Equation 2-1}$$

Rather than as a ratio, Carr (1965) defined powder compressibility (c) to quantify the powder compressibility and powder flowability, which is expressed as (McGlinchey, 2009):

$$c = \frac{\rho_t - \rho_b}{\rho_b} \times 100. \quad \text{Equation 2-2}$$

They are based on the geometric rearrangement of particles' ability, and they are also the indicator of the compressibility of bulk powder. The rationale is that cohesive materials have higher inter-particle forces enabling them to resist gravity and allowing particles to support themselves around void spaces. Therefore, when tapping process introduces additional force, overcoming these cohesive attractions and causing particle to settle into the void spaces,

thereby reducing the powder volume and increasing its bulk density. A low Hausner ratio value thus indicates weaker cohesion, signifying the powder shows better flowability. A Hausner ratio exceeding 1.25 is considered indicative of poor flowability. Similarly, a Carr index surpassing 25% suggests poor flowability, while a value below 15% signifies good flowability. Table 2-6 provides a flowability indication of powder from McGlinchey (2009); this indicator is used in this study.

Table 2-6: Flowability indicator prescribed by USP29-NF26, 2006 (McGlinchey, 2009).

Description of flow	Angle of repose (degree)	Carr's compressibility (%)	Hausner ratio (–)
Excellent/very free flow	25–30	<10	1.00–1.11
Good/free flow	31–35	11–15	1.12–1.18
Fair	36–40	16–20	1.19–1.25
Passable	41–45	21–25	1.26–1.34
Poor/cohesive	46–55	26–31	1.35–1.45
Very poor/very cohesive	56–65	32–37	1.46–1.59
Very very poor approx non-flow	>66	>38	>1.60

2.8.4.2 Angle of repose

Von Terzaghi (1925) defined the angle of repose, a critical parameter widely applied in the design of mass flow hoppers (McGlinchey, 2009). The angle of repose is defined as the angle formed by the free surface of a pile of powder with respect to the horizontal plane. This parameter serves as an indirect means to assess powder flowability. It's determined by factors like particle size, shape, and friction. Materials with higher cohesion and friction tend to have steeper angles of repose due to the cohesion overcome the gravity. Typically, an angle of repose instrument incorporates an inclined funnel through which the powder passes, settling on a flat circular surface. Carr (1965) incorporated a protractor, an indicator wire and a jarring device to measure the angle of repose, and offers valuable insights into powder flowability (Figure 2-16). Carr's classification, detailed in Table 2-6, categorises powder flowability based on the observed angle of repose. Powders with poor flow characteristics exhibit a steeper angle, while those with smoother flow spread more easily, resulting in a smaller angle. A lower angle of repose is indicative of improved flowability.

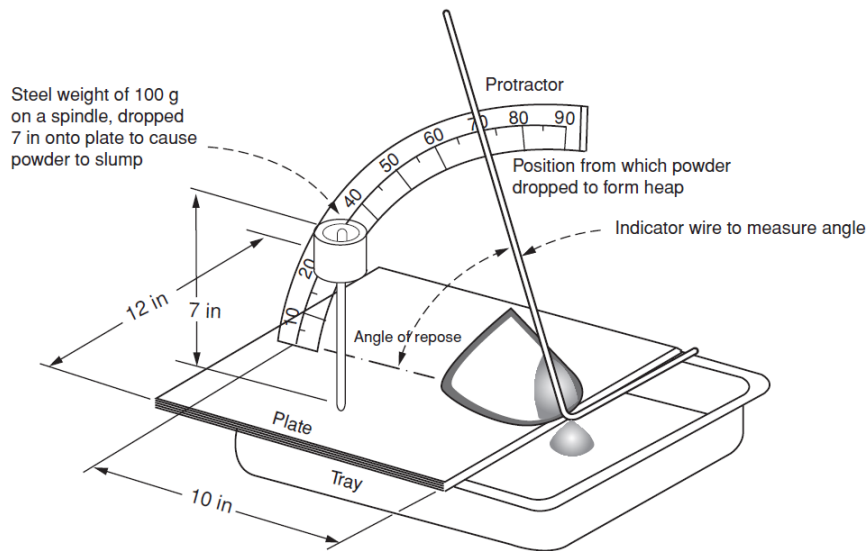


Figure 2-16: The apparatus of the angle of repose measurement by Carr, 1965 (McGlinchey, 2009).

Despite its simplicity and efficiency, the angle of repose method is a guide for evaluating powder flowability and is subject to limitations stemming from inconsistent measurements and its dependence on pile formation and operational methods. To address these challenges and enhance measurement accuracy, researchers have developed alternative methods such as injection/poured (Wouters and Geldart, 1996), discharge/drainage (Carrigy, 1970; Schulze, 2008), tilting table (Geldart et al., 2006), rotating drum methods (Carrigy, 1970) (Figure 2-17). These methods aim to provide more reliable assessments of the angle of repose by refining the experimental procedures and mitigating potential sources of variability.

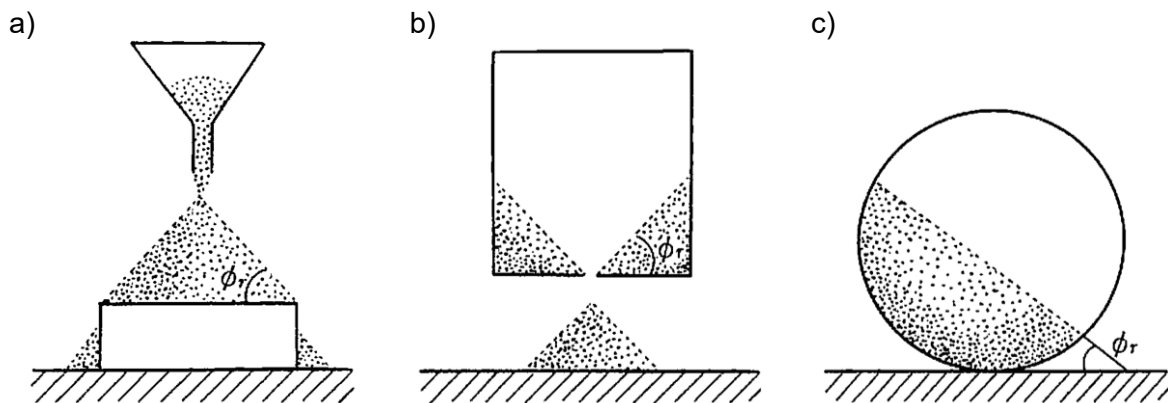


Figure 2-17: Measurement of angle of repose: a) injection method; b) discharge method; c) tilting method (Higashitani et al., 2020).

2.8.4.3 Critical orifice diameter

The critical orifice diameter is one of the powder flow measurement techniques. It indicates the minimum diameter required for gravity-induced powder discharge, ensuring the prevention of arching or clogging. Arching, characterised by interlocked powder particles forming stable bridges, impedes flow while clogging results in the complete blockage of the orifice. Notably,

materials with good flow characteristics exhibit a smaller critical orifice diameter. Determining the critical orifice diameter is achievable through established methods outlined in standard protocols such as USP29-NF24 (2006).

Lee et al. (2000) added depth to this understanding by conducting a comparative analysis that correlated critical orifice diameter results with Carr's index. This correlation emerged as a crucial factor for classifying powder flowability accurately. The evaluation of powder flowability has evolved over time, with a significant focus on monitoring the flow rates through an orifice.

Many researchers like Vemavarapu et al. (2009), Baserinia et al. (2016) and Baserinia and Sinka (2018) used this technique in their study to understand the intricate dynamics of powder behaviour of the tested materials. Figure 2-18 shows the apparatus of critical orifice measure used in (Baserinia et al., 2016) and (Baserinia and Sinka, 2018). A sealed cylindrical container with a shutter was employed, utilising opening diameters ranging from 1 to 30 mm. The smallest diameter at which powder discharged was recorded as the critical orifice diameter. They used the critical orifice diameter to determine the powder flowability for the tested materials.

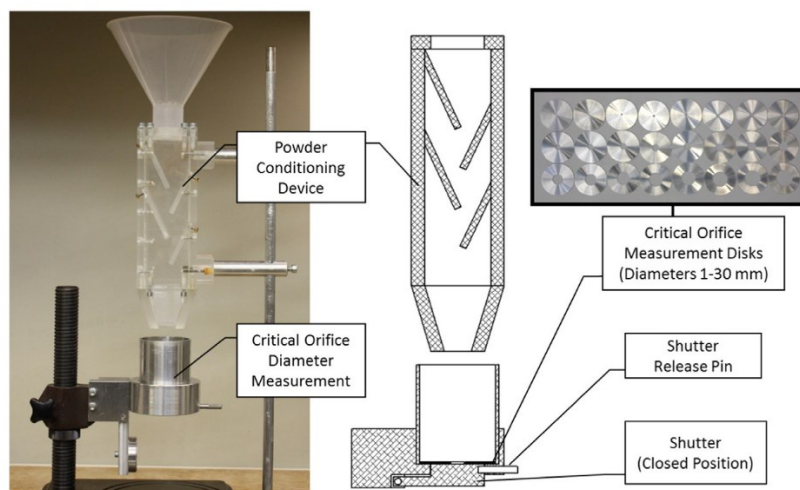


Fig. 4. Critical orifice diameter measuring device.

Figure 2-18: A critical orifice diameter measurement device (Baserinia et al., 2016b).

2.8.4.4 Carney and Hall flowmeters

Hall flowmeter, also known as a Hall-effect flowmeter, is a device used to assess the flow properties of bulk powders (Figure 2-19a). This instrument is named after Elbert J. Hall in 1945, who introduced the concept of using a standardised method for measuring powder flowability. The basic principle involves allowing a specified quantity of powder to flow through a standardised funnel or orifice with a specified diameter and measuring the time it takes for the powder to flow through a specified orifice by a gravitational force. Several international test standards, such as the International Organisation for Standardisation (ISO), 2014 and the

American Society for Testing and Materials (ASTM) are published to standardise the measurement of Hall flowmeter. They also standardise the geometry of the Hall flowmeter design for different applications, for example, ASTM 212 for the apparent density of free-flowing metal powder, ISO 3923 for the determination of apparent density for metallic powder, ISO 4490 for the determination of low flow rates, and ISO 14629 for fine ceramics.

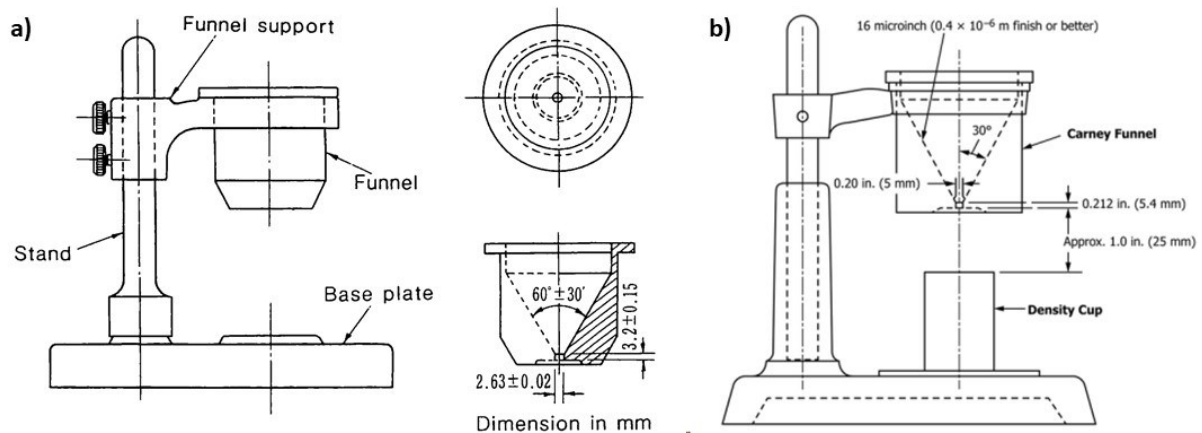


Figure 2-19: Flowmeter used for flow rate measurement of powder material: a) Japanese Industrial Standard Z 2502 Hall flowmeter (Higashitani et al., 2020) and b) ASTM standard B417-22 of the Carney flow meter (ASTM standard, 2022)

The Carney flowmeter (Figure 2-19b) is very similar to the Hall flowmeter. The difference is in the diameter of the holes. Carney flowmeter used a 5 mm diameter orifice. Therefore, it can handle more cohesive material than the Hall flowmeter. Irani et al. (1959) introduced a double-funnel technique featuring larger openings designed for cohesive powders. Jiang et al. (2009) devised an automated small-scale measurement system to assess the flowability of powders, utilising the vibrating capillary method. Seppälä et al. (2010) based on this principle and provided a single upward motion to break the vault structure to let the powder flow freely through the orifice to develop a method to get the reliable powder flow characteristics using very few materials. Vlachos and Chang (2011) improved a Hall flowmeter to investigate the flow properties of polydisperse mixtures of material powders.

2.8.4.5 Jenike's flow function

Jenike's flow function serves as a classification system for powder flowability. In 1964, Jenike introduced the flow function coefficient (ff_c) as a means of categorizing the flowability of bulk solids. This coefficient (ff_c) establishes a relationship between the major principal consolidation stress (σ_1) and the unconfined yield strength (σ_c) of the powder. The measurement process involves using a cylindrical specimen, consolidating it uniformly under a major (vertical) consolidation stress, and then removing both the consolidation stress and container. Subsequently, a vertical compressive stress is applied to induce collapse. The unconfined yield strength can be determined by employing Mohr's stress circle, which intersects tangentially with the material's yield locus. The varying consolidation stress values are

iteratively applied to determine the corresponding unconfined yield stress (Schulze, 2007). The expression for the flow function coefficient (ff_c) is given by:

$$ff_c = \frac{\sigma_1}{\sigma_c} \quad \text{Equation 2-3}$$

This coefficient is widely accepted as the primary parameter for designing mass flow hoppers and assessing powder flowability. A higher ff_c value indicates better flowability. Utilising the Jenike flow function coefficient, powders can be classified into different categories, as presented in Table 2-7. Various methods have been developed to determine the flow function of powders and evaluate their flowability under different consolidation stresses.

Table 2-7: A table of flow function coefficient and flowability of solid powder indicator, adapted from (McGlinchey, 2009)

Flow function coefficient	Flowability
$ff_c < 1$	Non-flowing
$1 < ff_c < 2$	Very cohesive
$2 < ff_c < 4$	Cohesive
$4 < ff_c < 10$	Easy-flowing
$10 < ff_c$	Free-flowing

2.8.4.5.1 Uniaxial compression test

A uniaxial compression test is a fundamental mechanical test used to determine powder flow by determining how a bulk powder responds to compression force along a single axis (Figure 2-20). A hollow cylinder with low-friction walls is first used to prepare a cylindrical specimen. The specimen is applied a uniaxial compression force (σ_1) along a single axis. This force is called the consolidation stress or major principal stress in the vertical direction. For the poorly flow bulk solid, the bulk density will increase. When the bulk density increases very little, the material is considered easy-flowing. In addition, we can observe that the strength of bulk solid specimens increases. The bulk solid is both consolidated and compressed. After consolidation, the hollow cylinder is removed to relieve the consolidation stress. The specimen will break if the bulk solid specimen is subsequently loaded with vertical compressive stress. At this point, the stress causing the breakage is called unconfined yield strength or cohesive strength, σ_c . By studying different consolidation stresses, different unconfined yield strengths can be obtained. Generating a graphical representation by plotting the unconfined yield strengths measured at different consolidation stresses on a diagram yields a curve known as the flow function. Nevertheless, the outcomes of uniaxial compression tests exhibit significant variability across different trials. This variability arises because stresses within the sample are not uniform, the cell wall does not allow for frictionless conditions, and the location of failure varies considerably (Schulze, 2007).

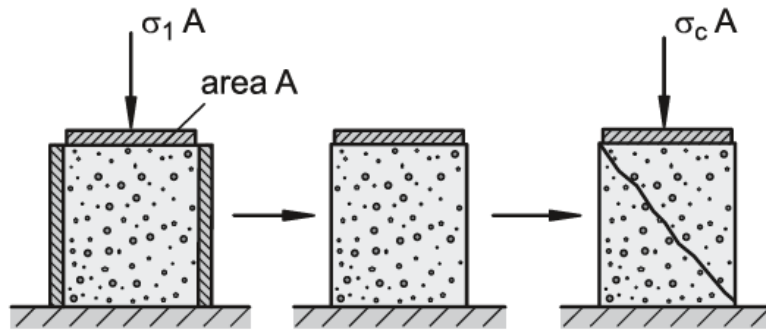


Figure 2-20: Uniaxial compression test for measuring the flow function of a powder (Schulze, 2007).

2.8.4.5.2 Shear testing

In a shear test, a bulk solid specimen undergoes the application of a vertically acting normal stress, denoted as σ . Subsequently, the specimen is sheared by displacing its upper and lower sides horizontally relative to each other. The resulting shear stress, τ , in the horizontal plane due to the deformation is then measured. When the relative displacement is translational, the shear tester is specifically referred to as a translational shear tester (Schulze, 2007). The translational shear tester (Figure 2-21a) was the first shear tester developed by Jenike (1964). Additional shear cell testers, including the ring shear tester (annular shear tester), have been introduced subsequent to the Jenike shear cell. Examples include the Schulze Ring Shear Tester (Figure 2-21b) developed by Schulze (2011), the Brookfield Powder Flow Tester (PFT) (Kerins et al., 2023; Lopes Neto et al., 2017; Peddapatla et al., 2016; Shah et al., 2023), and torsional testers (Figure 2-21c), which are commonly employed. In the ring shear tester, the powder is sheared by rotation of the lid.

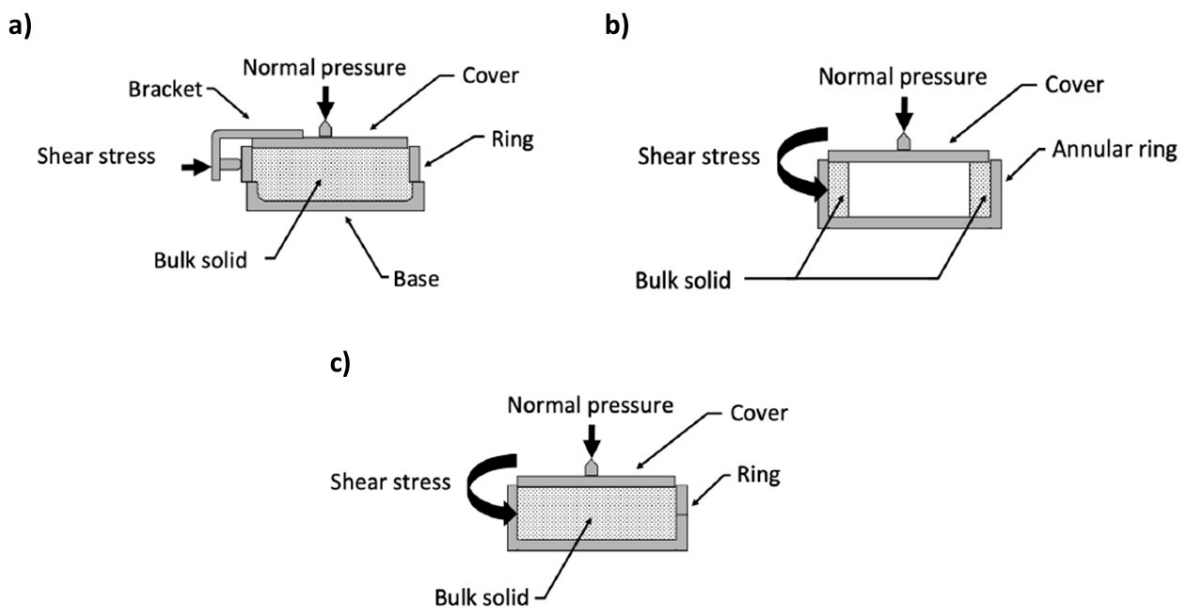


Figure 2-21: Shear tester: a) translational shear tester (Jenike), b) annular (ring) shear tester, and torsional shear tester (Mehos, 2018).

The shear testing process commences by addressing an initially under-consolidated bulk solid sample to ensure homogeneity. This involves a consolidation step, applying a normal stress (σ_{pre}) followed by shearing (Figure 2-22b). As shearing progresses, the shear stress undergoes an initial increase, culminating in a constant value (τ_{pre}), indicative of 'critical consolidation' under the given normal stress (σ_{pre}). After the pre-shear phase, the normal stress is reduced to $\sigma_{sh} < \sigma_{pre}$, leading to a gradual increase in shear stress during subsequent shearing. Upon reaching a sufficiently high shear stress, the specimen transitions into a flowing state, resulting in material dilation and a subsequent decrease in shear resistance and shear stress. The maximum shear stress (τ_{sh}) is achieved at the point of incipient flow. Before introducing another normal stress value, the sample undergoes preshearing to determine the corresponding yield point.

The temporal evolution of shear stress is visually presented in Figure 2-22c, while the resulting yield locus is considered linear within the measurement range, governed by the relationship: $\tau_{sh} = k\sigma_{sh} + \tau_c$. The slope (k) of the yield locus denotes the angle of internal friction, represented by $\varphi = \tan^{-1}(k)$. The intercept of the yield locus (τ_c) acts as an indicator of cohesion within the sample. Computation of bulk density (ρ_b) becomes feasible with knowledge of the sample weight and shear cell dimensions.

For a more nuanced exploration of stress states, the utilisation of Mohr stress circles is integral. A circle representing steady flow aids in determining consolidation stress (σ_1) (Schulze, 2008). Similarly, a circle representing the stress state at failure facilitates the calculation of unconfined yield strength (σ_c) (Schulze, 2008), as delineated in Figure 2-22d. The ratio of these two stresses (σ_1/σ_c) imparts valuable insights into the distinctive behaviour of the material.

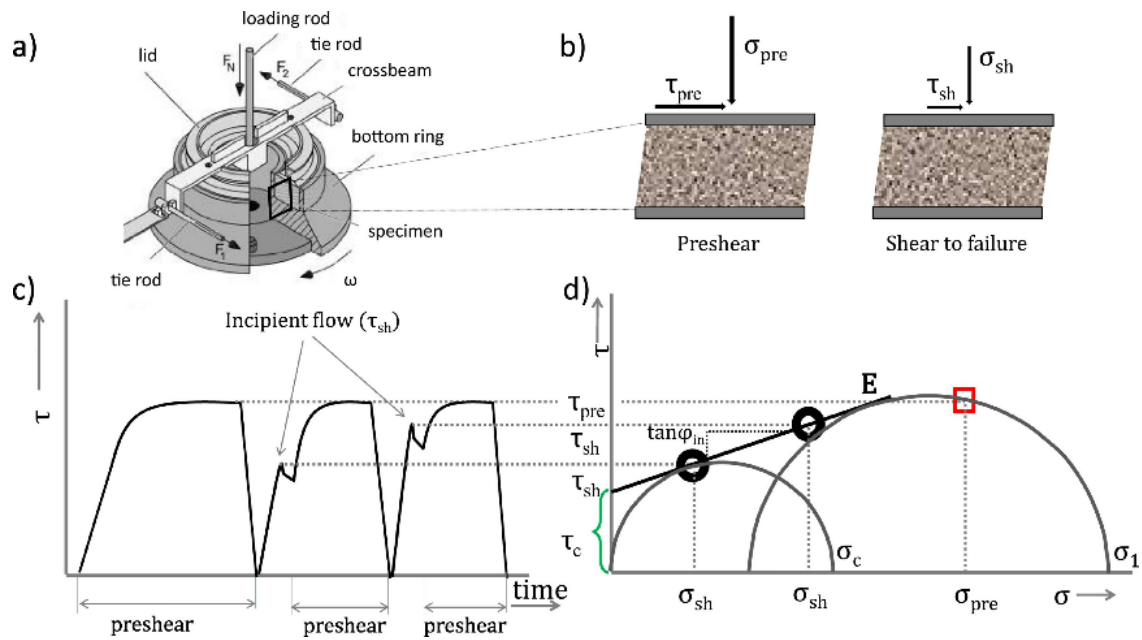


Figure 2-22: An example of ring shear tester: a) Shear cell of the Schulze ring shear tester, b) Schematic of the cross-section of the sample during preshear and shear to failure, c) Example of stress and tie data, d) Measurement of a yield locus by preshear and shear to failure from a ring shear tester (Deshmukh et al., 2019).

2.8.4.5.3 Ball indentation

The ball indentation method was first proposed by Tabor in 1948 (SI et al., 2022; Taylor, 1948). This method employs a ball, conical, or cylindrical indenter to create an indentation on a specimen under a consistent load (Figure 2-23). Analysing the load versus depth ($P-h$) curve allows for calculating stress and strain relationships, and a material's mechanical behaviour can be determined (Mehrabi et al., 2023). Hassanpour and Ghadiri (2007) expanded upon this technique at small scales and low compaction levels, discovering that the yield stress results obtained from indentation and unconfined compression measurements exhibit similarity. The classification of powder flowability can be performed using the yield stress obtained through indentation and the consolidation stress, employing Jenike's flow function. Numerical studies have been carried to enhance the ball indentation method to predict the bulk solid behaviour (Pasha et al., 2015; Tirapelle et al., 2020; Zafar et al., 2017).

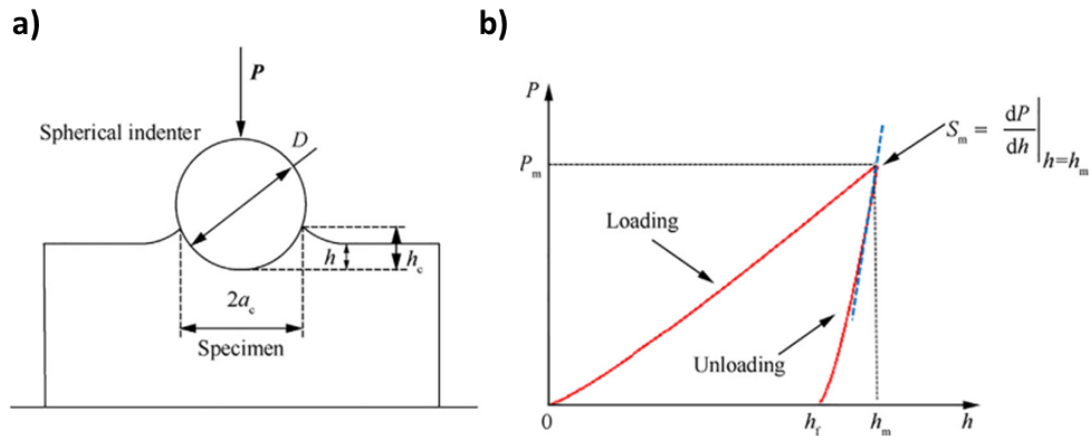


Figure 2-23: Ball indentation: a) definition of variables for ball indentation, b) indentation curve (SI et al., 2022).

2.8.4.6 Torque rheometers

A torque rheometer is an instrument used to measure the rheological properties of materials, particularly their flow behaviour (Freeman Technology Ltd, 2016; Mehos, 2018). Rheology is the study of the flow and deformation of materials under applied forces. Torque rheometers are commonly employed in the study of polymers, plastics, rubber, and other materials to understand their flow characteristics, viscosity, and other rheological properties. The fundamental concept underlying torque rheometer centres on exerting a regulated torque onto a specimen and gauging the ensuing deformation or flow. Torque indicates the rotational force imposed on the sample, and the material's reaction is observed to comprehend its flow characteristics. For example, the resistance encountered by the blade reflects the challenge in relative particle movement or the overall flow attributes. As particles exhibit greater resistance to motion, making it more challenging for the powder to flow, moving the blade becomes more arduous. Marketed rheometers possess the capacity to assess various parameters across a broad spectrum of powders, including specific energy, shear resistance, and others. This applies to powders ranging from those with free-flowing characteristics to cohesive ones, encompassing diverse particle sizes, such as FT4 powder rheometer (Figure 2-24).

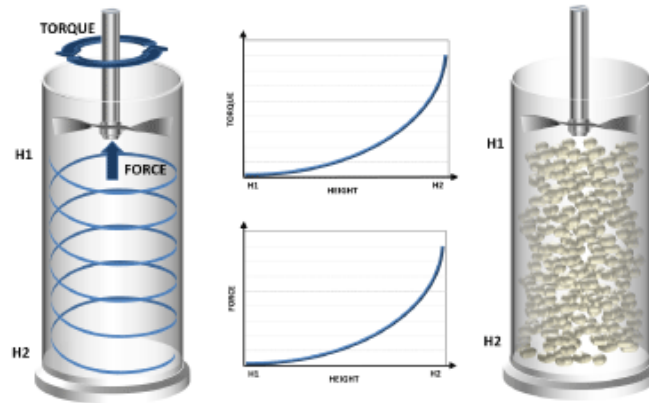


Figure 2-24: FT4 powder rheometer (Freeman Technology Ltd, 2016).

2.8.4.7 Permeability

The permeability of a powder denotes its capacity to permit the flow of air or another gas through it, playing a pivotal role in comprehending powder behaviour in diverse processes such as pneumatic conveying, fluidisation, and filtration. Numerous factors, including particle size, shape, and arrangement, contribute to the permeability of a powder bed (Richardson et al., 2002). The assessment of permeability frequently involves the application of Darcy's law equation (Darcy, 1856; Rhodes, 2008):

$$Q = -KA \frac{\Delta P}{L}. \quad \text{Equation 2-4}$$

Here, Q is the volumetric flow rate of the gas, K is the permeability of the powder bed, A is the cross-sectional area through which the gas flows, ΔP is the pressure drop across the powder bed, L is the length of the powder bed. Permeability (K) quantifies the ease with which gas can traverse the powder bed under a specified pressure drop, influenced by parameters like porosity, particle size distribution, particle shape, and particle arrangement.

The Darcy's law revised for spherical particle by Kozeny (1927), with Carman (1937) later modifying the equation to its present form (Rhodes, 2008):

$$\frac{\Delta p}{L} = -\frac{180\mu (1-\varepsilon)^2}{\phi_s^2 d_p^2 \varepsilon^3} u_s, \quad \text{Equation 2-5}$$

where ΔP is the pressure drop, L is the total height of the bed, u_s is the superficial velocity, μ is the viscosity of the fluid, ε is the porosity of the bed, ϕ_s is the sphericity of the particles in the packed bed, d_p is the diameter of the volume equivalent spherical particle. However, this Kozeny-Carman equation is only valid for laminar flow and mono-disperse spherical particles. Ergun (1952) introduced a widely accepted correlation for the pressure drop-flow rate relationship across packed beds, aiming to simulate incompressible flow through a bed of spherical particles (Rhodes, 2008):

$$\frac{-\Delta P}{L} = 150\mu \frac{(1-\varepsilon)^2 u_s}{\varepsilon^3 d_p^2} + 1.75\rho \frac{(1-\varepsilon) u_s^2}{\varepsilon d_p}, \quad \text{Equation 2-6}$$

The initial term accounts for viscous losses, which are predominant at lower fluid velocities, while the latter term represents kinetic energy losses, becoming more pronounced at higher velocities. Notably, the second term is negligible at low fluid velocities, rendering the equation akin to the Kozeny-Carman equation. Various scientists have developed alternative equations for different conditions, as reviewed and summarised by Erdim et al. (2015).

Illustrated in Figure 2-25 is a permeability testing apparatus. Determining permeability involves directing a gas through a powder bed within a cylinder. Throughout the testing process, the sample's mass, volume, and bulk density are computed using these volume metrics. Simultaneously, the pressure drop is gauged. Consequently, the permeability is computed using Darcy's Law, rearranged as follows:

$$K = \frac{QL\rho_b g}{A\Delta P}. \quad \text{Equation 2-7}$$

High permeability indicates that the powder bed allows easy passage of gas, while low permeability suggests resistance to gas flow. Understanding the powder permeability is crucial in designing and optimising processes involving the gas flow through powder beds. In pneumatic conveying systems, this knowledge aids in determining suitable conveying velocity and the pressure drop for efficient and stable material transport.

In industry, the permeability is measured experimentally using instruments like permeability cells or powder flow testers. The results play a crucial role in characterising powders and guiding the design of industrial processes that entail the handling and transporting of powder materials, such as preventing poor weight control into a die or hazardous flooding discharge from a hopper.

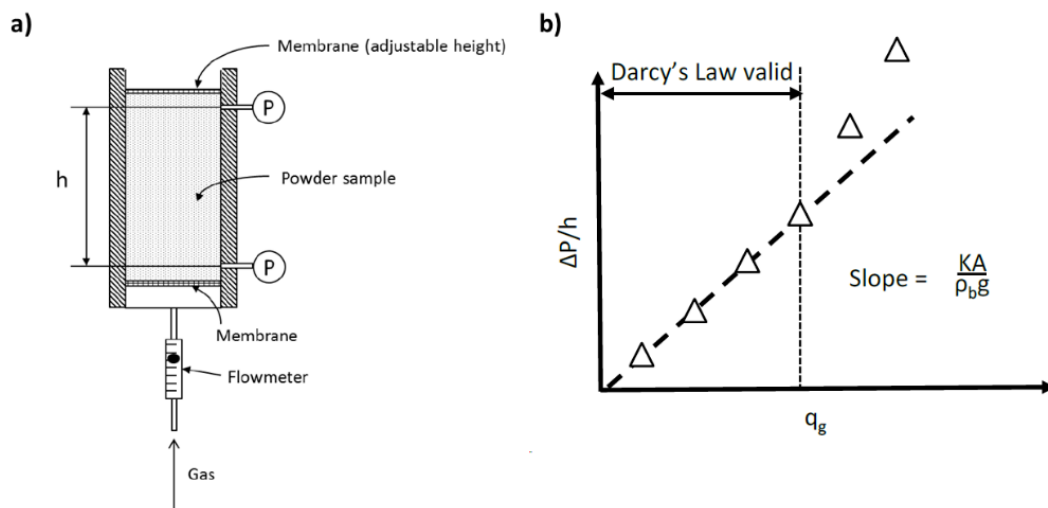


Figure 2-25: The measurement of permeability: a) permeability tester and b) determination of K from the test result (Mehos, 2018).

2.8.4.8 Geldart's classification

Geldart (1973) introduced a method for categorising fluidisable powders into four distinct groups in the context of aerated conditions. This empirical classification provides a preliminary assessment of powder behaviour during fluidisation, establishing a simple correlation between particle size and the disparity between particle and fluid densities. The Geldart classification is based on the balance of forces to categorise powder types. These forces include gravitational force, drag force, and intermolecular forces between particles, all of which vary depending on particle size. Geldart's classification, denoted as A, B, C, and D, is outlined below and visually depicted in Figure 2-26.

The Geldart classification system can be based on two dimensionless numbers: the Archimedes number (Ar) and the Reynolds number (Re) to determine the fluidisation behaviour and used to select the appropriate fluidisation equipment and operation conditions. The Archimedes number is defined as the ratio of buoyancy to gravitational forces $\left[\frac{\rho_g d_p^2 (\rho_p - \rho_g) g}{\mu^2} \right]$, while the particle Reynolds number assesses the viscous forces acting on a particle in a fluid $\left[\frac{\rho_f d_p U}{\mu} \right]$. Geldart's classification system divides powders into the following groups:

Group A: Aeratable powders

- Fine particles with a mean particle size between 50 and 100 μm
- $Ar < 10$ and $Re > 10$
- Low bulk density
- Good fluidisation and pneumatic conveying properties
- Examples: fumed silica, corn starch

Group B: Bubbling powders

- Intermediate particle size between 100 and 800 μm
- $Ar > 10$ and $Re < 10$
- Moderate bulk density
- Fluidisation and pneumatic conveying properties are less predictable
- Examples: sand, sugar

Group C: Cohesive powders

- Fine particles with a mean particle size of less than 50 μm
- $Ar > 10$ and $Re > 10$
- High bulk density

- Poor fluidisation and pneumatic conveying properties due to particle cohesion
- Examples: flour, toner

Group D: Spouted powders

- Coarse particles with a mean particle size greater than 800 μm
- $\text{Ar} < 10$ and $\text{Re} < 10$
- High bulk density
- Poor fluidisation properties but can be conveyed pneumatically
- Examples: gravel, pellets.

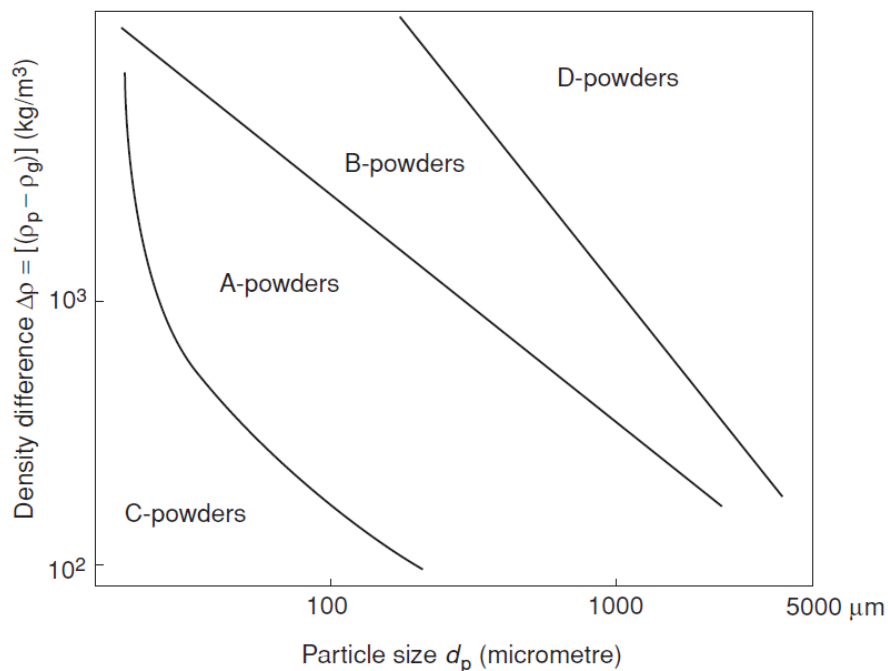


Figure 2-26: Geldart's classification of powder flowability in the aerated states (Geldart, 1973; McGlinchey, 2009).

Molerus (1982) and Rietema (1984) advanced Geldart's empirical classification by incorporating additional bulk powder properties, encompassing cohesion, gas viscosity, and gravity. They introduced the Geldart correction model, which juxtaposes the Archimedes number $\left[\frac{\rho_g d_p^3 (\rho_p - \rho_g) g}{\mu^2}\right]$ with the modified Reynolds number $\left[\frac{C}{\rho_g g d_p}\right]$, where C represents the cohesion factor. The Archimedes number is defined as the ratio of gravitational force to viscous force. This refined model expands upon the empirical Geldart fluidisation classification, as illustrated in Figure 2-27.

The inclusion of the cohesion factor and the modified Reynolds number in the Geldart correction model allows for a more comprehensive assessment of various powder handling processes, including mixing, transport, and separation. This enhanced classification system

offers dimensionless corrections considering a broader range of factors, providing a more accurate representation of powder behaviour.

Moreover, additional classifications have been proposed to account for factors such as pressure, temperature, and interparticle forces, as outlined by Grace (1986), Goossens (1998), Yang (2007) and Zhou et al. (2023). These expanded classifications contribute to a more thorough understanding of the complexities involved in powder handling under diverse conditions.

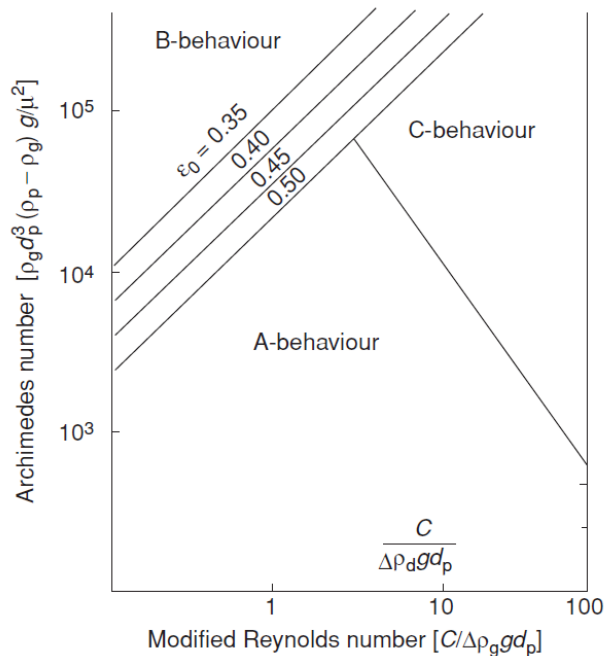


Figure 2-27: Modified Geldart's classification using Archimedes' number versus modified Reynolds's number (McGlinchey, 2009).

2.8.4.9 Die fill

The die filling process is a critical step in continuous direct compression or continuous direct capsule manufacturing (Jones-Salkey et al., 2023). The inconsistent die or capsule filling influences the accuracy of content uniformity, tensile strength and dissolution performance (Schomberg et al., 2020). However, highly cohesive, poorly flowing powders often used in pharmaceutical formulations can negatively impact die filling performance (Baserinia and Sinka, 2019; Zakhvatayeva et al., 2018). This is a particular issue in continuous direct compression tablet or continuous direct capsule manufacturing as there is not a granulation step to improve powder flow and processability. Therefore, the feeding to the die must be studied when design a feeder for a die or capsule filling. However, there are different mechanisms for die filling.

Various mechanisms for die filling exist, as observed by Schneider et al. (2007). They identified three mechanisms through high-speed camera observation: nose flow, bulk flow and

intermittent flow (Figure 2-28). Nose flow involves the initial acceleration of a shoe containing a fixed mass of powder. Friction between the powder mass and the base plate causes the powder to move towards the back of the shoe, forming a nose-shaped profile. As the nose translates across the die opening, material can flow over the surface of the nose, and it may avalanche into the die. This process is referred to as nose flow. Bulk flow occurs when the tip of the nose rapidly moves across the die opening at high speeds or if the die opening is small. The powder is delivered into the die by detaching from the bottom free surface of the powder mass. If this flow is reasonably continuous, it is referred to as bulk flow. Intermittent flow is characterised by the random detachment of individual particles or clusters of particles from the powder mass. This type of flow can result from discrete instabilities, releasing either small clusters of particles or large chunks of agglomerated powder into the die. In this work, they proposed a dimensional model to predict the mass transfer to the die based on shoe velocity. The dimensional model is expressed as:

$$\frac{m}{\rho_b D^2 L} = c \left(\frac{v_s}{\sqrt{gD}} \right)^{-(1+n)}, \quad \text{Equation 2-8}$$

where m is the powder mass transfer to the die, ρ_b is the bulk density, D is the opening size of the die, L is the length of the shoe, g is the gravity and v_s is the velocity of the shoe. The empirical parameters c and n depend on material properties and process parameters.

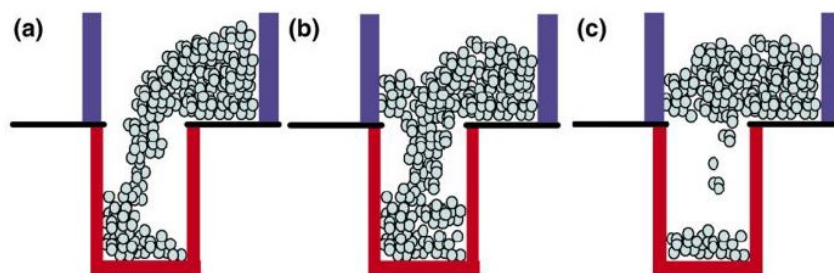


Figure 2-28: Powder flow into a die: a) nose flow, b) bulk flow and c) intermittent flow (Schulze, 2007).

In the studies of mass delivered into different die geometries, Sinka and Cocks (2009) assessed the powder flow behaviour tailored for die filling operations. They devised various experimental systems to scrutinise the gravity and suction filling of dies in air and vacuum environments. High-speed video observations unveiled crucial phenomena during powder deposition into dies, such as air pressure build-up and entrapment, impacting fill uniformity. The study defined critical fill velocity and dimensionless flowability measures to characterise powder flowability in die filling. Mills and Sinka (2013) extended this research by examining the influence of particle size and density on die filling. Smaller particle sizes exhibited more cohesion, resulting in intermittent flow during die filling, whereas larger particles displayed enhanced free-flowing characteristics. For gravity filling, a consistent

correlation emerged between particle size and critical flow velocity, with larger particles requiring higher critical velocities. Comparisons of particle density indicated that lower bulk density powders outperformed higher density powders of the same nominal size. This finding emphasised the improved flowability associated with lower bulk density for materials of the same particle size. The study identified optimal powder bed height, suction velocity, and other process parameters to maximise die fill performance.

Baserinia and Sinka (2019) developed advanced models for predicting powder flow into dies in pharmaceutical tablet manufacturing. These models incorporated separate terms for gravity and suction filling, allowing them to capture distinct air-powder interaction mechanisms. By integrating measured pressure differentials and powder height effects, the models offered more accurate estimates of mass flow rates, particularly for fine cohesive powders where small pressure changes significantly impacted flow. Despite requiring calibration, these models demonstrated enhanced predictive capability for die filling behaviour compared to previous approaches. This improvement is expected to aid in pharmaceutical process design and optimisation, particularly when dealing with poor-flowing powders sensitive to air effects. Overall, the study underscored the importance of modelling pressure differentials and suction effects for accurate dosing predictions.

Understanding the complex relationships between powder properties and process parameters poses a challenge when attempting to broadly rank powders' flowability. Nevertheless, in die filling processes, factors influencing formulations and process parameters can be discerned to optimise specific powder characteristics. Mills and Sinka (2013) calculated empirical constants, denoted as c and n , showing their dependence on different process parameters and material properties.

Mendez et al. (2010) explored how the feed frame influences powder flow properties and the weight uniformity of powder filling into the die. They observed that an increase in feed frame speed, including disc speed, resulted in a decrease in the resident time of the powder and an associated increase in die filling weight. Additionally, in 2012, they identified that changing the feeder impacted the particle size distribution, leading to increased bulk and tap densities (Mendez et al., 2012). This investigation aimed to identify an optimal combination of process parameters to minimise variability in tablet weight.

Several techniques have been identified to overcome poor die filling with cohesive powders. Increasing paddle speed in forced feeders allows cohesive powders to essentially move as a solid block, improving die fill weight consistency. Introducing air flow enhances particle flow and reduces vertical segregation. But air can also create pressure build up that resists powder flow. Suction filling helps overcome poorly flowing powders by creating negative pressure and

lowering segregation. It improves packing density compared to gravity filling. These techniques should be considered in feeder design.

In summary, studying die fill, primarily through a screw feeder, involves understanding the relationships between powder feeding and die filling, considering factors such as screw speed control, screw selection and feeder outlet design.

2.9 Design Guides

2.9.1 Pneumatic Conveying

Pneumatic conveying is a method of bulk solid material handling that uses air, gas or other conveying mediums to transport particles or powders from one place to another. This technique is commonly employed in industries such as agriculture, pharmaceuticals, and food processing, where the efficient and controlled movement of granular materials is essential (Abbas et al., 2020; Abrar et al., 2020; Kaur et al., 2017; Kuang et al., 2019). The essential components of a pneumatic conveying system include a source of compressed air, a feeding device to introduce the material into the air stream, a conveying pipeline, and a separation device to remove the material from the air at the destination point. The pneumatic conveying system can be classified as high, low and negative pressure conveying. Material flow rates can be controlled and monitored for this reason, and it gains interest in various industries (Abbas et al., 2020; Y. S. Huang et al., 2022; Kaur et al., 2017; Kuang et al., 2019; Zhang et al., 2016). Two modes of conveying are recognised: dilute phase conveying and dense phase conveying. In dilute phase conveying, the concentration of material in the air stream is relatively low, and the particles are fully suspended in the air, allowing for efficient and economical material transport. Compared to dilute phase conveying, dense phase conveying involves a higher concentration of material in the airstream and slower air velocities. The dense phase conveying results in the material moving in a denser, more concentrated manner through the pipeline (McGlinchey, 2009; Mills, 2016b; Rhodes, 2008a). The air velocity for the dilute phase conveying is typically 10 m/s to 12 m/s for fine powder and 16 m/s for fine granular and high-density materials. For the dense phase conveying, air velocities can be lower than 3 m/s (McGlinchey, 2009; Mills, 2016b; Rhodes, 2008). Zenz and Othmer (1960) introduced a qualitative phase diagram for the pneumatic conveying in a horizontal pipeline, as illustrated in Figure 2-29 (Rhodes, 2008). The saltation velocity in the horizontal pipeline is the boundary between suspension and non-suspension flow.

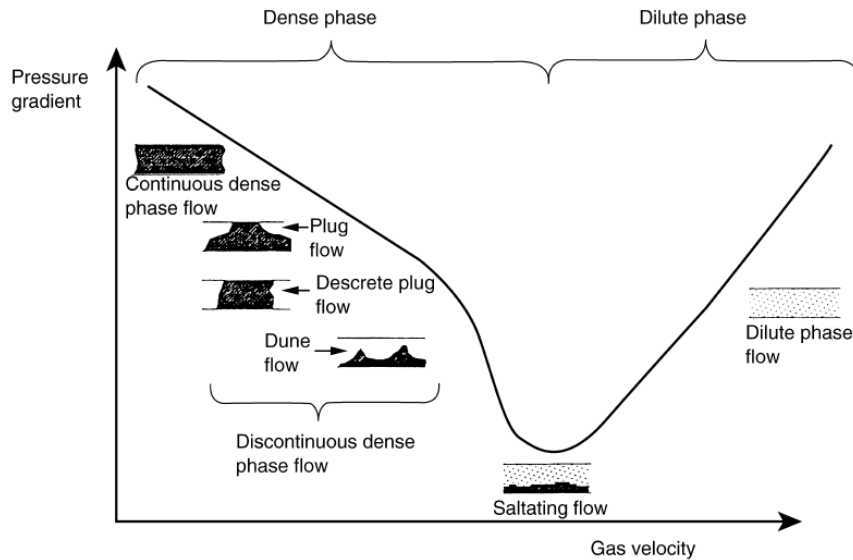


Figure 2-29: Flow patterns in horizontal pneumatic conveying (Rhodes, 2008).

Numerous studies (Hartman et al., 2006; Kaur et al., 2017; Lim and Yao, 2009) have used the dimensionless quantity, phase density or solid loading ratio to define the boundary between suspension and non-suspension flow. The solid loading ratio helps characterise the concentration of solid material in the conveying air. It becomes an essential parameter in designing and analysing pneumatic conveying systems, influencing the system's performance, pressure drop, and energy consumption.

The solid loading ratio is a term used in pneumatic conveying to quantify the amount of solid material being transported in relation to the conveying air. It is defined as the ratio of the mass flow rate of the solid material to the mass flow rate of the conveying air. The solid loading ratio is expressed as a percentage or a fraction. It is a dimensionless form and, mathematically, given by the formula:

$$\phi = \frac{\dot{m}_p}{\dot{m}_{air}}, \quad \text{Equation 2-9}$$

where \dot{m}_p is the mass flow rate of solid powder (kg/h), and \dot{m}_{air} is air mass flow rate (kg/h). In dilute phase conveying, where the concentration of solid material in the air stream is low, the solid loading ratio is typically below 15 (15 kg of material conveyed with 1 kg of air) (McGlinchey, 2009; Mills, 2016b).

The solid loading ratio is a critical factor in determining the appropriate design and operating conditions for a pneumatic conveying system. It influences the pressure drop along the pipeline, the conveying velocity, and the overall efficiency of the system. Different materials and applications may require varying solid loading ratios for optimal performance. In industries, engineers use the solid loading ratio to design systems that ensure effective and reliable

material transport while minimising issues such as pipeline wear, blockages, and excessive energy consumption.

Powder entrainment is a critical aspect of pneumatic conveying, especially in its application to dry powder inhalers. Over the past three decades, researchers have extensively investigated powder entrainment in pneumatic conveying systems (Annamalai et al., 1992; Hartman et al., 2006; Ikumi et al., 1986; Kuang et al., 2019; Matsusaka and Masuda, 1996; Suri and Horio, 2009).

Literature suggests that both adhesive and separation forces influence particle entrainment. The adhesive force, influenced by particle properties like size, shape, and surface characteristics, adds complexity to the analysis of this mechanism (Higashitani et al., 2020; Mills, 2016b). Kousaka et al. (1980) delved into the re-entrainment mechanism of small aggregate particles from flat surfaces, revealing that bending stress induced by drag force is crucial in causing re-entrainment (Figure 2-30). The critical diameter of particles prone to re-entrainment is linked to the $-2/3$ power of the velocity gradient at the surface. Matsusaka and Masuda (1996) investigated the re-entrainment of fine particle aggregates from a powder layer in turbulent air flow, both experimentally and theoretically. Their model considers factors such as adhesive strength distribution, powder surface renewal, and time-delay associated with turbulence and aggregate adhesion forces. Experimental data on particle flux versus air velocity and time in steady and accelerated flows validate the model.

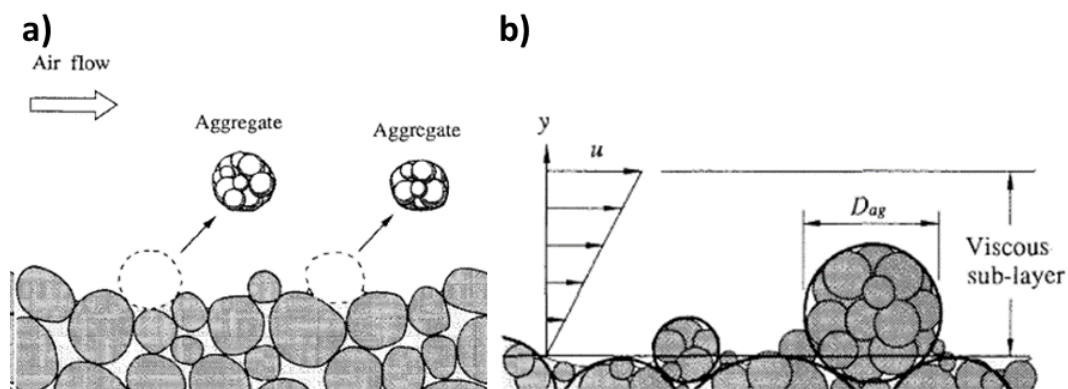


Figure 2-30: Mechanism of aggregate entrainment: a) Illustration depicting the concept of powder entrainment from the surface of a powder layer and b) the entrainment process driven by bending and shearing stress of an aggregate within the powder layer (Matsusaka and Masuda, 1996).

Hartman et al. (2006) conducted experiments to explore the minimum horizontal transport velocity (U_{tr}) and vertical entrainment velocity (U_t) of different particulate materials in pneumatic conveying. Their findings, encompassing materials like silica sand, alumina, ceramsite, dry sewage sludge, and wood shreds, led to the proposal of empirical correlations relating Reynolds numbers to Archimedes numbers for horizontal transport and vertical entrainment. These correlations, fitting well across material variations, contribute valuable

insights for designing and operating solids feeding systems, particularly for unconventional materials like sludge and wood shreds intended for fluidised bed combustion/gasification. Empirical correlations are proposed relating the Reynolds numbers at U_{tr} and U_t to the Archimedes number for horizontal transport and vertical entrainment:

$$Re_{tr} = 4.82Ar^{0.322} \text{ (for horizontal transport)} \quad \text{Equation 2-10}$$

$$Re_{tr} = 0.368Ar^{0.621} \text{ (for vertical transport)} \quad \text{Equation 2-11}$$

These correlations, fitting well across different materials, offer insights for designing and operating solids feeding systems, particularly for unconventional materials in processes like fluidised bed combustion/gasification. These studies provide valuable insights for developing a pneumatic micro-feeder in both research and practical applications in this thesis.

2.9.2 Gas-solid separation – Cyclone separator

Gas-solid separation devices are integral components in numerous industrial processes aimed at removing solid particles from gas streams. These devices are pivotal for environmental compliance, protecting downstream equipment, and maintaining air quality. Common gas-solid separation devices that can be found in the industry are cyclone separators, bag filters, electrostatic precipitators, gravity settlers and venturi scrubbers. The choice of a particular gas-solid separation device is contingent on factors like particle size, concentration, and the unique demands of the industrial process (Mills, 2016). Generally, a particle size larger than 100 μm can be separated by gravity settling, and less than 10 μm will need filtration, wet scrubbing, and electrostatic precipitation (Figure 2-31).

Bag filters utilise fabric bags to capture particles as the gas passes through, with periodic cleaning methods like reverse air or pulse jet cleaning. Foundries, asphalt plants, and metalworking industries commonly employ bag filters. Electrostatic precipitators (ESPs) rely on electrostatic forces to separate particles, charging them and attracting them to collector plates. ESPs are prevalent in power plants, metallurgical processes, and incineration facilities. Gravity settlers, or sedimentation chambers, enable gas to flow through, allowing particles to settle under gravity's influence, commonly used for coarse particle separation. Venturi scrubbers use the venturi effect to create a high-velocity gas stream, injecting liquid to capture particles through impaction, interception, and diffusion. Widely applied in air pollution control, venturi scrubbers find use in chemical plants and metal processing facilities. In pneumatic conveying systems dealing with medium and fine powder, the cyclone separator is frequently employed.

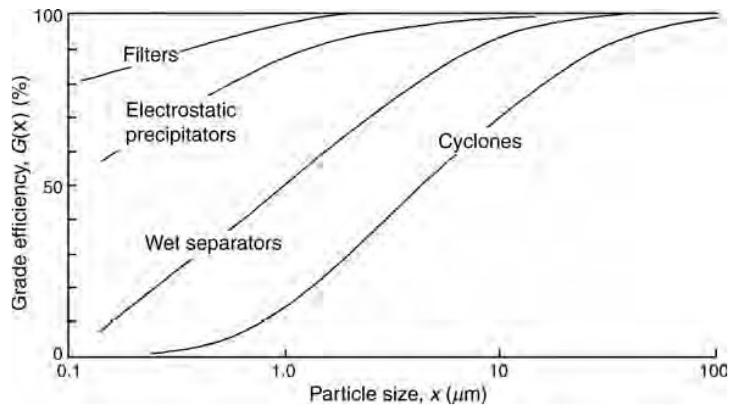


Figure 2-31: Typical grade efficiency curves for gas-solid separators (Rhodes, 2008).

Among these separators, cyclone separators are widely used due to its simple design and low-cost maintenance. Cyclone separators use centrifugal force to separate particles from a gas stream by inducing a swirling motion, causing heavier particles to settle on the outer wall. Widely used in power generation, cement manufacturing, and chemical processing, cyclone separators are effective in particle segregation.

The common cyclone is the reverse flow type, illustrated in Figure 2-32. In the reverse cyclone, the gas-solids inlet is rotated by introducing it tangentially to the cylindrical shell and creating a spiral flow downward. It uses a centrifugal force to separate the gas and particles. The solid particles are then collected from the outlet at the bottom of the separator while the cleansed gas blows in the opposite direction through the top outlet. Increasing the entry velocity or decreasing the cylinder diameter increases the separation efficiency of finer particles ($>10 \mu\text{m}$) (Rhodes, 2008).

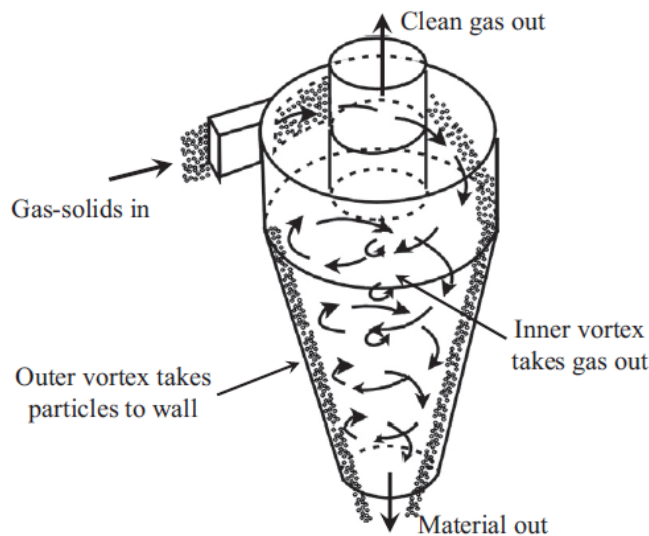


Figure 2-32: Illustration of a reverse flow cyclone separator (Mills, 2016).

The cyclone design is based on Stokes's law to determine the terminal velocity (u_t), which can be expressed as

$$u_t = \frac{g \cdot d_p^2}{18 \cdot \mu_f} \cdot (\rho_p - \rho_f) \quad \text{Equation 2-12}$$

where, d_p is the particle diameter, ρ_p is the true density of the particle, ρ_f is the density of the fluid, μ_f is the viscosity of the fluid, and g is the acceleration of gravity. Therefore, the minimum diameter of the separator (D_s) can be determined by using the terminal velocity:

$$D_s = \sqrt{\frac{4 \cdot Q_f}{\pi \cdot u_t}} \quad \text{Equation 2-13}$$

where Q_f is the volumetric flow rate of air and powder from the fluidised bed. Typical proportions of dimensions of a cyclone can follow the guide in Figure 2-33. For the high collecting efficiency, the cross-sectional area of the inlet, gas outlet and diameter of cyclone can be reduced. The multiple parallel units are also considered to increase the collecting efficiency for fine particles.

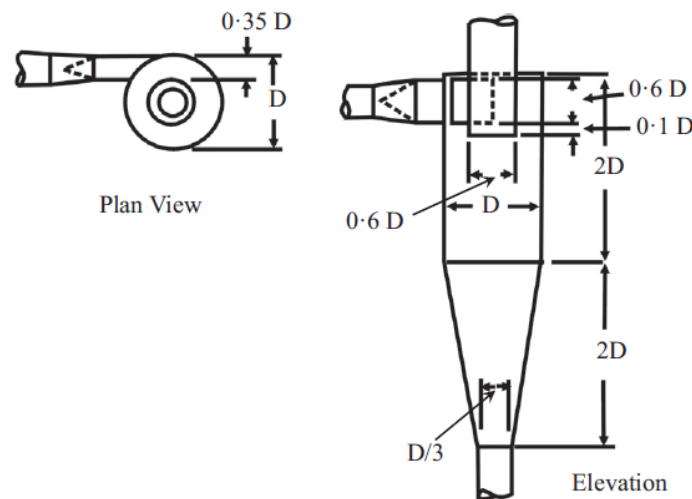


Figure 2-33: Typical proportions of a cyclone separator (Mills, 2016).

Numerous research efforts have been undertaken to enhance the collection efficiency of cyclones by considering factors such as cyclone dimensions and the characteristics of the gas and solid particles or using machine learning and computational fluid dynamics (CFD) to simulate the powder flow (Baltrėnas and Chlebnikovas, 2019; Kashan Bashir, 2015; Park, 2020; Taiwo et al., 2016; Zhou et al., 2019). However, a universally accepted theoretical expression for predicting cyclone performance remains elusive. Figure 2-34 shows the examples of a high-efficiency cyclone and a high-throughput cyclone, revealing a trade-off between efficiency and throughput. The figure highlights a significant drop in cyclone efficiency when dealing with particles smaller than 20 μm . Consequently, to improve both the throughput

cyclone and efficiency cyclone simultaneously, a strategy involving using multiple cyclones in parallel has been introduced.

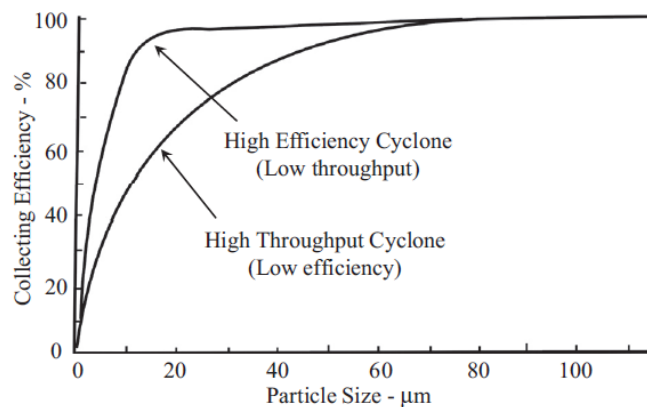


Figure 2-34: Performance curves for typical cyclone separators (Mills, 2016).

Furthermore, when utilising a cyclone, it is crucial to take into account the potential abrasion and breakage of solids. Typically, cyclones are constructed from stainless steel, and at times, they are lined with other materials to reinforce the cyclone body. Solid breakage tends to occur predominantly in larger particles. Hence, when selecting and designing a cyclone as a gas and solid separator, one must carefully consider these factors. This thesis involves designing a cyclone to separate air and solids, enabling the powder settling on a precision balance for the feed rate measurement. The detailed design calculations are outlined in Section 5.2.4.5.

2.9.3 Screw feeder design

Screw feeders have been widely used in industry to feed the bulk solid based on their simple mechanism operation, accurate throughput control and great flexibility of design. The performance of the screw feeder is affected by the feeder geometry and size, the properties of the materials being fed and the operating parameters such as screw rotational speed and angle. The design of the screw feeder is still being studied to understand the powder flow in the screw feeder and optimisation for its application in various applications (Haaker et al., 1993; Hou et al., 2014; Li et al., 2018; López et al., 2020; Minglani et al., 2021). It is important to know the powder flow and behaviour in the screw feeder so that engineers can optimise the hopper, screw and control system and have more accurate control of powder feeding.

Numerical investigations have been undertaken to explore theoretical models governing particle motion during transportation (Carleton et al., 1969; Metcalf, 1965; Mi et al., 1991; Roberts et al., 1992; Wada et al., 1990). Screw pitch, diameter, shaft diameter and clearance between screw and tube influence the feed capacity and power requirement. Roberts et al. (1992) and Haaker et al. (1993) analysed material motion and discharge output in the screw both theoretically and experimentally and found a good match between the theoretical

expression for vortex motion of the grain to the experiment results. Roberts et al. (1992) found that the observed vortex motion of material within a screw undergoes a transition from a compelled vortex at low speeds to a consistent, tangential-speed vortex at higher speeds. Hörmann-Kincses et al. (2022) introduced a workflow to predict the feedability of various powder feeders with distinct configurations. This methodology facilitates early-stage feeder selection for initial process assessment during early-phase development.

The prediction of feed capacity is very good information for the screw feeder design, and it is affected by the screw diameter, inclination and screw and screw speed (Kumar, 2023). Metcalf (1965) and Carleton et al. (1969) provided a fundamental study of screw feeders from the mechanics studies and factors affecting the volumetric flow rate and torque of screw feeders by assuming the gravity and centrifugal forces were negligible and the screw was filled. Roberts (1996), Roberts et al. (1992), and; Roberts and Wiche (1993) analysed the effect of uniform drawdown to the stable feed rate by assuming the force exerted on the screw flights is uniformly distributed along the screw length and further studied the mechanics of screw feeder performance in relation to bulk solid draw down characteristics in the hopper. Haaker et al. (1994 & 1993) investigated the improvement of screw geometry for better drawdown performance and provided two theoretical calculations for volumetric efficiency based on deformation in the bulk solid and plug flow of the bulk material.

A comprehensive investigation by Carleton et al. (1969) delved into the factors influencing the performance of screw feeders, including rotation speed, screw diameter, screw pitch, and degrees of fill, using sand, gravel, and calcite. The experimental results were compared with theoretical predictions, revealing that experimental feed rates surpassed theoretical projections. Notably, variations were more pronounced at higher pitch and diameter ratios (p/d), especially when dealing with cohesive materials. Bates (1969) also introduced the theoretical model for the motion of particles as a function of screw dimensions and the angle of friction of bulk solid on the flight face of a screw. This paper also introduces the concept of mean radius for computing volumetric efficiency and transported volume. Bates in 1986 discussed the effect of the flow pattern in the hopper on the screw feeder (Bates, 1986). Wada et al. (1990) further investigated the transportation mechanism inside of screw by studying the screw rotating speed and pressure of material inside of the hopper and introduced a model on the required power and feed rate (Figure 2-35):

$$V_F(r) = \frac{P}{2\pi r} \left(\frac{2\pi N r}{60} - V_r(r) \right), \quad \text{Equation 2-14}$$

where V_F is the velocity of V_A axial direction, and V_A is particle motion direction velocity, P is the pitch, N is rotation speed, r is radius and V_r is the rotation velocity of V_A .

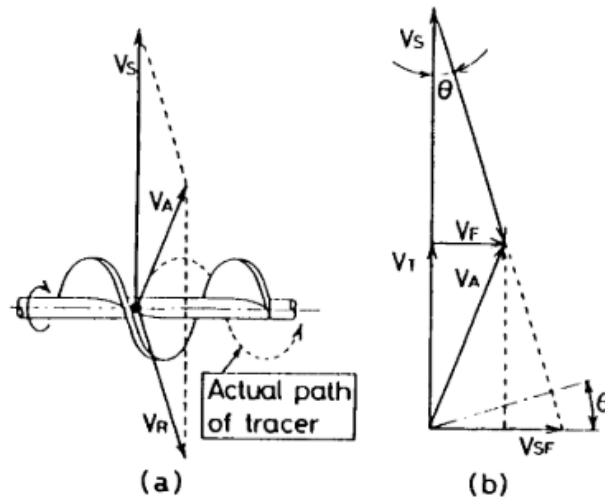


Figure 2-35: The velocity diagram for particle (Wada et al., 1990).

Carleton's (1972) contribution, focusing on the free-discharge flow rate of granular solids from hoppers, complements the contemporary understanding of critical orifice dynamics. The equation derived from Carleton's work considers multiple forces acting on particles, providing a successful approach for modelling granular flow rates from hoppers, particularly in cases where wall friction forces become significant. This equation considers the fine particles sensitive to the air flow returning from the discharge point and opposing the material flow.

$$\frac{4V_0^2 \sin\theta}{D} + \frac{15\rho_{air}^{1/3} \mu_{air}^{2/3} V_0^{4/3}}{\rho_p d_p^{5/3}} = g, \quad \text{Equation 2-15}$$

$$\dot{m} = \rho_b A V_0, \quad \text{Equation 2-16}$$

where V_0 is the average velocity of solid discharge, ϑ is the angle of hopper. This knowledge is paramount for designing powder handling systems, ensuring reliable hopper discharge, and ultimately enhancing the efficiency of dosage processes.

Other studies investigated theoretical models to predict the torque requirement for single screw feeders (Bates, 1969; Dai and Grace, 2008; Yu and Arnold, 1997). Dai and Grace (2008) developed and validated a theoretical model to predict the torque requirements of a screw feeder for feeding biomass materials. By analysing the mechanics of the bulk solid within a screw pocket and the forces acting on the different surfaces, they estimated the torque contributions from components like the shear surface, core shaft, trailing flight, and choke section (Figure 2-36). Key parameters influencing torque include vertical stress, clearance, compression, and wall friction. The model demonstrates good ability to predict experimentally measured torque and power for feeding various woody biomasses like wood pellets, sawdust, and hog fuel. The analysis highlights the significant contribution of the choke section to torque requirements.

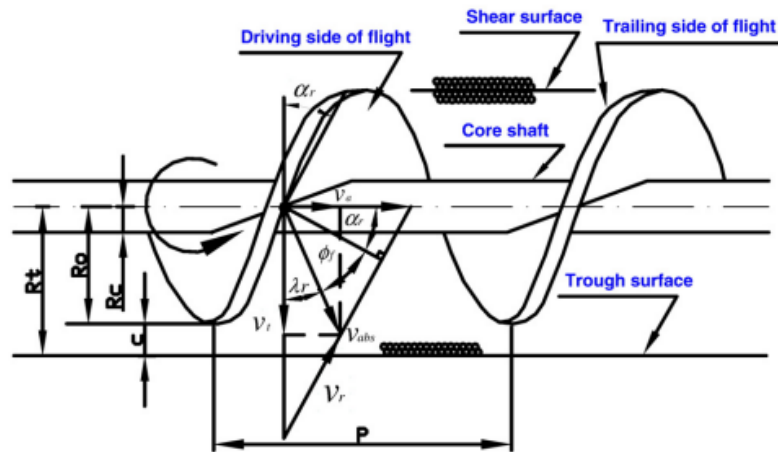


Figure 2-36: Five boundary surfaces in a screw pocket (Dai and Grace, 2008).

Nevertheless, theoretical models made certain assumptions that restrict their accuracy and hinder their ability to address effects such as cohesion and adhesion (Minglani et al., 2020). Discrete element method (DEM) currently have been widely used in predicting the powder behaviour in e.g., blenders, feed frame (Sierra-Vega et al., 2019) or roller compaction (Cartwright et al., 2013; Hanson, 2018; Jaspers et al., 2021; Mazor et al., 2018; Rogers et al., 2013; Scheibelhofer et al., 2013; Simonaho et al., 2016).

Numerous DEM simulation studies have delved into modelling intricate feeding processes, including feed frames for presser and roller compaction. In a study by López et al. (2020), DEM was applied to investigate the impact of increased cohesion on continuous pharmaceutical powder conveying. They calibrated paracetamol properties and analysed adhesive stiffness (K_{adh}) and impeller rotation rates. They found that higher K_{adh} enhanced particle velocity in the conveying barrel and hopper. Maintaining constant K_{adh} while varying speeds increased overall particle velocity. The study explored power consumption and identified arching at $K_{adh} > 0.5$, affecting particle structures and feed consistency. Inconsistencies in flow were linked to improper screw pitch filling, impacting mass flow rate. The study proposed supporting findings on friction's minimal effect on powder flow consistency reported by Leung et al. (2017) using DEM simulation tools.

Similarly, Cundall and Strack (1979) used DEM for predicting powder flow behaviour in screw feeders for bulk materials handling. Subsequent studies by Moysey and Thompson (2005), Hou et al. (2014), and Orefice and Khinast (2017) applied DEM to analyse particle motion in screw feeders, with Hou et al. (2014) explicitly investigating cohesive powders. Owen and Cleary (2009) utilised DEM simulations to explore the impact of operating conditions on screw conveyor performance, providing detailed insights into particle speeds, mass flow rate, energy dissipation, and power consumption. DEM enables a close estimation of particle behaviour under various operational conditions, allowing for a thorough comparison between theoretical

relationships and experimental data to understand flow patterns in different sections of screw feeders.

2.9.3.1 Hopper Design

A hopper is used to store and supply feed material. The design of the hopper is often underestimated as it can be affected by the powder properties and the quantity of materials to be handled (Schulze, 2007). One common problem is that powder flows through the hopper discharge orifice. Many studies have been done to understand and improve the powder flow from the hopper. Jenike (1964) categorised the flow in hopper as mass flow hoppers and core flow hoppers. In mass flow, all powder in the hopper is in motion during discharge (Figure 2-37a). Core flow is the moving solids forming a channel to the hopper outlet and stationary solids remaining around the walls (Figure 2-37b). However, for the feed delivery system, a uniform flow hopper is preferred to ensure a smooth flow of material supply to the screw. In mass flow, the powder motion is uniform and steady state and the bulk density of the discharge powder is constant, providing a consistent powder flow rate. However, the mass flow is only possible when the wall friction is very low or at a very steep wall hopper. The flow pattern is significantly influenced by the powder properties and hopper design. In addition, the arching, segregation, and residence time distribution should be considered in the hopper design stage.

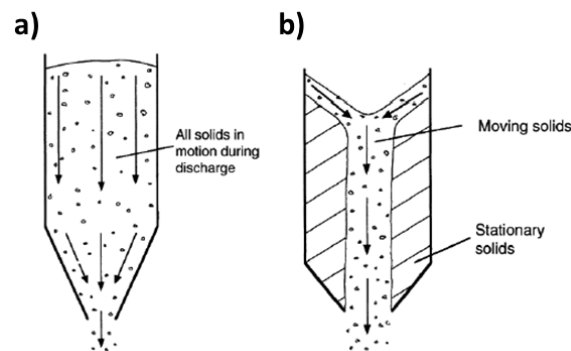


Figure 2-37: Flow profiles: a) mass flow hopper and b) funnel flow hopper (Rhodes, 2008).

There are numerous ways in which the discharge rate from a hopper can be determined theoretically, with many relationships between material properties and the rate of discharge being available in the literature (Beverloo et al., 1961; Carleton, 1972; Mehos, 2023, 2020; Rhodes, 2008). The outlet of discharge of a powder under gravity depends on many parameters such as powder properties, outlet shape and size, and hopper inclination (Demming and Mehring, 1929). Empirical and dimensional analysis has been conducted in many works of literature. Beverloo et al. (1961) introduced a well-known model for a circular outlet for coarse powder (>400 μm). The equation is given by:

$$\dot{m} = C\rho_b\sqrt{g}(D - kd)^{2.5}, \quad \text{Equation 2-17}$$

where $C = 0.55-0.65$, ρ_b is the bulk density, and D is the orifice diameter, d is the particle diameter and $k = 1.5 -3.0$ for free-flowing coarse powder. k is dependent on the particle shape (1.6 for spherical particles and 2.5 for non-spherical particles). Nedderman et al. (1982) presented a basic equation for estimating the mass flow rate of granular powders based on Hagen (1852)'s study and suggested the equation should be used for particle diameters in the range 0.4 mm to $D/6$. British Materials Handling Board (McGlinchey, 2009) suggests the equation should consider the hopper inclination (θ) through the factor k_θ ; therefore, the equation is modified and expressed by:

$$\dot{m} = 0.58\rho_b\sqrt{g}(D - kd)^{2.5}k_\theta \quad \text{Equation 2-18}$$

$$k_\theta = (\tan\theta)^{-0.35} \quad \text{for hopper inclination } \theta < 45^\circ$$

$$k_\theta = 1 \quad \text{for hopper inclination } \theta \geq 45^\circ$$

Other modifications, such as Artega and Tüzün (1990), modified the Beverloo equation to consider a bidisperse mixture:

$$\dot{m} = C\rho_m\sqrt{g}(D - k_md_m)^{2.5}, \quad \text{Equation 2-19}$$

where ρ_m is mixture density, k_m is a fitted coefficient of mixture particle, and d_m is a mixture diameter. Johanson (1965) included the cohesive strength to determine the hopper outlet size for the desired discharge rate of a coarse cohesive bulk material:

$$\dot{m} = \rho_b A \sqrt{\frac{Dg}{2(1+m)\tan\theta} \left(1 - \frac{ff}{ff_a}\right)}, \quad \text{Equation 2-20}$$

where m is equal to 1 for conical hopper and 0 for wedge hopper. ff signifies the flow factor, which is the ratio of the major principal stress to the stress on the abutments of an arch, whereas ff_a represents the actual flow factor.

Bulsara et al. (1964) carried out a study of the effect of air pressure on the bulk flow rate and found that the mass flow rate is related to the differential pressure by:

$$\dot{m} \propto \Delta p^{0.5}. \quad \text{Equation 2-21}$$

McDougall and Knowles (1969) modified this relation by considering the adverse pressure gradient required to prevent flow, ΔP_0 , and expressed the equation:

$$\dot{m} \propto (\Delta P + \Delta P_0)^{0.5}. \quad \text{Equation 2-22}$$

Crewdson et al. (1977) considered the influence of air effects on particles and modified the particles' acceleration, considering the influence of an interstitial pressure gradient as an additional force in addition to the gravitational force causing acceleration due to weight ($\rho_b g$). Consequently, an adaptation of the Beverloo correlation for hoppers was derived from this analogy, resulting in the following modification:

$$\dot{m} = \dot{m}_B \left(1 + \frac{\Delta P}{\rho_b g r_o}\right)^{0.5}, \quad \text{Equation 2-23}$$

where r_o is the radius of the free fall arch. Verghese and Nedderman (1995) investigated the effect of a negative pressure gradient and noted that a reduction in particle size led to an increase in the pressure gradient near the orifice. Subsequently, this observation introduced a model to predict the mass flow rate:

$$\dot{m} = \dot{m}_B \left(1 + \frac{\lambda}{\rho_b g d^2}\right)^{0.5}. \quad \text{Equation 2-24}$$

Here, λ represents a function associated with the compressibility of the material and gas properties. Other researchers, Donsì et al. (2004) and Barletta et al. (2007), proposed models to consider the cohesive powder.

Investigations by Baserinia et al. (2016) and Baserinia and Sinka (2018) have also deepened our understanding of critical orifice dynamics. These studies explored the impact of applying vacuum or negative pressure differentials on initiating flow from arching powders in hoppers. Noteworthy findings indicate that even minimal pressure reductions (100-300 Pa) can significantly decrease the critical orifice size required for flow, demonstrating the sensitivity of powder flow initiation to pressure variations.

Moreover, dimensional analysis models derived from these studies have provided predictive insights into the pressure needed for flow initiation (Baserinia et al., 2016b; Baserinia and Sinka, 2018). These models incorporate crucial parameters like powder density, particle size, bed height, and orifice diameter. The agreement between these models and experimental results on pharmaceutical powders underscores their utility in designing reliable hopper discharge systems.

Additionally, pneumatic discharge aids such as air injectors, along with mechanical discharge aids like vibrators or agitators, can improve the flow during discharge (Figure 2-38). It's important to note, however, that the incorporation of these elements will introduce added complexity to the prediction process.

Tardos and Lu (1996) and Zhang et al. (2010) introduced vibration to the hopper to enhance screw fill efficiency and improve feed rate consistency. Heinrich et al. (1998) invented fitting an internal and external paddle agitation on a flexible wall to improve hopper flow. Papazoglou and Pyle (1970) utilised air assistance to improve powder flow. Engisch and Muzzio (2015) investigated the impact of hopper refill on feed rate variability. Other studies have employed DEM simulations to model these intricate systems, contributing to a better understanding of the influence of process parameters on feeder performance (Datta et al., 2008; Hemph et al., 2019; X. Huang et al., 2022; Ketterhagen and Hancock, 2010).

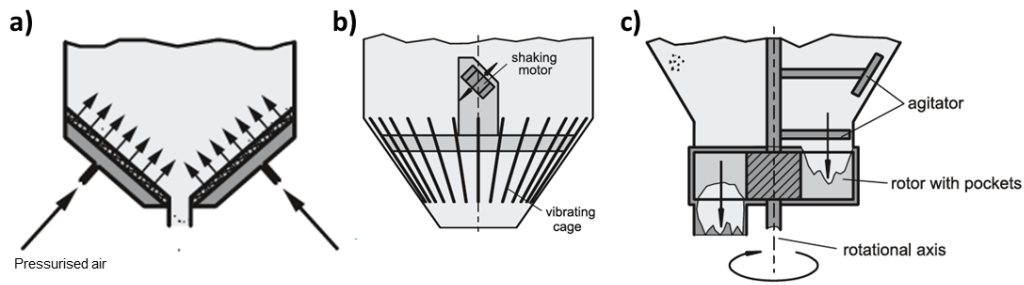


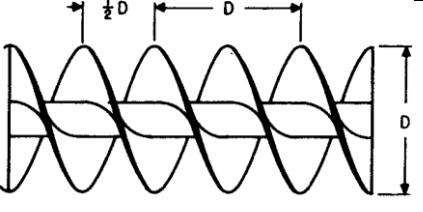
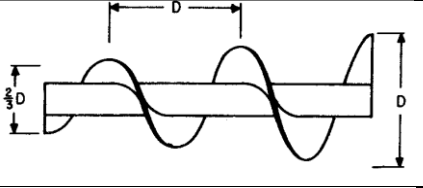
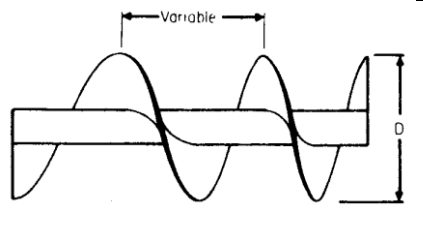
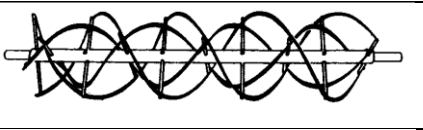
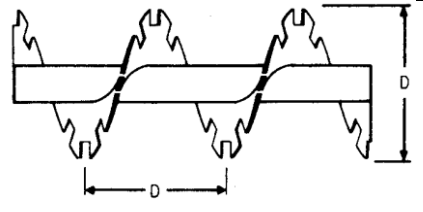
Figure 2-38: Flow promoting devices: a) pneumatic discharge aids, b) vibrating insert, c) rotary valve with vertical axis and agitator (Schulze, 2007).

2.9.3.2 Screw design

The screw design is an essential class in the screw feeder design or screw feeder selection as it influences the cost of fabrication, accurate throughput control, and volumetric efficiency. The selection or design of a screw depends upon many factors, such as the properties of the material being fed, screw geometry and size, and operating parameters. Theoretical models have been developed to describe the motion of particles (Bates, 1986). Kumar (2023) indicated that shaftless screws result in smooth movement of bulk materials without clogging and be able to handle high moisture content materials or sticky and sluggish materials. Also, shaftless screw provides higher conveying efficiency and less friction on the particles (Kumar, 2023).

A large number of screws are used in various industries. The screws are designed to address varying characteristics of materials fed. Table 2-8 describes different types of screw design used in the industry. The selection of the screw type of the screw feeder is a function of the powder properties such as particle size, bulk density, tap density, and flowability.

Table 2-8: Common screw design (adapted from Conveyors Incorporated, 2023).

Single flight pitch	The most common type of screw configuration. Frequently used to convey or feed powder, different pitch is used for the material.	
Tapered pitch	For withdrawing the material from the hopper.	
Variable pitch screw	For withdrawing the material from the hopper or controlling the powder flow.	
Multiple ribbon flight	For mixing purpose and handling sticky materials.	
Cut flight	It is used in a process where alight-moderate agitation of material or aeration of material is required.	

2.9.3.2.1 Screw blade angle and pitch

Bates (2000) provides comprehensive guidance on the design, selection, and application of screw feeders. A crucial consideration to prevent logging is to ensure that the pitch exceeds one-half the height of the flight, as indicated by the inequality (Mehos, 2018):

$$\frac{P}{(D-d)} \geq 1. \quad \text{Equation 2-25}$$

However, the selection of pitch must also take into account the material properties. For cohesive powders, a larger pitch may be necessary to prevent clogging, while higher speeds may warrant a smaller pitch. The use of a tapered pitch can be advantageous in controlling powder flow. The equation gives the recommended angle (θ) of the screw:

$$\theta = \tan^{-1} \frac{\pi D}{P}. \quad \text{Equation 2-26}$$

Although this equation is considered conservative in its approximation, it acknowledges that surface pressure may be expected to be the largest near the shearing plane at the periphery of the flight. However, it can be used as the start point of the screw angle design.

2.9.3.2.2 Throughput prediction

When designing a screw, predicting the discharge rate is crucial. The flow rate prediction for a screw feeder must consider several factors such as the flow characteristics and bulk density of the bulk material being fed, capacity, the inlet opening of the screw feeder, and the height of bulk materials in the hopper (KWS Manufacturing Company Ltd., 2015; Liu et al., 2020). Drawing inspiration from screw conveyors, the feed capacity (\dot{m}_p) of a screw feeder is determined by the formula:

$$\dot{m}_p = F\rho VC \quad \text{Equation 2-27}$$

F is the cross-sectional area of the feed layer in the tank, V is the axial movement speed of the feed in the tank, ρ is the feed density, and C is the coefficient of inclination. The cross-sectional area of the feed layer (F) is given by:

$$F = \varphi A, \quad \text{Equation 2-28}$$

here φ is the filling coefficient, and A is the cross-sectional area of the rotating screw. The axial moving speed of the feed in the screw (V) is determined by:

$$V = P\omega, \quad \text{Equation 2-29}$$

where P is the screw pitch, and ω is the rotation speed of the screw. Combining Equation 2-27, Equation 2-28, and Equation 2-29, the theoretical maximum feed capacity is expressed as:

$$\dot{m}_p = 60 \frac{\pi}{4} (D^2 - d^2) P \rho \omega, \quad \text{Equation 2-30}$$

where D is the screw diameter, d is the shaft diameter. Considering inclination, horizontal orientation, and powder flowability, a correction factor for the inclination of the screw (C), loading ratio (φ) are introduced, leading to the modified equation:

$$\dot{m}_p = 60 \frac{\pi}{4} (D^2 - d^2) P \rho \omega C \varphi. \quad \text{Equation 2-31}$$

The correction factor for inclination and the loading ratio can be located in Table 2-9 and Table 2-10, respectively. Table 2-9 aligns with the discovery made by Li et al. (2018). An alternative mass flow rate prediction, based on volumetric efficiency (η_v), is expressed as:

$$\dot{m}_p = 60 \frac{\pi}{4} D^2 P \rho \omega \eta_v, \quad \text{Equation 2-32}$$

The discussion of volumetric efficiency (η_v) is elaborated on in the following section.

Table 2-9: The correction factor for screw inclination (PowderProcess.net, 2022).

Inclination (°)	Correction factor, C
0	1
5	0.9
10	0.8
15	0.7
20	0.65
30	0.55

Table 2-10: the loading ratio of the screw according to the flow properties of the solid (PowderProcess.net, 2022).

Material	Min loading ratio	Max loading ratio
Free flowing	0.4	0.45
Average flowability	0.25	0.30
Not free flowing	0.12	0.15

2.9.3.2.3 Volumetric efficiency

The volumetric efficiency is defined as the ratio of the volume of material conveyed in a single screw revolution to the volume of a pitch length at the specified position (Bates, 2000; Yu and Arnold, 1997):

$$\eta_v = \frac{Q_{con}}{\pi P (R_o^2 - R_c^2)}, \quad \text{Equation 2-33}$$

where Q_{con} is volume conveyed per revolution within a pitch, R_o is the outside radius of screw flight, and R_c is the radius of the core shaft. The thickness of the screw flight (t) is disregarded in this equation. Volumetric efficiency is influenced by the rotational motion, including screw geometry and fullness, as well as friction between the bulk solid and the flight surface. According to Roberts (1999), higher volumetric efficiency is achieved with lower screw speed and inclination angles. Figure 2-39 illustrates bulk solid sliding on the screw surface of a flight in a direction related to the angle of friction on the surface and angle of the flight face.

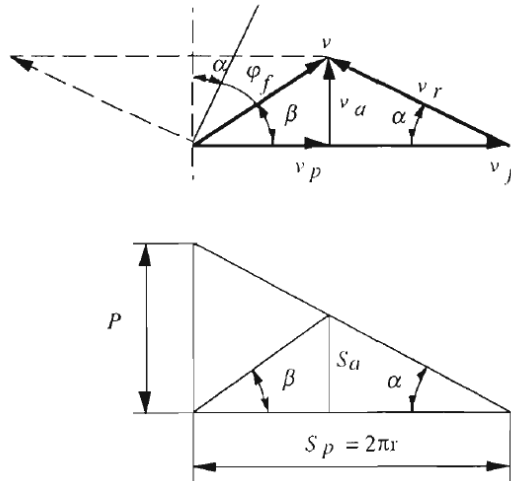


Figure 2-39: Velocity and displacement for material in contact with the flight surface (Yu, 1997).

In the case of the feeder running 100% full, the volumetric efficiency of the material fed can be expressed as:

$$\eta_v = \frac{\tan \beta}{\tan \alpha + \tan \beta}, \quad \text{Equation 2-34}$$

here α is the flight helical angle, and β is the helical angle of bulk material motion. The relationship between α and β is determined by

$$\alpha + \beta = 90^\circ - \phi_f, \quad \text{Equation 2-35}$$

where ϕ_f is the wall friction angle of bulk solid on flight surface. The actual volumetric efficiency can be expressed as:

$$\eta_v = \frac{Q_{act}}{Q_t}, \quad \text{Equation 2-36}$$

where Q_{act} is the actual volumetric throughput, and Q_t is the theoretical maximum throughput. Various factors affect volumetric efficiency, such as rotational speed and friction between the bulk material and the flow channel. Several studies have developed methods for more accurate predictions, including those based on material plug flow (Yu and Arnold, 1997), mean radius (Bates, 1969), or an average ratio of radius to pitch by A.W Robert in 1994 (Yu and Arnold, 1997). DEM is also widely used to simulate powder flow behaviour in screw feeding (Hou et al., 2014; Tanida et al., 1998; Wang et al., 2019; Owen and Cleary, 2009).

2.9.3.2.4 Feed factor

The term "feed factor" in the context of powder feeders or conveyors refers to the amount of material conveyed or fed per revolution (rev) of the feeding mechanism. This factor helps quantify the feeding efficiency and capacity of the feeder. Mathematically, the feed factor (FF) is expressed as:

$$FF = \frac{\dot{m}_p}{\omega}, \quad \text{Equation 2-37}$$

where \dot{m}_p is the material feed rate, and ω is screw rotation speed. This formula expresses the mass of powder the feeder delivers per revolution. The feed factor can be influenced by various factors, including the design of the feeder, the characteristics of the powder being conveyed, and the operating conditions (Tahir et al., 2020). The feed factor is used as a valuable metric for assessing and optimising the performance of screw feeders in screw feeder design, especially in the gravimetric feeder design.

2.10 Summary of gaps in literature

The preceding literature study highlights several gaps/challenges regarding micro-feeders in drug manufacturing. Here is a summary of the identified gaps/challenges:

Challenges with Cohesive Materials: Handling cohesive materials, especially in small quantities (under 50 g/h), poses a substantial challenge. Cohesion leads to poor flowability, causing adherence to equipment surfaces and reduced feeder performance (Blackshields and Crean, 2018; Sacher et al., 2021; Stranzinger et al., 2023; Wang et al., 2018a).

Limited Focus on Micro-Feeding: While there is extensive research on optimising feed consistency at higher feed rates, there is a significant gap in the literature concerning micro-feeding. The available works often concentrate on achieving consistent feed rates at higher levels (0.5 kg/h), neglecting the challenges associated with micro-feeding (Besenhard et al., 2017; M O Besenhard et al., 2015; Qi et al., 2011; Sacher et al., 2020).

Long-term operation: The existing literature reveals a deficiency in comprehensive solutions that adequately address the intricate challenges associated with handling cohesive materials, achieving precise dosing in small quantities, and ensuring sustained operational stability over the long term (Bekaert et al., 2022; Blackshields and Crean, 2018; Burcham et al., 2018; Teżyk et al., 2016).

Refill Issues: Refilling gravimetric feeders presents a challenge, as the transition from gravimetric to volumetric modes during the refill process can cause disruptions, affecting the bulk density and, consequently, feed consistency (Engisch and Muzzio, 2015; Hanson, 2018; Janssen et al., 2022; Peterwitz et al., 2022).

Hopper Design Influence: The design of the feeder's hopper is crucial, significantly impacting powder flow to the screw fill and contributing to inconsistent feeding. Hopper level also influences consistent feeding (Fernandez et al., 2011; Hemph et al., 2019; X. Huang et al., 2022).

Variability and Standard Deviation: The need for a micro-feeder with a small standard deviation in feed rate is emphasised. Variations in the feeding process must be minimised for accurate and consistent performance (Blackshields and Crean, 2018; Hanson, 2018; Jones-Salkey et al., 2023; F. Stauffer et al., 2019; Teżyk et al., 2016).

Reliability and Repeatability: Achieving reliability and repeatability, especially in volumetric feeding, is challenging due to powder compression. The existing designs may struggle to meet these goals (Gad, 2007; Janssen et al., 2022; Jaspers et al., 2021; Markarian, 2022).

Real-time Feedback and Process Analytical Technology (PAT): Incorporating real-time feedback control and PAT for more accurate and consistent feeding is identified as a gap in the literature (Y. S. Huang et al., 2022; Pauli et al., 2020; Ruiz-Carcel et al., 2018; Singh et al., 2015).

Powder Flow Behaviour Modelling: Despite numerous studies attempting to predict powder flow behaviours using Discrete Element Method (DEM), a gap persists in achieving high accuracy in modelling the complex powder flow dynamics within feeders (Hou et al., 2014; López et al., 2020; Orefice and Khinast, 2017; Wang et al., 2019).

Integration with Process Equipment: Ensuring seamless integration of micro-feeders with other processing equipment in pharmaceutical production lines is essential for efficient operation (Pauli et al., 2020; Sacher et al., 2020; Teżyk et al., 2016).

In summary, the gaps in the literature suggest a need for comprehensive and innovative solutions in the design and development of micro-feeders, particularly in addressing challenges associated with cohesive materials, small quantities, and long-term operational accuracy.

3 Material and Material Characterisations

3.1 Particles shape and particle size distribution measurement

A dynamic imaging instrument, QIC/PIC (VIBRI/L, Sympatec GmbH, Germany), was used to determine the average particle size (D_{50}), sphericity (S_{50}) and particle size distribution (PSD). QIC/PIC is a morphological characterisation tool for particle size and shapes measurement from 0.5 micrometres to several millimetres. It uses a microscope to capture high-resolution images of individual particles coupled with an image analysis system to give the number distribution of size and shape by calculating various diameters from the particles' projected image. In order to efficiently disperse the particles, 2 g of material was dispersed using a RODOS powder disperser with a speed of 100 m/s in this study. All measurements were performed in triplicate. The result is summarised in Table 3-3.

3.2 Powder density

True density (ρ_p) is measured by a gas pycnometer (MicroUltrapyc 1200, Quantachrome instrument, Graz, Austria). The pycnometer employs Archimedes' principle of fluid displacement and the technique of gas expansion (Boyle's Law) to measure the actual volume of solid materials using gas to penetrate fine pores. First, the powder was placed into a 1.0725 cm³ stainless steel sample cell. The powder's sample cell was then placed on a precise balance, and the net powder weight was recorded. The sample cell was placed in the measuring chamber of the gas pycnometer, and recorded the average volume. True density is defined as the particle mass divided by the volume of the particle occupied.

$$\rho_p = \frac{W_p}{V_p}, \quad \text{Equation 3-1}$$

where W_p is the particle weight, and V_p is the volume of the particles. All samples were measured in triplicate.

Bulk density (ρ_b) is defined as the ratio between the mass of a given bulk solid and the occupied volume. The bulking properties of a powder are dependent upon the preparation, treatment and storage of the sample. Particles can be packed to have a range of bulk densities, and the slightest disturbance of the powder bed may result in a change in bulk density. Thus, the bulk density of a powder is often challenging to be fixed. USP<616> provide three guideline procedures to measure the bulk density into a graduated cylinder (Method I), a volumeter (Method II) and a stainless-steel measuring vessel (method III). In this study, Method I was chosen to measure the bulk density. Bulk density was measured using a volumetric cylinder and a precise balance. A precise balance weighs a fixed weight of powder. The powder was then freely placed into a graduated glass cylinder and record its occupied

volume. In this study, the bulk density is measured following the USP<616> method I. The bulk density was then determined as

$$\rho_b = \frac{W}{V_b}, \quad \text{Equation 3-2}$$

where W is the measured value of free-loaded powder weight, V_b is the volume of powder occupied in the graduated glass cylinder. The average of three replicates was used to determine the bulk density of the sample powders.

Tapped density (ρ_t) was determined by using Autotap (AT-6, Quantachrome instrument, Graz, Austria) following the USP<616> method II. Tap density is the mass of the powder divided by the volume the powder occupies after tapping. Tapping is done by shaking the powder under controlled conditions to obtain packing. The tapping density can be determined as

$$\rho_t = \frac{W}{V_t}, \quad \text{Equation 3-3}$$

where V_t is the volume that powder occupies after tapping. The average of three replicates was used to determine the tapped density of the sample powders.

3.3 Flowability

3.3.1 Hausner ratio and Carr Index measurement

Hausner ratio (H) was determined by calculating the ratio of tapped density (ρ_t) to bulk density (ρ_b), as per Equation 2-1. We conducted bulk and tapped density measurements, as detailed in Section 3.2, and employed Equation 2-1 to derive the Hausner ratio. Referring to Table 2-6, we interpreted the obtained Hausner ratio to provide insights into the flowability of the powder under investigation.

3.3.2 Flow function coefficient measurement

A Brookfield Powder Flow Tester (PFT) was used to assess the tested materials in this study. Material is loaded into the annular tray and evenly levelled, and then a cupped lid of known mass is applied. The Brookfield PFT is able to measure the shear stress generated via a reaction torque sensor attached to the stationary lid. A load is applied to the shear cell lid, consolidating the material to a known and repeatable bulk density. Material is then sheared to failure through the rotation of the annular tray round a central point at a constant velocity. The shear stress generated is recorded to increase with time until a steady state is reached; at this point, a shear plane is generated and the material exhibits incipient flow. Once this point has been reached, the rotational direction is reversed and the material is returned back to its original state. This initial shearing procedure of material is referred to as pre-shear and is repeated after each subsequent load has been applied and the material has been sheared.

Repeating the pre-shear procedure allows a reliable and known bulk density to be attained before shearing under each subsequent normal load. After the measurement of the pre-shear point has been carried out, the load on the shear cell lid is reduced, the material is sheared, and the shear stress required to generate incipient flow is recorded. The rotation of the annular tray is then reversed as with the measurement of the pre-shear point to return the material back to its original condition. The material is reconsolidated using the pre-shear load and then sheared to failure. This process is repeated with a number of normal loads in order to generate a yield locus made up of normal stress and shear stress points. A reliable result can be generated with as few as three normal loads. That is, if the normal loads are sufficiently spaced apart to generate shear planes in different regions of the bulk material. Essentially, the greater the normal load applied, the further down into the bulk material the shear plane will be generated. Therefore, using sufficiently spaced loads ensures new shear planes are created under each normal load applied. Using normal loads that are only marginally spaced will generate shear planes in broadly the same region.

In this study, a shear cell tester was also employed to evaluate the cohesive strength, internal friction, compressibility, and wall friction of various types of powder across a range of pressures. The flow function coefficient (ff_c), which is calculated by dividing the major principal consolidation stress (σ_1) by the unconfined yield strength (σ_c) of the powder, was determined in order to assess the flowability of each sample. The flow function coefficient (ff_c) can be calculated using the equation:

$$ff_c = \frac{\sigma_1}{\sigma_c}, \quad \text{Equation 3-4}$$

which is widely accepted as the main parameter for designing mass flow hoppers and assessing the flowability of powders. Higher ff_c values indicate better flowability. To ensure consistency, the samples were prepared in accordance with the Brookfield equipment handbook, and all experiments were conducted in triplicate using the default mode, which produced five shear wrappings for each sample. Based on the Jenike flow function coefficient, the flowability of the powders was classified into various categories, which are presented in Table 3-1. This table provides a useful guideline for the flowability of powders and has thus been used extensively throughout our research endeavours. The flow function diagram of tested materials in this study can be found in Figure 3-1.

In low stress and/or dynamic environments, such as in the presence of an aerated powder state, it diminishes the applicability of shear cell testing. The aforementioned testing method for powder flowability is considered less valuable in such conditions (Bruni et al., 2007; Clayton, 2019; Pingali et al., 2009).

Table 3-1: A table of flow function coefficient and flowability of solid powder indicator, adapted from (McGlinchey, 2009)

Flow function coefficient	Flowability
$ff_c < 1$	Non-flowing
$1 < ff_c < 2$	Very cohesive
$2 < ff_c < 4$	Cohesive
$4 < ff_c < 10$	Easy-flowing
$10 < ff_c$	Free-flowing

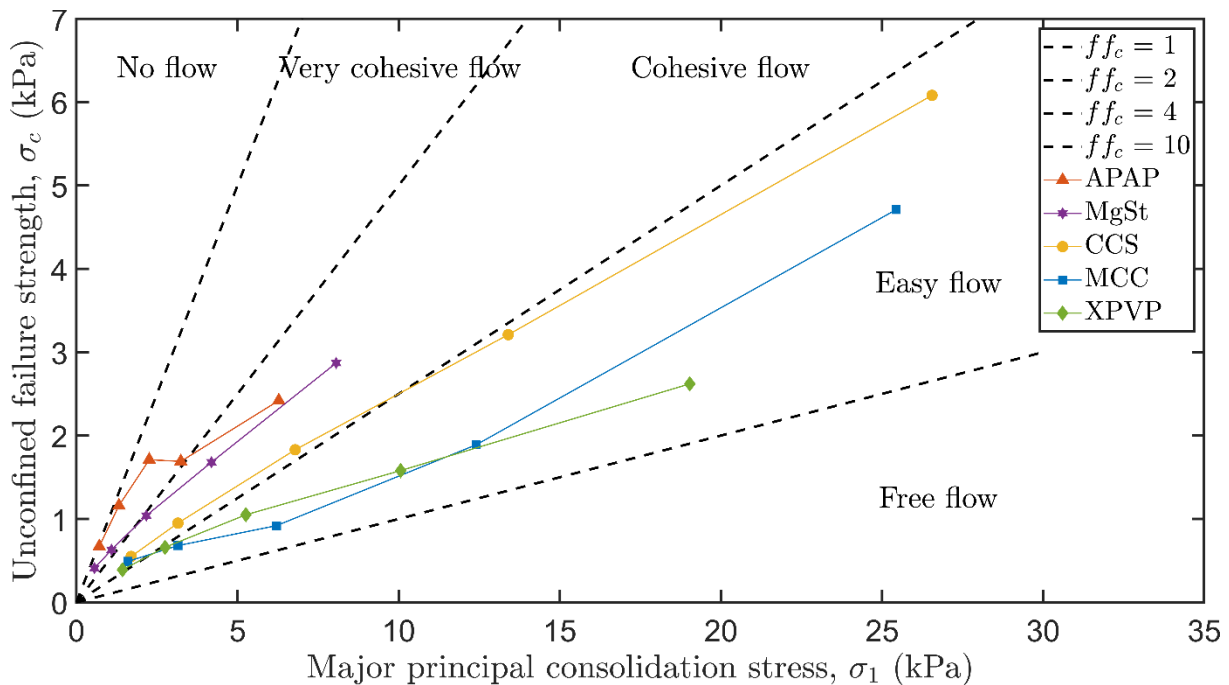


Figure 3-1: Flow function of investigated pharmaceutical powders measured using a PFT shear cell tester.

3.4 Materials and characterisation results

It is widely acknowledged that the characteristics of the powder significantly impact the feeder's effectiveness. Therefore, the development of a new design must encompass a broader range of powder properties, accommodating materials ranging from easy-flowing to poor-flowing substances.

A wide range of powder properties was used to assess the performance of the feeder design in this study. The following five materials were used in this study: microcrystalline cellulose (MCC, VIVAPUR 112 from JRS pharma, Germany), croscarmellose sodium (CCS, SDW-802, JRS pharma, Germany), crospovidone (XPVP, Microgranule Grade, Kollidon® CL, BASF), magnesium stearate (MgSt, LIGAMED MF-2-V from Peter Greven Nederland C.V., Nederland)

and an active pharmaceutical ingredient, paracetamol (APAP, 1680 Special Granular Grade, Ph Eur Powder from Mallinckrodt Pharmaceuticals, Ireland). These materials were selected also based on a raw material database (Snick et al., 2018) and literature (Table 3-2) and details are discussed below.

Table 3-2: Pharmaceutical material selection and its feed rate in literatures.

Material	Function	Feeder model	Feed rate (kg/h)	Operating principle	Reference
MCC	Diluent/Filler	K-Tron KT20	10.64 – 16.64	Coarse concave or coarse auger	(Engisch and Muzzio, 2014)
XPVP	Disintegrant	K-Tron MT12	0.480 – 0.750	Fine concave	(Engisch and Muzzio, 2014)
CCS	Disintegrant	K-Tron KT20	0.5 – 0.84	Coarse concave	(Hanson, 2018); (Bostijn et al., 2019); (Fathollahi et al., 2020)
MgSt	Lubricant	K-Tron MT12	0.177 – 0.278	Coarse concave	(Engisch and Muzzio, 2014); (Bostijn et al., 2019)
APAP	API (average particle size of 45 µm)	K-Tron KT20 and KT35	0.1 – 5.0	Concave style twin screws were used with two different size pitches, coarse and fine	(Hanson, 2018);
		MT12	0.1 – 0.55	Concave coarse screws (D 12mm and Pitch 5.75 mm)	(Bostijn et al., 2019);
		Schenck-Accurate	0.9 – 1.35	Helix	(Vanarase and Muzzio, 2011)

The selected MCC is a common material used as a filler in typical tablet formulations. Due to its easy-flowing nature and large particle size, it is extensively employed to examine feeder performance (Hörmann-Kincses et al., 2022) and other equipment, such as die fill (Mills and Sinka, 2013; Schneider et al., 2007). In this study, it is chosen for initial testing and understanding of the system, aiming to adapt the system allowing it to handle different powder properties.

XPVP serves as a disintegrant in tablet formulations, exhibiting powder properties similar to the selected MCC but with slightly inferior flowability. As a screw feeder can relatively feed it with no significant problems, it is selected for testing and comparison purposes with market screw feeders. Typically, a concentration of 2-5%wt/wt of XPVP is utilised in tablet production, with tablet presses yielding anywhere from 8,000 to 2,000,000 tablets per hour. For a 500 mg

tablet, such as an example, the XPVP feed rate can range from 80 to 200 g/h, and a lower flow rate may be desired for the smaller tablets or even mini-tablets (Sierra-Vega et al., 2019; IPharmachine, 2023).

CCS is a commonly employed disintegrant in oral pharmaceutical formulations, offering comparable flowability but smaller particle size and higher bulk density than XPVP. Typically used at 2%wt/wt in direct compression and 3% in wet granulation, CCS has been extensively studied in various pharmaceutical contexts (Augsburger and Hoag, 2008; Hickey, 2001; Narang and Badawy, 2019; Shaikh et al., 2018; Engisch and Muzzio, 2014). In addition, both XPVP and CCS have been previously employed in the literature to assess the performance of new powder feeder designs (Fathollahi et al., 2020).

MgSt, widely employed as a lubricant in tableting, serves the dual purpose of functioning as a flow agent. Its propensity to undergo easy shearing enables the formation of a protective barrier between ingredients and machinery, preventing cohesion during the formulation process. However, these beneficial properties also present challenges in handling, as MgSt is known to be shear-sensitive and can lead to equipment coating (Engisch and Muzzio, 2014; F Stauffer et al., 2019). The situation worsens when the API or excipient mass fraction is lower. For instance, a typical lubricant mass fraction of 0.2% translates to 40 g/hr (Nagy et al., 2020).

The majority of APIs exhibit poor flowability and highly cohesive characteristics. APAP, a widely utilised drug, is particularly known for its highly cohesive and electrostatic nature, leading to challenges in feeding and a notable reduction in the accuracy of powder flow rate (Vanarase and Muzzio, 2011; Bekaert et al., 2021). It is frequently chosen as a representative material to assess the performance of designed powder feeders when handling poorly flowing materials and typical powder properties of APIs, making it a pertinent choice for this study (Seppälä et al., 2010). Notably, the amount of API feeding typically ranges from 0.2 to 1.0 kg/h, balancing considerations of material cost and safety (Engisch and Muzzio, 2014; F Stauffer et al., 2019). For HPAPI feeding, lower feed rates are preferred due to safety concerns and the cost of material (Besenhard et al., 2017; Fathollahi et al., 2020). In laboratory or small clinical trials, minimising material usage is desirable to conserve resources, time, and enhance the efficiency of dosage form development (Wang et al., 2017b). Table 3-3 summarises the material's powder properties.

Table 3-3: Powder properties of materials investigated to assess the performance of the designed micro-feeders.

Powders	D_{10} (μm)	D_{50} (μm)	D_{90} (μm)	VMD (μm)	S_{50} (-)	True Density (g/cm^3)	Bulk Density (g/cm^3)	Tapped Density (g/cm^3)	Hausner ratio (-)	Flow function coefficient (-)	Flowability*
Microcrystalline cellulose (MCC)	56.6 \pm 4.0	139.4 \pm 11.7	238.9 \pm 6.2	144.6 \pm 8.4	0.63 \pm 0.007	1.542 \pm 0.001	0.314 \pm 0.036	0.447 \pm 0.036	1.43 \pm 0.061	4.75 \pm 0.74	Cohesive
Crospovidone (XPVP)	30.1 \pm 0.1	103.4 \pm 0.3	244.0 \pm 1.0	124.5 \pm 0.5	0.73 \pm 0.001	1.183 \pm 0.003	0.334 \pm 0.001	0.451 \pm 0.001	1.35 \pm 0.000	4.22 \pm 0.32	Cohesive
Croscarmellose Sodium (CCS)	29.9 \pm 0.1	50.0 \pm 0.1	74.2 \pm 0.1	51.8 \pm 0.1	0.72 \pm 0.003	1.537 \pm 0.010	0.529 \pm 0.001	0.715 \pm 0.001	1.35 \pm 0.000	3.79 \pm 0.48	Cohesive
Magnesium Stearate (MgSt)	7.1 \pm 0.2	24.4 \pm 0.6	48.4 \pm 0.6	26.9 \pm 0.7	0.80 \pm 0.001	1.074 \pm 0.001	0.207 \pm 0.007	0.349 \pm 0.009	1.69 \pm 0.008	2.23 \pm 0.09	Non-flowing
Paracetamol (APAP)	23.6 \pm 0.1	67.9 \pm 0.4	178.1 \pm 3.8	87.3 \pm 1.6	0.63 \pm 0.003	1.291 \pm 0.002	0.310 \pm 0.003	0.495 \pm 0.005	1.60 \pm 0.029	1.63 \pm 0.33	Non-flowing

The shown values are the mean \pm standard deviation of all measurements in triplicate.

D_{10} , D_{50} , and D_{90} are, respectively, the mean particle size below which 10%, 50%, or 90% of all particles are contained.

Volume median diameter (VMD): Median particle size diameter per volume of the particles.

S_{50} is the sphericity below 50% of all particles contained.

*The classification is based on Hausner ratio.

4 Definition of terms

Several values are calculated to assess the performance of the micro-feeder:

Powder flow rate (\dot{m}_p) is a metric that characterises the mean powder flow rate. It is determined based on data collected from a catch scale, which records the mass dispensed every second. The calculation of \dot{m}_p is given by Equation 4-1:

$$\dot{m}_p = \frac{1}{n} \sum_{j=1}^n (m_{t_{j+1}} - m_{t_j}) / (t_{j+1} - t_j), \quad \text{Equation 4-1}$$

where m_j and m_{j+1} are the accumulated powder weights at measurement times t_j and t_{j+1} . j is the measurement index corresponding to 1-s intervals, while n is the total number of samples.

Average powder flow rate ($\overline{\dot{m}_p}$) is the average of a powder flow rate of three repeated experiments:

$$\overline{\dot{m}_p} = \frac{1}{3} \sum_{i=1}^3 \dot{m}_{p,i}. \quad \text{Equation 4-2}$$

with i as the number of experiments.

Standard deviation (σ) represents a measure of differences in powder flow rates from the mean powder flow rate:

$$\sigma = \sqrt{\frac{1}{n-1} \sum_{j=1}^n |\dot{m}_j - \dot{m}_p|^2}, \quad \text{Equation 4-3}$$

where \dot{m}_j represents an individual powder flow rate.

Relative standard deviation (RSD) is obtained by dividing the standard deviation by the powder flow rate. In this study, this value indicates the variation of the powder flow rate from the mean powder flow rate. The high value indicates a higher variation and indicates poorer accuracy of powder feeding:

$$RSD = \sigma / \dot{m}_p \cdot 100\%. \quad \text{Equation 4-4}$$

Average relative standard deviation (\overline{RSD}) is the mean of relative standard deviations of three repeat experiments:

$$\overline{RSD} = \frac{1}{3} \sum_{i=1}^3 RSD_i. \quad \text{Equation 4-5}$$

Repeatability (r) is the standard deviation of powder flow rates of three repeat experiments divided by the average powder flow rate:

$$r = \sqrt{\frac{1}{2} \sum_{i=1}^3 |\dot{m}_{p,i} - \overline{\dot{m}_p}|^2} / \overline{\dot{m}_p} \cdot 100\%. \quad \text{Equation 4-6}$$

Stability (σ_{RSD}) is the standard deviation of three relative standard deviations from three repeat experiments. It provides insight into the variability of variations, which is used to assess the stability and reliability of powder feeding. It is defined as

$$\sigma_{RSD} = \sqrt{\frac{1}{2} \sum_{i=1}^3 |RSD_i - \overline{RSD}|^2} \cdot 100\%. \quad \text{Equation 4-7}$$

5 Development and implementation of a pneumatic micro-feeder for poorly-flowing solid pharmaceutical materials

5.1 Chapter Summary

Consistent powder micro-feeding (<100 g/h) is a significant challenge in manufacturing solid oral dosage forms. Low-dose feeding can well control the content consistency of the dosage forms, improving drug efficiency and reducing manufacturing waste. Current commercial micro-feeders are limited in their ability to feed <50 g/h of cohesive (i.e. powders of poor flowability) active pharmaceutical ingredients (API) and excipients (e.g. lubricants) with low fluctuation. To breach this gap, this chapter presents an advanced micro-feeder design capable of feeding a range of pharmaceutical-grade powders consistently at flow rates with low flow rate variation.

As previously mentioned in Section 2.8.1, consistent powder feeding is highly dependent on powder properties, such as particle size distribution, cohesion force between particles and adhesion force between particles to the equipment contact surface. In reality, new APIs and many excipient powders are classified as cohesive or poorly flowing materials. Cohesive materials are susceptible to aggregate, reduce powder's movement and stick to the equipment, eventually causing high variations in the flow rate. It is a great challenge to develop a powder feeder that can continuously and reproducibly feed powder with high consistency regardless of its powder properties.

Powder entrainment in pneumatic conveying has been studied in the last 30 years (Annamalai et al., 1992; Hartman et al., 2006; Matsusaka and Masuda, 1996; Suri and Horio, 2009). This powder entrainment principle is utilised in the pneumatic micro-feeder developed in this chapter. The papers indicate that the moment forces: adhesion force, drag force and gravity are required to entrain a particle. In this study, the sum of these forces is called "entrainment force". This force is seen as the minimum force to pick up a particle from stationary status. Based on this principle, when a constant force (fixed air pressure and flow rate) is continuously supplied to the system, it will only entrain a certain amount of particles. Slight adjustments in entrainment force overcome time-to-time variations in cohesion and particle size distribution.

This chapter presents a pneumatic micro-feeder that enables highly consistent feeding. This system is based on the effect of powder entrainment to control the powder flow rate. The particle entrainment concept is deployed to minimise agglomeration as the air flow minimises particle-particle and particle-wall contacts (Francis et al., 2010; Kousaka et al., 1980; Theerachaisupakij et al., 2003). This study describes the detailed principle and equipment setup (section 5.2.2). It assesses the effect of process parameters and equipment

configurations (section 5.3.3) on feeding performance (section 5.3.4) using four pharmaceutical-grade powders to cover various powder properties.

5.2 Materials and method

5.2.1 Materials

The present chapter aims to select a broad scope of powder properties to evaluate the performance of the pneumatic micro-feeder. Specifically, four powder properties were selected, namely, the easy-flowing material (microcrystalline cellulose, MCC and crospovidone, XPVP), the cohesive material (croscarmellose sodium, CCS), and the active pharmaceutical ingredient's very cohesive material (paracetamol, APAP). These properties were chosen based on their relevance to the performance of the pneumatic micro-feeder in accurately feeding powders.

A thorough characterisation of the selected powder properties was carried out, and the detailed results can be found in Chapter 3. This information is essential for a comprehensive understanding of the experiments conducted and the conclusions drawn in this chapter. By expanding the range of powder properties considered, this study provides a more holistic assessment of the performance of the pneumatic micro-feeder, which can be useful in the development of more accurate and efficient powder feeding systems.

5.2.2 Pneumatic micro-feeder

The pneumatic micro-feeder uses a powder supply unit to feed powder into the system and control the mean powder flow rate. A stable air flow is then to entrain and convey the particles and, importantly, minimise powder flow rate variations. Figure 5-1 shows the flow diagram of this pneumatic micro feeder prototype.

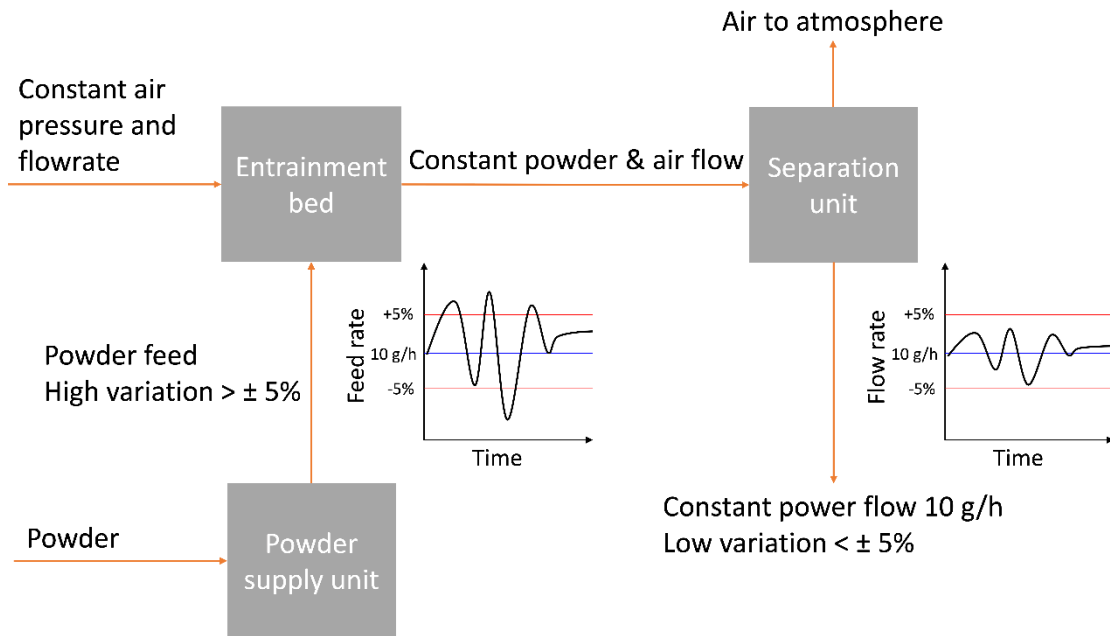


Figure 5-1: A process flow diagram for the proposed micro-feeder's conceptual design.

Figure 5-2a depicts the pneumatic micro-feeder design with a validation balance comprising an air supply line, an entrainment bed, a powder supply unit and a cyclone separator. The pneumatic micro-feeder is designed in modules, where each component can be independently manufactured, modified and replaced. The modular design facilitates to analyse and identify the critical components that affect the system's performance; each component can then be optimised individually. A photo of the pneumatic micro-feeder is shown in Figure 10-1.

The air supply line provides constant air pressure and flow rate to the system. It comprises a pressure regulator (Norgren-E74H-4GK-QD1-NFG-QPB, Norgren) and a variable area air flowmeter (WZ-32460-48, Masterflex, Cole-Parmer). The powder supply unit is a powder pump (Figure 5-2b) adapted from Besenhard et al. (2017). Its purpose is the supply of powder material into the entrainment bed and controls the mean powder flow rate. The use of the powder pump provides a relatively simple feeding mechanism compared to other feeders that involve a complex mechanical design, such as a vibration-generation system. The powder pump length is 120 mm in this study. The effect of piston speed is discussed in section 5.3.3.1.

The entrainment bed (Figure 5-2c), where the powder is entrained, produces the air-powder mixture. The entrainment bed is an adapted 1/2 inch PFA union tee with a tube fitting (PFA-820-3, Swagelok). In this prototype, inserts (Figure 5-2e) and plugs (Figure 5-2f) are applied to narrow the chamber of the entrainment bed and the process and air lines. Figure 5-2e depicts the air supply line insert types to regulate the air velocity to the entrainment bed, and the process lines insert types to maintain the powder-air flow velocity. The inserts are labelled according to their free cross-section area, e.g. 1/4D corresponds to a circular segment with a

height equal to $1/4$ of the tube diameter. Figure 5-2f depicts plug positions to regulate air velocity in the chamber. The plug positions are labelled according to position in the chamber, e.g. $1/3D$ corresponds to a circular segment with a height equal to $2/3$ of the tube diameter. The size of the process line insert is $1/4D$ cut, as shown in Figure 5-2e. Therefore, the plug and the insert are used to 1) maintain the desired air velocity and pressure drop with low air supply; 2) increase the entrainment rate and efficiency; 3) enable the system to handle a wider range of material properties; 4) minimise the accumulation built up in the chamber; 5) reduce the air consumption and workload to the separator. The effects of insert size and plug position are discussed in sections 5.3.3.2 and 5.3.3.3. The mathematic model and design calculation can be found in Section 5.2.3 and 5.2.4

A cyclone separator is a well-developed technique with no moving parts and a small number of control parameters. It is used to separate the powder-air stream (Figure 5-2d). Eight vertical baffle rods are installed inside the separator to improve the separation efficiency through impinging particles on the vertical baffle rods. In addition, the separator can be equipped with a vibration motor (Seeed Studio 105020003 Grove-Vibration Motor) to minimise the powder fouling formed on the separator wall due to the adhesive forces. To measure the powder flow rate, a lab-scale balance (60 | 120 g, ± 0.01 | ± 0.1 mg, Sartorius Quintix 125D-1S, Germany) is mounted beneath the cyclone separator outlet. The balance was calibrated before the daily experiments, followed by an annual calibration and maintenance. The design calculation of a cyclone used in this study can be found in Section 5.2.4.5.

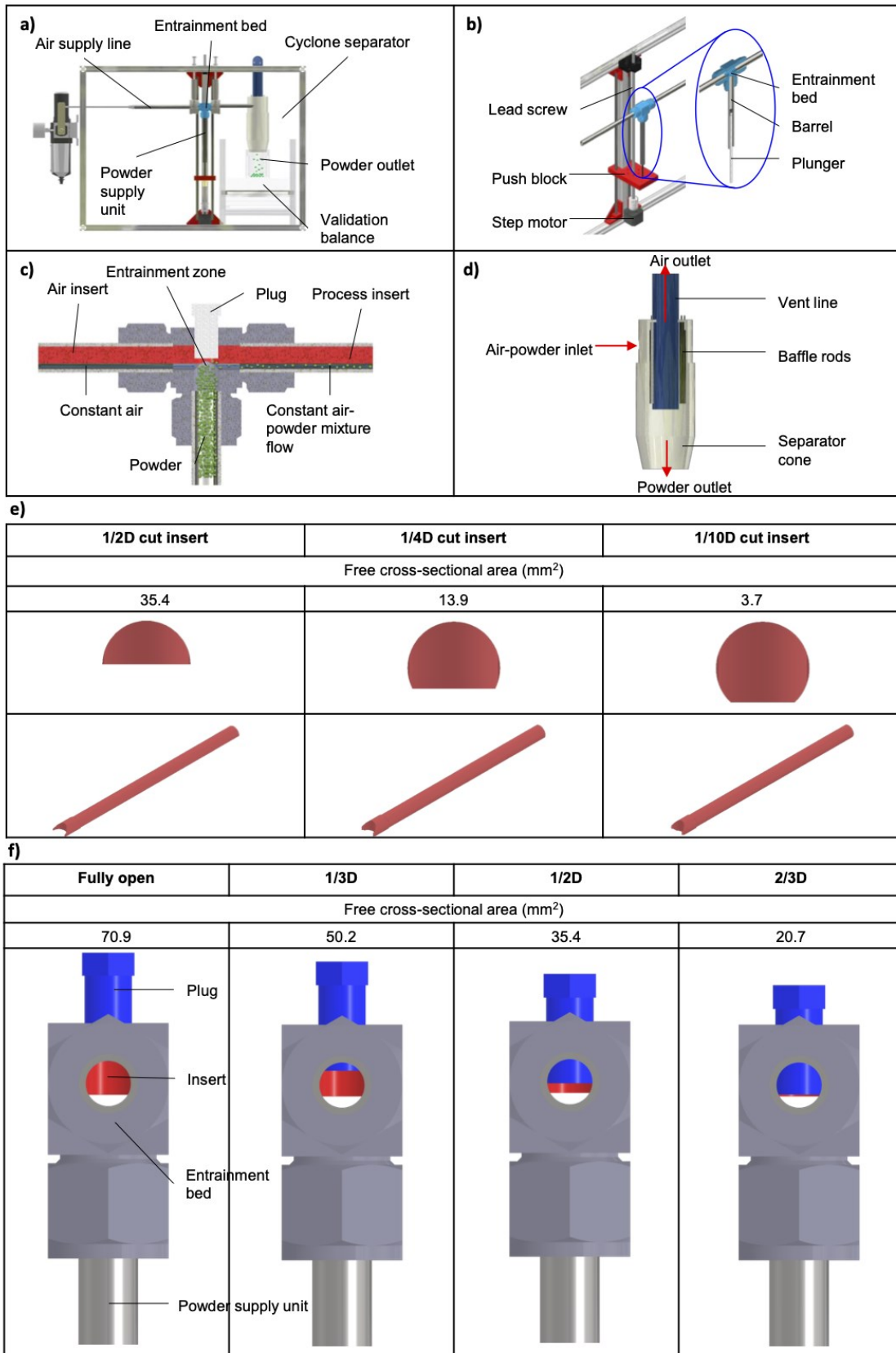


Figure 5-2: Prototype of the micro-feeder system with (a) overview, (b) powder pump, (c) entrainment bed half-section view, (d) cyclone separator, (e) air supply line and process lines insert types (side view and top-front-right view), (f) plug position to regulate air velocity in the chamber (side view).

5.2.3 Mathematic model of pneumatic micro-feeder

This section presents the mathematical models developed for the pneumatic micro-feeder design. The predictions of the model will be compared with experimental data. In the light of this comparison, the key parameters will be discussed.

5.2.3.1 Modelling the relationship between piston speed and powder mass flow rate

The aim is to model the relationships between the piston speed (S) and the powder mass flow rate (\dot{m}_p) in the powder pump section. The cross-section area of the barrel (A_b) is given as

$$A_b = \frac{\pi}{4} d_b^2, \quad \text{Equation 5-1}$$

where d_b is the internal diameter of the barrel. As $d_b = 9.52$ mm in this design, therefore, A_b is equal to 71.18 mm^2 , and is constant in this design. The powder volumetric (Q_p) flow rate is known as,

$$Q_p = \frac{\dot{m}_{p,b}}{\rho_b}, \quad \text{Equation 5-2}$$

where $\dot{m}_{p,b}$ is the powder flow rate from the powder pump, and ρ_b is the bulk density of the powder in the powder pump. The relationship between the piston speed (S) and powder volumetric flow rate (Q_p) is given by

$$S = \frac{Q_p}{A_b}, \quad \text{Equation 5-3}$$

Combining Equation 5-2 and Equation 5-3 yields

$$\dot{m}_{p,b} = S \rho_b A_b, \quad \text{Equation 5-4}$$

Equation 5-4 shows that the powder mass flow rate is proportional to the piston speed. However, it shows that bulk density variation heavily impacts the variation of mass flow rate while the S and A_b are the fixed parameters. Therefore, the stabilisation of bulk density becomes an important factor. The bulk density depends on the solid fraction. The solid fraction (ϕ) is the volume solid material occupies in the total volume. It is defined as

$$\phi = \frac{V_{\text{solid}}}{V}, \quad \text{Equation 5-5}$$

with V_{solid} as the total solid volume and V as the total volume. It is related to the bulk density from powder pump (ρ_b) by

$$\rho_b = \phi_b \rho_p, \quad \text{Equation 5-6}$$

where ϕ_b is the solid fraction of powder in the powder pump and ρ_p is the true density of the powder. Therefore, the powder mass flow rate (Equation 5-4) can be written as:

$$\dot{m}_{p,b} = \phi_b \rho_p S A_b. \quad \text{Equation 5-7}$$

Equation 5-7 indicates that the control of the solid fraction can control the variation of powder mass flow rate such as compaction. However, it is not possible to keep the solid fraction constant by compressing the powder.

5.2.3.2 Modelling the relationship between air flow rate and mass flow rate

Section 5.2.3.1 indicates that solid fraction deviation causes the instability of the mass flow rate, but the solid fraction cannot easily be overcome by compaction. Therefore, the entrainment bed is expected to reorganise the bulk density to be aeration bulk density. The aeration bulk density is controlled by adjusting the air flow rate to control the mass flow. This section aims to develop a model describing the relationships between the air flow rate, solid fraction and powder mass flow rate. Figure 5-3 shows a schematic of the powder flow in the entrainment bed. Simply, it can be divided into two stages: In the first stage, the powder is introduced from the powder pump and entrained by the moving gas in the entrainment zone. The second stage is the steady powder-air flow.

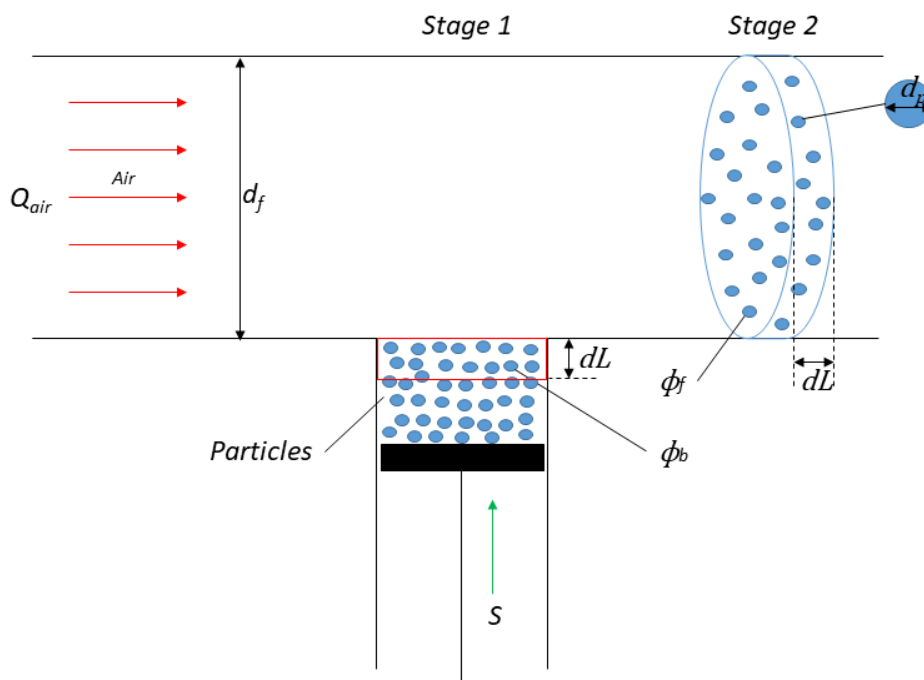


Figure 5-3: Schematic of the powder behaviour in the fluidised bed section.

For the minimum transport velocity of air in the horizontal pipes, Hartman, Phořelý & Trnka, (2006) expressed the relationship of the Reynolds number and the Archimedes number as shown in Equation 2-10. In Equation 2-10, Re_{tr} is the Reynolds number at minimum gas velocity needed to transport (pickup) particles through a horizontal pipe ($Re_{tr} = \frac{\bar{d}u_{tr}\rho_{air}}{\mu_{air}}$), where \bar{d} is mean particle size, u_{tr} is the minimum air velocity required to pick-up particles through a horizontal tube, ρ_{air} is air density which is a function of pressure and temperature, μ_{air} is the dynamic viscosity of air which is a function of temperature. Ar is the Archimedes number ($Ar = \frac{\bar{d}^3 g \rho_{air} (\rho_p - \rho_{air})}{\mu_{air}^2}$), where g is the acceleration due to gravity ($g = 9.807 \text{ m/s}^2$) and ρ_p is true density of the particles. Therefore, Equation 2-10 can be rearranged to

$$u_{tr} = 4.82 \left(\frac{\mu_{air}}{\bar{d}\rho_{air}} \right) \left(\frac{\bar{d}^3 g \rho_{air} (\rho_p - \rho_{air})}{\mu_{air}^2} \right)^{0.322} . \quad \text{Equation 5-8}$$

The density (ρ_{air}) and dynamic viscosity (μ_{air}) of the air can be determined from the formulae

$$\rho_{air} = 3.485 \frac{P}{T} \quad \text{Equation 5-9}$$

and

$$\mu_{air} = 1.81 \times 10^{-5} \left(\frac{T}{293} \right)^{0.66} . \quad \text{Equation 5-10}$$

P is the air supply pressure (kPa), T is the air supply temperature (K). According to Matsumoto (1977), the particle transfer velocity (u_p) can be estimated by Konno's empirical equation:

$$\frac{u_p}{u_{air}} = 1 - \frac{1.35 \times 10^{-3}}{d_f \left(\frac{u_t}{\sqrt{g d_f}} \right)^{0.65}} , \quad \text{Equation 5-11}$$

where u_t is the terminal velocity of particles and d_f is the pipe diameter of fluidised bed. This equation shows the relationship between air velocity and particle velocity in a horizontal pipe. The u_{air} in Equation 5-11 can be replaced by Equation 5-8; therefore, the minimum particle velocity can be predicted. For spherical particle, the terminal velocity is expressed as

$$u_t = \sqrt{\frac{4g\bar{d}}{3C_d} \left(\frac{\rho_p - \rho_{air}}{\rho_{air}} \right)} . \quad \text{Equation 5-12}$$

C_d is the drag coefficient, the terminal velocity can be seen as a constant when the lifting media, air, are in the same operation conditions, P and T are constant. In addition, the powder mass flow rate in stage 2 can be expressed as

$$\dot{m}_{p,f} = u_p A_f \phi_f \rho_p . \quad \text{Equation 5-13}$$

ϕ_f is the solid fraction in the fluidised bed. A_f is the cross-section area of the fluidised bed ($A_f = \frac{\pi}{4} d_f^2$). Combining Equation 5-8, Equation 5-11 and Equation 5-13 yields

$$\dot{m}_{p,f,tr} = u_{tr} A_f \phi_f \left(1 - \frac{1.35 \times 10^{-3}}{d_f \left(\frac{u_t}{\sqrt{g d_f}} \right)^{0.65}} \right) \rho_p , \quad \text{Equation 5-14}$$

where $\dot{m}_{p,f,tr}$ is the transported powder flow rate by minimum air velocity. Also, $Q_{tr} = u_{tr} A_f$, where Q_{tr} is the minimum air flow rate required for transferring the powder. Therefore, Equation 5-14 can be expressed as

$$\dot{m}_{p,f,tr} = Q_{tr} \phi_f \left(1 - \frac{1.35 \times 10^{-3}}{d_f \left(\frac{u_t}{\sqrt{g d_f}} \right)^{0.65}} \right) \rho_p . \quad \text{Equation 5-15}$$

The introduction of a minimum air flow rate to transfer the solid powder represents that the variation of solid fraction in the powder pump is shifted to the fluidised bed. Air flow rate plays an important role in stabilising particle velocity and influencing mass flow rate. Equation 5-15 shows that the change of solid fraction and the change of air flow rate influence powder flow rate. However, this solid fraction is a function of air flow rate and air pressure, and the change of solid fraction can be restored by adjusting air flow rate to keep mass flow rate constant. Equation 5-15 also reveals that the powder mass flow rate is proportional to air volumetric flow rate. This equation will be assessed by comparing the calculated values with the measured values in samples collected at the outlet of the pipe.

In addition, Equation 5-8 can be adapted to predict the minimum volumetric air flow rate required for transferring the powder, which is expressed as:

$$Q_{tr} = 3.79 d_f^2 \left(\frac{\mu_{air}}{\bar{d} \rho_{air}} \right) \left(\frac{\bar{d}^3 g \rho_{air} (\rho_p - \rho_{air})}{\mu_{air}^2} \right)^{0.322} \quad \text{Equation 5-16}$$

The estimated minimum air flow rate for pick-up particles can be found in Section 5.2.4.3. Based on the above mathematical modelling study, when the air flow rate maintains at a minimum superficial velocity of a gas stream needed to entrain solid particles through a horizontal tube, particles can consistently be picked up by the entrainment force. Therefore, the desired powder flow rate can be maintained by adjusting the air flow rate.

There are two scenarios: Scenario 1 refers to overdosing the powder to the fluidised bed from the powder pump. When the air flow rate is maintained at the setpoint, powder overdosed from the powder pump theoretically will not influence powder mass flow rate. The constant air flow rate will maintain the mass flow rate in this scenario. However, exceed powder can slowly be generated in the chamber. It eventually impacts the mass flow rate due to the powder build-up. The powder build-up would narrow the cross-section area and increase a pressure drop. Scenario 2 would be underdosing either from the powder pump or caused by inadequate air supply. If the air flow rate is below setpoint, it is increased to the required setpoint. If the air flow is on setpoint, then the powder pump speed must be increased.

5.2.4 Design Calculation

5.2.4.1 Fluidisation categorisation based on Geldart's classification

Table 3-3 presents essential data regarding the particle size and particle density of the tested materials. This information enables us to generate a plot on Geldarts classification figure,

revealing insightful categorisations (Figure 5-4). According to Geldarts classification during the aeration phase, materials such as MCC, XPVP, CCS, and APAP fall under the category of type A powder. This implies characteristics suitable for effective fluidisation and handling in industrial processes. In contrast, MgSt is classified as a type C powder, signifying different attributes that may affect its behaviour during aeration. These classifications offer insights into the diverse powder characteristics, aiding in the optimisation and selection of insert and parameter setting.

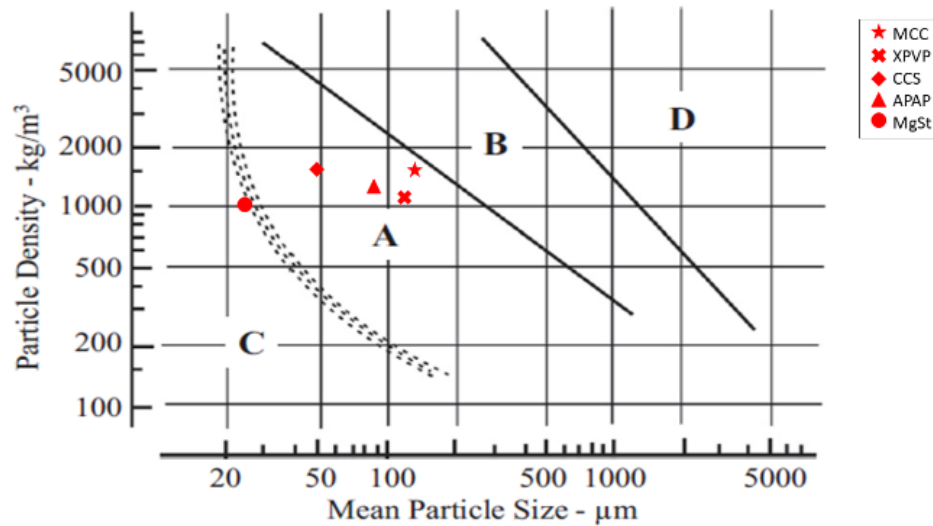


Figure 5-4: Geldart's classification of fluidisation behaviour for tested materials.

5.2.4.2 Classification of powder transfer phase

The analysis of our results involves an examination of the solid loading in relation to the mass flow rate and air flow rate, allowing us to discern the flow pattern within the equipment. Notably, our findings reveal that, irrespective of the relatively low air flow rates employed in the experimental conditions, all tested materials exhibit a dilute phase flow (Table 5-1). This implies that, even with minimal air flow, the materials maintain a dispersed state within the system. This observation that no accumulation appears in the process line which can influence the consistency of the powder feeding, and this system has a good control of the particle entrainment.

Table 5-1: Flow pattern identification through solid loading.

Material	\dot{m}_p (g/h)	Q (l/min)	P (kPa)	\dot{m}_{air} (g/h)	ϕ (-)	Flow phase
MCC	1.6	3	25	52.6	0.03	Dilute phase
	3	4	25	70.1	0.04	Dilute phase
	6	5	25	87.7	0.07	Dilute phase
	11	8	25	140.3	0.08	Dilute phase
XPVP	1.3	4	25	70.1	0.02	Dilute phase
	2.6	4.5	25	78.9	0.03	Dilute phase
	5.3	5	25	87.7	0.06	Dilute phase
	9.2	5	25	87.7	0.10	Dilute phase
CCS	8.3	4	25	70	0.12	Dilute phase
	14.2	4	25	70	0.20	Dilute phase
	21.2	5	25	88	0.24	Dilute phase
APAP	0.7	7	55	270	0.00	Dilute phase
	1.8	9	25	158	0.01	Dilute phase
	3.3	9	30	189	0.02	Dilute phase
	5.7	10	50	351	0.02	Dilute phase

Operation Temperature, T = 25 °C

5.2.4.3 Estimate the minimum entrainment air pressure and volumetric flow rate

As an example of estimating the air flow rate and cross-sectional area (insert) selection, as noted previously, the minimum air flow rate required to pick up the particles can be expressed

$$Q_{tr} = 3.79d_f^2 \left(\frac{\mu_{air}}{\bar{d}\rho_{air}} \right) \left(\frac{\bar{d}^3 g \rho_{air} (\rho_p - \rho_{air})}{\mu_{air}^2} \right)^{0.322} \quad \text{Equation 5-17}$$

Operation conditions:

Air supply pressure (P) = 25 kPa

Air supply temperature (T) = 20 C = 293 K

The dry air is used in this study. From Equation 5-9, air density:

$$\begin{aligned} \rho_{air} &= 3.485 \frac{P}{T} \\ &= 3.485 \times \frac{126}{293} \\ &= 1.5 \text{ kg/m}^3 \end{aligned}$$

From Equation 5-10, air dynamic viscosity:

$$\begin{aligned} \mu_{air} &= 1.81 \times 10^{-5} \left(\frac{T}{293} \right)^{0.66} \\ &= 1.81 \times 10^{-5} \times \left(\frac{293}{293} \right)^{0.66} \end{aligned}$$

$$= 1.81 \times 10^{-5} \text{ Pa} \cdot \text{s}$$

In the estimation study, MCC (VIVAPUR112) was employed as a case study. Analysis of Section 3.4 revealed that the mean particle size (\bar{d}) of MCC is approximately 141 μm , with a true density (ρ_p) of 1500 kg/m^3 and assuming the use a $\frac{1}{2}$ cut insert. Based on Equation 5-16, the air flow rate required to pick up the particle in the entrainment bed is given by:

$$\begin{aligned} Q_{tr} &= 3.79 d_f^2 \left(\frac{\mu_{air}}{\bar{d} \rho_{air}} \right) \left(\frac{\bar{d}^3 g \rho_{air} (\rho_p - \rho_{air})}{\mu_{air}^2} \right)^{0.322} \\ &= 3.79 \times (9.52 \times 10^{-3} / 2)^2 \times \left(\frac{1.81 \times 10^{-5}}{141 \times 10^{-6} \times 1.5} \right) \\ &\quad \times \left(\frac{(141 \times 10^{-6})^3 \times 9.81 \times (1500 - 1.5)}{(1.81 \times 10^{-5})^2} \right)^{0.322} \\ Q_{tr} &= 3.49 \times 10^{-5} \text{ m}^3 / \text{s} \\ &= 0.08 \text{ m}^3 / \text{h} \\ &= 1.3 \text{ l/min (at } 20^\circ\text{C \& 25 kPa)} \end{aligned}$$

5.2.4.4 Estimate the piston speed

The piston speed can be estimated using Equation 5-4

$$\dot{m}_{p,b} = S \rho_b A_b .$$

Operation conditions:

Powder mass flowrate ($\dot{m}_{p,b}$) = 10 g/hr

Average bulk density of the VIVAPUR112 (ρ_b) = 0.36 $\text{g}/\text{cm}^3 = 3.6 \times 10^{-4} \text{ g}/\text{mm}^3$

The internal diameter of powder pump barrel (D_b) = 9.52 mm

Therefore, the cross-section area (A_b) = $\frac{\pi}{4} D_b^2 = 71.18 \text{ mm}^2$

Therefore,

$$\begin{aligned} S &= 10 / (3.6 \times 10^{-4} \times 71.18) \\ &= 390.2 \text{ mm/h} \\ &= 6.5 \text{ mm/min} \end{aligned}$$

5.2.4.5 Cyclone separator

The cyclone separator is used to separate the particles from gas by inertial forces. By changing the direction of gas flow, the trajectories of the particles deviate from the gas streamlines. The gas-solid flow enters the cyclone separator chamber where it creates a spiral vortex. Because a solid has more momentum than gas, it is not influenced by the vortex. The particles hit the wall and drop down and discharge from the separator cone. The gas then escapes out from the separator venting tube.

In this thesis, the design of a cyclone separator follows the equation outlined in Section 2.9.2. To determine the required diameter for treating 5 l/min of ambient air (viscosity: 1.8×10^{-5} Pa s; density: 1.5 kg/m^3) containing APAP solids with a density of 1290 kg/m^3 and a particle size of $30 \text{ }\mu\text{m}$. The resulting tangential velocity (u_t) is calculated to be 0.035 m/s using Equation 2-12. Subsequently, the cyclone diameter is computed as 60 mm diameter using Equation 2-13. Consequently, the overall dimensions, as depicted in Figure 5-5, can be designed accordingly. Figure 5-5 shows the cyclone separator module. The separator is 3D-printed with acrylonitrile butadiene styrene (ABS) and then polished using papers 200, 600, 1000, 1500, 2000 and coated with an anti-static agent (Licro Crystal™, Tchspray, USA). The cyclone separator is also added with 6 rods as baffles to increase its separation efficiency.

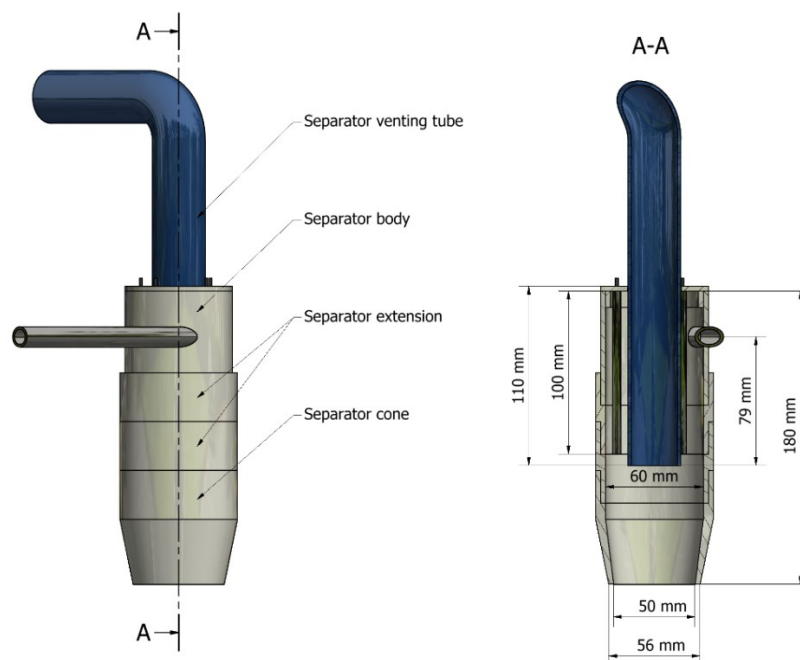


Figure 5-5: Overall dimensions of cyclone separator

5.2.5 Methods

Four pharmaceutical-grade powders (Table 3-3) at three piston speeds were studied to assess the performance of the pneumatic micro-feeder. The appropriate insert size and plug positions were selected to suit different powder properties, as shown in Figure 5-2e and f, respectively. The piston speed is the displacement speed at which the powder is pushed upwards. This speed was controlled by a stepper motor which had been calibrated prior to the experiments, i.e. 1 rpm of motor speed equals 1 mm/min of piston speed in the current setup (Appendix 10.1.2). The air pressure and air flow rate were fixed for each experiment. This is given for each experiment in the caption of each figure. In addition, there was no pre-conditioning of the powder needed for the application of the pneumatic micro-feeder. The accumulated powder weight (g) was recorded every second. Section 5.3.2 examines each variable's effects on the stability and repeatability of the system.

Chapter 4 of this study has defined the terms used to an evaluation of the micro-feeder's performance through the computation of various metrics, including powder flow rate (\dot{m}_p), relative standard deviation (RSD), stability (σ_{RSD}), and repeatability (r). Notably, the reported powder flow rate (\dot{m}_p) in this chapter corresponds to the average flow rate during the plateau phase (Phase III) of powder flow. As exemplified in Figure 5-6, the plateau phase of powder flow extends from 20 to 59 minutes at an air flow rate of 4 l/min and piston speed of 2 mm/min for MCC. In Equation 3-1, the number of samples during Phase III is represented by 'n,' which is equal to 2340 for the case presented in Figure 5-6 (corresponding to the time interval from 20 to 59 minutes). Based on this, a powder flow rate of 3 g/h can be obtained for Figure 5-6.

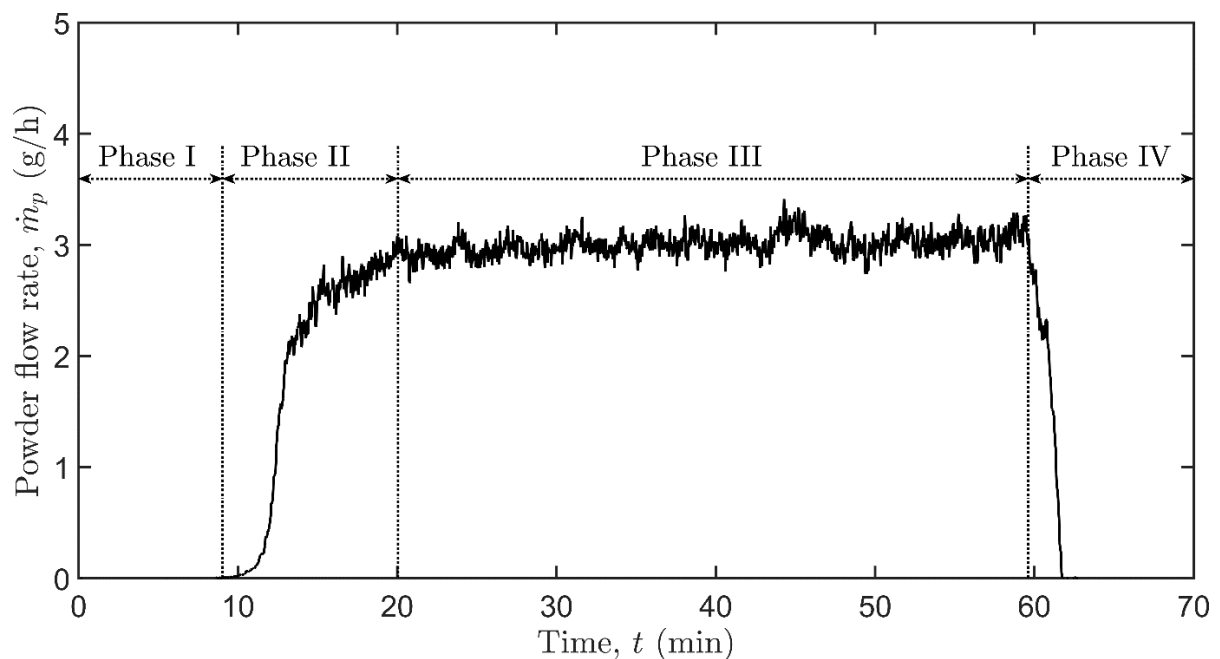


Figure 5-6: MCC powder feeding process at a feed rate of 3 g/h. Process parameters: piston speed of 2 mm/min; air pressure of 25 kPa; air flow rate of 4 l/min.

5.3 Results and discussions

5.3.1 Micro-feeder performance statistics

For the performance analysis, the powder weight is recorded at 1 Hz via a data logger. The powder flow rate is expressed as $\dot{m}_p(t) = \Delta m / \Delta t$, where Δm is the powder mass accumulated within a certain time window Δt . Figure 5-7 shows an example of raw data of MCC feeding, demonstrating that the raw data closely follows a linear trend.

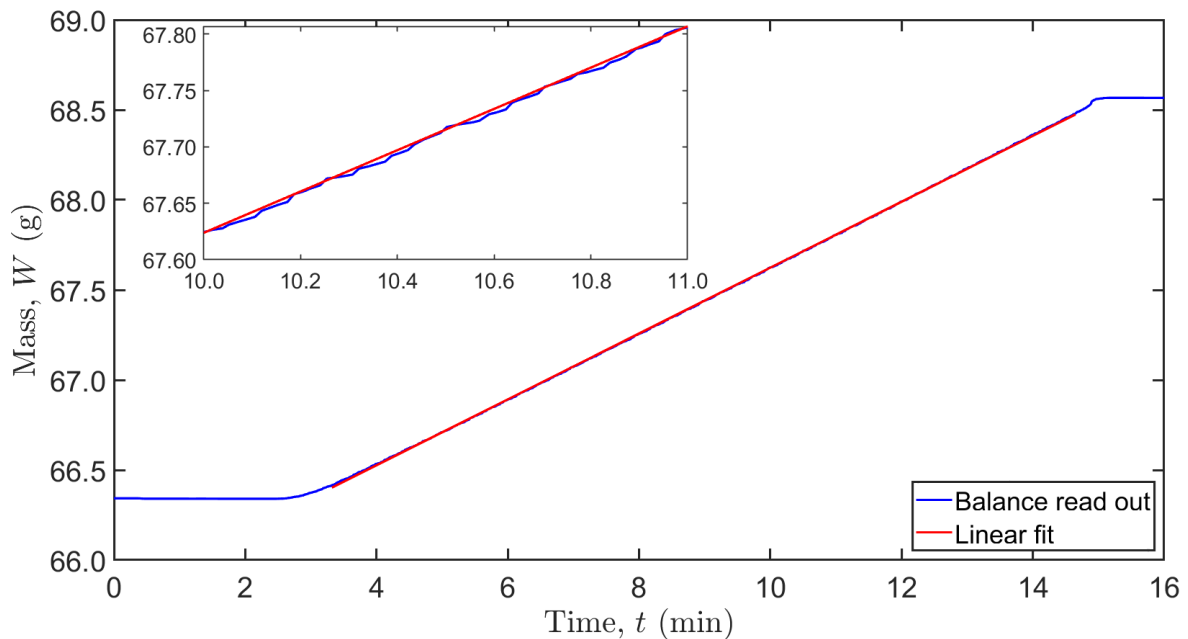


Figure 5-7: An example of MCC recorded powder weight at 8 mm/min of piston speed with a linear line fit (red line). The enlarged view depicts a close view from 10 to 11 min, demonstrating that the actual dispensed powder weight was close to the linear regression line. It implies consistent powder feeding.

Due to the measurements being recorded in an ‘unstable’ condition, this lab-scale balance used in this study provides an average value of two or three mass measurements, i.e. a data point recorded from the balance at a rate of 1 s interval is an average of two or three individual mass measurements in a second internally in the balance. For continuous feeding, the balance cannot reach a stable condition; hence, measurement noise appears in the data recorded at a 1 s interval. A moving mean was introduced to suppress this measurement noise. To ensure the application of a moving mean on the raw data does not eliminate actual feed rate variations, the moving mean method was compared to a time change data analysis method. The time change data analysis method reads the accumulated powder weight (read-out from the balance) at time intervals equal to the moving mean window size. Figure 5-8 shows the standard deviations of the time change and moving mean data analysis methods. As the standard deviations of both methods are in good agreement, the application of a moving mean on the raw data does not eliminate actual feed rate variations. The data from both methods demonstrated that a moving mean with a 60 s window is required to suppress the

measurement noise. A 60 s moving mean is also accepted in industrial applications (Enabling Technologies Consortium, 2020). Therefore, a 60 s moving mean was applied to all data shown in this study with flow rates >2 g/h. A 120 s window is used when the powder flow rate is under 2 g/h due to the decrease of balance accuracy at low weight measurements.

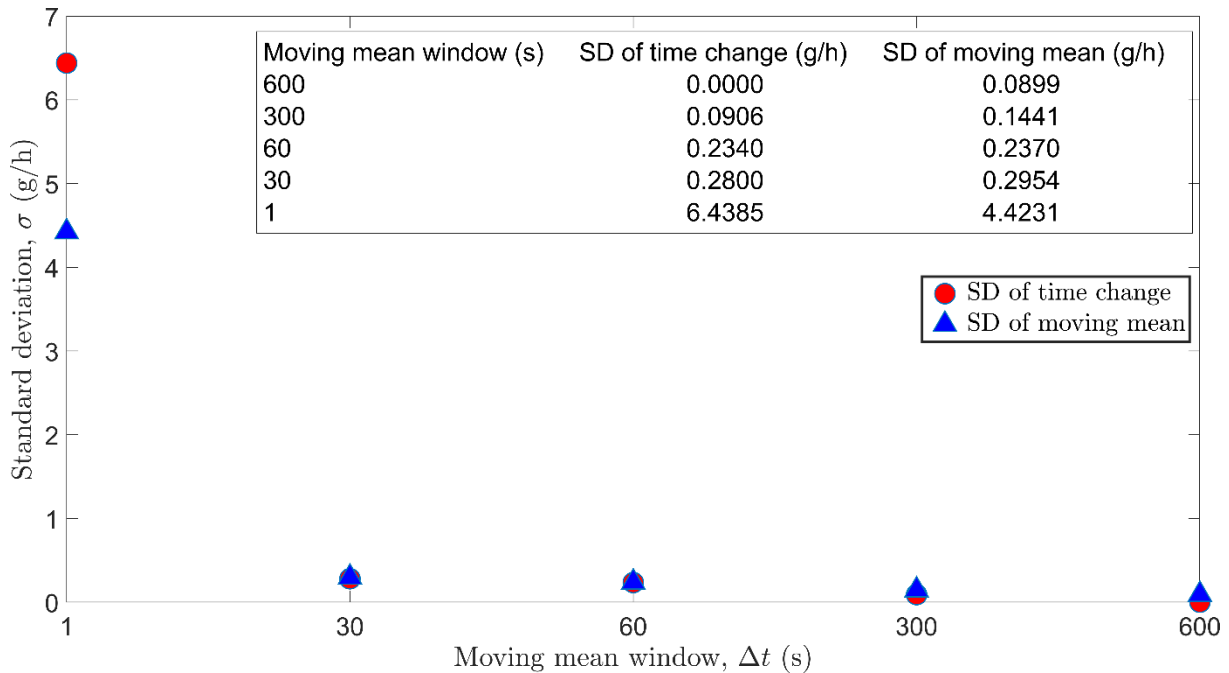


Figure 5-8: Standard deviations as a function of applying time changes and moving mean windows for a powder feeding at 11 g/h.

5.3.2 Micro-feeding process analysis

The operation of the pneumatic micro-feeder is discussed on the basis of the MCC results (Figure 5-6). The results clearly show a degree of similarity to the powder pump performance investigated by Fathollahi et al. (2020) but without the significant gradual increase of powder flow rate as a function of time.

The feeding process can be broken down into four phases:

1. Phase I - powder compression phase. This system does not require a pre-treatment of the powder. As the powder is freely filled into the powder pump, the powder is compressed by the piston before it is transported upwards towards the entrainment bed. The duration of phase I depends primarily on the compressibility of the powder and the piston speed. This phase can be eliminated by a pre-run. The details of the pre-run are shown in Section 10.1.3 and Figure 10-6. It should be noted that the pre-run does not affect the feeding accuracy in Phase III.
2. Phase II - acceleration phase. This phase follows the powder compression phase. The particles are entrained, transferred to the separator, air-solid separated and then settle

to the receiver. The duration of phase II depends on particle size, true density, cohesion, air flow rate, powder feed rate, and separator dimensions.

3. Phase III - stable feeding phase. The system provides consistent powder feeding. Figure 5-6 shows a gradual upward slope. It results from the powder compression caused by the wall friction. The powder compression causes two phenomena: 1. The increase of powder bulk density; 2. The excess powder is fed to the entrainment bed. The powder is then slowly accumulated in the entrainment bed and narrowed cross-sectional area. The decrease in the cross-sectional area increases the air velocity, which leads to more particles being picked up. This issue can be minimised by the introduction of automation on adjusting the plug position in future work.
4. Phase IV - shutdown phase. A rapid downward trend occurs as soon as the powder pump stops.

5.3.3 The influence of equipment configurations and process parameters

5.3.3.1 Piston speed

Compressibility (C) is defined as the compression degree of the material being compressed in the powder pump due to the wall shear stress. The material compressibility is estimated by considering the dead space of 9 mm in the connection of the powder pump to the chamber of the entrainment bed. The actual compression length of Figure 5-6 is 7.4 mm for MCC, yielding a compressibility of 6.2%. The compressibility is determined by the powder pump diameter, length, powder property and operation. Table 5-2 summarises phases I and II at different piston speeds. The results indicate that phase I is nearly halved when the piston speed is doubled. The table also shows that the compressibility varies depending on the powder filling.

The lower the feed rate (piston speed) for Phase II, the more prolonged phase II lasts for the same material. This can be attributed to a) the slow particle velocity due to the lower powder flow rate using a low air flow rate; b) the fouling in the separator, where particles initially adhere to the separator until the gravity force is greater than the adhesive force. At this point, the system reaches a stable feeding process (phase III). As the fouling rate is nearly constant from our observation, a lower feeding rate at the same equipment setting requires longer to achieve the required fouling quantity. These findings suggest that the duration of phase II is influenced by the powder properties, air flow rate, powder feeding flow rate, and separator dimensions. In addition, phase III gets shorter when the piston speed increases.

Table 5-2: A summary of phases I, II and III at various piston speeds for the different materials.

Material	Piston speed, S (mm/min)	Air pressure, P (kPa)	Air flow rate, Q (l/min)	Air mass flow rate, \dot{m}_{air} (g/h)	Average	Compression length, $L_{c,actual}$ (mm)	Compressibility, C (%)	Acceleration phase, $t_{Phase II}$ (min)	Stable feeding phase, $t_{Phase III}$ (min)
					compression phase, $t_{Phase I}$ (min)				
MCC	8	25	9	157.7	2.1 ± 0.0	17.0 ± 0.3	6.7 ± 0.2	1.9 ± 0.2	10.9 ± 0.2
	7	25	8	140.2	2.6 ± 0.0	17.9 ± 0.3	7.4 ± 0.2	1.8 ± 0.1	12.8 ± 0.2
	4	25	5	87.6	4.4 ± 0.1	17.4 ± 0.4	7.0 ± 0.4	5.2 ± 0.3	20.5 ± 0.2
	2	25	4	70.1	8.7 ± 0.5	17.5 ± 1.0	7.1 ± 0.8	10.8 ± 1.6	40.5 ± 1.1
	1	25	3	52.6	21.0 ± 2.4	21.0 ± 2.4	10.0 ± 2.0	12.8 ± 1.5	86.3 ± 2.8
APAP	7	50	10	350.5	5.6 ± 1.1	39.0 ± 7.8	25.0 ± 6.5	5.1 ± 1.8	6.5 ± 0.7
	4	30	9	189.3	8.9 ± 0.2	35.4 ± 0.6	22.0 ± 0.5	7.1 ± 1.2	14.1 ± 1.2
	2	25	9	157.7	18.3 ± 2.8	36.6 ± 5.6	23.0 ± 4.7	19.9 ± 4.6	21.8 ± 1.9
	1	55	7	269.9	33.9 ± 4.9	33.9 ± 4.9	20.8 ± 4.1	19.8 ± 2.4	66.3 ± 6.8
CCS	10	25	5	87.6	2.3 ± 0.2	22.6 ± 2.1	11.3 ± 1.8	2.3 ± 0.4	7.4 ± 0.4
	7	25	4	70.1	3.0 ± 0.2	20.7 ± 1.6	9.7 ± 1.4	3.7 ± 0.6	10.4 ± 0.4
	4	25	4	70.1	5.3 ± 0.2	21.3 ± 0.9	10.2 ± 0.7	5.0 ± 0.8	19.7 ± 0.7
XPVP	7	25	5	87.6	3.5 ± 0.2	24.7 ± 1.5	13.1 ± 1.2	1.9 ± 0.3	11.7 ± 0.1
	4	25	5	87.6	6.2 ± 0.0	24.7 ± 0.2	13.1 ± 0.2	2.6 ± 0.2	21.2 ± 0.2
	2	25	4.5	78.9	12.5 ± 0.4	24.9 ± 0.8	13.3 ± 0.7	5.0 ± 0.1	42.6 ± 0.4
	1	25	4	70.1	24.0 ± 0.8	24.0 ± 0.8	12.5 ± 0.7	10.7 ± 1.5	85.3 ± 2.1

Compression length ($L_{c,actual}$) = $t_{phase I} \times S$.

Compressibility (C) = $((L_{c,actual} - 9)/120) \times 100\%$, where 120 mm is the length of the powder supply unit.

Compression phase ($t_{Phase I}$) is average of compression phases of three repeat experiments.

Acceleration phase ($t_{Phase II}$) is average of acceleration phases of three repeat experiments.

Stable feeding phase ($t_{Phase III}$) is average of stable feeding phases of three repeat experiments.

5.3.3.2 Air supply line and process line inserts

The use of an insert in the air supply line and the process line plays a vital role in controlling powder flow rate stability. The air supply line insert controls the air velocity into the entrainment bed. It prevents back pressure in the air supply line that could cause the powder to settle in the air supply line. The process line insert maintains the air-powder velocity and ensures the particles are suspended in the air. The inserts also minimise the supplied air flow rate, which reduces the workload of the separator.

Figure 5-9 depicts the RSDs of powder flow rates for MCC and APAP as a function of the insert sizes (free cross-section areas). It shows the influence of three different sizes of inserts on the stability of the MCC and APAP powder flow rate. The results demonstrate that an inappropriate insert size causes a higher RSD.

In addition, Figure 5-9 demonstrates that the non-flow material (APAP) requires a small insert, whereas the cohesive material (MCC) yields lower RSDs with a large insert. 1/2D insert is required for MCC, whereas 1/10D insert is required for APAP to stabilise the powder flow rate. The kinetic energy of air flow is termed the entrainment energy in this study. As known, the reduction in insert size (free cross-sectional area) increases the air velocity when the air flow rate is constant. It dramatically raises the air flow kinetic energy based on the kinetic energy equation of air flow. Without the insert, a higher air flow rate would be required to achieve the desired air velocity, adding excess entrained energy to the system and causing fluctuations. It would also require a wide range of air flow rate meters and controllers to achieve the ideal air velocity. Therefore, the appropriate insert size selection for individual materials helps to maximise entrainment efficiency and entrainment rate.

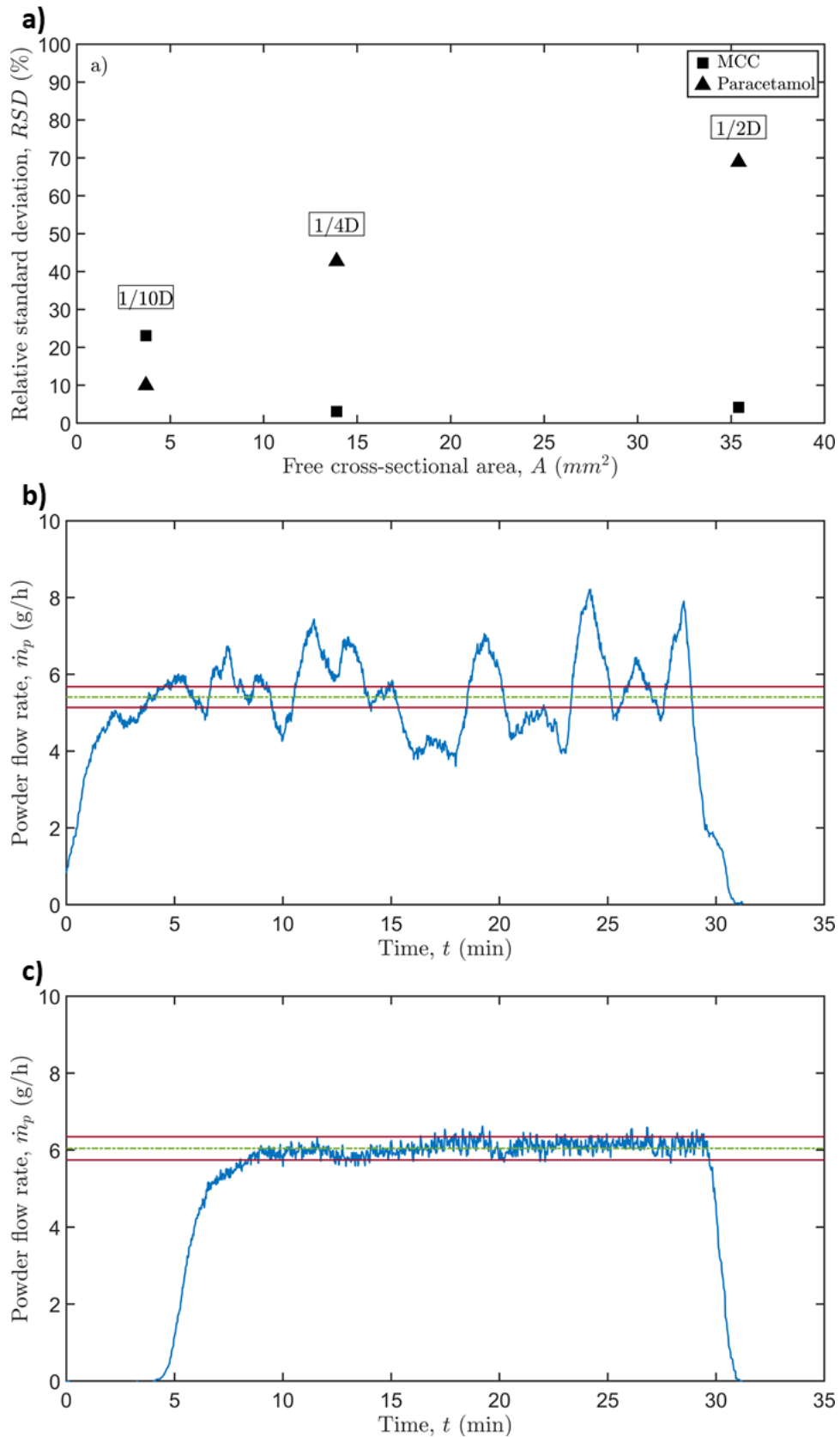


Figure 5-9: a) The relative standard deviation of APAP mass flow rate as a function of the cross-section area in the process line controlled by three different insert sizes at a fixed plug position (open position/highest level of the plug). 30 kPa and 9 l/min of air flow rate for the mean powder rate of APAP at 3.4 g/h, 25 kPa of air pressure and 6 l/min of air flow rate for the mean powder rate of MCC at 6.0 g/h; b) the MCC feeding trend using 1/10D cut insert; c) the MCC feeding trend at 1/4D cut insert.

5.3.3.3 Plug position

Adjustment of the plug position regulates the air velocity and pressure drop in the entrainment chamber. This study investigated the influence of four discrete positions (full open chamber, 1/3D, 1/2D and 2/3D) on the stability of the powder flow rate. Figure 5-10 illustrates the RSDs of MCC and APAP powder flow rate as a function of three different plug positions using the same insert size. It suggests that a 1/10D cut insert with the plug position at 1/2D provides stable feeding for APAP, and the use of a 1/4D cut insert with the plug position at 1/3D results in stable feeding for MCC. It was found that placing the plug below the optimal position will increase the air velocity and entrainment energy and cause strong turbulence in the chamber. This turbulence will dig out powder from the powder feed unit, entrain excess powder to the outlet, and cause fluctuations in the powder flow rate. On the contrary, when the position of the plug is higher than the optimal position, the low air velocity (low entrainment energy) will result in poor entrainment efficiency, which in turn causes the system to be blocked by the accumulation of powder in the chamber. Therefore, the selection of plug position together with the insert size are critical settings in terms of the stability of the powder flow rate.

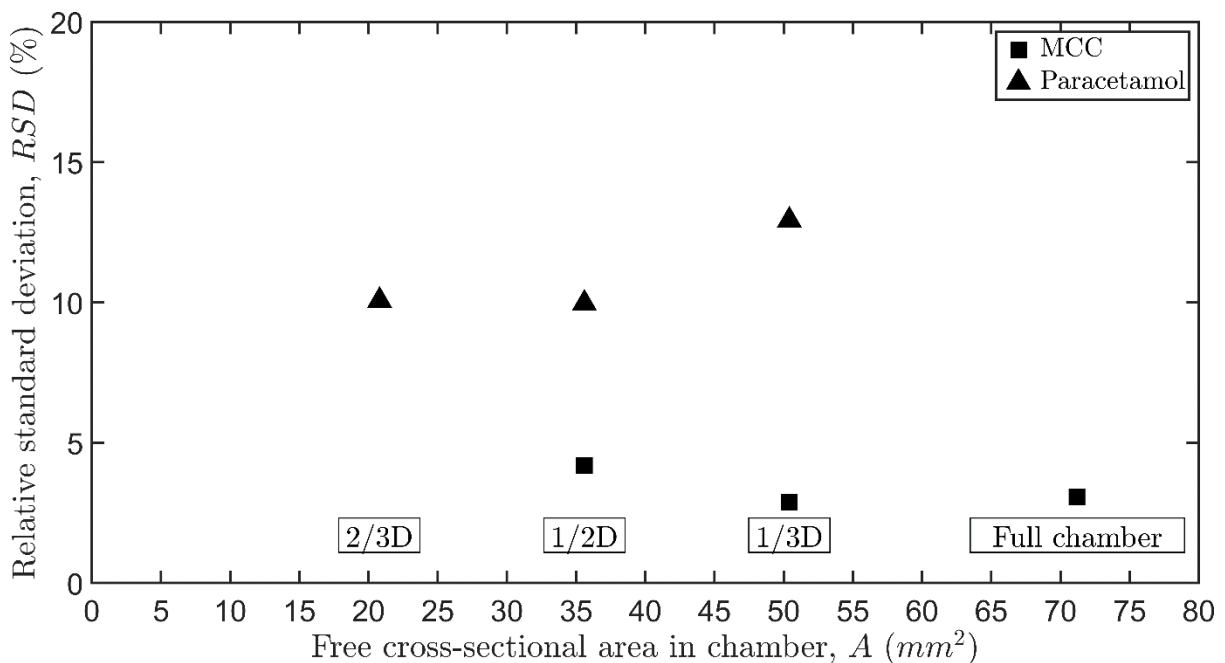


Figure 5-10: The relative standard deviation of the MCC flow rate (6 g/h) and APAP flow rate (3.3 g/h) as a function of different plug positions in the entrainment bed using the same insert size (1/10D cut insert for APAP, 1/4D cut insert for MCC) at same air flow rate and pressure settings (30 kPa and 9 l/min of air flow rate for APAP, 25 kPa of air pressure and 6 l/min of air flow rate for MCC).

5.3.3.4 Air pressure

The air pressure affects the chamber's air velocity and air flow rate influencing the entrainment energy. Figure 5-11 shows the RSDs of APAP and MCC powder flow rate as a function of air pressure at 9 l/min of air flow rate. A plug position of 1/2D and an insert size of 1/10D cut were set for APAP feeding, and a plug position of the full chamber and an insert size of 1/2D cut

were set for MCC feeding. The figure indicates that the optimal air pressure point should be around 30 kPa for APAP and 25 kPa for MCC, where lower or higher air pressure leads to severe fluctuations.

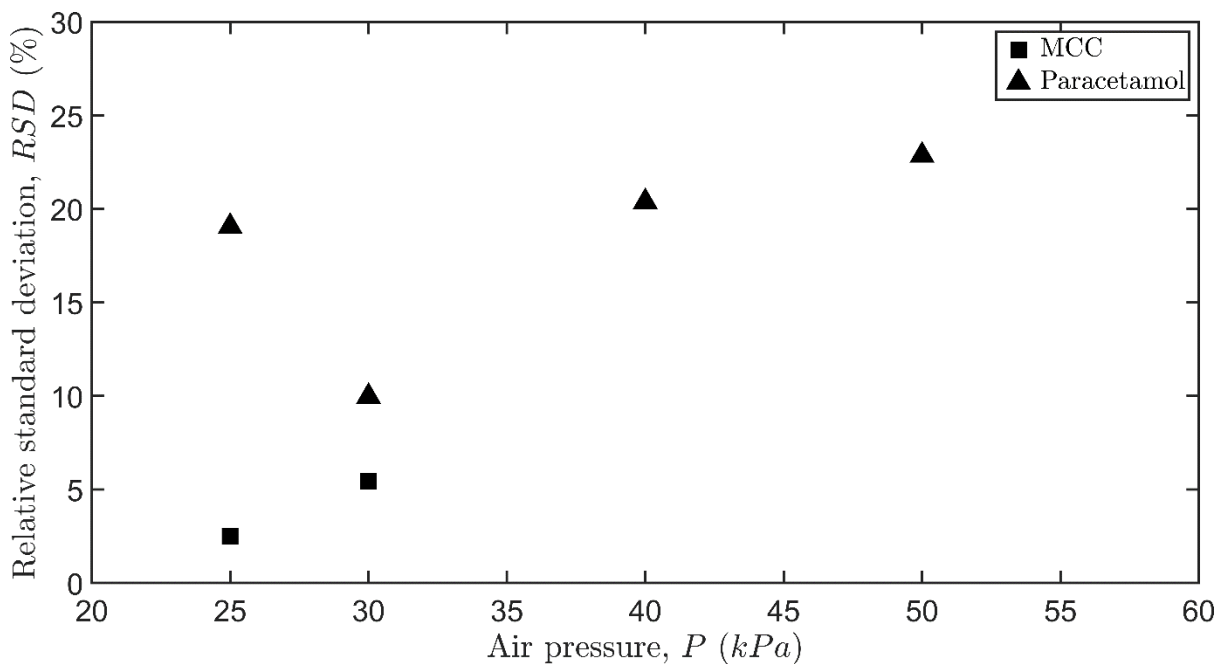


Figure 5-11: The relative standard deviation of the APAP flow rate (3.5 g/h) and MCC flow rate (6 g/h) as a function of the air pressure at 9 l/min of air low rate. A plug position of 1/2D and an insert size of 1/10D cut was set for APAP, and a plug position of full chamber and an insert size of 1/2D cut for MCC

5.3.3.5 Air flow rate

The air flow rate is used to minimise the variations in the powder flow rate. Figure 5-12 clearly shows that the variations were minimised by reducing the air flow rate, and a stable MCC powder feeding rate was achieved using an air flow rate of 5 l/min. It is found that the RSDs increase with raising the air flow rate for MCC. The powder flow rate can be stabilised through air entrainment, which can also be clearly observed for APAP feeding.

Figure 5-12 shows that three phenomena occur when the air flow rate is not close to the optimal value: First, when the air flow rate is higher, the air acts as a scraper. Due to the compression in the powder pump, the powder density is reduced across the displacement. Therefore, the powder flow rate tends to increase gradually. The obtained metrics from this scenario would be similar to the powder pump's original design (Besenhard et al., 2017; Fathollahi et al., 2020). Second, fluctuations occur for air flow rates higher than the optimal value due to large agglomerates entrained, especially for cohesive materials. Third, blockage occurs when the air flow rate is lower than optimal. This is because powder feeding from the powder pump to the entrainment bed is faster than the powder flow entrained by the air, which leads to accumulation in the chamber. According to these findings, the exact ratio between piston speed and air flow rate is vital for stabilising the powder flow rate.

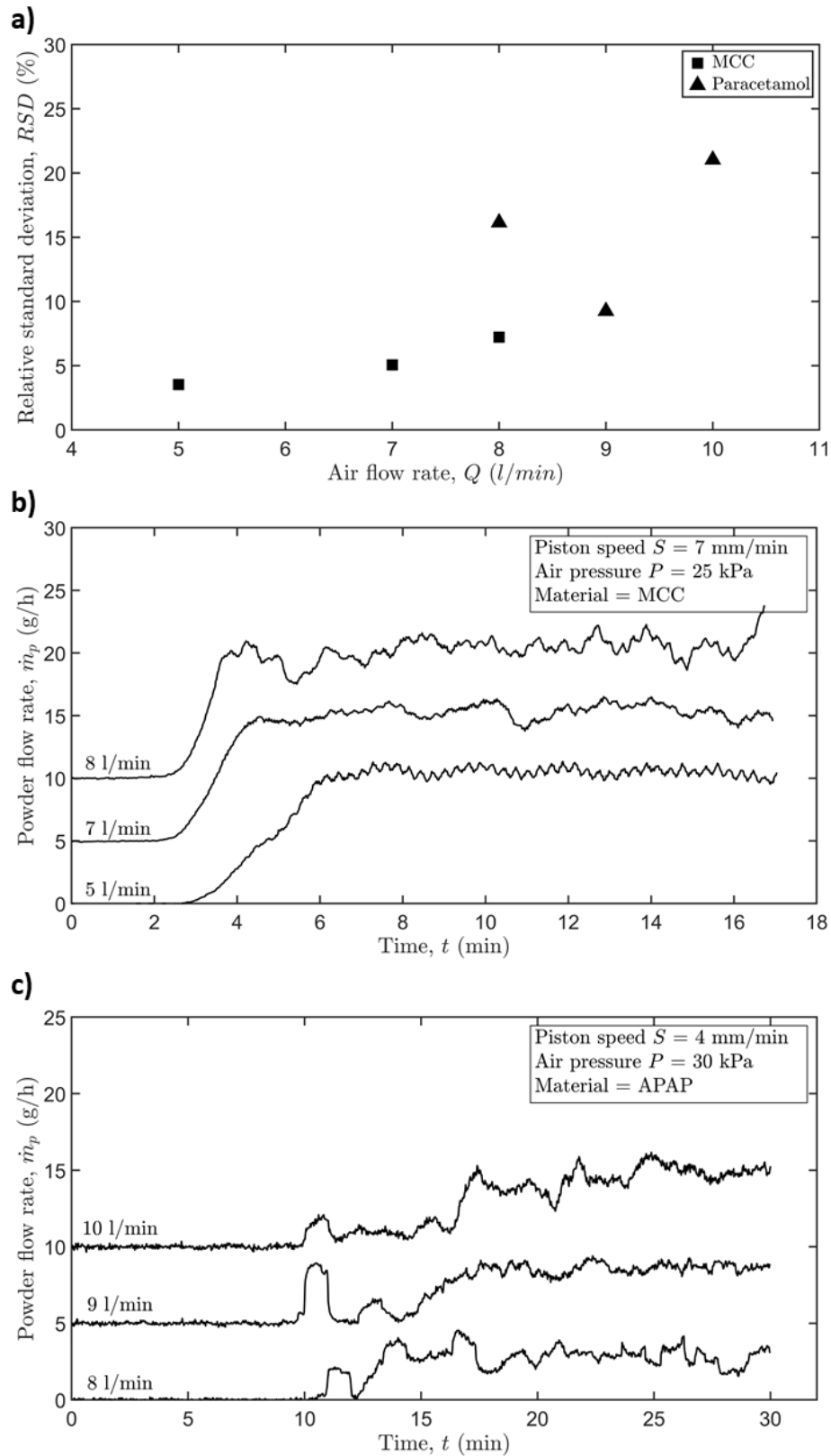


Figure 5-12: Feeding performance of MCC and APAP for a different setting. a) The effect of air flow rate on the MCC flow rate (6 g/h) and APAP flow rate (3.5 g/h) at a fixed piston speed and equipment setting. It shows the RSDs of MCC (■) and APAP (▲) powder flow rate as a function of the air flow rate at fixed air pressures (25 kPa and 30 kPa) and plug positions (full chamber and 1/2D) with the same insert size (1/2D cut and 1/10D cut); b) the effect of air flow rate on the MCC powder flow rate; c) the effect of air flow rate on the APAP powder flow rate.

5.3.3.6 Equipment and operational guideline

Based on the influence of equipment configurations and process parameters, a recommendation can be made for equipment and operational settings. The equipment settings and process parameters can be determined and broken down into four steps to finding the optimal equipment setting and process parameters. These stages can be defined as follows:

Step 1 - Set the piston speed

In order to predict the piston speed setting, the piston speed (S) and the mean powder feed rate ($\dot{m}_{p,b}$) were estimated following

$$\dot{m}_{p,b} = S\rho_b A_b / (1 - C) , \quad \text{Equation 5-18}$$

where ρ_b is the powder bulk density, A_b is the cross-section area of the powder pump. In this study, A_b is 71.18 mm². C is the powder compression. The full derivation steps can be found in Section 10.1.4. Equation 5-18 helps estimate the piston speed setting when the desired powder flow rate is known. In this study, the current motor can only set integer values. In future work, a wider range of motor speed settings will provide a more accurate powder flow rate.

Step 2 - Select insert

We know from section 5.3.3.2 that non-flow materials (APAP) require a small free cross-sectional area insert. In contrast, the cohesive material (MCC) requires a large free cross-sectional area insert. Therefore, a suitable inset size requires several tests and needs to consider the flowability of the material.

Step 3 - Position of the plug

The plug's positioning starts from half of the insert size, e.g. the plug would be positioned at 1/3D for a selected 1/4D cut insert and is then increased or decreased until the optimal plug position is found.

Step 4 - Set air pressure and air flow rate

Using MCC as a baseline, MCC used 25 kPa of air pressure in this study. For cohesive material, high entrainment energy is expected, which can be achieved by increasing the air velocity or air mass flow rate. To increase the air velocity, it is by adjusting the air pressure and air flow rate. The higher air pressure would also be considered to increase the air mass flow rate. For example, we know that APAP has a higher cohesion force between particles than MCC. Therefore, 30 kPa of air pressure was selected in APAP feeding experiments. The air flow rate is then slightly adjusted to minimise the RSDs. As a rule of thumb, the more cohesive the material, the higher the air pressure and air flow rate should be. In addition, the air flow rate should be increased when powder accumulation is observed in the process line.

When the powder flow rate is seen to fluctuate, the air flow rate should be reduced. Figure 5-13 summarises the equipment and operational guideline.

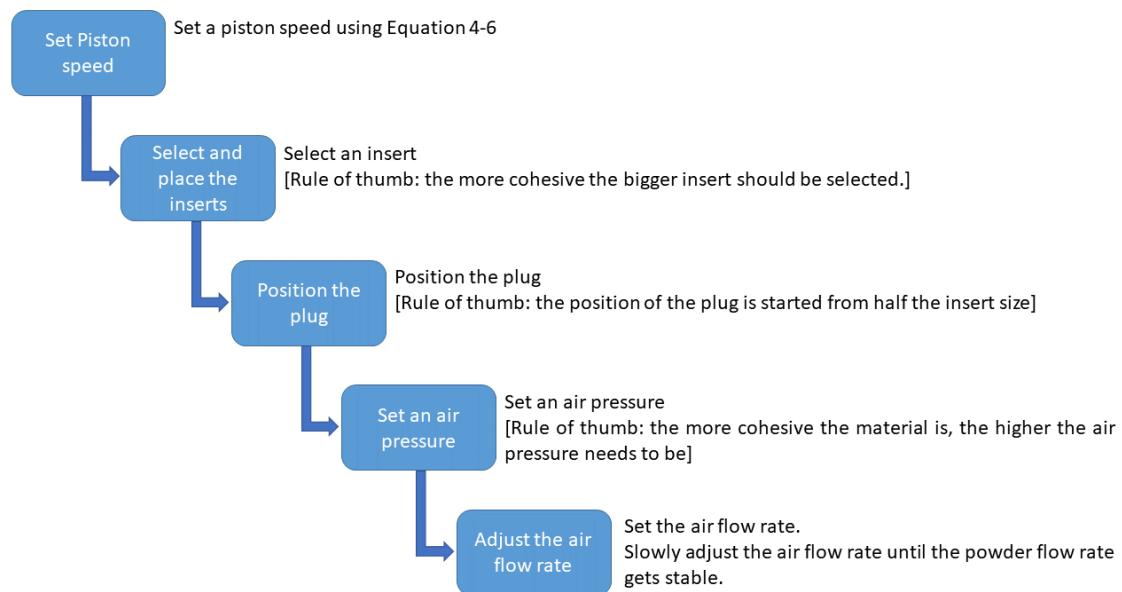


Figure 5-13: The equipment and operational guideline.

5.3.4 Feeding performance of different materials

Figure 5-14 shows the feeding performance of MCC for five powder flow rates between 1.6 g/h and 12.7 g/h. It clearly demonstrates a consistent feeding and a positive correlation between the piston speed and powder flow rate. Further analysis showed that the air flow rate adjustment minimises the RSDs to below $\pm 5\%$. The system can consistently feed for 80 minutes for the lowest MCC feeding performance (1.6 g/h).

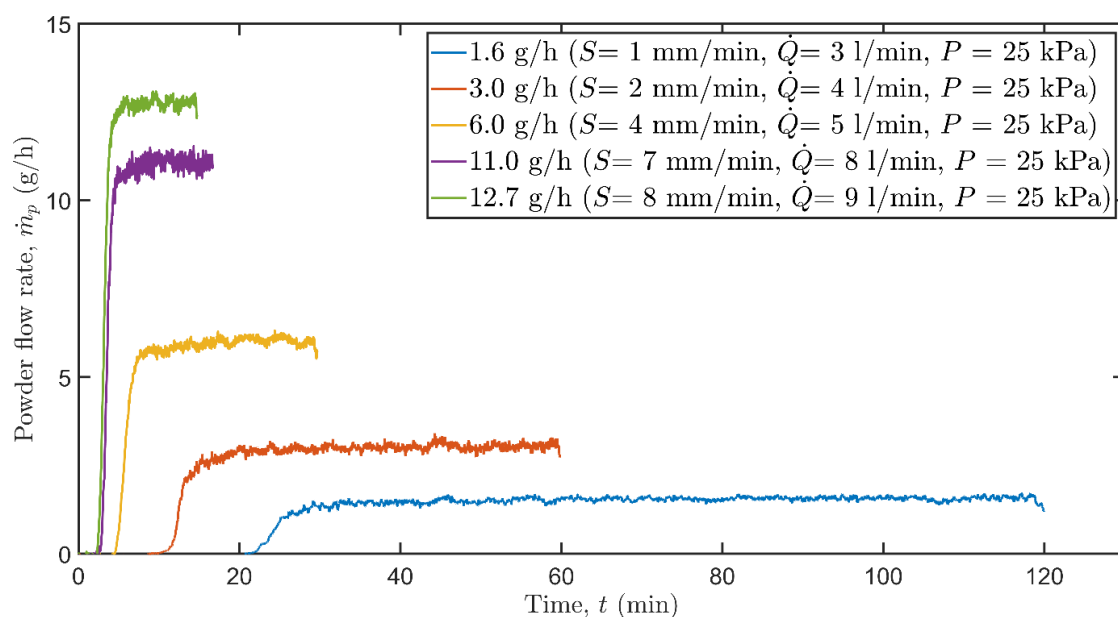


Figure 5-14: Feeding performance of MCC using the pneumatic micro-feeder. The air pressure, P , was set at 25 kPa. The air flow rate, \dot{Q} , was adjusted to stabilise the powder flow rate. The piston speed, S , was varied to adjust the average powder flow rate.

Figure 5-15 summarises the average powder flow rate for four materials as a function of piston speed. As expected, the powder flow rate increases linearly with increasing piston speed. However, the currently available data do not provide sufficient information to confirm the relationship of the slopes to cohesion, particle size or bulk density.

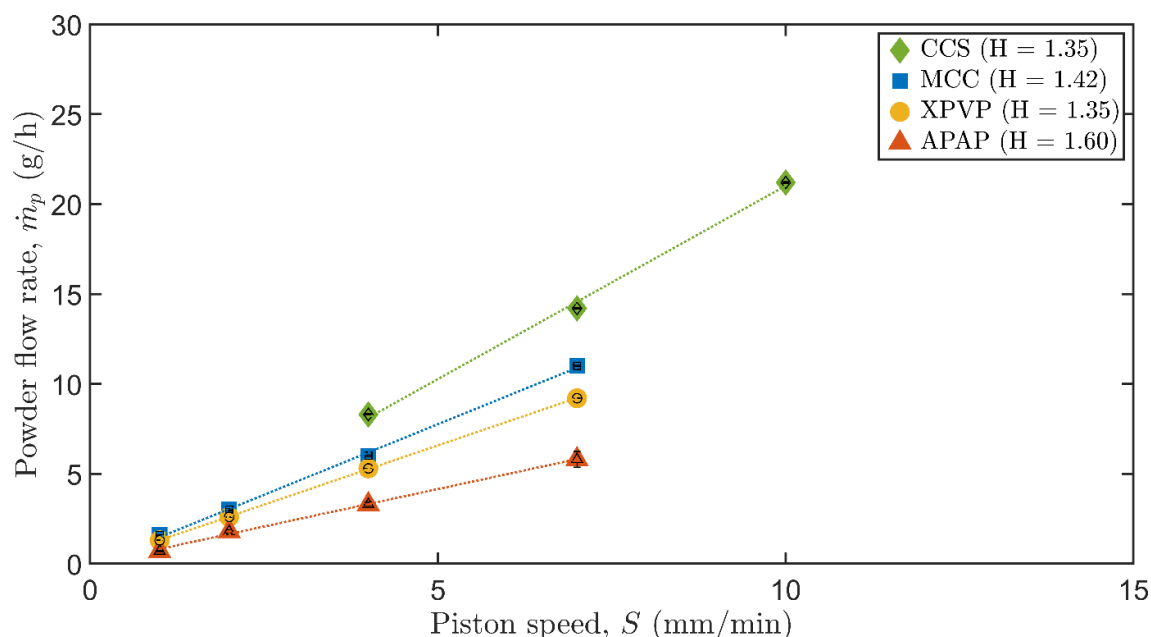


Figure 5-15: Average powder mass flow rate with standard deviations of three repeat experiments as a function of piston speed for four different materials. H represents the Hausner ratio.

Table 5-3 summarises the overall feeding performance of the four materials. Across all materials, the pneumatic micro-feeder demonstrated high repeatability and can consistently feed powders within the range of 0.7 g/h to 21.2 g/h with an RSD of less than ± 5 -20% (depending on the material).

In the case of cohesive powder (MCC), the micro-feeder was able to achieve feed rates ranging from 1.6 ± 0.07 g/h to 11 ± 0.22 g/h with RSDs of $< \pm 5\%$, high repeatability ($< 1.5\%$) and high stability ($< 0.5\%$). For the non-flow material APAP, the current equipment setting can feed APAP from 0.7 g/h ($< \pm 20\%$) to 5.8 g/h ($< \pm 10\%$) with repeatability of $< 8\%$ and stability of $< 5\%$. Applied to a powder with a low Hausner ratio of 1.35, the micro-feeder was able to feed CCS from 8.3 g/h to 21.2 g/h with an RSD $< 16\%$, repeatability of $< 5\%$ and stability of $< 1.5\%$. And it was shown to be capable of feeding XPVP at a feed rate from 9.2 g/h $\pm 5\%$ to 1.3 g/h $\pm 10\%$ with a repeatability of less than 1.5% and better than 1.3% stability. Although CCS and XPVP have a similar Hausner ratio ($H = 1.35$), CCS increased the RSD at a low powder flow rate. Conversely, the feeder performance for XPVP was significantly better. Comparing the particle size of both materials, XPVP ($D_{50} = 104.9 \mu\text{m}$) particles are, on average, twice as large as CCS particles ($D_{50} = 54.9 \mu\text{m}$). These results indicate that the particle size also affects the feeding consistency.

Table 5-3: Summary of the feeding performance of different powder flow rates. The definitions of all listed parameters can be found in section 5.3.2.

Materials	Piston speed, S (mm/min)	Air pressure, P (kPa)	Air flow rate, Q (l/min)	Air mass flow rate, \dot{m}_{air} (g/h)	Powder flow rate, \dot{m}_p (g/h)	Standard deviation, σ (g/h)	Relative standard deviation, RSD (%)	Average powder flow rate, \bar{m}_p (g/h)	Average standard deviation, $\bar{\sigma}$ (g/h)	Average relative standard deviation, RSD (%)	Repeatability, r (%)	Stability, σ_{RSD} (%)
Microcrystalline cellulose (MCC)	7	25	8	140.2	11.0	0.2151	2.0	11.0	0.2191	2.0	0.20	0.13
					11.0	0.2068	1.9					
					11.0	0.2354	2.1					
	4	25	5	87.6	5.9	0.1740	2.9	6.0	0.1699	2.9	0.78	0.12
					5.9	0.1615	2.7					
					6.0	0.1742	2.9					
	2	25	4	70.1	3.0	0.1049	3.5	3.0	0.1152	3.8	1.31	0.44
					3.0	0.1291	4.3					
					3.1	0.1116	3.6					
	1	25	3	52.6	1.6	0.0680	4.3	1.6	0.0716	4.5	0.55	0.39
					1.6	0.0682	4.3					
					1.6	0.0787	5.0					
Paracetamol (APAP)	7	50	10	350.5	6.2	0.3670	5.9	5.8	0.3645	6.4	7.56	1.15
					5.7	0.3154	5.5					
					5.4	0.4112	7.7					
	4	30	9	189.3	3.4	0.3913	11.6	3.3	0.3631	10.6	3.05	0.86
					3.6	0.3548	10.0					
					3.4	0.3433	10.2					
	2	25	9	157.7	1.7	0.1732	10.0	1.8	0.1612	9.0	4.80	1.17
					1.8	0.1353	7.7					
					1.9	0.1752	9.3					
	1	55	7	269.9	0.7	0.0964	13.6	0.7	0.1317	19.2	2.72	4.93
					0.7	0.1421	21.1					
					0.7	0.1567	22.9					
Croscarmellose sodium (CCS)	10	25	5	87.6	20.2	1.7250	8.5	21.2	1.7889	8.4	4.32	0.50
					21.4	1.6867	7.9					
					22.1	1.9550	8.9					
	7	25	4	70.1	13.9	1.8041	13.0	14.2	1.6779	11.8	2.46	1.29
					14.1	1.7086	12.1					
					14.6	1.5210	10.4					
4	25	4	70.1	8.6	1.5276	17.7	8.3	1.3488	16.2	3.14	1.52	
				8.1	1.1958	14.7						
				8.2	1.3232	16.1						
Crospovidone (XPVP)	7	25	5	87.6	9.1	0.2800	3.1	9.2	0.3286	3.6	0.97	0.45
					9.2	0.3414	3.7					
					9.2	0.3643	4.0					
	4	25	5	87.6	5.3	0.2493	4.7	5.3	0.2312	4.3	0.54	0.34
					5.3	0.2128	4.0					
					5.4	0.2317	4.3					
	2	25	4.5	78.9	2.7	0.1910	7.2	2.6	0.2238	8.5	1.32	1.22
					2.6	0.2472	9.5					
					2.6	0.2332	8.9					
	1	25	4	70.1	1.3	0.1312	9.9	1.3	0.1241	9.5	0.72	0.43
					1.3	0.1225	9.4					
					1.3	0.1185	9.1					

Powder flow rate: the average of each calculated powder flow rate after the flow rate stabilised (Phase III)

Average powder flow rate: the average of powder flow rate of three repeat experiments

Standard deviation (SD): the average of standard deviation after the flow rate stabilised (Phase III)

Average SD: the average of standard deviations of three repeat experiments

Relative Standard Deviation (RSD) = SD/powder flow rate

Average RSD: the average of RSD of three repeat experiments

Repeatability = standard deviation of powder flow rates/average powder flow rate

Stability = standard deviation of RSDs of three repeat experiments

According to Table 3-3, APAP with a Hausner ratio greater than 1.60 is classified as a non-flowing material. APAP, therefore, represents a challenging material to assess the capabilities of this design. Figure 5-16 compares the feeding performance of APAP and MCC at similar powder flow rates. APAP requires a higher piston speed (7 mm/min) to achieve the same powder flow rate as MCC (4 mm/min). This is due to the higher compressibility of APAP (Table 4); APAP is twice as compressible as MCC. Phase I of APAP is thus longer than that of MCC. Additionally, the acceleration phase of APAP is 6.9 min compared to 4.8 min of MCC, which is primarily attributed to the higher cohesive forces of APAP. APAP also adheres more strongly to the inner wall of the separator, which leads to an extended phase II. APAP particle size is smaller than MCC's, extending the particle settling time. Due to the extension of phases I and II, the stable phase of APAP becomes shorter compared to the stable phase of MCC. Table 5-3 shows that the air mass flow rate of APAP is almost twice of that of MCC. This finding, while preliminary, suggests that a higher air entrainment rate is required to overcome cohesion. Further work should be undertaken to investigate the relationship between the air entrainment rate and cohesion.

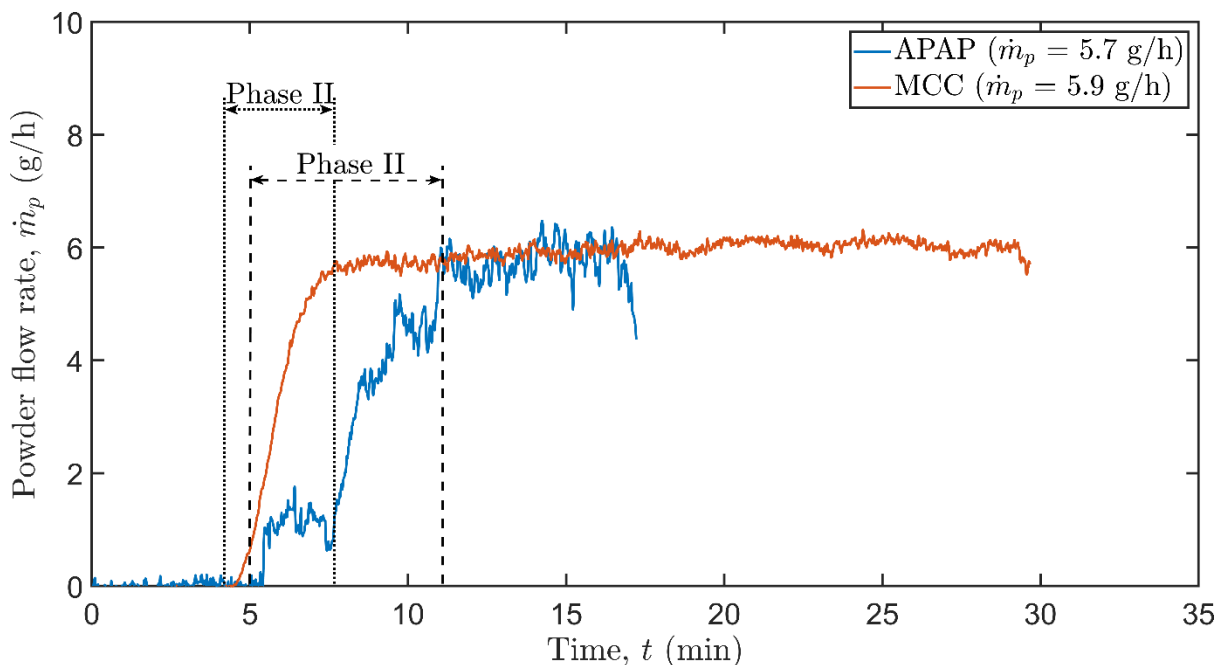


Figure 5-16: Comparison of MCC and APAP at similar feed rates. The parameters of MCC were set to 4 mm/min of piston speed, 25 kPa of air pressure and 5 l/min of air flow rate. APAP was fed at 7 mm/min of piston speed, 50 kPa of air pressure and 10 l/min of air flow rate.

5.3.5 Segregation and particle degradation

The particle size distribution of APAP in the feed, on the separator and in the receiver was analysed to study the degree of segregation in the pneumatic micro-feeder. Table 5-4 shows that most of the fine paracetamol particles are trapped on the inner wall of the separator due to adhesion. The data also showed that the particle sizes collected in the receiver ranged from

66.9 μm to 186.7 μm , indicating that fine particles are easily captured on the inner walls of the separator. Therefore, improving the fouling problem and minimising segregation are crucial to reducing the segregation effect.

Due to the low velocity, the particle degradation was not observed from this result. However, the result shows that there is some aggregation in the receiver. This could be the environment moisture or the centrifugal force compressed the powder during the powder conveying and separation processes.

Table 5-4: Particle size distribution along with the system for APAP. All experiments were conducted in triplicate.

Powder	Location	D_{10} (μm)	D_{50} (μm)	D_{90} (μm)	VMD (μm)
Paracetamol	Feed	23.6	67.9	178.1	87.3
	Separator	23.2	63.1	136.9	72.8
	Receiver	66.9	186.7	314.4	195.5

5.3.6 Current limitations of the pneumatic micro-feeder

However, its current limitations can be summarised as follows (the details of limitation and disturbance can be found in Sections 10.1.5):

- Fouling in the separator, especially for materials with a particle size $<50 \mu\text{m}$ (Table 5-4); further research will investigate the effectiveness of minimising the fouling using an ultrasonic vibrator.
- Segregation of non-flow materials such as APAP; like the first point (fouling in the separator), the application of ultrasonic vibration is expected to minimise segregation.
- Relatively short stable feed time; further research will introduce a continuous powder feeding unit to replace the limitation of the powder pump.

5.4 Conclusions

A novel pneumatic micro-feeder was developed, and its performance was demonstrated for four different pharmaceutical-grade materials. This system shows its potential for delivering consistent powder flow rate controlled by adjusting the air flow rate. This system has only a few moving parts, is composed of simple components, and is easy to operate. The effects of process parameters and equipment configurations on feed performance, including different insert sizes, plug positions, air pressure, air flow rate, and piston speed were investigated. The overall results show that this system can feed a powder flow rate of 0.7 to 20 g/h, with an RSD of ± 20 to 5%, depending on the powder properties. The feeder demonstrates a high degree of repeatability and stability. The results of this work can be summarised as follows:

- The powdery material does not need to be pre-conditioned.

- The powder flow rate has no significant increase of powder flow rate over time as the powder pump has.
- The system can consistently feed powder down to 0.7 g/h of powder flow rate.
- The system can handle a wide range of powder properties.
- The system provides good repeatability and stability of low-quantity powder feeding.
- The system shows its controllability of a constant flow rate for a range of powder flow rates by adjusting the piston speed and air flow rate.
- This system does not require high air pressure and flow rate, and the air can be replaced by another gas, such as nitrogen, for various purposes.

In conclusion, this system's high consistency and low dose/flow rate will be particularly beneficial for manufacturing future solid oral dosage forms, such as HPAPI products. Future work will develop a continuous powder micro-feeder and introduce automation into the system to improve its accuracy and to meet current good manufacturing practice (cGMP) industrial applications.

6 Design and development of the pneumatic micro-feeder: A systematic approach

6.1 Chapter Summary

Chapter 5 presents a promising solution to the challenge of continuous and consistent powder feeding - a pneumatic micro-feeder that incorporates an innovative insert and plug mechanism to adjust the cross-sectional area and finely tune the air flow rate (Hou *et al.*, 2023). Unlike existing products in the market, this pneumatic micro-feeder presented offers the advantage of an adjustable insert and plug position, enabling control over the cross-sectional area. This adjustable feature allows the system to handle powders with varying flowability, including easy-flowing, cohesive, and non-flowing powders. By providing a narrow channel of cross-sectional area, the insert and plug configuration ensures high-precision adjustment of the air flow rate, consequently controlling the entrainment energy with exceptional accuracy.

The primary objective of this study is to conduct a comprehensive analysis of the data obtained from Chapter 5 to gain a deeper understanding of the operational principles underlying the pneumatic micro-feeder. Specifically, we focus on four key parameters: stable feed rate, air velocity, air mass flow rate, and entrainment energy. By employing mathematical analysis techniques, we aim to extract valuable insights into the system's performance and establish predictive models that can guide the selection of optimal parameter settings for different powder properties.

The significance of this research lies in its better understanding of revolutionising the pneumatic micro-feeder and optimising its ability to achieve more stable feed rates and precisely control the entrainment energy. In the following sections, we will delve into the methodology employed for data analysis, present the obtained results, and discuss their implications.

6.2 Materials and method

6.2.1 Material

The material properties are in accordance with section 5.2.1.

6.2.2 Pneumatic micro-feeder

The specifics of the pneumatic micro-feeder are presented in section 5.2.2. The pneumatic micro-feeder operates by utilising a powder supply unit to introduce powder into the system and supplying a steady air flow rate and air velocity to entrain and transport the particles to achieve a consistent powder flow rate. The pneumatic micro-feeder is composed of an air supply line, an entrainment bed, a powder supply unit, and a cyclone separator (Figure 6-1).

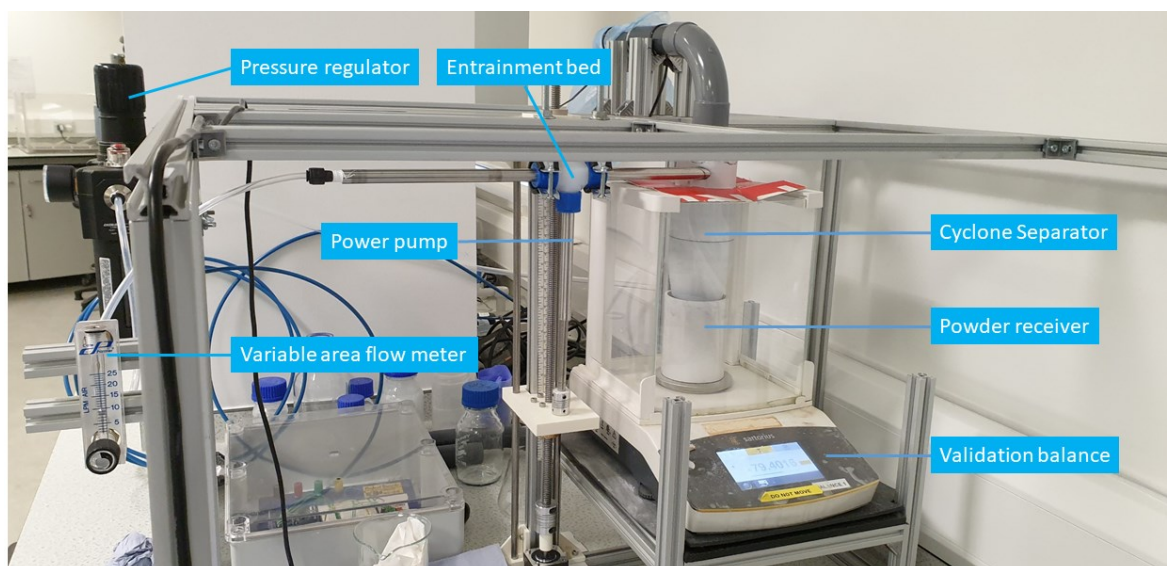


Figure 6-1: A photo of a pneumatic micro-feeder prototype.

6.3 Result and discussion

6.3.1 Relationship between powder flow rate and piston speed.

The aim of this section is to investigate the relationship between powder flow rate, piston speed, and flowability. The experimental results are compared and discussed with the mathematical model presented in Section 5.3.3.6.

A linear correlation is investigated between the powder flow rate and piston speed for all powders (Figure 6-2) in all tested materials. This correlation indicates a relationship between the slope and flowability, where the slope increases as the flowability decreases. The slope also indicates that the higher slope, the more sensitive the piston speed control requires in order to provide a consistent powder feed rate. Figure 6-2 demonstrates that CCS exhibits a steeper slope compared to MCC and APAP, consistent with the fact that APAP has higher flowability than MCC and CCS. However, there is an exception to this trend with XPVP. Despite its anticipated higher slope due to its high flowability, the result shows that XPVP falls between MCC and APAP in terms of slope. This observation could be attributed to the powder compression as MCC and XPVP exhibit very similar powder properties, but XPVP displays a higher compression compared to MCC. Overall, the figure unveils a linear relationship between powder flow rate and piston speed, which is beneficial in designing control systems.

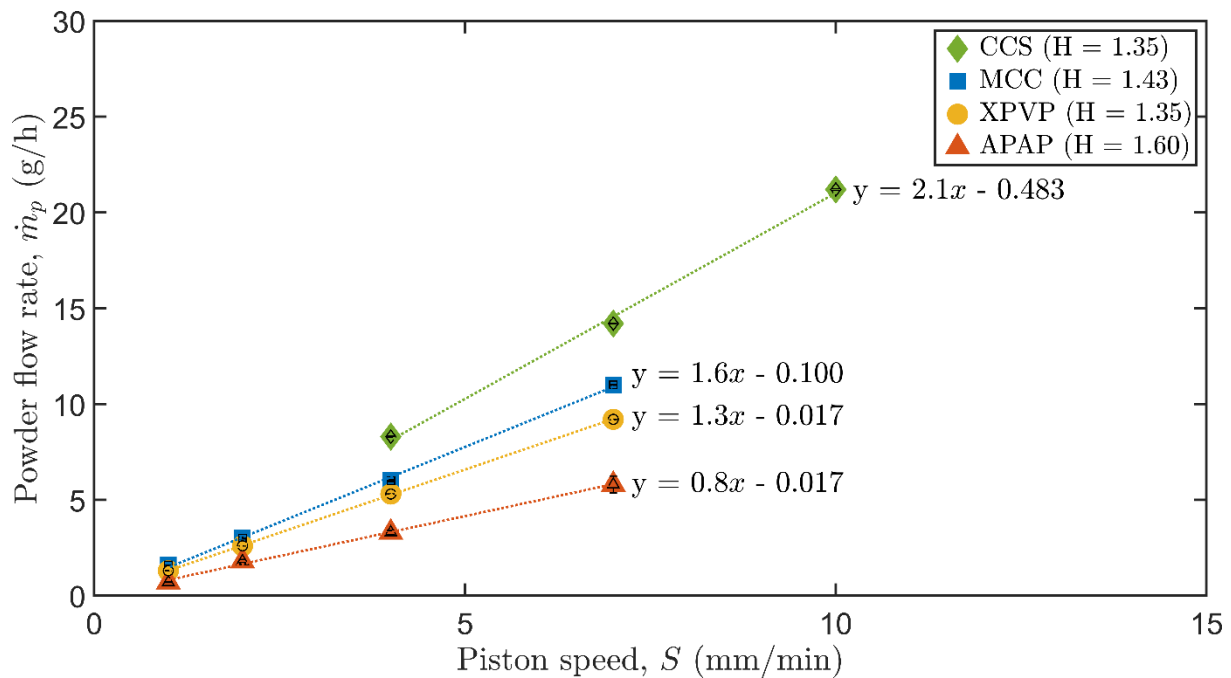


Figure 6-2: Linear relationship between average powder flow rate (averaged over three repeat experiments) with standard deviations shown as error bars, and piston speed for four different materials (MCC, CCS, XPVP, and APAP). H represents the Hausner ratio.

By employing Equation 5-18, the powder flow rate is computed, and the slopes of the materials are subsequently determined. The slopes of CCS, XPVP, and MCC are found to be 2.5, 1.6, and 1.4, respectively (Figure 6-3). The outcome closely aligns with the results depicted in Figure 6-2, the slope values of 2.1, 1.3, and 1.6. Notably, a significant deviation is observed between the experimental (0.8) and predicted (1.6) slopes for APAP. This deviation is attributed to the high degree of cohesion exhibited by APAP. Additionally, it is observed that the MCC and XPVP trends are inverted compared to those depicted in Figure 6-2. It should be noted that the difference in compression degree between MCC and XPVP, as it is highly dependent on the powder properties and operating conditions.

The results obtained herein indicate that Equation 5-18 can be used to extrapolate the piston speed required for cohesive and easy-flowing materials. However, for non-flowing materials, the predicted piston speed may be twice as high as the predicted value to ensure accurate performance. Therefore, when estimating the piston speed for non-flowing materials, it is crucial to consider the cohesion of the material.

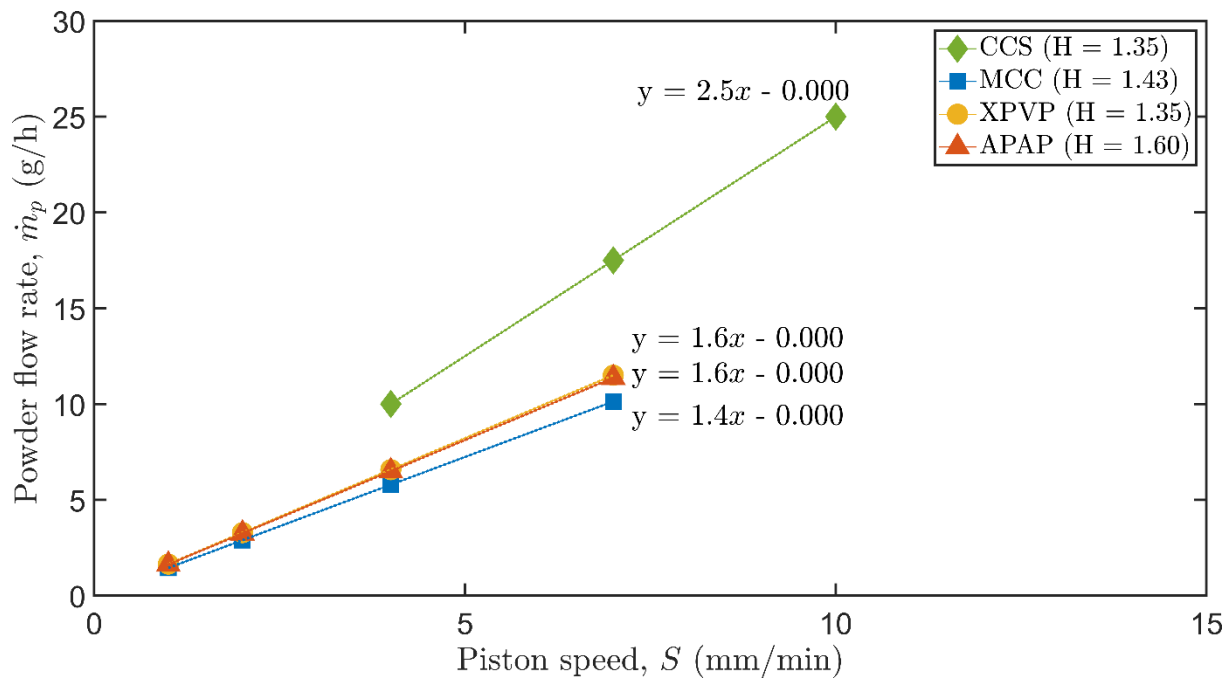


Figure 6-3: Predicted powder flow rate as a function of piston speed for four materials (MCC, CCS, XPVP, and APAP) using Equation 5-18. H represents the Hausner ratio.

6.3.2 Relationship between powder flow rate and air velocity.

The calculation of air velocity is a crucial factor in selecting the appropriate insert size, particularly for materials sensitive to entrainment energy, which includes air mass flow rate (mass) and velocity (momentum). Air velocity can be determined by dividing the air volumetric flow rate by the insert's free cross-sectional area.

Figure 6-4 demonstrates a nearly flat line, implying that a very small increase in air velocity was observed across changes in powder flow rate. However, this seems to confirm that the influence of air velocity on the average powder flow rate is minimal. Additionally, the figure shows that APAP has a considerably higher air velocity than the other three easy-flowing and cohesive materials due to its high cohesive force. This necessitates greater entrainment energy for efficient powder transport. Further discussion on this matter will be presented in Section 6.3.4. The result also indicates that the air velocity requirement has no direct relationship to the particle size.

The study confirms that the air velocity required for consistent powder feeding varies depending on the material properties. The air velocity remains nearly constant for the same material, suggesting that the required entrainment energy mainly depends on the air mass flow rate.

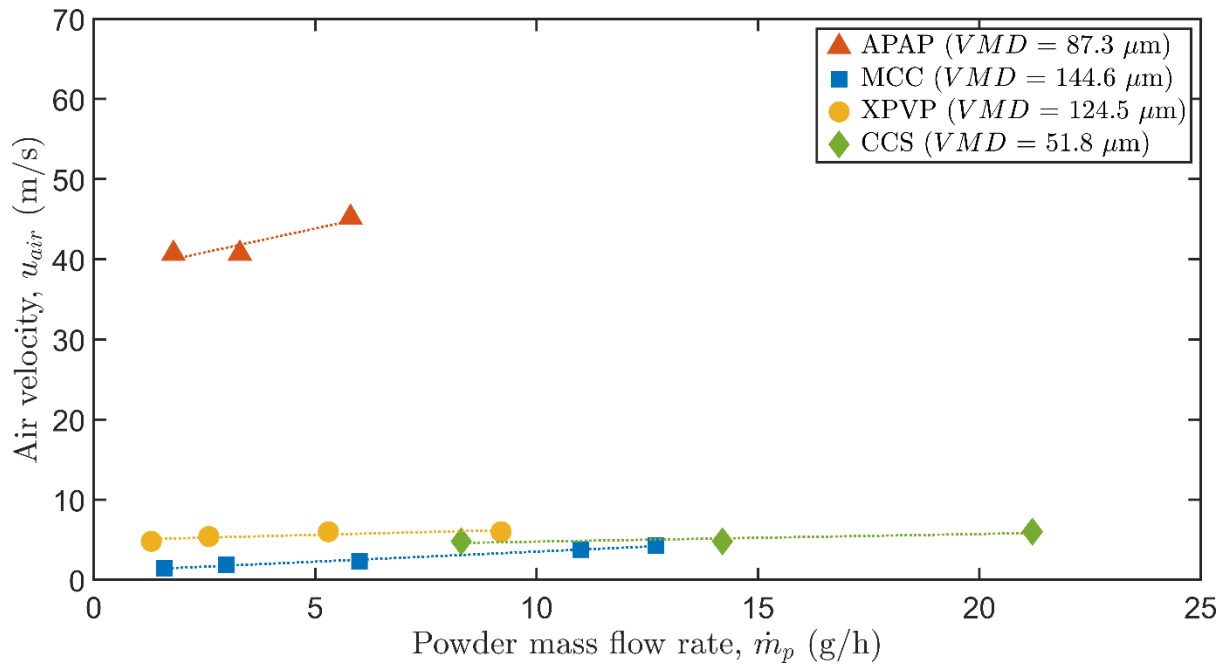


Figure 6-4: The relationship between air velocity and powder flow rate for four materials. The air velocity is calculated by the air volumetric flow rate divided by the insert's free cross-sectional area. For all materials, the effect of air velocity on powder flow rate is minimal, with slight variation observed in air velocity across changes in powder flow rate. *VMD* represents the volume median diameter.

6.3.3 Relationship between powder flow rate and air mass flow rate.

In this feeding system, flowability is a critical parameter that directly influences the efficiency of powder transport. Poor flowability of materials requires higher entrainment energy to achieve powder transport due to the cohesive forces between particles. As mentioned in the previous section, the air velocity remains nearly constant in the consistent powder feeding in the pneumatic micro-feeder. As such, this section examines the influence of air mass flow rate on powder flow rate and flowability.

Figure 6-5 shows that APAP exhibits significantly higher air mass flow rates than MCC, XPVP, and CCS, indicating its high cohesive force. For easy-flowing materials like XPVP and CCS, the closely flat line implies that nearly constant air mass flow rates are required, highlighting their sensitivity to air mass flow rate and difficulty adjusting the air flow rate during experiments. The figure also reveals a positive correlation between the Hausner ratio and the air mass flow rate required, meaning that the material with high Hausner ratio materials requires a high air mass flow rate as the powder flow rate increases and vice versa.

In summary, poor flowability necessitates a higher air mass flow rate and an incremental increase of air mass flow rate as the powder flow rate increases. Easy-flowing materials require a much lower air mass flow rate than non-flowing materials, but adjusting the air mass flow rate becomes more sensitive in the former case.

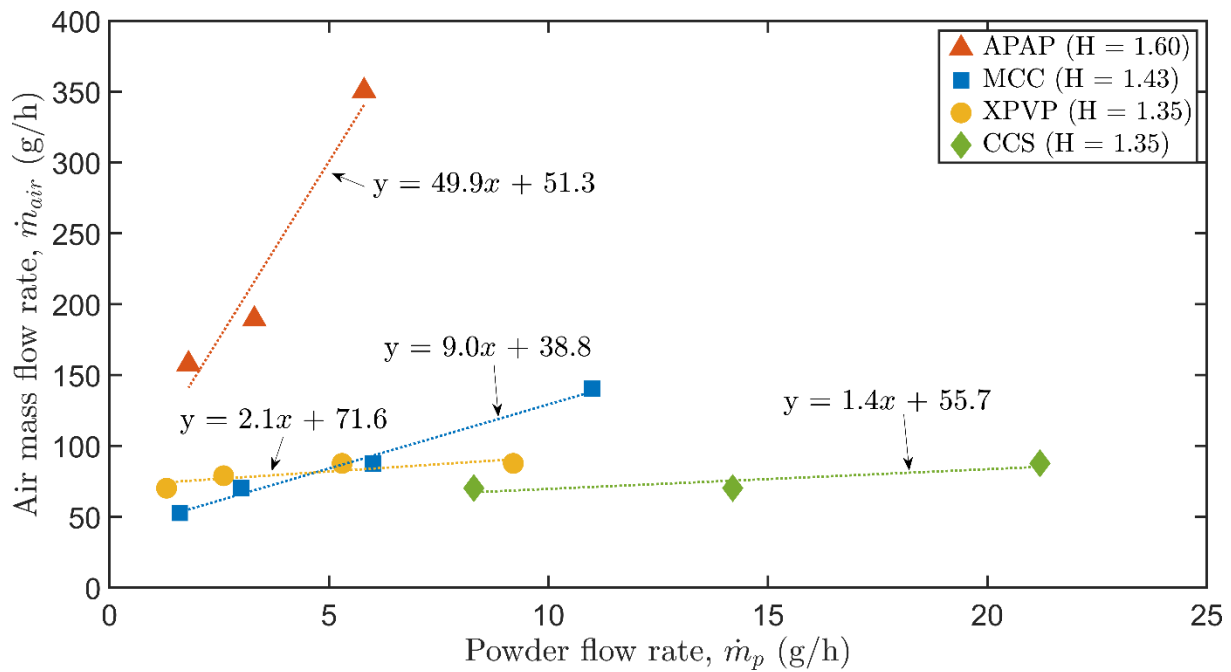


Figure 6-5: Relationship between powder flow rate and air mass flow rate for four different materials.

6.3.4 Relationship between powder flow rate and air entrainment energy.

We discussed the effect of air velocity and air mass flow rate on the powder feeding rate and flowability. In this section, we investigate the relationship between powder flow rate and air entrainment energy in the system. By neglecting the energy loss, the energy balance in the system can be represented by Equation 6-1, where the air entrainment energy is equivalent to the air kinetic energy provided to entrain the particles.

$$E_{air} = E_{entrainment} \cdot \quad \text{Equation 6-1}$$

The air kinetic energy can be calculated using Equation 6-2, which represents the kinetic energy of air based on the air mass flow rate and velocity.

$$E_{air} = KE_{air} = \frac{1}{2}mv^2. \quad \text{Equation 6-2}$$

Utilising the correlation between the entrainment energy and powder flow rate, a logarithmic scale linear graph was constructed, depicted in Figure 6-6. The graph signifies a logarithmic increase in the entrainment energy requirement with the rise in powder flow rate for the same materials. Notably, the entrainment energy requirement for MCC exhibited an unexpected significant increase with the increase in powder flow rate, despite still being substantially lower than the requirement for APAP. Conversely, APAP, which was anticipated to possess a high slope, demonstrated a nearly flat slope. This observation proposes that particle weight might be the primary factor influencing the increase in entrainment energy requirement in the same material instead of only cohesion. Nevertheless, further investigation is warranted to confirm this phenomenon in future studies.

In summary, if the entrainment energy requirement can be predicted, then the powder flow rate can be controlled more consistently, providing a succinct guideline for predicting parameter settings such as the selection of insert size, plug position, air flow rate, and air pressure. However, the calculation of entrainment energy must consider cohesion and particle weight.

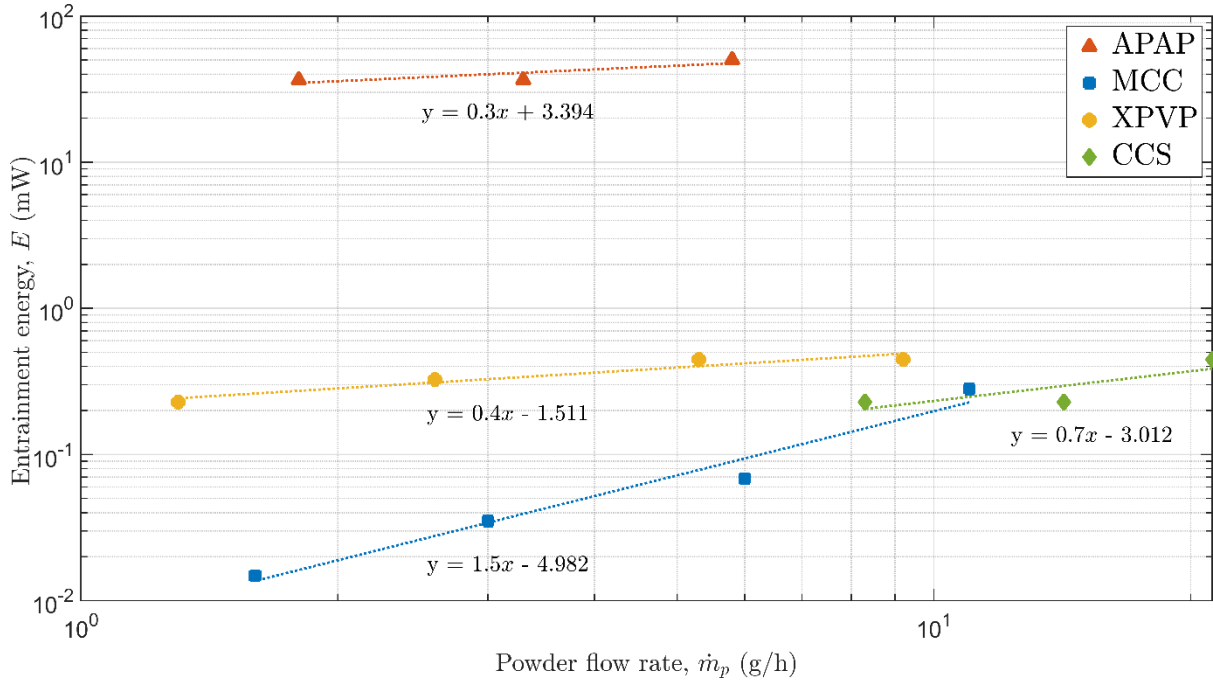


Figure 6-6: Entrainment energy as a function of powder flow rate for four different materials.

6.4 Conclusion

In this chapter, a comprehensive analysis of the data obtained from Chapter 5 is conducted to enhance our understanding of this system. The study focuses on examining the relationship between powder flow rate, air velocity, air mass flow rate, and entrainment energy, leading to the following key findings:

- A positive correlation exists between piston speed and powder flow rate, indicating that higher piston speeds result in increased powder flow.
- Air velocity does not exert a significant influence on the powder flow rate, suggesting that variations in air velocity have minimal influence on the feeding process.
- An increase in air mass flow rate directly leads to an increase in the powder flow rate.
- Easy-flowing materials are particularly sensitive to changes in air mass flow rate, indicating that adjustments in this parameter significantly affect the feeding of such materials.
- Increasing the powder flow rate necessitates a corresponding increase in entrainment energy, highlighting the relationship between these two variables.
- Poorly flowing materials demand higher entrainment energy to achieve consistent powder feeding, underscoring the importance of tailored energy inputs for different powder properties.

The innovative design allows for precise control of entrainment energy, effectively regulating the powder flow rate and minimising variations. By enabling reasonable control over these parameters, the pneumatic micro-feeder demonstrates its potential for consistent and reliable powder feeding in various applications.

7 A continuous micro-feeder for cohesive pharmaceutical materials

7.1 Chapter Summary

Over the past decade, continuous manufacturing has garnered significant attention in the pharmaceutical industry. Still, numerous continuous unit operations need development, such as powder blending and feeding at high and low throughputs. Especially the continuous and consistent feeding of solid drug substances and excipients at low feed rates remains challenging. The most common powder feeders in the pharmaceutical sector are screw feeders. Screw feeders are normally built on a load cell and rely on gravitational control to attain the preferred powder flow rate and reduce fluctuations through adjusting the screw speed. Numerous studies focus on the improvement of loss-in-weight (LIW) screw feeders through the refinement of the screws (Barati Dalenjan et al., 2015; Engisch and Muzzio, 2014; Santos et al., 2018) and the optimisation of the feedback control system (Blackshields and Crean, 2018). Despite these advancements, refilling LIW screw feeders remains a challenge due to their dependence on the load cell and the feedback control, resulting in additional variations in the mass flow rate during the refilling process (Blackshields and Crean, 2018; De Souter et al., 2023; Engisch and Muzzio, 2015). Other difficulties for LIW screw feeders that affect the consistency and precision of powder feeding include issues such as bridging, adhesion, cohesion, powder compression and vibrations (Janssen et al., 2022; Minglani et al., 2020; Peterwitz et al., 2022).

Owen and Cleary (2009) utilised discrete element method (DEM) simulations to analyse particle flow in inclined screw conveyors. The simulations revealed two main flow patterns that depended on the angle and fill level - a recirculating, heap-like flow at low angles versus a shearing flow in a uniform bed at higher angles. The simulations provided insights into how operating parameters like inclination angle, screw speed, and fill level impacted axial and swirling particle velocities, power draw, and collision energies in complex, non-linear ways. Overall, the inclination angle is suggested to be able to apply for optimising feeder design and performance. Therefore, we also introduce the inclination to our design.

This chapter introduces a new micro-feeder technology that combines an inclined screw feeder with a double-screw agitated hopper to enable highly consistent feeding of typical pharmaceutical materials at rates below 10 g/h. The double screw agitator speed controls the powder flow rate, while the feeding screw speed regulates the powder flow rate variation. The effects of feeding screw pitches, agitator speed, and screw speed are investigated in this chapter. The feeding performance and the mechanisms of the micro-feeder were investigated

using three grades of pharmaceutical powder: croscarmellose sodium (cohesive), magnesium stearate (non-flowing), and an active ingredient, paracetamol (non-flowing).

7.2 Materials and method

7.2.1 Material characterisation and material properties

Three poorly flowing powders were used: croscarmellose sodium (CCS, JRS pharma, Germany), magnesium stearate (MgSt, LIGAMED MF-2-V from Peter Greven Nederland C.V., Nederland), and an active pharmaceutical ingredient, paracetamol (APAP, Ph Eur Powder from Mallinckrodt Pharmaceuticals, Ireland). The details of material characterisation and properties of the materials used in this study can be found in Chapter 3.

7.2.2 Design Calculation

7.2.2.1 Hopper estimate

Carleton (1972) formulated a theory aimed at predicting the discharge rate of fine material from a hopper, with the theoretical discharge rate (\dot{m}) defined by Equation 2-16:

$$\dot{m} = \rho_b AV_0 \quad \text{Equation 2-16}$$

The expression for V_0 is given by:

$$\frac{4V_0^2 \sin\theta}{D} + \frac{15\rho_{air}^{1/3} \mu_{air}^{2/3} V_0^{4/3}}{\rho_p d_p^{5/3}} = g \quad \text{Equation 2-15}$$

In the present design, the properties of APAP powder were employed to determine the hopper size. Using a 25 mm orifice diameter and a hopper discharge angle of 15°, the powder flow velocity (V_0) was calculated as 0.00056 m/s through Equation 2-15. Substituting this value into Equation 2-16 yielded a discharge rate (\dot{m}) of 307 g/h, ensuring efficient screw fill. Figure 7-1 illustrates the schematic of the hopper.

To regulate the flow rate and homogenise bulk density within the hopper, an agitator was incorporated. Consequently, the investigation of the actual flow rate is detailed in Section 7.3.3.2.

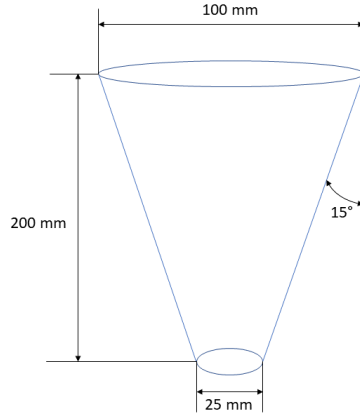


Figure 7-1: Hopper dimensions.

7.2.2.2 Screw blade angle design

The design of the screw blade angle adheres to the equation presented by Bates (2000), where the angle (θ) is expressed as:

$$\theta = \tan^{-1} \frac{\pi D}{P}. \quad \text{Equation 7-1}$$

In our specific design, a commercial tube with an internal diameter of 9.52 mm is employed. However, considering the variation in material properties, four different pitches (7 mm, 10 mm, 15 mm, and 25 mm) are analysed to assess the effectiveness of each. Figure 7-3 illustrates the schematic of the screw for a given pitch. The table provides the corresponding screw blade angles for each of the specified pitches. Table 7-1 displays the screw blade angles for each of the specified pitches.

Table 7-1: Screw blade angles

P (mm)	7	10	15	25
θ ($^{\circ}$)	76	71	63	50

7.2.2.3 Inclined screw flow rate estimate

According to Section 2.9.3.2.2, the feed screw capacity is given by the equation:

$$\dot{m}_p = 60 \frac{\pi}{4} (D^2 - d^2) P \rho \omega C \phi. \quad \text{Equation 2-31}$$

In this investigation, a stainless steel tube with an inner diameter of 9.52 mm was chosen, and the inclination angle was set to 30°, resulting in a C value of 0.55. The loading ratio was estimated to be 0.45 for CCS, whereas for MgSt and APAP, it was 0.15. Subsequently, Table 7-2 was generated to display the estimated feed screw capacity for three tested materials, along with design parameters.

Table 7-2: the design parameters and design calculation.

Material	Screw diameter, D (mm)	Inclination correction factor, C (-)	Loading ratio, φ (-)	Bulk density, ρ_b (kg/m ³)	Screw pitch, S (mm)	Screw speed, ω (rpm)	Screw capacity, \dot{m}_p (g/h)
CCS			0.45	529	7	5	19.6
						3	11.7
						1	3.9
MgSt	9.52	0.55	0.15	207	25	5	9.1
						3	5.5
						1	1.8
APAP			0.12	310	25	5	10.9
						3	6.6
						1	2.2

7.2.3 Micro-feeder design

The inclined screw feeder (Figure 7-2) is composed of three key design features: a feeding screw (Figure 7-3), a double-screw agitator (Figure 7-4) and a piping bag hopper. The feeding screw and double-screw agitator were fabricated using a high-precision stereolithography (SLA) printer (Form 2, FormLab, USA), while the screw housing was printed using a fused deposition modelling (FDM) printer (Ultimaker 3, Ultimaker, Netherlands). This fabrication approach enabled the system to be fine-tuned and optimised, providing maximum flexibility in design adjustments.

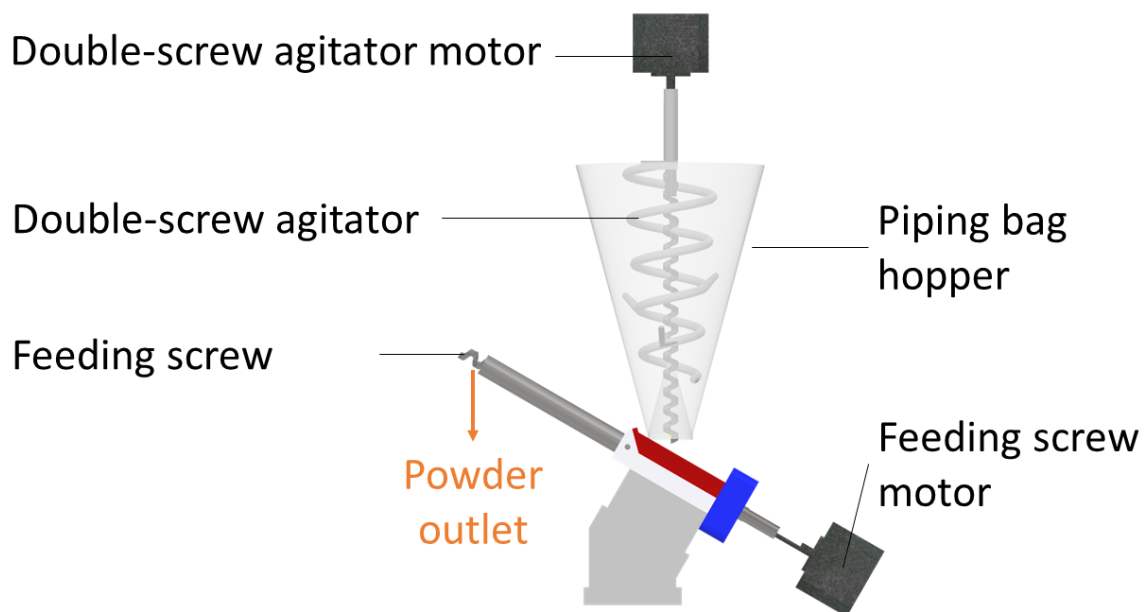


Figure 7-2: An overview of a schematic inclined micro-feeder.

7.2.3.1 Feeding screw

The unique feeding screw in this study is a design between an auger and a spiral screw. Unlike the auger screw, it eliminates the need for a central shaft, resulting in an increased screw pocket capacity and reduces powder compression due to shear stress on the wall and shaft. In contrast to spiral screws, this design does not have a hollow shaft, which eliminates the risk of unstable powder feeding caused by a steep drop of the powder flowing back into the screw housing. To investigate the effect of screw pitch on various powder properties, the study examined four screw pitches (7 mm, 10 mm, 15 mm, and 25 mm) to identify the optimal screw pitch.

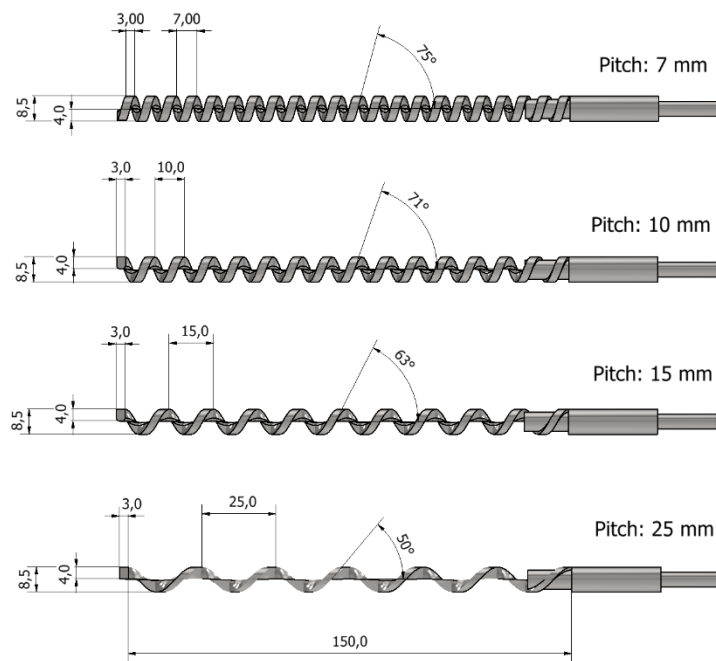


Figure 7-3: Schematic diagram of the feeding screws in four pitches: 7 mm, 10 mm, 15 mm and 25 mm.

7.2.3.2 Double-screw agitator

The double-screw agitator comprises a central feeding screw and an outer spiral screw tapered at 5° and a pitch of 25 mm, printed as two separate components, providing design versatility. This unique design allows the powder to circulate vertically in the hopper, effectively homogenising the bulk density and eliminating common issues such as rat holes and bridging, which are frequently observed in traditional LIW feeders.

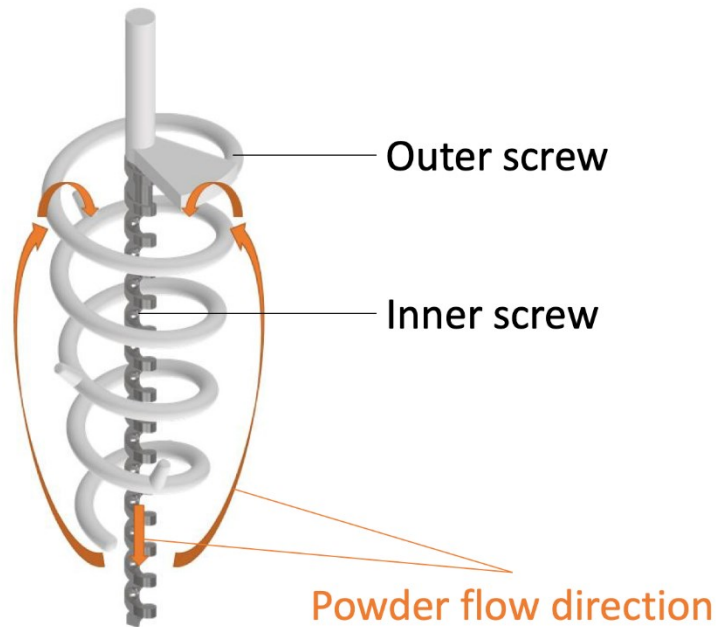


Figure 7-4: Schematic diagram of the double-screw agitator.

7.2.4 Operation

Initially, the powder must be added to the hopper until it reaches a level exceeding 50% of its total capacity. Subsequent refilling of the hopper should be initiated when the powder level falls below 20% of its total capacity, with each refilling involving the addition of approximately 80 mL of powder. To operate the feeder, two process parameters must be configured: the speeds of the feeding screw and the double-screw agitator. Each of these speeds can be regulated using stepper motors connected to an Arduino controller (Arduino Mega 2560). Both speeds can then be set by an operator in a MATLAB-designed graphical user interface (Figure 10-12 in Appendix). The inner screw of the double-screw agitator feeds the powder into the inclined feeding screw within the screw housing. The inclined screw transports the powder to a receiver positioned below the feeding screw outlet. Throughout this study, a pre-run was conducted before each measurement to ensure that the space of the feeding screw was filled with the powder. If the subsequent experiment employs the same parameter setting as the previous one, the pre-run is deemed unnecessary. A lab-scale balance (Sartorius Quintix 125D-1S, Germany) recorded the accumulating powder weight per second, which was then converted to a powder flow rate (g/h). An operator observed the powder level, and manual refilling was done when it went below one-fifth of the hopper level. Within the context of this study, the term "double-screw agitator speed" refers to the motor rotation rate (rpm) of the double-screw agitator, whereas the feeding screw speed refers to the motor rotation rate (rpm) of the feeding screw.

7.3 Results and discussions

7.3.1 Mass flow rate analysis

To analyse the performance of the powder feeding process, the weight of the powder was recorded using a catch scale at a frequency of 1 Hz (Figure 7-5). The acquired experimental mass was then used to calculate the mass flow rate, $\dot{m}_p(t) = \Delta m / \Delta t$, which represents the rate of powder mass accumulated within a certain time window, Δt . The experimental mass data exhibited a close approximation to a linear trend, as depicted by the red-dashed line in Figure 7-5.

In continuous powder feeding processes, fluctuating weight measurements can arise from various factors, such as the height of the feeding position (the effect of feed height on the measurement was investigated and presented in Appendix 10.2.2) and the weight of the material fed. In this study, measurement noise was identified to be caused by a vibrating spring in the balance due to the initial and subsequent drops arriving at the balance pan, preventing the balance from reaching a stable equilibrium.

To mitigate the influence of measurement noise on powder feeder performance analysis, a 60-second moving mean filter was employed. This technique, widely used in spectral data and powder feeding analysis in previous studies (Beretta et al., 2023; Bostijn et al., 2019; Fathollahi et al., 2020; Y. S. Huang et al., 2022; Johnson et al., 2022), was applied to the weight difference of the powder fed per second. While complete elimination of these factors may not be feasible, the implementation of this filter serves to minimise their influence on further analyses. Figure 7-5 depicts the CCS powder feeding process with the additional application of a 60-second moving mean window to the generated data (g/s), which was subsequently converted to g/h. This data is then further used to calculate the mean powder flow rate, SD, and RSD.

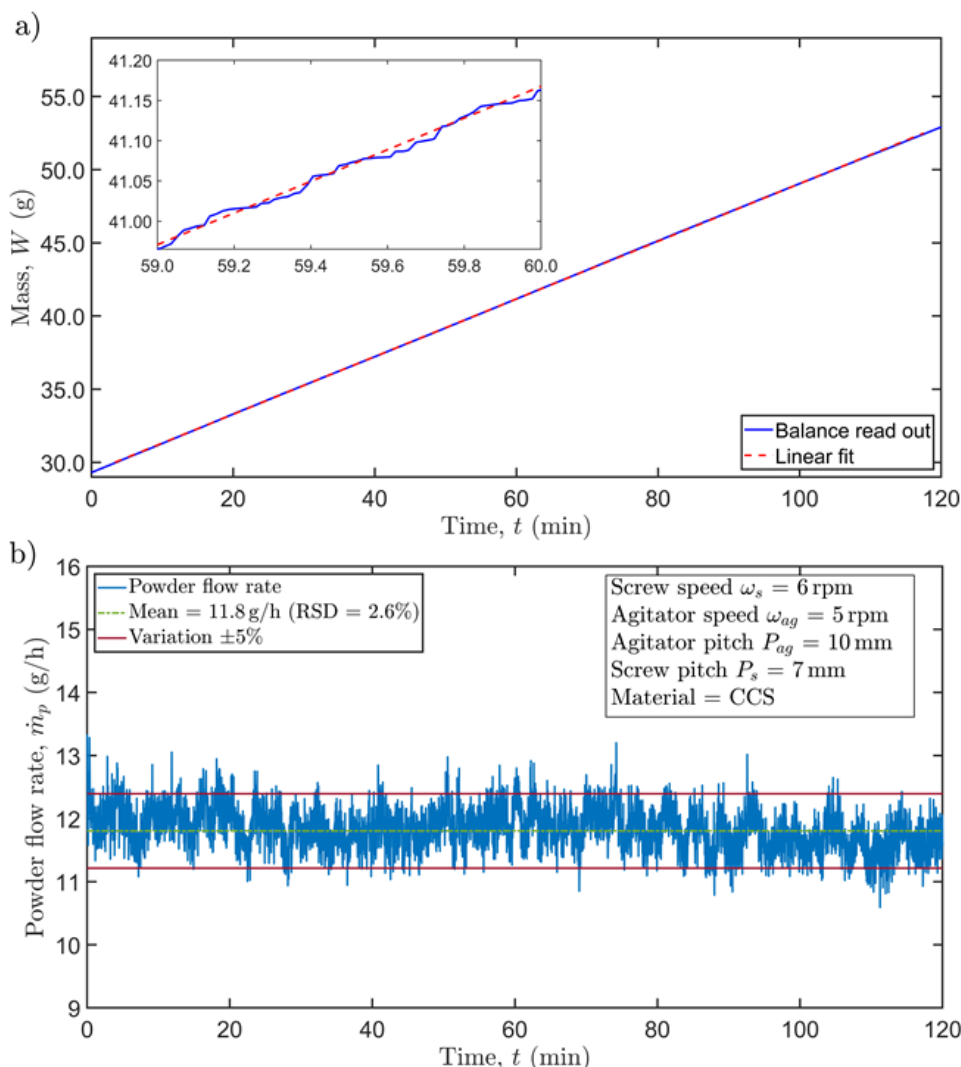


Figure 7-5: Data acquisition and analysis of continuous CCS powder feeding at 6 rpm feeding screw speed and 5 rpm double speed agitator speed over 2 hours: a) experimental mass acquired at 1-second intervals from the catch scale; b) filtered mass flow rate using a 60-second moving mean window. The green dashed line represents the mean powder flow rate, while the upper and lower solid red lines denote the predetermined range of variation, set at $\pm 5\%$ for this particular experiment.

To ensure the moving mean filter does not remove real variability, 30- and 60-second manual measurement experiments were conducted at identical operational conditions without applying any filter. Figure 7-6 depicts an example of APAP feeding over a period of 30 minutes, with manual measurements taken at one-minute intervals, alongside automatic data acquisition with the implementation of a 1-minute moving mean filter. Figure 7-6 provides a comprehensive summary of the outcomes derived from both manual and automatic measurements. The results indicate that the RSDs using the moving mean filter are larger (or equal to the highest CCS flow rate) than the RSD of the manual measurements. The findings reveal that this particular manual measurement variation yields lower results compared to applying a 60-second moving mean. This indicates that using the 60-second moving mean filter does not eliminate genuine data points. In addition, the difference in RSDs between

moving mean and manual measurement reduces with increasing powder flow rate. This is attributed to the fact that the time it takes the balance to stabilise has a stronger influence on the RSD at low flow rates. Overall, using a time window of 60 seconds with the moving-mean filter technique can effectively reduce the measurement noise without compromising the actual data. However, a longer time window of 120 seconds is necessary when dealing with lower powder flow rates below 2 g/h due to the limited accuracy of the balance. By applying moving-mean, the balance spring vibrations caused by continuous feeding can be minimised, leading to more reliable and accurate measurements. The comparison between applying moving mean filter and Savitzky-Golay derivative filter is investigated and presented in Appendix 10.2.3.

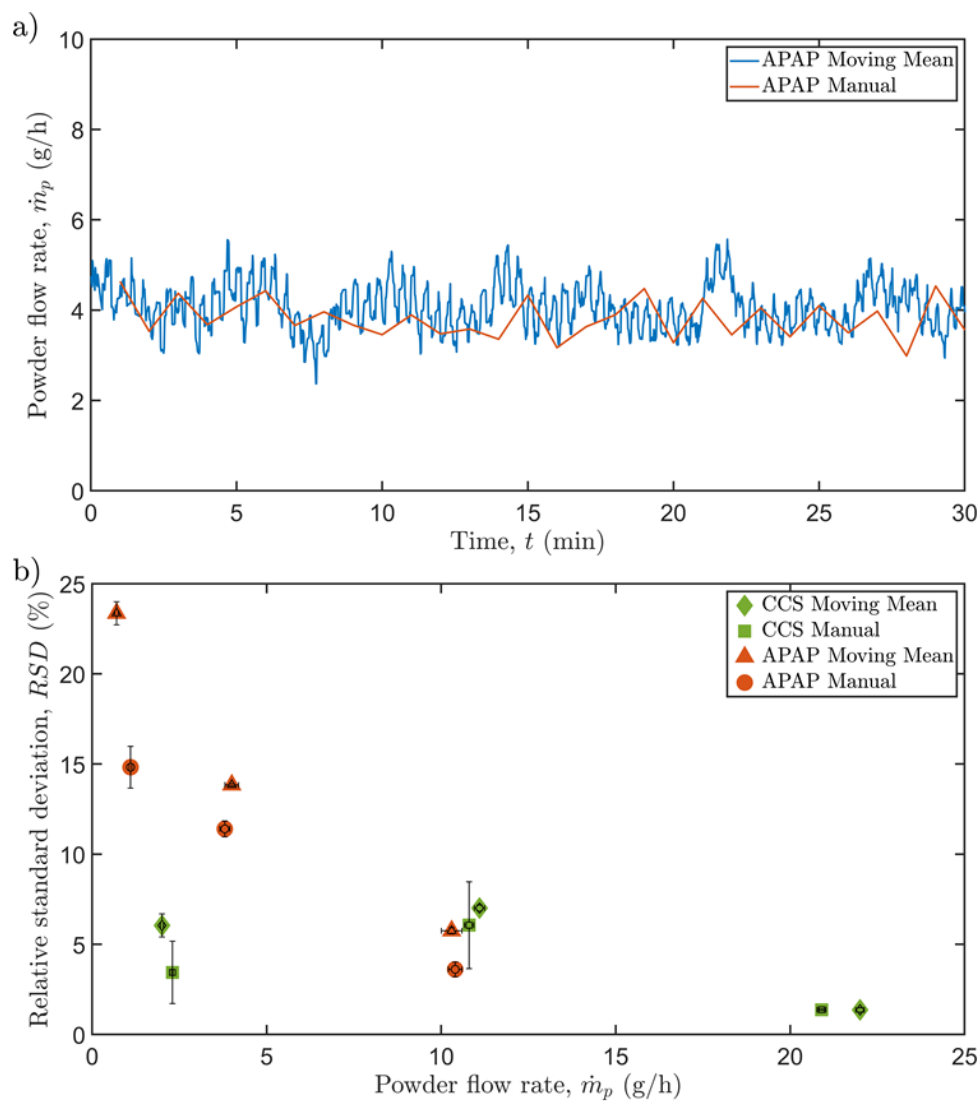


Figure 7-6: Effect of powder flow rate on RSD for automation and manual operation with 60-second window measurement, and APAP with lowest powder rate at 120-second window measurement. a) an illustration of APAP feeding conducted over a 30-minute duration, with manual measurements recorded at one-minute intervals, juxtaposed with automatic data acquisition utilising a 1-minute moving mean filter; b) a comprehensive summary of the results obtained from both manual and automatic measurements. Each measurement was done in triplicate ($n = 3$).

7.3.2 Refilling

Numerous investigations have explored the influence of hopper refill and fill level on feeding consistency, with notable studies conducted by Janssen et al. (2022), Van Snick et al. (2017), Hörmann-Kincses et al. (2022), Tahir et al. (2020). Figure 7-7 present distinct case studies involving various powder materials and feeder types.

In Figure 7-7a, Janssen et al. (2022) conducted repeated lactose feedings ($H = 1.21$, fair-flowing material) using a 22 mm double concave screw in volumetric mode. Figure 7-7b, based on Tahir et al.'s (2020) work, illustrates the application of a GEA compact feeder for MgSt feeding with a 20 mm concave screw (Bin# = hopper fill level). Figure 7-7c showcases Van Snick et al.'s (2017) exploration of different powder properties using a concave screw. Lastly, Figure 7-7d highlights Hörmann-Kincses et al.'s (2022) investigation into M200 grade mannitol feeding using different types of feeders.

Consistent findings across all experiments reveal a gradual decrease in the feed factor with changes in the hopper fill level. Compression at the bottom of the powder results in a higher bulk density. As the feeding progresses and the hopper level decreases, the bulk density lowers, resulting in a gradual reduction in the powder flow rate. This trend is particularly pronounced in highly compressible powders such as MgSt and APAP. Additionally, materials with poor flow characteristics exhibit lower feed factors due to alterations in powder density within the hopper.

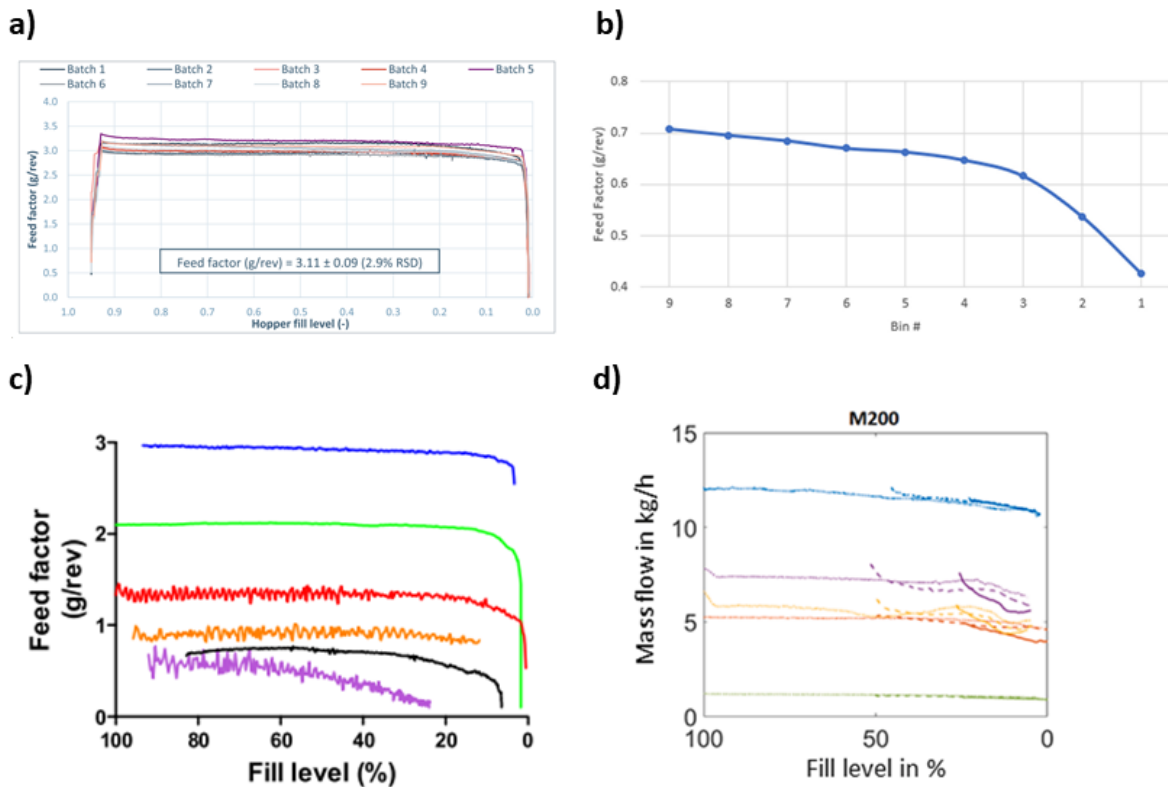


Figure 7-7: Illustrations depicting the impact of hopper fill level on the consistency of powder feeding. a) Feed factors plotted against hopper fill level for six iterations of spray-dried lactose ($H = 1.21$ – fair-flowing) in volumetric mode, utilising a 22 mm double concave screw (Janssen et al., 2022). b) Feeding of MgSt with hopper fill level variation (Bin#) using a GEA compact feeder equipped with a 20 mm concave screw (Tahir et al., 2020). c) Feed factor variations across six different materials – Colour codes: Starch1500 (blue), Methocel DC2 (red), NAP+SiO₂ (orange), MgSt (black) and NAP (purple) (Van Snick et al., 2017). d) Diverse feeders delivering M200 grade mannitol with a coarse concave screw at 50% screw speed – Colour codes: Coperion-KTron KT20 (blue), Compact feeder (yellow), Compact feeder with adapted hopper (purple), ZD12FB (orange), and Brabender MT-S (green) (Hörmann-Kincses et al., 2022).

The hopper in this study was refilled approximately every 20 minutes, with the amount of powder added varying depending on the feed rate. On average, around 80 millilitres of powder were added to the hopper during each refill. The effectiveness of the refilling process was monitored and analysed through Figure 7-8, which captures the feeding process over a period of 2 hours for three different materials. The results revealed that no significant excessive variations were observed during the feeding process, indicating that the design of the double-screw agitator used in this study effectively mitigated any variations caused by the refilling. In contrast to current industrial feeders, the double-screw agitator eliminates variations in the mass flow rate induced by refilling.

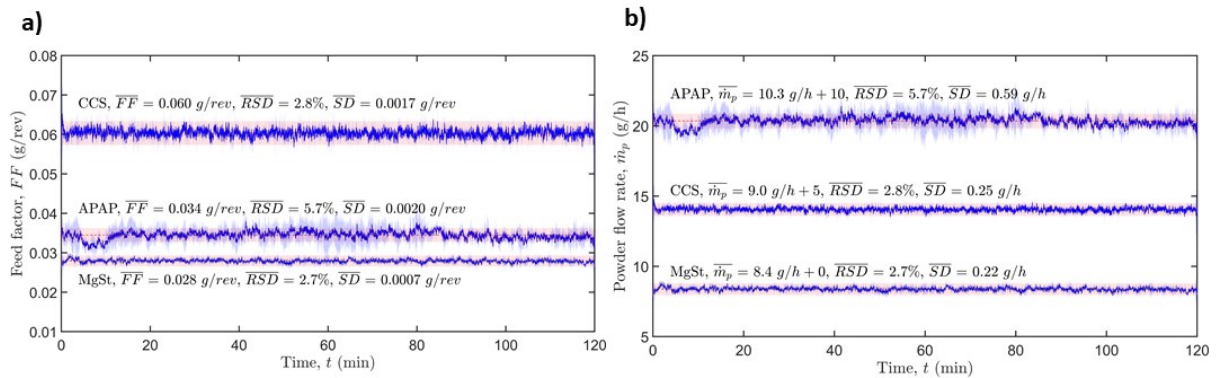


Figure 7-8: Refilling every 20 mins in continuous feeding demonstrated in three different materials: a) Variation in feed factor over feeding time, b) Changes in powder flow rate with respect to feeding time. All experiments were performed in triplicates ($n = 3$). The blue line is the mean powder flow rate. The blue shadow represents the SD of three repeated experiments. The red shaded belt represents $\pm 5\%$.

Another aspect challenging consistent powder feeding is the hopper refill, as depicted in Figure 7-9, where it induces inconsistent feeding marked by sudden peaks at the refill point. Interestingly, our feeding figure does not exhibit this issue, indicating that the hopper refill does not affect feeding consistency in this design. This is attributed to the action of the agitator, which continuously circulates the powder in the hopper. Upon addition to the hopper, the refill is promptly circulated, preventing the powder compression, which leads to a decrease in bulk density and, consequently, results in a higher feed rate, particularly beneficial for sensitive compressible materials.

As a result of the increase in bulk density resulting from powder compression, it also prompts a decrease in screw speed in gravimetric control. In scenarios where refill occurs, the compression and increased bulk density can cause a sudden spike in feed rate, leading to unstable control. In contrast, the absence of an influence on feed rate in our design suggests that the agitator plays a crucial role in homogenising bulk density within the hopper. This, in turn, ensures a more stable and consistent powder feeding experience across various fill levels.

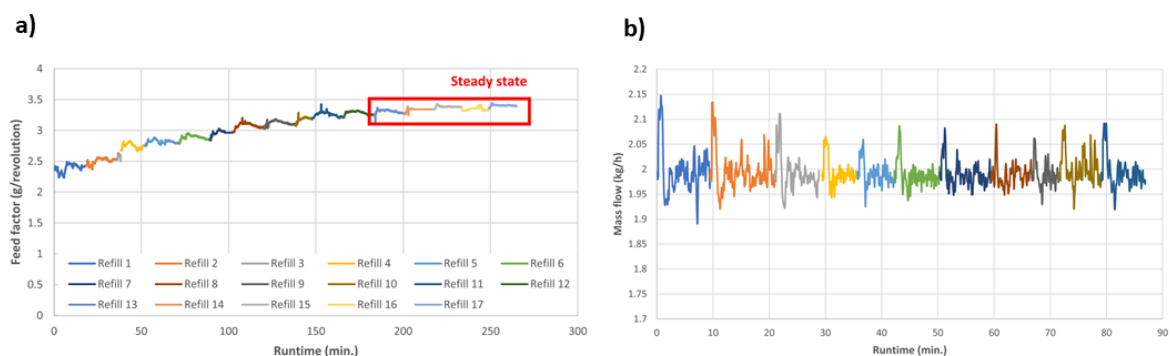


Figure 7-9: Illustration depicting the effect of hopper refill on powder feeding performance. a) Feed factor profile for paracetamol during a single feeding period. b) Mass flow profile of paracetamol powder across 11 refills in a feeding period, highlighting observable refill overshoots after each refill (Bekaert et al., 2022).

7.3.3 Effect of equipment configuration and process parameters on feeding performance

7.3.3.1 Feeding screw pitch

Figure 7-10 presents the effect of screw pitch on feeding three different powders - APAP, MgSt, and CCS. The results reveal that a screw pitch of 25 mm leads to a lower SD of 0.44 g/h for APAP, while a pitch of 7 mm gives a lower SD of 0.67 g/h for CCS. Although a pitch of 25 mm yields a slightly higher SD of 0.41 g/h for MgSt compared to a pitch of 10 mm (0.37 g/h), it provides better stability ($\sigma_{SD}=2.3\%$) for MgSt using a 25 mm pitch, whereas 10 mm pitch results in $\sigma_{SD}=16.3\%$. These findings suggest that using a screw pitch of 25 mm for MgSt can maintain better precision and consistency in the powder feeding process. Furthermore, it is observed that the application of a 7 mm pitch for APAP and MgSt results in screw clogging. Based on these findings, it is recommended that highly cohesive materials such as APAP and MgSt are better suited for larger screw pitches to stabilise the feeding process, while materials with better flowability, like CCS, benefit from smaller screw pitches.

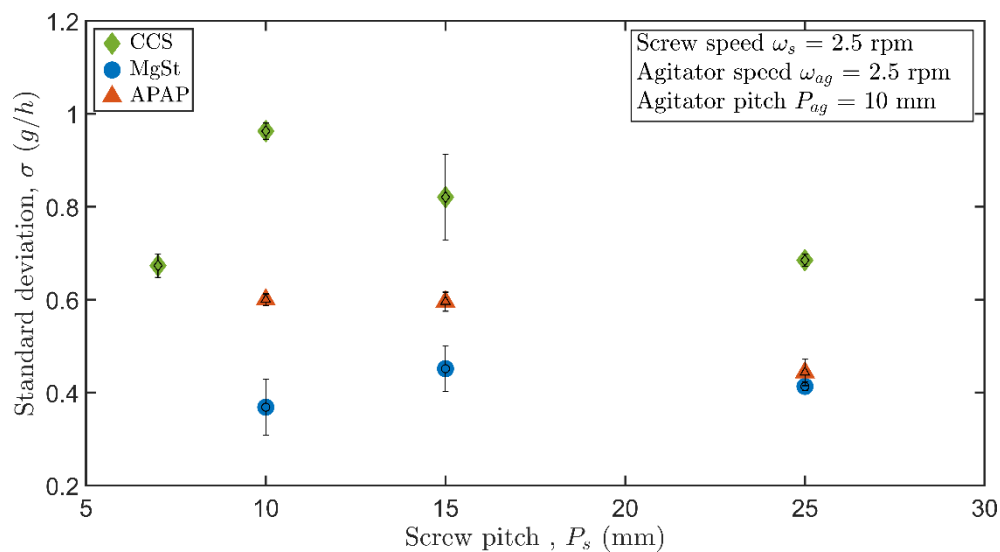


Figure 7-10: Standard deviation as a function of screw pitches for CCS, MgSt and APAP. Each measurement was done in triplicate ($n = 3$).

When designing a screw feeder, the volumetric efficiency emerges as a crucial parameter intricately linked to factors such as feeder load, bulk solid properties, and screw configuration. Employing an analytical solution for volumetric efficiency calculation enables a comprehensive grasp of how the pitch influences the volumetric efficiency in our screw design. The estimation of volumetric efficiency utilises the equation introduced in Section 2.9.3.2.3. Figure 7-11 provides the volumetric efficiency values obtained from the equation and compares them with the observed volumetric efficiency at various P/D ratios. As depicted in Figure 7-11, the calculated volumetric efficiency decreases with an increase in the P/D ratio. The observed volumetric efficiency follows a similar trend but at significantly lower efficiency levels. Difference between the predicted and observed volumetric efficiency stems from the omission

of factors such as the friction coefficient of the bulk solid and the inclination of the screw in this calculation.

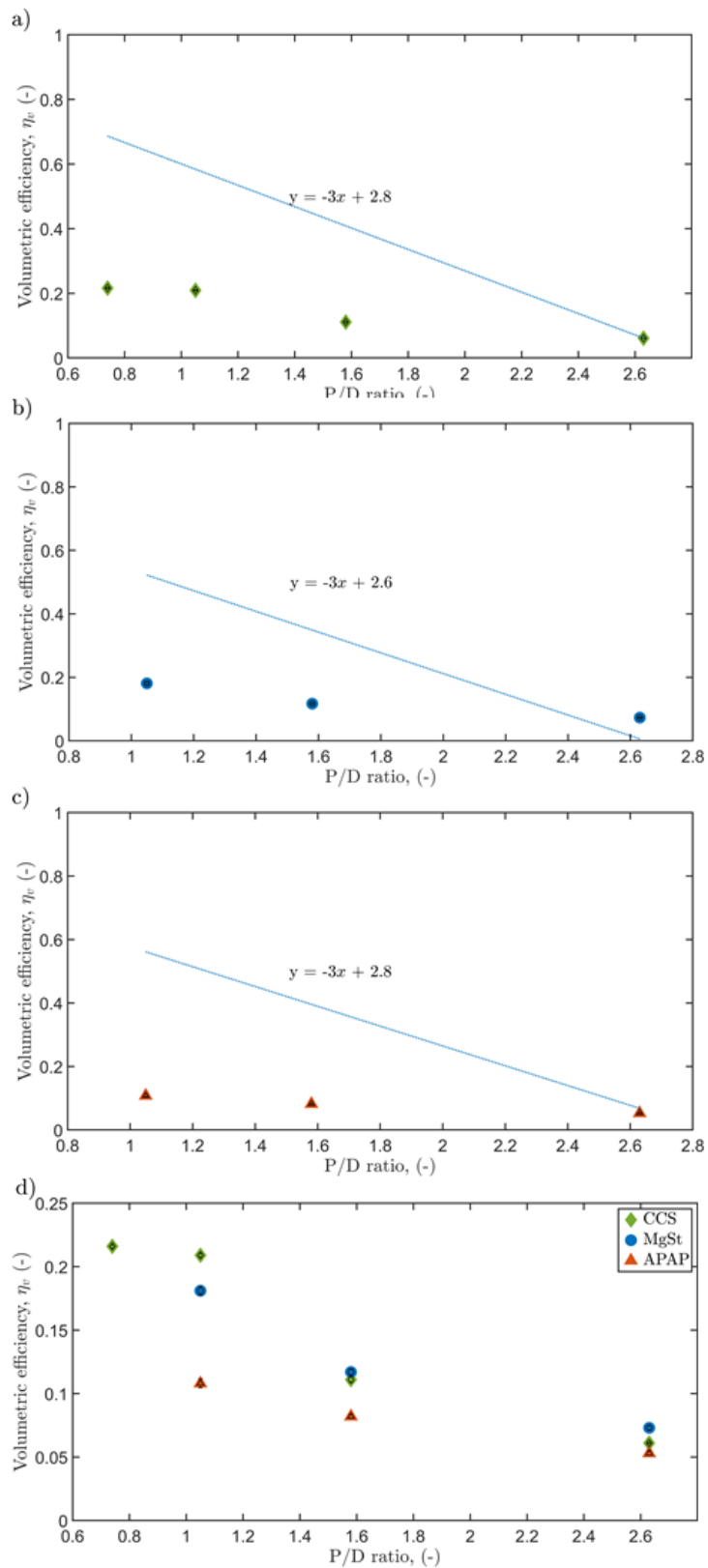


Figure 7-11: Effect of P/D on η_v in different tested materials a) CCS, b) MgSt, c) APAP, and d) summary of volumetric efficiency of all tested material. The speed of the feeding screw is configured to 2.5 rpm, and the agitator operates at a speed of 2.5 rpm.

Furthermore, the assessment of the feed factor is a pivotal parameter for evaluating screw design. The prediction suggests that an increase in the P/D ratio should lead to a corresponding increase in the feed factor. However, Figure 7-12 demonstrates that the feed factor remains relatively consistent at a constant speed across different pitches at constant screw and agitator speeds. This indicates that the screw pitch is not a major factor influencing the powder flow rate. This finding deviates from the suggestion in the literature by Hou et al. (2014). The actual feed factor is considerably lower than predicted. Several factors contribute to this result, including the omission of inclination and loading ratio in the prediction. In this particular design, the loading ratio is influenced by the agitator. Further exploration of this phenomenon is detailed in Section 7.3.3.2 and 7.3.5. In conclusion, the screw pitch in the design has minimal impact on the powder flow rate itself but affects the variation in powder flow rate. Hence, the selection of the pitch is still a crucial step in ensuring consistent feeding during the practical implementation of this design.

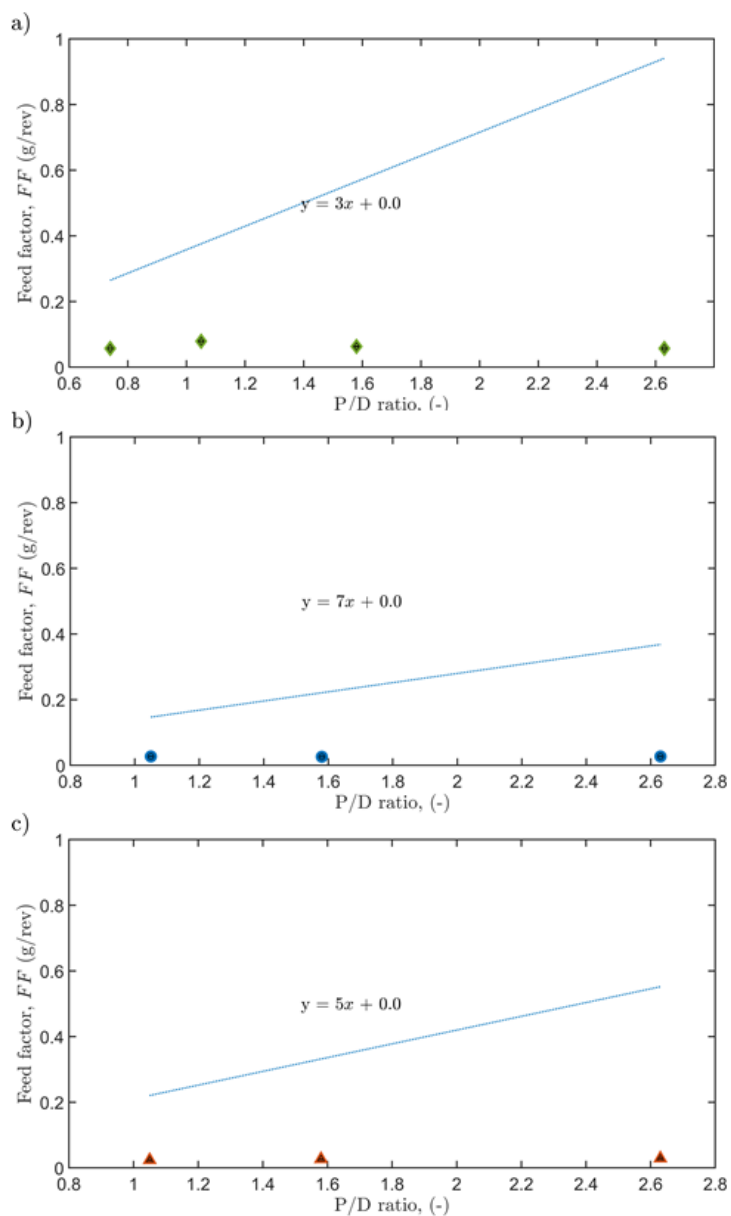


Figure 7-12: Effect of P/D Ratio on Feed Factor (FF) in a) CCS, b) MgSt, and c) APAP.

7.3.3.2 Double-screw agitator speed

Increasing the agitator speed while maintaining a constant feeding screw speed leads to a considerable increase in the powder flow rate (Figure 7-13). Moreover, Figure 7-13 indicates that as agitator speed increases, the SD also increases with the increase in powder flow rate for APAP and MgSt. Conversely, the outcome of CCS feeding reveals a contrasting pattern, whereby an augmentation in the increase of agitator speed leads to a decrease in the SD. The results also demonstrate that increased agitator speed leads to a decrease in the RSD for the three tested materials (Figure 7-13). Figure 7-13 shows that the agitator and feeding screw speeds are critical parameters that influence the powder flow rate and the RSD. However, the effect of these parameters on the powder flow rate and RSD depends on the powder

properties and agitator design, necessitating careful consideration when optimising the performance of the inclined screw feeder.

The experimental results confirm the critical role of the agitator in ensuring consistent powder feeding. In the absence of the agitator, issues such as rat holing and bridging arise, making continuous feeding impossible. The application of a double-screw agitator also helps to overcome the refilling issues that current LIW feeders face.

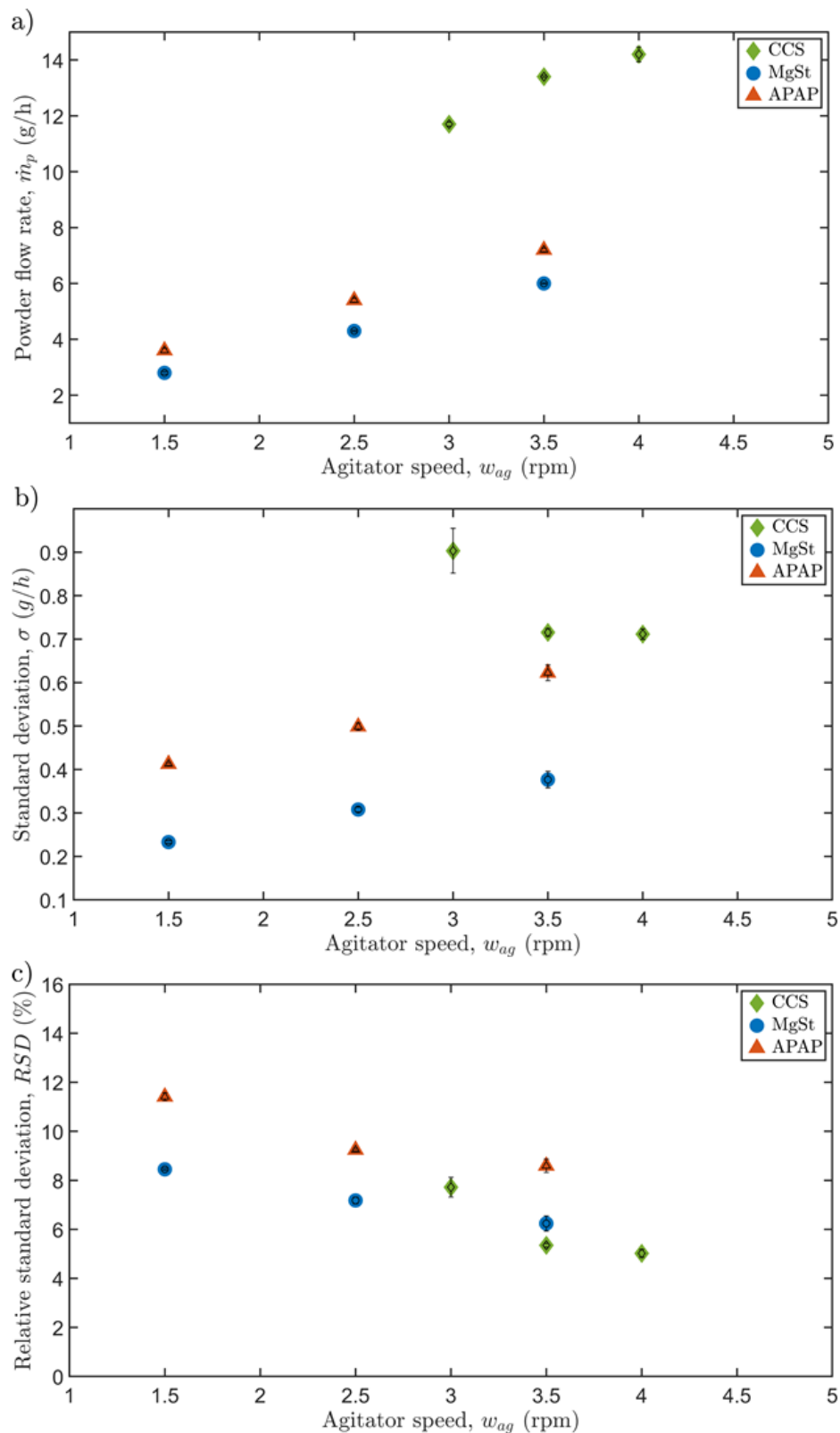


Figure 7-13: The effect of double-screw agitator speed on powder flow rate, SD and RSD. a) The mean powder flow rate from three repeated experiments ($n = 3$) is plotted in relation to agitator speed for three different powder properties at a fixed feeding screw speed of 3.5 rpm. b) SD is plotted in relation to agitator speed. c) RSD is plotted in relation to agitator speed.

Figure 7-14 illustrates a clear trend: as the agitator speed rises, so does the feed factor at a constant screw speed. This underscores the impact of agitator speed on the powder feed rate. With an increase in agitator speed, the powder flow rate shows a consistent rise across all materials. Notably, in cases examined in this study, the relationship proved to be linear, indicating a consistent filling of the screw flights by the powders. This observation implies that calibration or calculation of the feed factor for volumetric operation can be reliably undertaken.

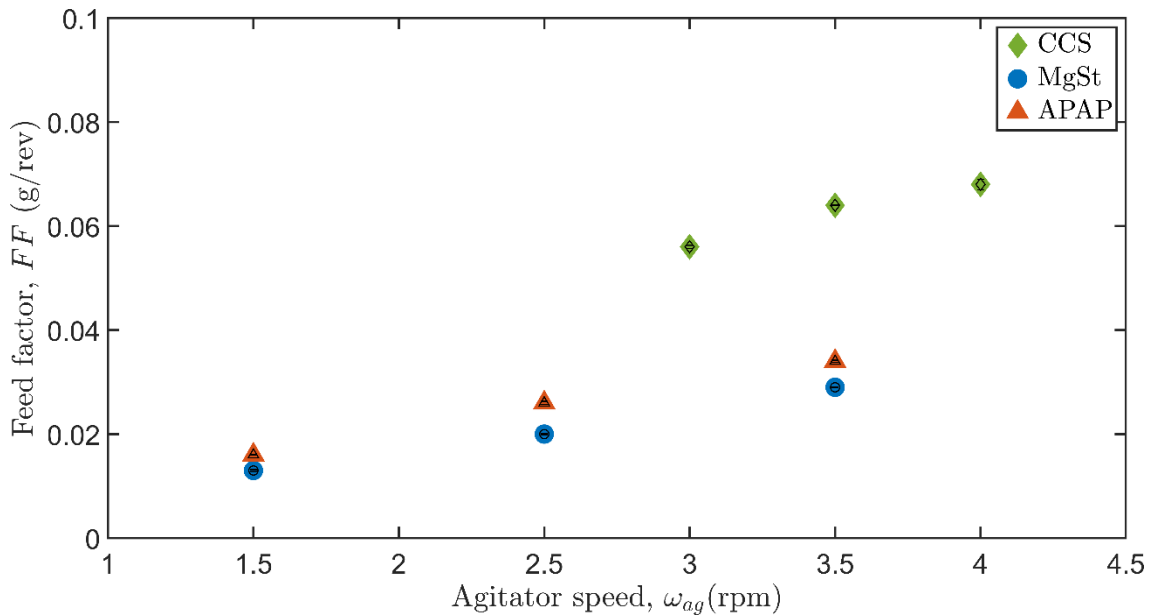


Figure 7-14: Feed factor as a function of agitator speed at a constant screw speed of 3.5 rpm.

7.3.3.3 Feeding screw speed

For process optimal process settings, it is vital to understand the influence of various ratios between feeding screw speed and double-screw agitator speed on the stability of the powder flow rate in the system. Figure 7-15 indicates that all investigated materials exhibit a close to constant feeding rate with variations below 5%, indicating stable and consistent feeding.

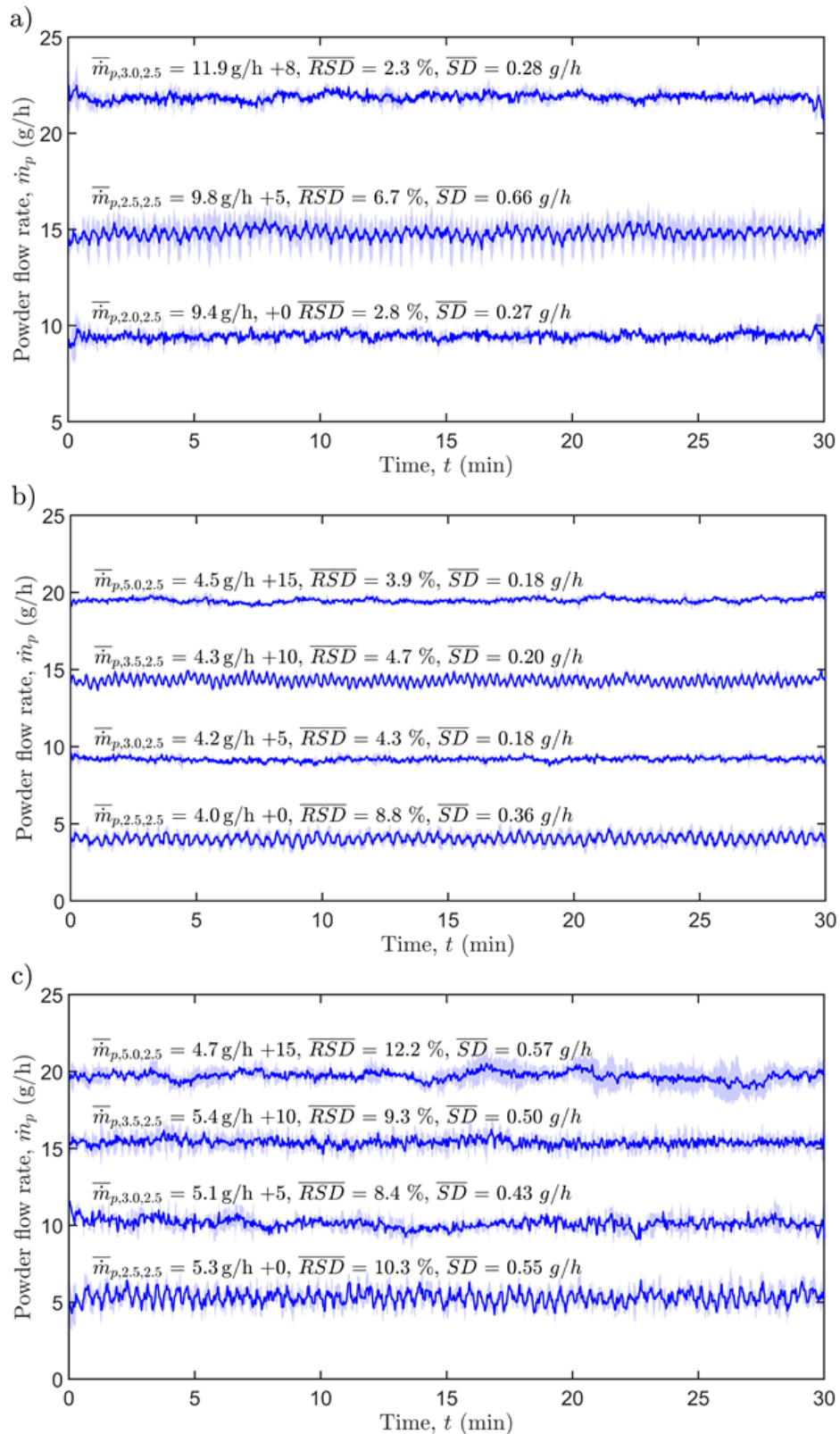


Figure 7-15: Effects of feeding screw speed on powder flow rate, SD and RSD for three distinct powder properties. a) CCS, b) MgSt, and c) APAP powder feeding at varying feeding screw speeds and a constant agitator speed of 2.5 rpm. The blue line is the mean powder flow rate. The blue shadow represents the SD of three repeated experiments.

Figure 7-16 shows that the screw speed has a relatively minor influence on the powder flow rate compared to the more significant influence of agitator speeds, as discussed in Section 7.3.3.2. Nevertheless, it indicates that increasing the feeding screw speed slightly enhances the CCS powder flow rate but has an insignificant influence on the flow rates of MgSt and APAP powders.

Figure 7-16, on the other hand, emphasises the notable influence of feeding screw speed variation on SD and RSD while maintaining a constant double-screw agitator speed. The results demonstrate fluctuations in both SD and RSD as the feeding screw speed increases. Nevertheless, the results of these experiments reveal that the system demonstrates the best stable and consistent powder feeding for CCS and APAP when the agitator speed is 0.5 rpm higher than the feeding screw speed. Moreover, MgSt has its optimal point at 2.5 rpm (twice the feeding screw speed). This result suggests the existence of an optimal value for a specific screw speed to agitator speed ratio, and adjusting this ratio can enhance the consistency of powder feeding.

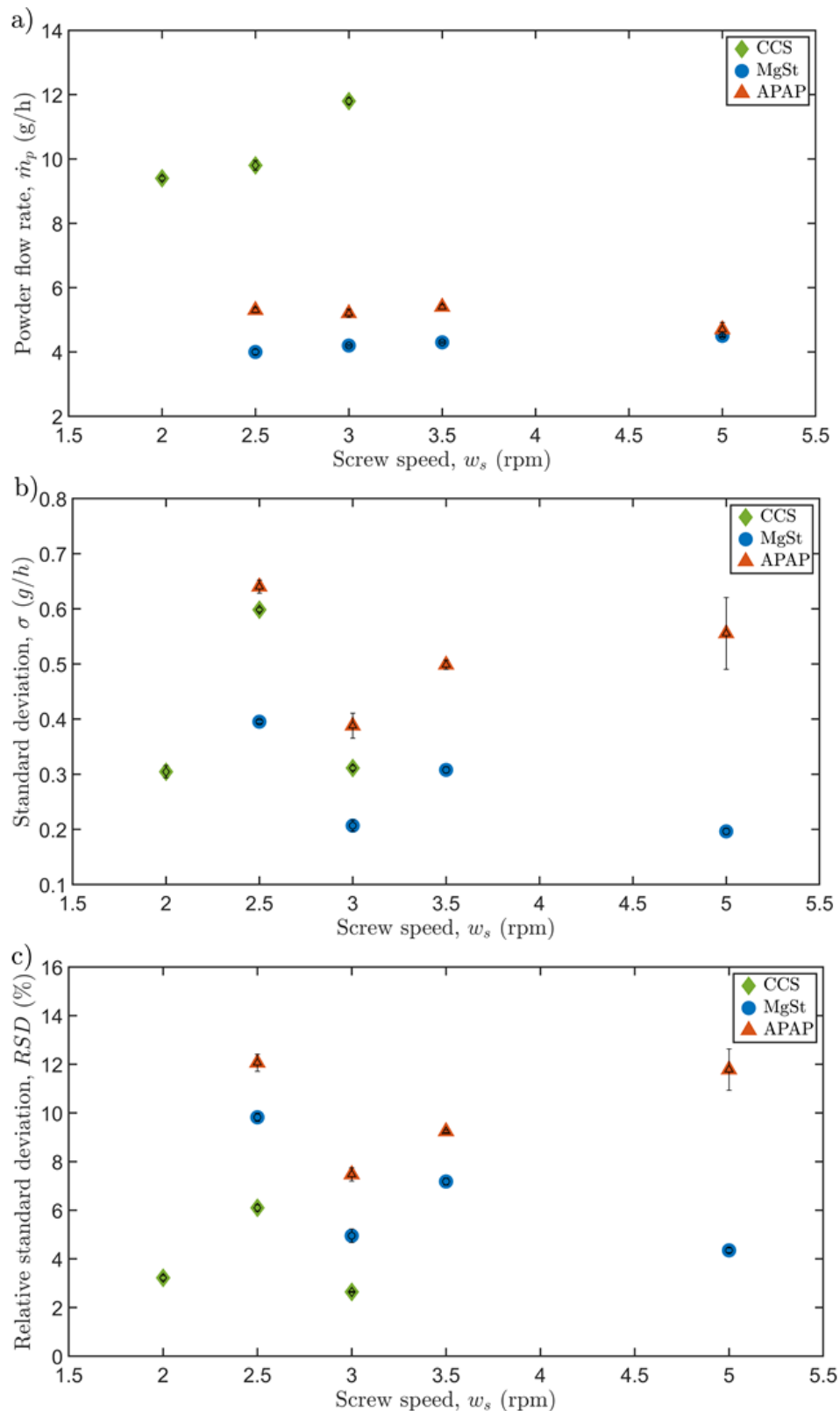


Figure 7-16: Effects of feeding screw speed on powder flow rate, SD and RSD for three distinct powder properties. a) Mean powder flow rate of three repeat experiments as a function of feeding screw speed for three different powder properties at a constant double-screw agitator speed of 2.5 rpm; b) standard deviation as a function of feeding screw speed at 2.5 rpm of double-screw agitator speed; c) relative standard deviation as a function of feeding screw speed at 2.5 rpm of double-screw agitator speed.

Figure 7-17 indicates that variations in screw speed exert only a slight influence on the feed factor when maintaining a constant agitator speed. An increase in screw speed marginally diminishes the screw fill. In comparison to the impact of agitator speed, screw speed emerges as a less significant parameter affecting the powder flow rate. However, this suggests that the consistent ratio between agitator speed and screw speed can yield a steady powder flow rate. This inference is drawn from the observed linear relationships between the feed factor and screw speed at a constant agitator speed and between the feed factor and agitator speed at a constant screw speed. Consequently, the next section aims to identify the optimal points based on these relationships.

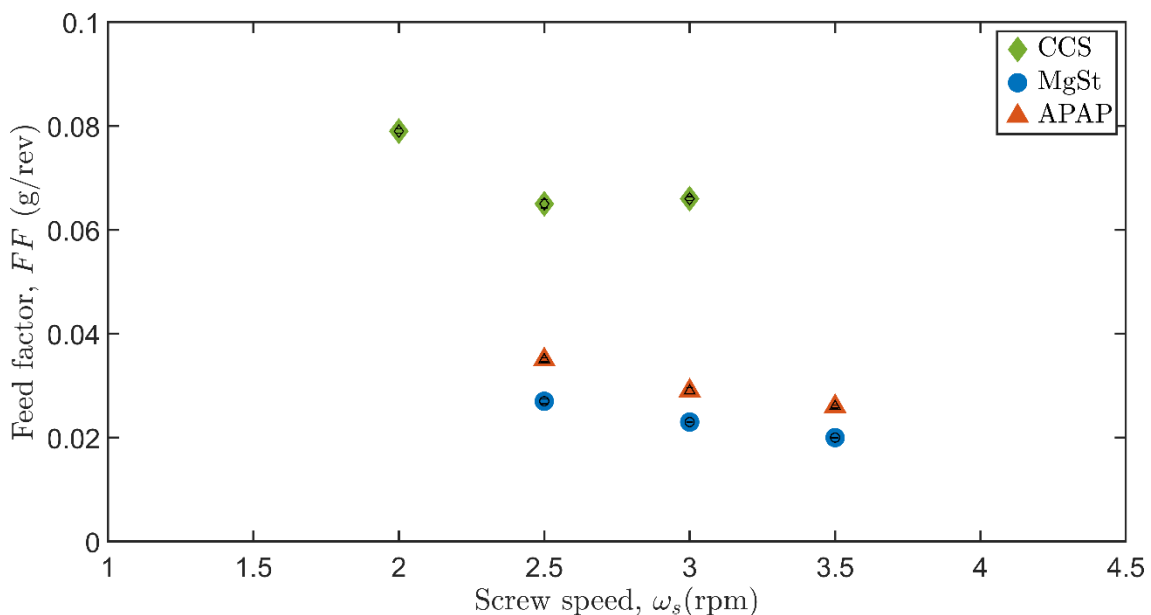


Figure 7-17: Feed factor as a function of screw speed at a constant agitator speed of 2.5 rpm.

7.3.4 Performance statistics

An experimental investigation was conducted to determine the optimal ratio of screw speed to agitator speed for a given material. The summary tables of feeding performance for all tested materials can be found in Table 10-1, Table 10-2, and Table 10-3 in Appendix. Figure 7-18 depicts the temporal consistency of powder feeding for the three materials investigated under optimal conditions without the implementation of feedback control. The findings establish that powder feeding maintains consistent performance over time at different powder feed rates. The optimal ratio was found to be when the screw speed was 0.5 rpm higher than the agitator speed for APAP and CCS, while no clear optimal ratio pattern was observed for MgSt.

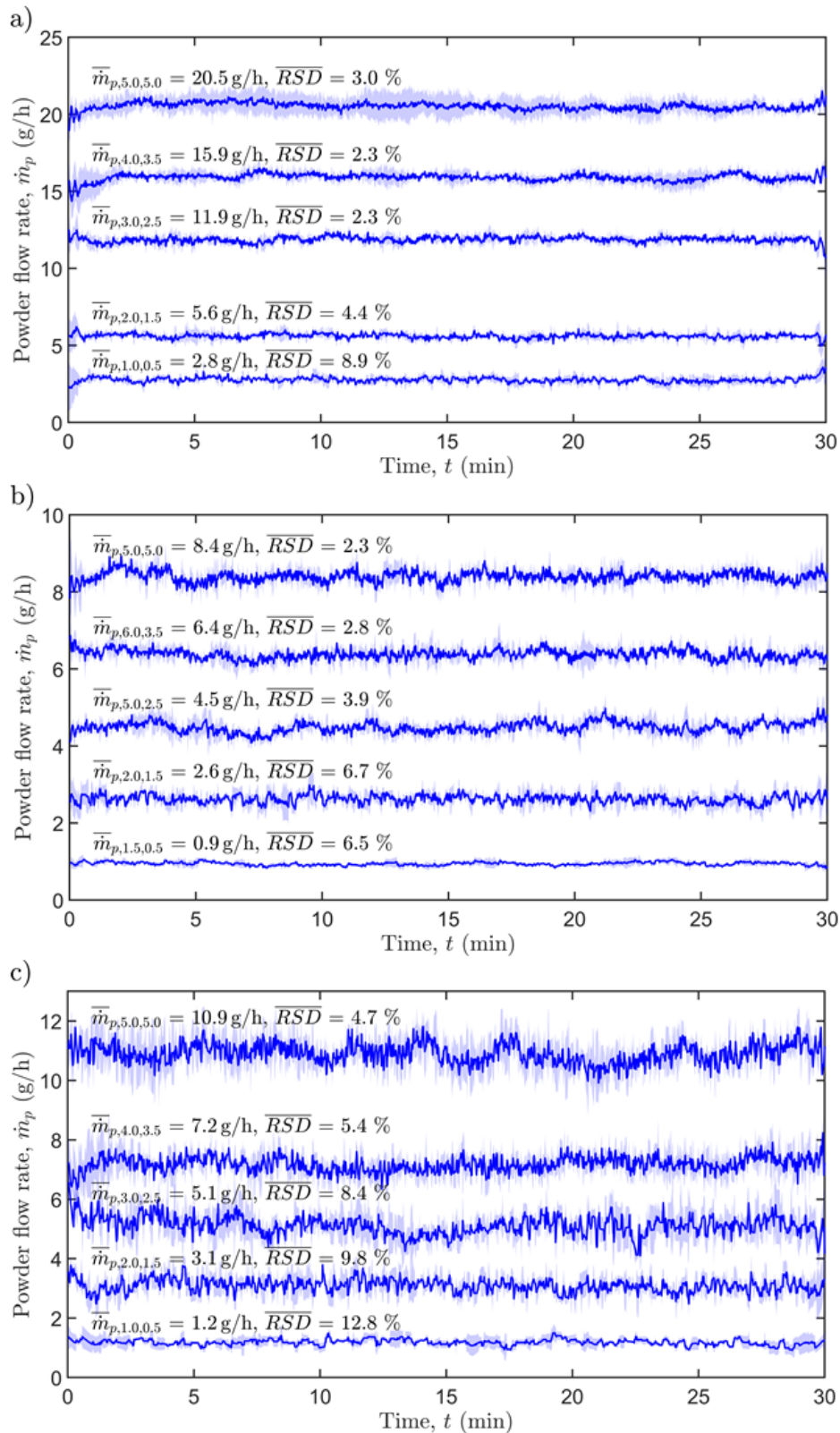


Figure 7-18: Consistent feeding of optimal ratios was observed in three repeat experiments without feedback control for (a) CCS, (b) MgSt, and (c) APAP. The blue line is the mean powder flow rate. The blue shadow represents the SD of three repeated experiments.

It is important to note that the RSD between the equal (screw speed = agitator speed) and optimal ratios decreases as the powder flow rate increases for all tested materials (Figure

7-19). The findings indicate that the powder flow rate remains relatively stable when the agitator speed is held constant, regardless of whether the feeding screw speed is increased or decreased. This observation highlights the dominant influence of the agitator speed, that it controls the powder flow rate, with the screw speed exerting a minor influence, particularly when the powder cohesion is high. These results further support the idea that the screw speed governs the screw volumetric efficiency and reduces the powder flow rate variation. The decrease in the RSD gap with increasing powder flow rates can be attributed to the concurrent rise in screw volumetric efficiency, leading to the screw pocket approaching its maximum capacity. During this phase, the influence of screw speed on the variation in powder flow rate diminishes significantly.

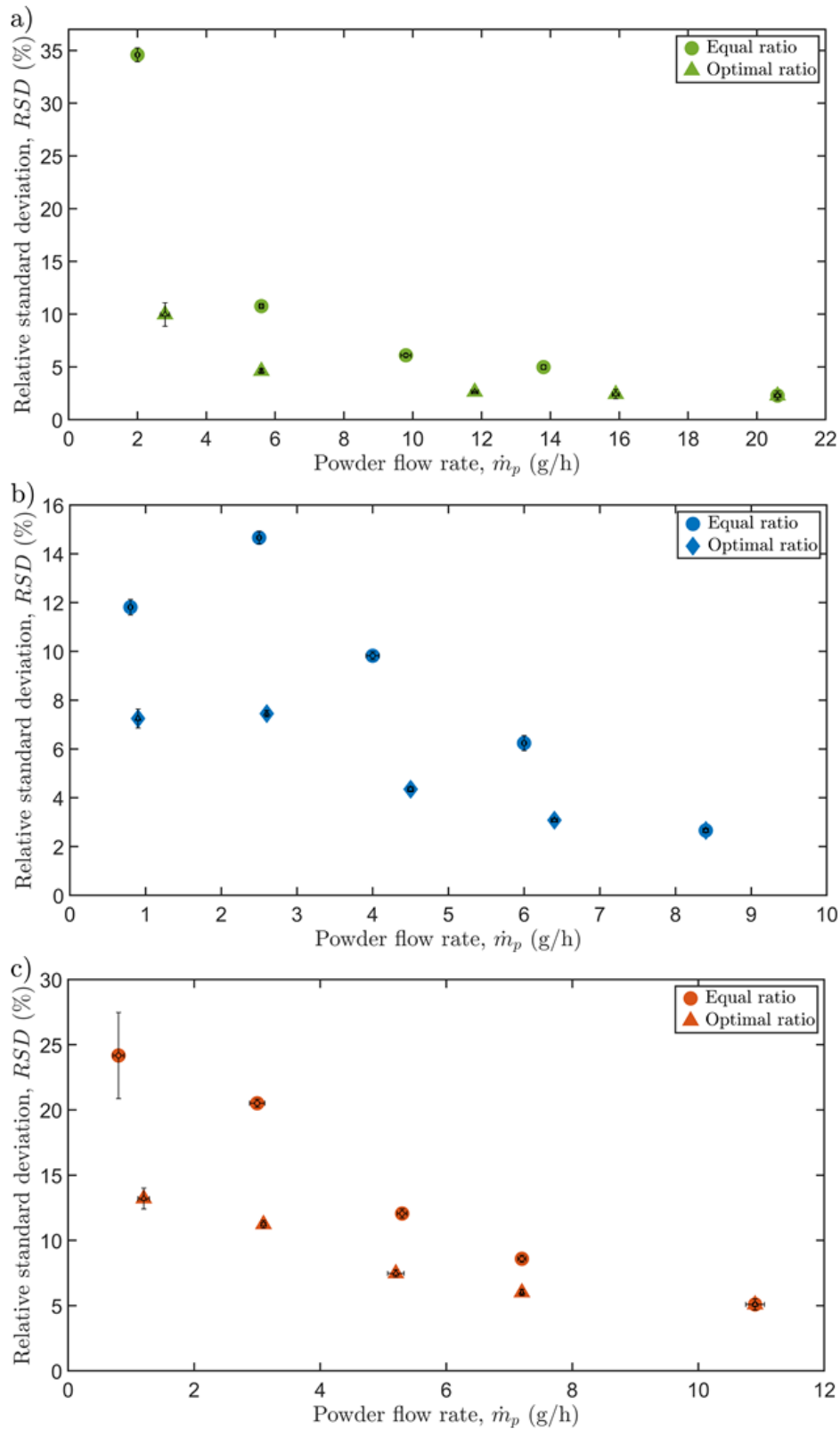


Figure 7-19: The summary statistics of the powder flow rates and RSDs for the three materials. RSDs as a function of powder flow rate at the equal and optimal ratio of screw and agitator speed: a) CCS; b) MgSt; c) APAP. Horizontal and vertical errors represent the SDs of the powder flow rates and RSDs of triplicate experiments. Each measurement was done in triplicate ($n = 3$).

The investigation reveals that materials with poor flowing characteristics exhibit good repeatability when subjected to flow rates exceeding 4 g/h (Figure 7-20). In terms of stability, the results indicate that satisfactory stability under 0.4% is attained when the flow rates are above 2 g/h for all three tested materials. However, stability declines when CCS and APAP are fed at flow rates under 2 g/h. This is because the feeder may have achieved its minimum feed rate at this configuration. A comparison of repeatability and stability of the equal and optimal ratios can be found in Figure 10-15 and Figure 10-16 in Appendix.

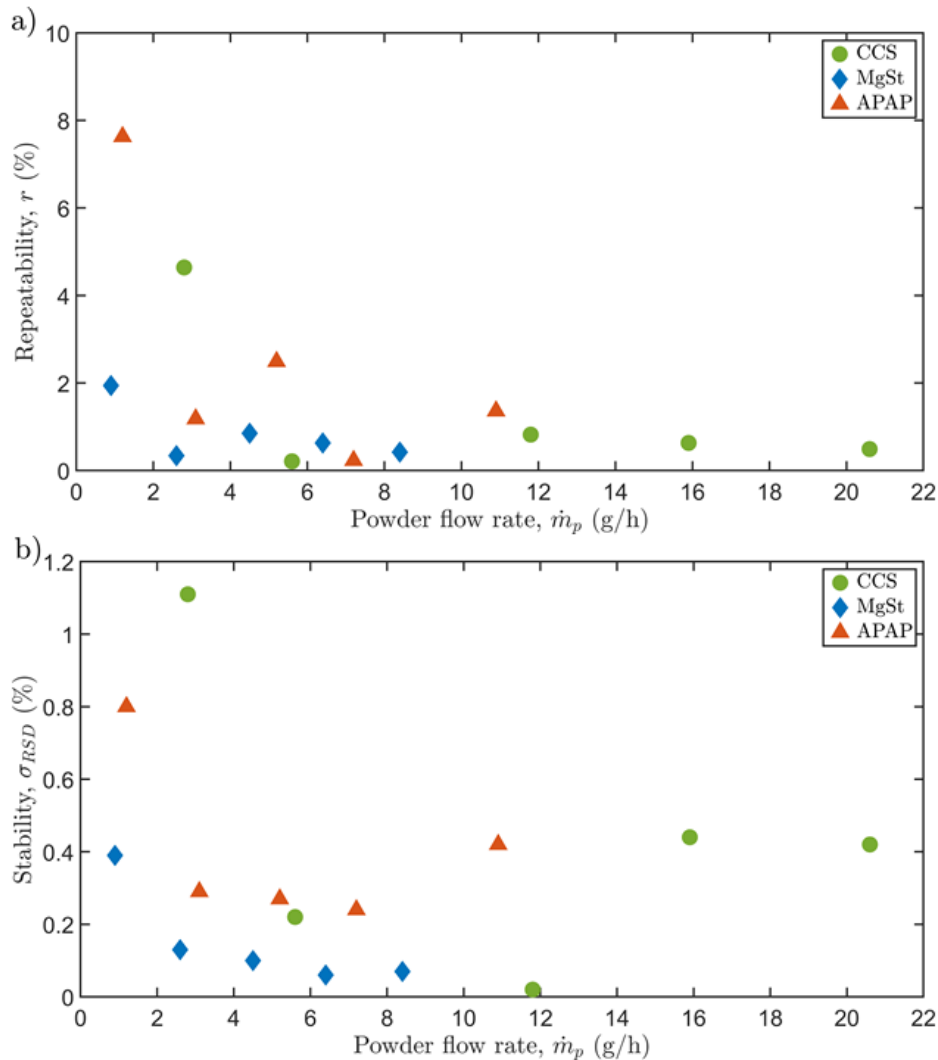


Figure 7-20: Repeatability and stability at the optimal ratios were investigated for the three materials. a) repeatability and b) stability as a function of powder flow rate at the optimal ratio.

To sum up the experimental results from the optimal ratios, a linear correlation between the powder flow rate and agitator speed can be observed in Figure 7-21. The observed linear relationship between the powder flow rate and agitator speed suggests that adjusting the appropriate agitator speed, tailored to the specific powder properties, enables the attainment of the desired powder flow rate.

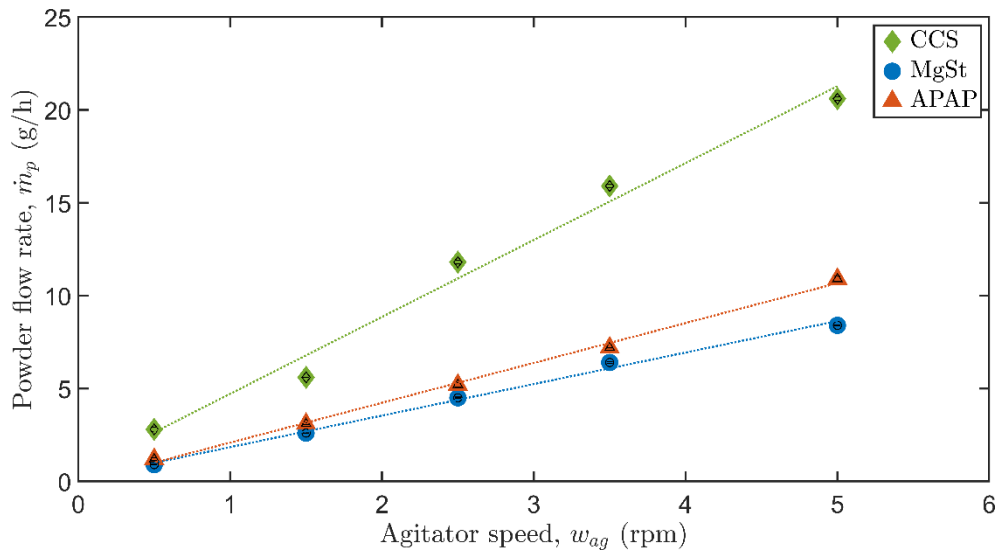


Figure 7-21: The summary of the powder flow rate as a function of agitator speed for the three different materials at optimal ratios, demonstrating a linear relationship. Experiments were conducted in triplicate ($n = 3$).

7.3.5 Volumetric efficiency, feed factor and feed rate analysis

Figure 7-22 juxtaposes the theoretical and observed volumetric efficiency for three tested materials. Notably, the theoretical predictions exhibit consistency across screw speeds, as these predictions omit considerations for the rotational motion of the bulk material and friction between the bulk materials and the flow channel induced by screw speed. In fact, as rotational speed increases, rotational motion diminishes, leading to an increase in volumetric efficiency. Figure 7-22 illustrates that the actual volumetric efficiency of the screw feeder experiences a slight increase as the screw and agitator speeds enhances. However, discerning a linear relationship becomes challenging due to the influence of the screw speed-to-agitator speed ratio on volumetric efficiency. Additionally, the figure reveals that the actual volumetric efficiency of the screw feeder falls below the theoretical volumetric efficiency and vice versa for MgSt. This discrepancy arises from the absence of inclination and the influence of agitator consideration in the calculation.

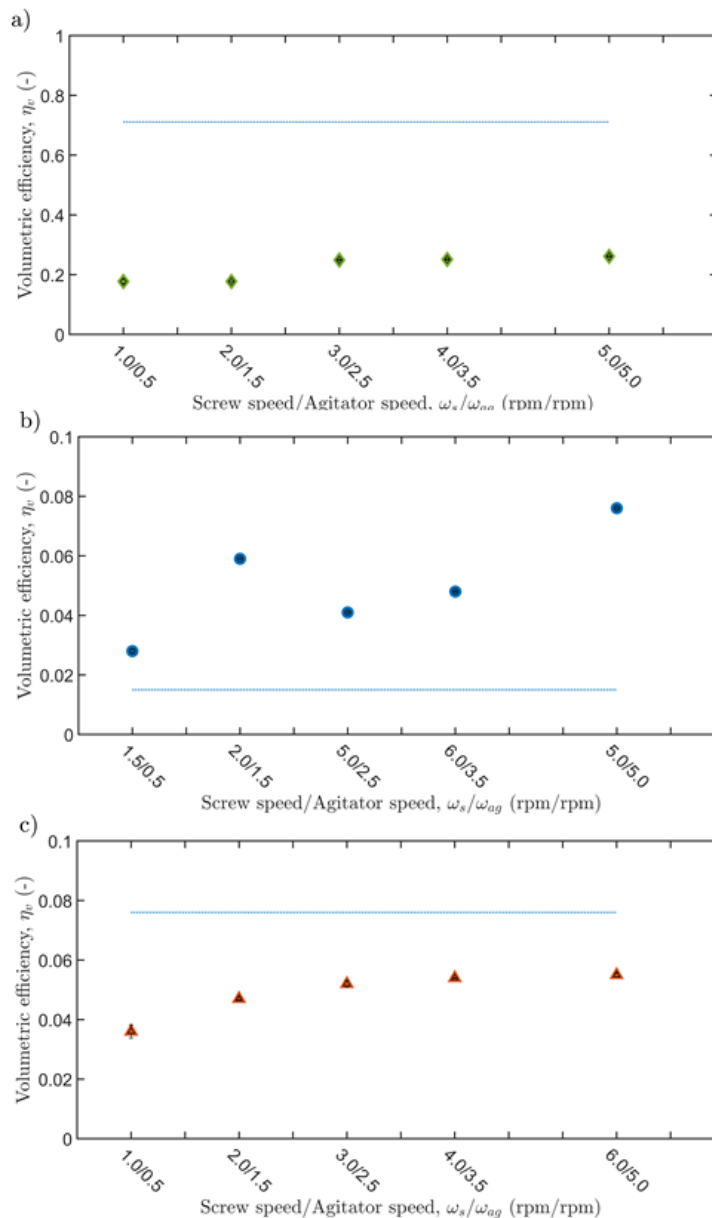


Figure 7-22: Effect of screw speed/agitator speed on the volumetric efficiency: a) CCS with a 7 mm pitch screw, b) MgSt with a 25 mm pitch screw, and c) APAP with a 25 mm pitch screw. The predicted volumetric efficiency is indicated by the blue dashed line.

Figure 7-23 illustrates the impact of agitator speed on the feed factor for three distinct materials within the same feeder. The linear regression lines for each material type demonstrate varying slopes and intercepts. These differences underscore that the influence of agitator speed on the feed factor is material-specific.

Upon analysing the experimental data, it becomes evident that the feed factors exhibit a linear increase with increasing agitator speed for all tested materials. The figure emphasises that the agitator continues to play a crucial role in governing the powder flow rate, aligning with the assertion in Section 7.3.3.2 regarding agitator control over the powder flow rate.

Further insights emerge a decrease in feed factor as the Hausner ratio increases, as illustrated in Figure 7-23. This reinforces the understanding that feed factor is inversely related to flowability, highlighting the intricate interplay between material characteristics and the control parameters of the feeder system.

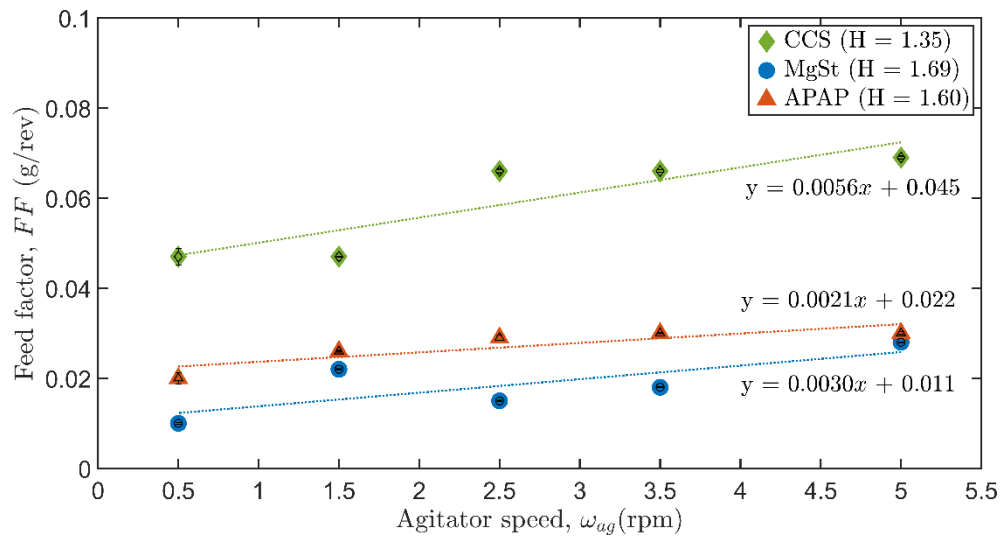


Figure 7-23: Effect of agitator speed on the feed factor. Different symbols depict data points for CCS (green), MgSt (blue), and APAP (red), and linear regression lines for each material type demonstrate varying slopes and intercepts.

In Figure 7-24, we conducted a comparative analysis of the maximum theoretical flow rate (Equation 2-30), theoretical flow rate as per Equation 2-31, theoretical flow rate using Equation 2-32, and the observed flow rate. This examination allows us to evaluate which equation serves as a more accurate predictor of powder flow rates.

The results of the analysis reveal that, across all materials, Equation 2-31 emerges as a robust predictor of powder flow rates. It consistently provides a good estimation compared to the observed flow rates. However, specific nuances arise for individual materials. In the case of MgSt, the utilisation of Equation 2-32 results in an underestimation of the observed flow rate. This discrepancy can be attributed to the low volumetric efficiency associated with MgSt. On the other hand, for APAP, both Equation 2-31 and Equation 2-32 demonstrate effective predictions of the powder flow rate, with Equation 2-31 exhibiting a slightly superior performance. For CCS, the observed flow rate has a close prediction by using Equation 2-31.

This deviation between Equation 2-31 and Equation 2-32 is attributed to the fact that Equation 2-32 does not account for factors such as inclination and flowability, which are crucial considerations. It indicates that gravity significantly influences the screw fill efficiency and the powder flow rate.

In summary, the comparative analysis underscores that Equation 2-31 generally outperforms the other equations in predicting powder flow rates.

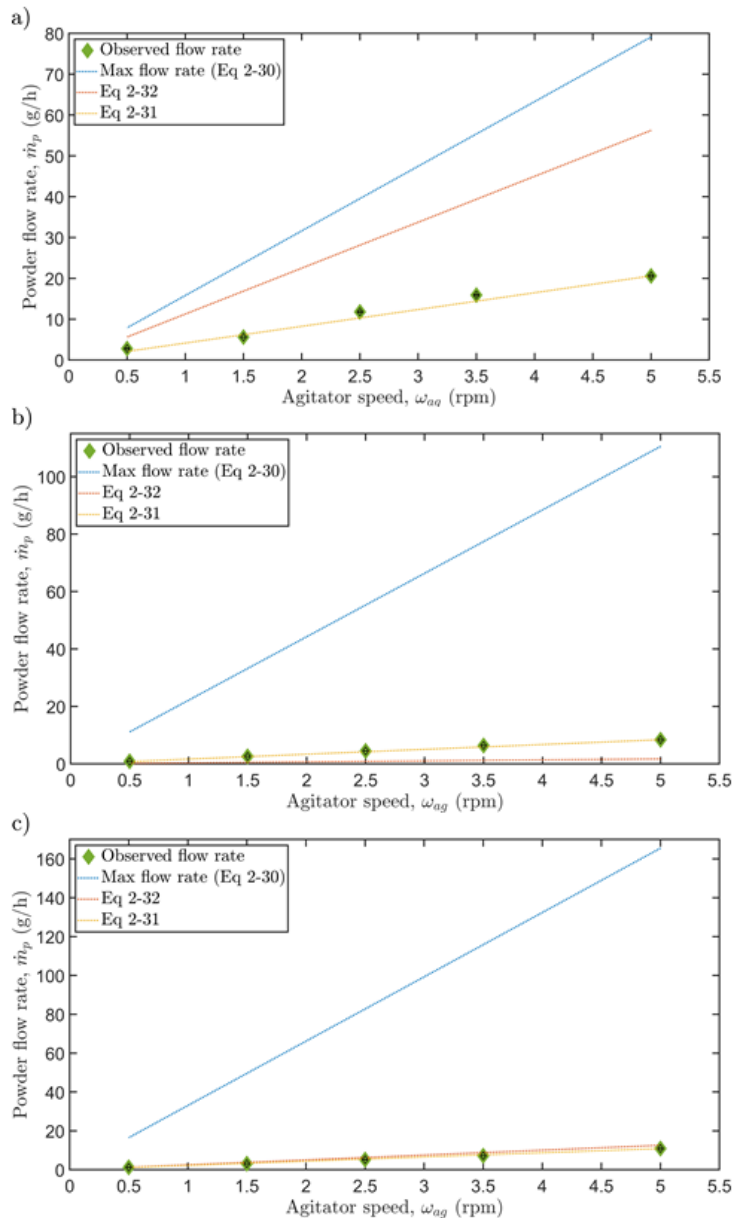


Figure 7-24: Comparative analysis of theoretical powder flow rates (depicted by lines) for a) CCS, b) MgSt, and c) APAP. In Equation 2-31, the inclination correction factor, C , is set at 0.55 for all tested materials, with loading ratios of 0.474 for CCS, 0.138 for MgSt, and 0.120 for APAP. The blank experiment at an agitator speed of 5 rpm determines loading ratios.

Figure 7-25 displays the theoretical (Equation 2-31) and observed powder flow rates, accompanied by an analysis of the R-squared values. The results highlight the excellent performance of the predictive model across the three distinct materials: CCS (cohesive), MgSt (non-flowing), and APAP (non-flowing).

The elevated R-squared values of 0.9699 for CCS, 0.9941 for MgSt, and 0.9934 for APAP indicate a robust correlation between the predicted and actual feed rates. This high level of agreement demonstrates the model's efficacy in capturing the nuances of material behaviour during powder flow. Notably, the model excels in accuracy for non-flowing materials, with MgSt and APAP achieving R-squared values surpassing 0.99.

The marginal decrease in the R-squared value for CCS (0.9699) may be attributed to the inherent variability observed in easy-flow materials. Despite this, the value still signifies a strong predictive capability, highlighting the model's adaptability even in the presence of material-specific intricacies.

In conclusion, the consistently high R-squared values affirm the model's effectiveness in accurately predicting feed rates for both easy-flow and non-flowing materials. This performance suggests practical applications in process optimisation or control, where reliable predictions of powder flow rates are essential for achieving desired outcomes.

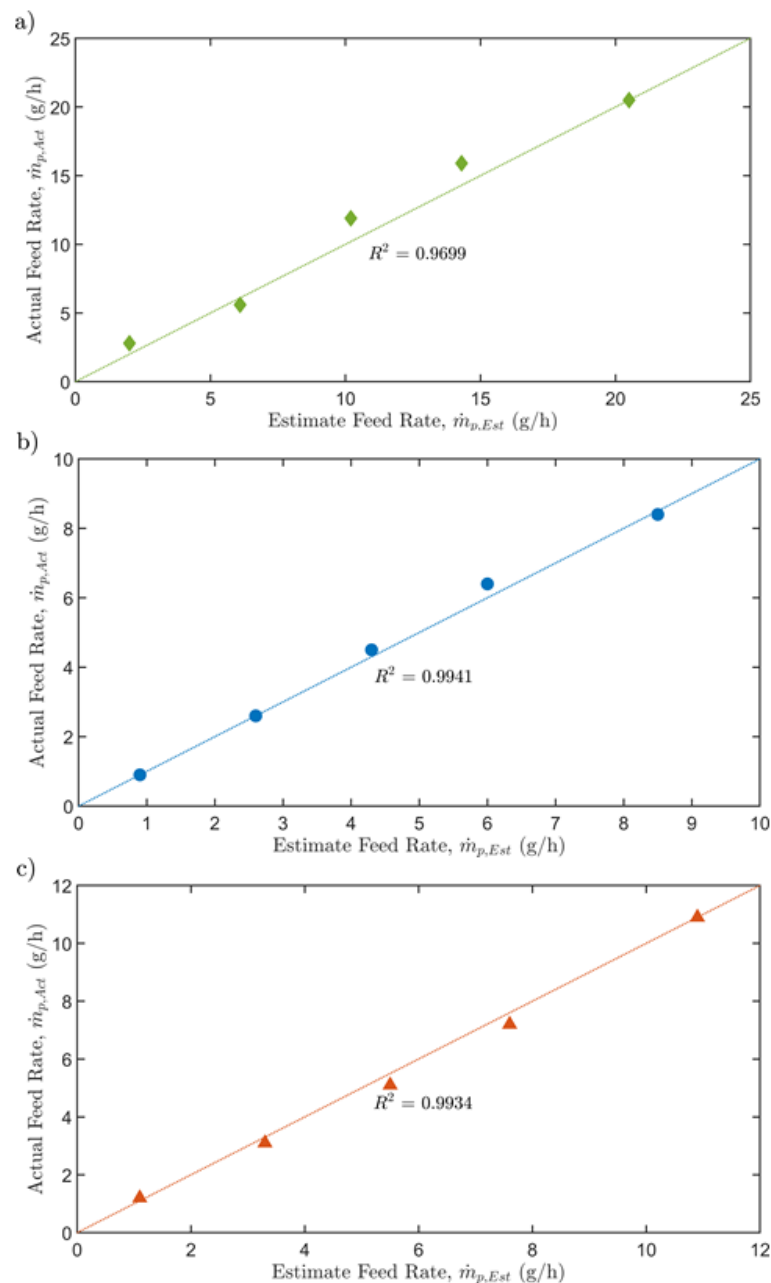


Figure 7-25: Comparison of the theoretical flow rate (Equation 2-31) and observed flow rate for a) CCS, b) MgSt, and c) APAP.

7.4 Conclusions

In summary, this study unveils a new micro-feeder, introducing a new concept that contributes to the field. This micro-feeder, featuring a unique combination of a feeding screw and a double-screw agitator design, stands out as a solution capable of achieving consistent and uninterrupted powder feeding without the reliance on feedback control or susceptibility to refilling disruptions. The development of this micro-feeder addresses common hopper issues and provided enhanced feeding stability and repeatability.

A contribution of this study is the introduction of a unique feeding mechanism that employs a double screw agitator in conjunction with screw speed adjustment to enhance screw volumetric efficiency and minimise variations in powder flow rate. A noteworthy finding is the agitator's role in regulating powder flow rates, particularly evident in cohesive materials, where challenges like rat holing and bridging are effectively addressed.

The experimental results reveal good repeatability (below 8%) and stability (below 6% at low flow rates and below 15% at high flow rates for cohesive materials) across a diverse range of tested materials and flow rates (0.5 g/h to 22 g/h). The micro-feeder's independence from refilling disruptions, as highlighted in section 7.3.2, underscores its potential for long-term and reliable feeding operations. The scrutiny of mass flow rate predictions, particularly the high accuracy demonstrated by Equation 2-31 (with a coefficient of determination of 0.99 in section 7.3.5), adds control of powder flow rate can be reliably undertaken.

Moreover, the modular and compact design of the micro-feeder, highlighted in this study, opens up new possibilities for versatile applications in both industrial and research settings. The emphasis on future work, focusing on refining the system for higher levels of consistent flow rates, especially for non-flowing materials.

8 Maximising performance and efficiency of inclined screw feeders

8.1 Chapter Summary

Chapter 7 presented an inclined micro-feeder based on the volumetric principle, designed to enable consistent and continuous powder feeding across a range of feed rates and various powder properties in industrial applications. The micro-feeder comprises a double-screw agitator and a feeding screw. The double-screw agitator consists of an outer and an inner screw, with the former moving the powder upward and the latter feeding it downward into the feeding screw. This arrangement allows the powder to circulate vertically like a liquid in the hopper, potentially eliminating the influence of refilling and preventing arching during the feeding. The feeding screw helps to minimise feed rate variations. By adjusting the speeds of the double-screw agitator and feeding screw, the system can achieve the desired powder flow rate with low variation.

The aim of the study in this chapter was to enhance the performance of the inclined micro-feeder previously designed in Chapter 7 and gain a deeper understanding of the design. To achieve this objective, a series of experiments were conducted to evaluate the effects of various modifications to the inclined micro-feeder system. The experiments were designed to assess the effect of independent variables, such as feeding screw inclination angles, feeding screw flight configurations, and inner screw pitch of the double-screw agitator, on dependent variables, including powder flow rate, relative standard deviation (RSD), standard deviation (SD), stability, and repeatability (Figure 8-1). Two types of pharmaceutical powders, croscarmellose sodium (CCS) and paracetamol (APAP), were selected to represent commonly used powders in industrial applications. The outcomes from the optimised inclined micro-feeder were compared with the performance of the inclined micro-feeder developed in Chapter 7. The findings of the study were used to draw conclusions regarding the effectiveness of the modifications made to the system and their influence on feeding performance. In addition, this study presents an evaluation of the performance of an optimised inclined micro-feeder compared to two commercial feeders, namely the Brabender MiniTwin Feeder, the FlexWall Feeder and literature. The objective of this experimental investigation was to evaluate the efficacy of the inclined micro-feeder design when juxtaposed with commercial feeders.

In summary, this study builds upon the original design of the inclined micro-feeder and seeks to optimise its performance through experimentation and analysis. The optimisation of the inclined micro-feeder involves several improvements, including adjustments to feeding screw

inclination angles, flight configurations, and the inner screw pitch of the double-screw agitator. The findings presented in this chapter are then contrasted with the commercial micro-feeders and literature.



Figure 8-1: Optimising the inclined micro-feeder: A step-by-step process for enhancing feeding performance.

8.2 Material and methods

8.2.1 Material characterisation and material properties

In this study, two materials were utilised: Croscarmellose sodium (CCS) from JRS Pharma, Germany, and paracetamol (APAP) from Mallinckrodt Pharmaceuticals, Ireland. The selection of CCS aimed to represent cohesive materials, whereas APAP was chosen to represent non-flow materials. A thorough examination of the material properties and associated analyses are presented in Chapter 3, offering detailed information such as particle size distribution, bulk density, true density and flowability.

8.2.2 Inclined micro-feeder and operation

The presented inclined micro-feeder in this study operates on the volumetric principle, as shown in Figure 8-2. The inclined micro-feeder comprises a double-screw agitator and a feeding screw to facilitate the efficient transfer and delivery of powder. The double-screw agitator effectively agitates the powder in a vertical direction, resulting in a homogenised powder density within the hopper. The feeding screw transfers the powder to a catch balance beneath the feeder's outlet to minimise feed rate variation.

During the experimental setup, the hopper initially contained around 100 ml of raw material, which was refilled once or twice during the feeding process, depending on the feed rate and operation time. The agitator and screw speeds were pre-set and held constant throughout the feeding process, ensuring the consistency of the feed rate. The fed powder was continually monitored, and its weight was recorded at 1-second intervals. Subsequently, the recorded data was converted into the corresponding mass flow rate.

To reduce the influence of measurement noise, a moving mean of 60-second windows was implemented. This approach was previously validated in Chapter 7, demonstrating its efficacy in minimising measurement noise without compromising the quality of the actual data.

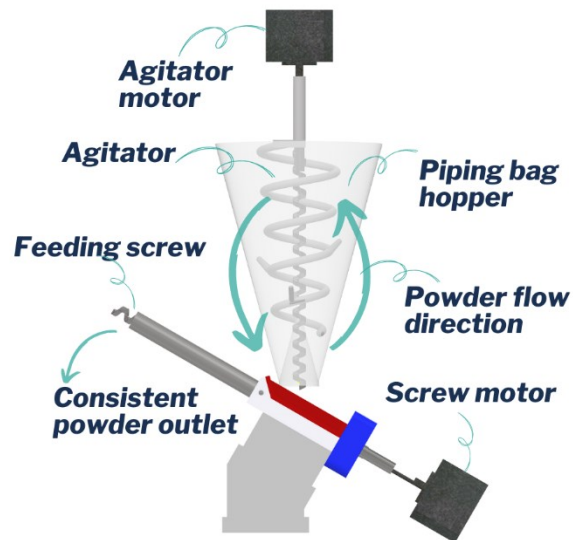


Figure 8-2: Inclined micro-feeder schematic: A double-screw agitator and feeding screw facilitate efficient powder transfer and delivery.

8.3 Results and discussions

8.3.1 The effect of screw angles on the powder feeding performance

In Chapter 7, the study presented encouraging results indicating that the inclined micro-feeder offers a viable solution for consistent powder feeding. Nevertheless, to further improve the design, it is important to explore how different feeding screw angles affect the powder feeding consistency and stability (Figure 8-3). By evaluating the performance of the inclined micro-feeder across these angles, the study aimed to gain a comprehensive understanding of how the feeding screw angle affects the overall feeding process. Such insights are essential to refine and optimise the micro-feeder's design, ensuring that it meets the industry's high standards for powder feeding consistency and stability.

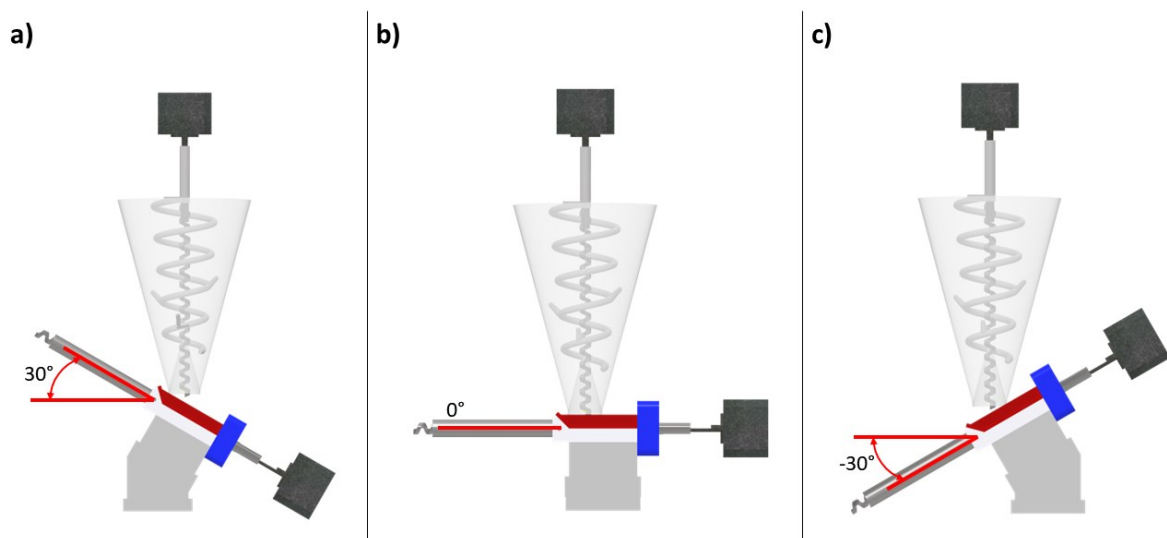


Figure 8-3: The effect of three distinct feeding screw angles: a) 30° inclination, b) 0° horizontal, and c) -30° declination.

Figure 8-4 reveals that the powder flow rate of cohesive materials slightly increases as the feeding screw angle decreases, while for non-flowing materials, there is not much change in powder flow rate across different angles, but at a feed rate above 10 g/h. The results also indicate that the SDs of CCS and APAP at -30° inclined screw feeding falls within the range of 0.2 g/h to 0.4 g/h, while the other two angles (0° and -30°) have an SD within the range of 0.3 g/h to 0.8 g/h. These results suggest that both cohesive and non-flowing materials fed at a 30° inclined screw feeding angle exhibit less SD as compared to the other angles. This clearly demonstrates the significant role of the inclined feeding screw system in this design.

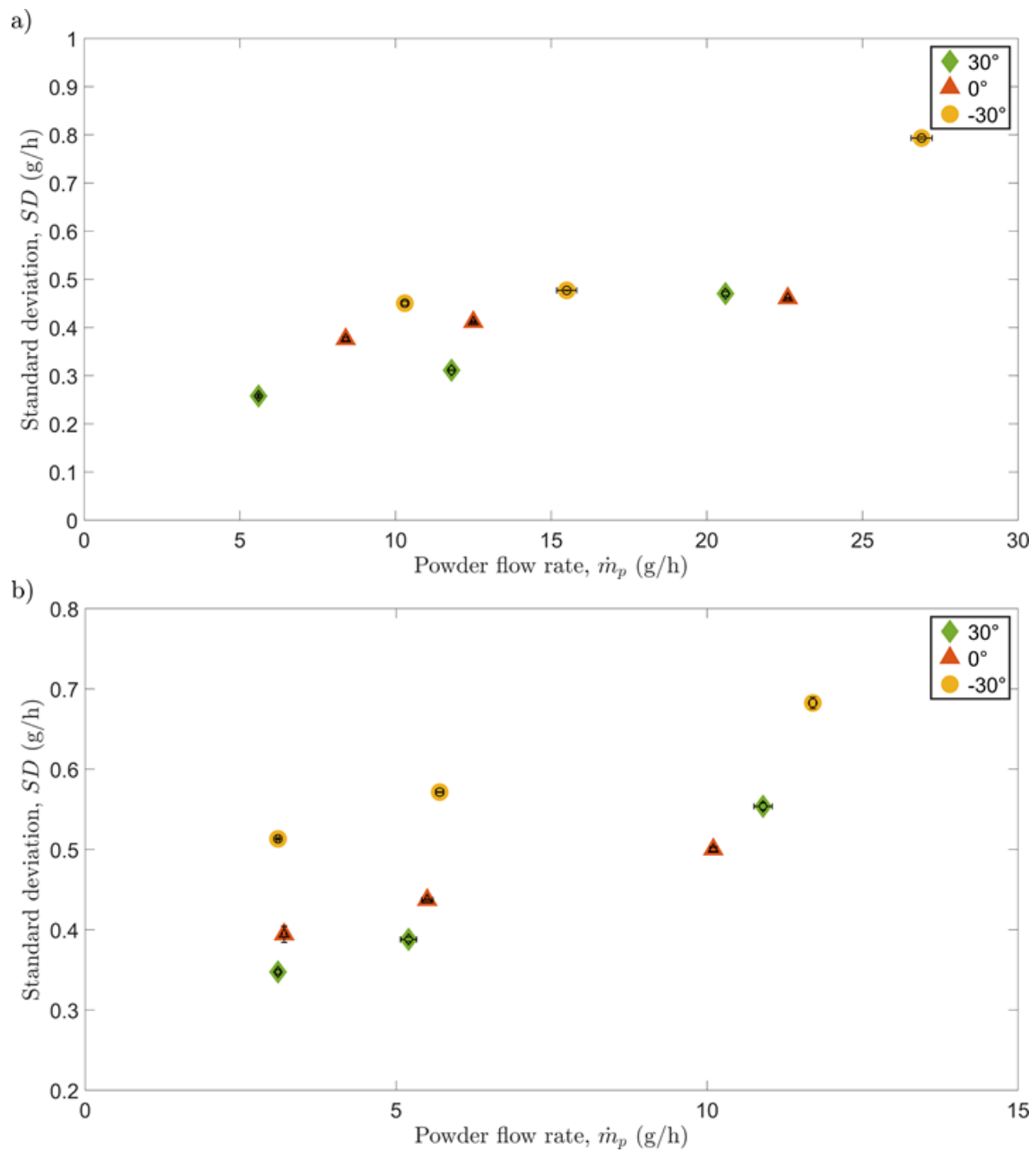


Figure 8-4: SD as a function of powder flow rate at optimal ratios of a) CCS and b) APAP for three different screw feeder angles: 30° inclination, 0° horizontal, and -30° declination.

The results in Figure 8-5 suggest that changes in the feeding screw angle are not the primary factor affecting the repeatability of cohesive materials. However, for non-flowing materials, the decreasing angle of the feeding screw improves repeatability. More specifically, the 30° feeding screw demonstrates better repeatability for cohesive material, while the -30° feeding screw shows good repeatability for non-flowing material.

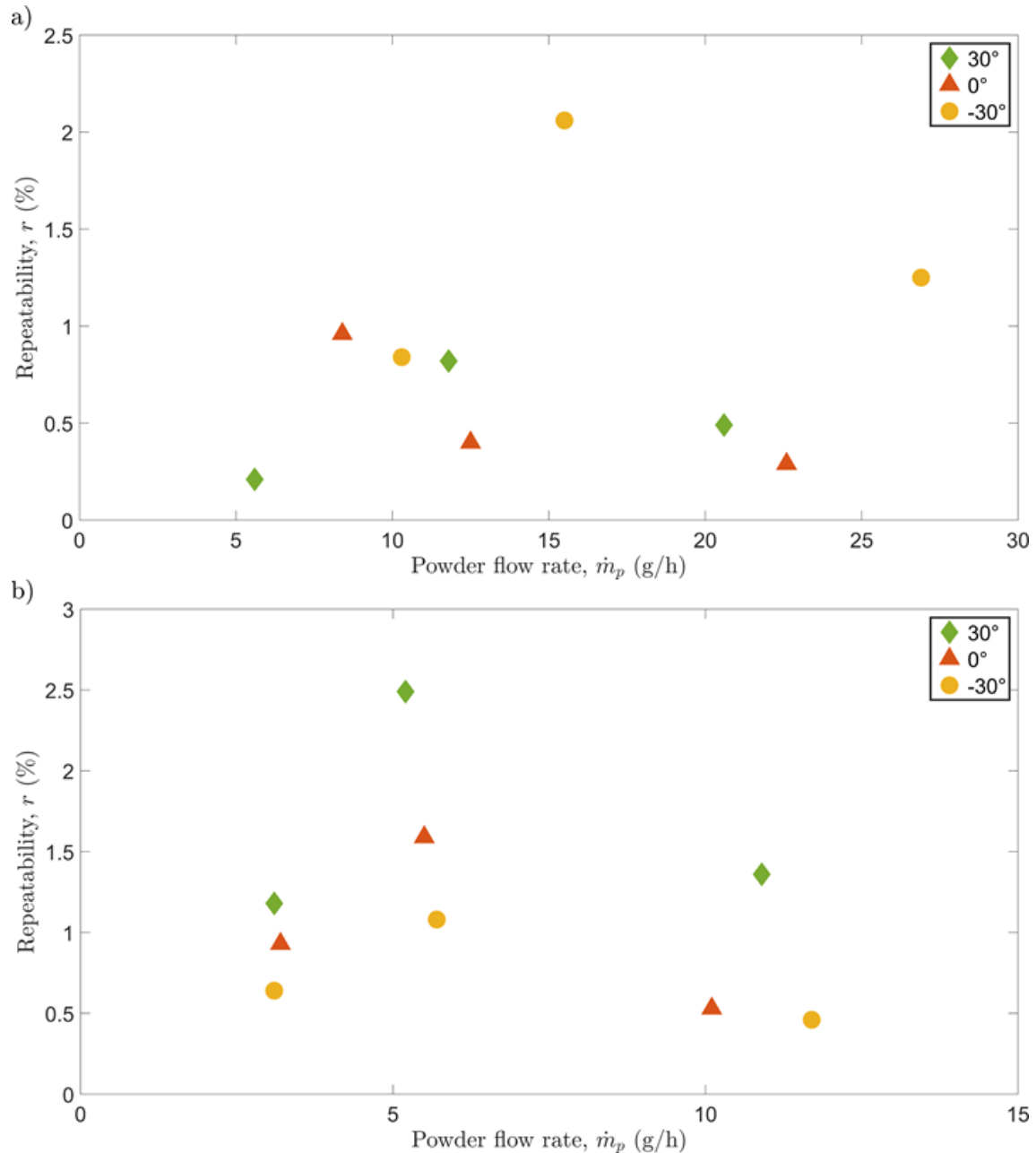


Figure 8-5: Effect of feeding screw angle on repeatability as a function of powder flow rate: (a) CCS and (b) APAP. The graph shows the repeatability of powder feeding for two materials (CCS and APAP) as a function of the powder flow rate for different feeding screw angles. The results suggest that the feeding screw angle can influence the repeatability of powder feeding for different materials, with varying influences on the powder flow rate.

Figure 8-6 demonstrates that the stability of the system has no clear pattern in the changes of feeding screw angles for cohesive material. For non-flowing materials, the -30° declination of

the feeding screw stands out as having excellent stability at flow rates under 10 g/h. However, the 30° inclination demonstrates more constant stability at approximately 0.4% across the powder flow rates. The findings suggest that the 30° inclination is the practical design for maintaining stability in powder micro-feeder, although the specific choice of feeding screw angles may depend on the properties of the powder being processed and the desired flow rates.

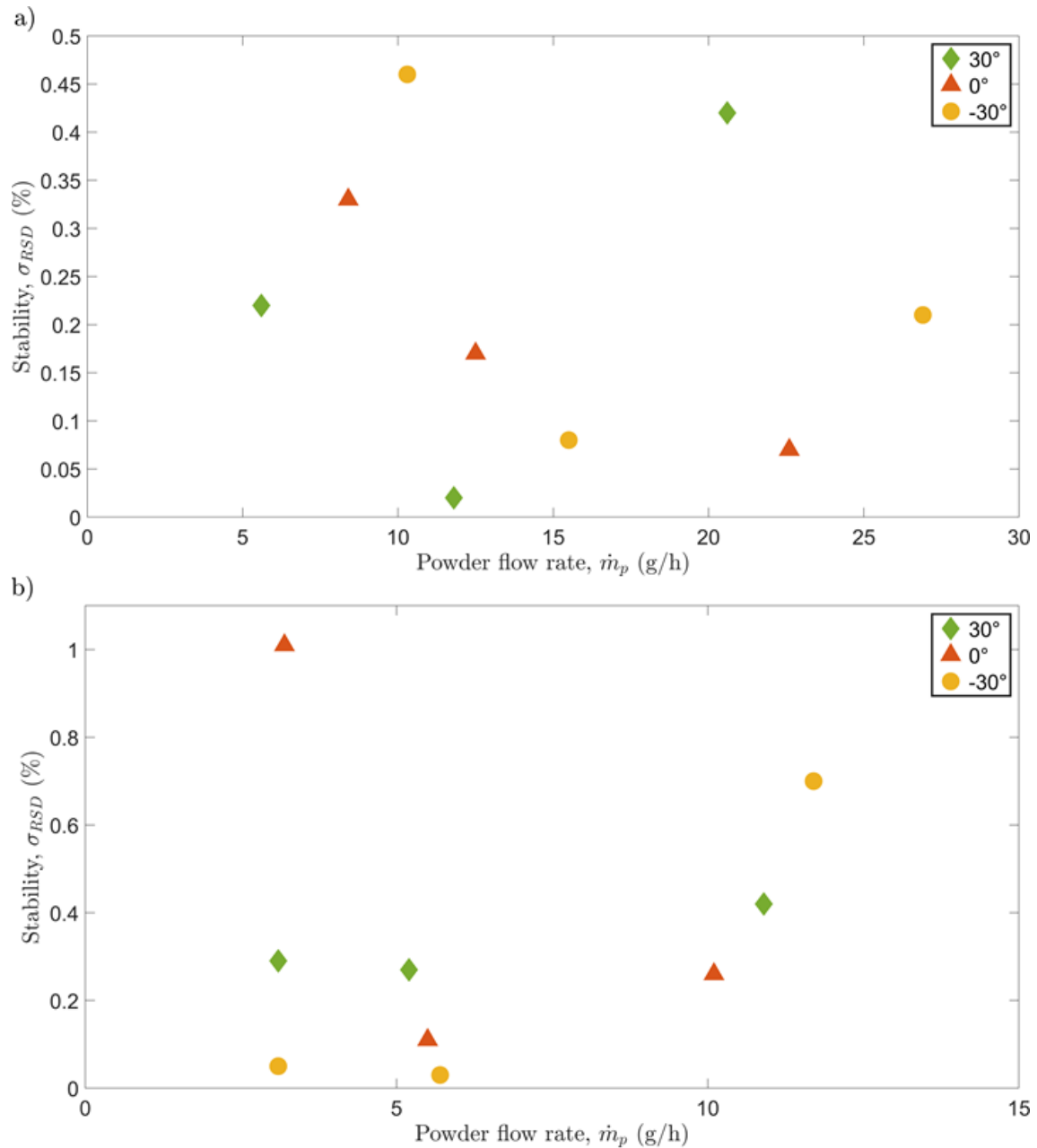


Figure 8-6: Stability as a function of powder flow rate: a) CCS b) APAP. The results suggest that the 30° inclination of the feeding screw provides more consistent stability across varying powder flow rates for both materials.

The feed factor analysis in Figure 8-7 provides insights into how screw speed influences the efficiency of powder feeding for CCS and APAP, offering a view of feeding dynamics under different screw inclinations.

In Figure 8-7, a nearly flat relationship is observed between screw speed and feed factor at -30° and 0° inclination angles for CCS, suggesting that increases in screw speed at these angles are less sensitive to changes in powder flow rate. Small adjustments to the screw speed in these two angles result only in small differences in the feed factor, posing a challenge to fine-tuning the powder flow rate through speed variations alone. Conversely, at a 30° inclination angle, Figure 8-7 shows a more pronounced change in the feed factor with increasing screw speed, displaying a non-linear relationship. Initially, the relationship between screw speed and feed factor increases but then tends to flatten after reaching 3 rpm, indicating a potential limitation in the system. For the APAP (non-flowing) powder feeding, an increase in screw speed leads to a significant rise in the feed factor at three different screw inclination angles. At a 30° inclination angle, a good linear relationship is observed between feed factor and screw speed, simplifying control and optimisation. This linear relationship suggests a consistent behaviour of the feeder across a range of screw speeds, advantageous for maintaining product quality and process stability. Linear relationships, especially in control systems using proportional-integral-derivative (PID) controllers, allow for predictable responses to changes in screw speed. Notably, the system may not have reached its limitation at 5 rpm yet, indicating the potential for higher feed rates in feeding APAP in this equipment setting. In summary, based on these results, a 30° inclination angle is a favourable choice for optimising the control of powder flow rate.

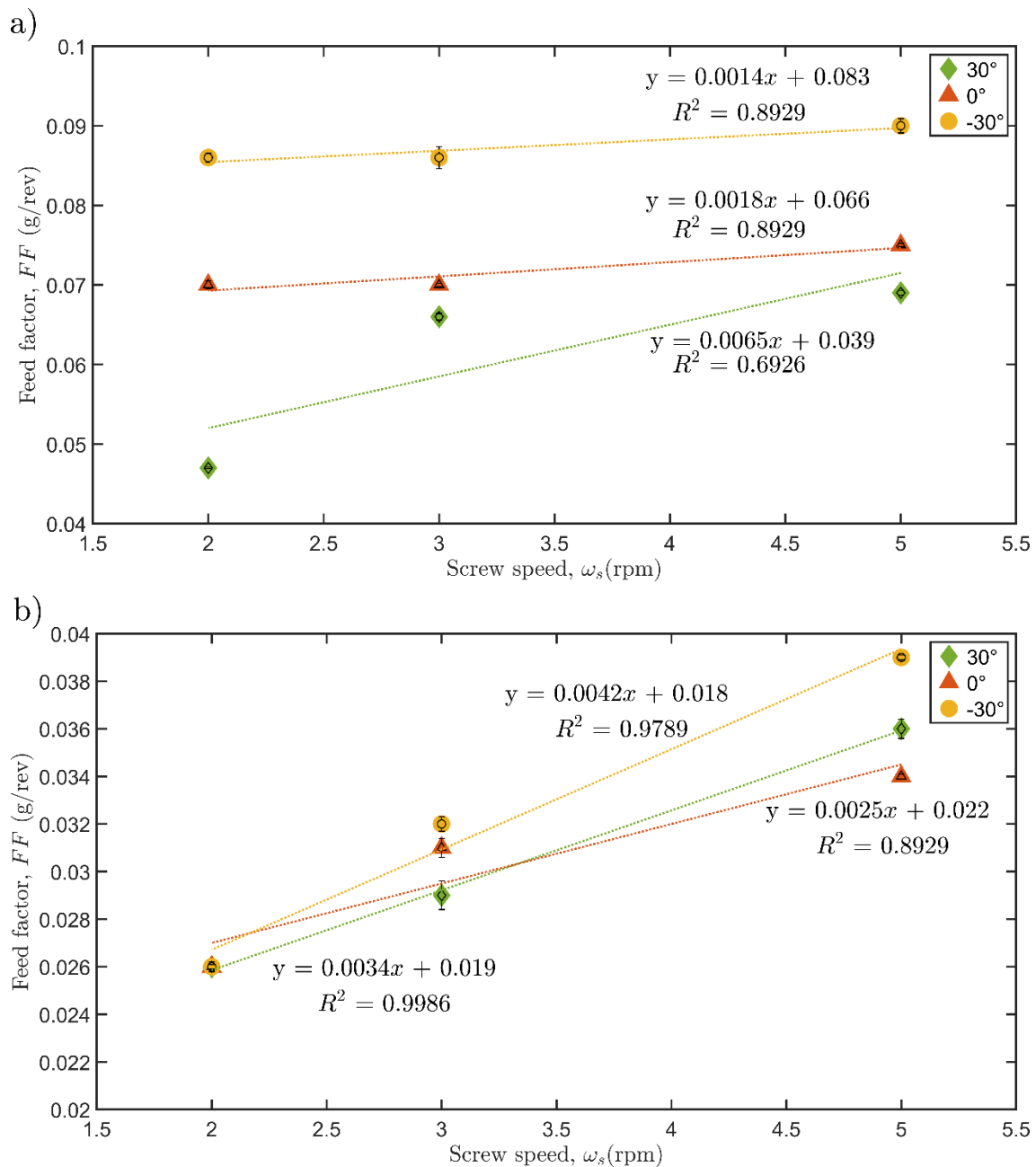


Figure 8-7: Feed factor as a function of screw speed in the powder feeding process of a) CCS, b) APAP at inclination angles of 30°, 0°, and -30°.

8.3.2 The effect of feeding screw flight configuration at various feeding screw speeds

To minimise variation and improve feeding consistency, this study explores the modified outlet (Figure 8-8a) and four types of modified feeding screws for each tested material (Figure 8-8b and c). Various flight configurations offer opportunities to regulate flow rate and enhance its consistency. For instance, tapered flights facilitate material compression and flow rate control. The choice of the suitable flight configuration for accurate powder feeding relies on the powder properties. A comprehensive grasp of these elements enables us to refine the volumetric feeding procedure effectively. The screw flight configuration in this study are categorised as compression and non-compression, with compression referring to a screw tapered at minus

2.5° at the end section. Furthermore, both compression and non-compression screws have two types of end sections: equal pitch and increased pitch. The equal pitch end refers to a screw with a consistent pitch from the body to the end section. On the other hand, the increased pitch end means that the pitch is higher in the end section compared to the body sections. For both compression and non-compression screws, there are variations with equal pitch and increased pitch. For example, the 50/25 compression screw indicates an increase in pitch from 25 mm (body section) to 50 mm (end section) at the compressed section, and so on.

The study focuses on the effect of these screws on the flow rate and feeding consistency of both non-flowing and cohesive materials. Specifically, the non-flowing material was tested using the 50/25 compression, 50/25 non-compression, 25/25 compression and 25/25 non-compression screws, while the cohesive material was tested using the 15/7 compression, 15/7 non-compression, 7/7 compression and 7/7 non-compression screws.

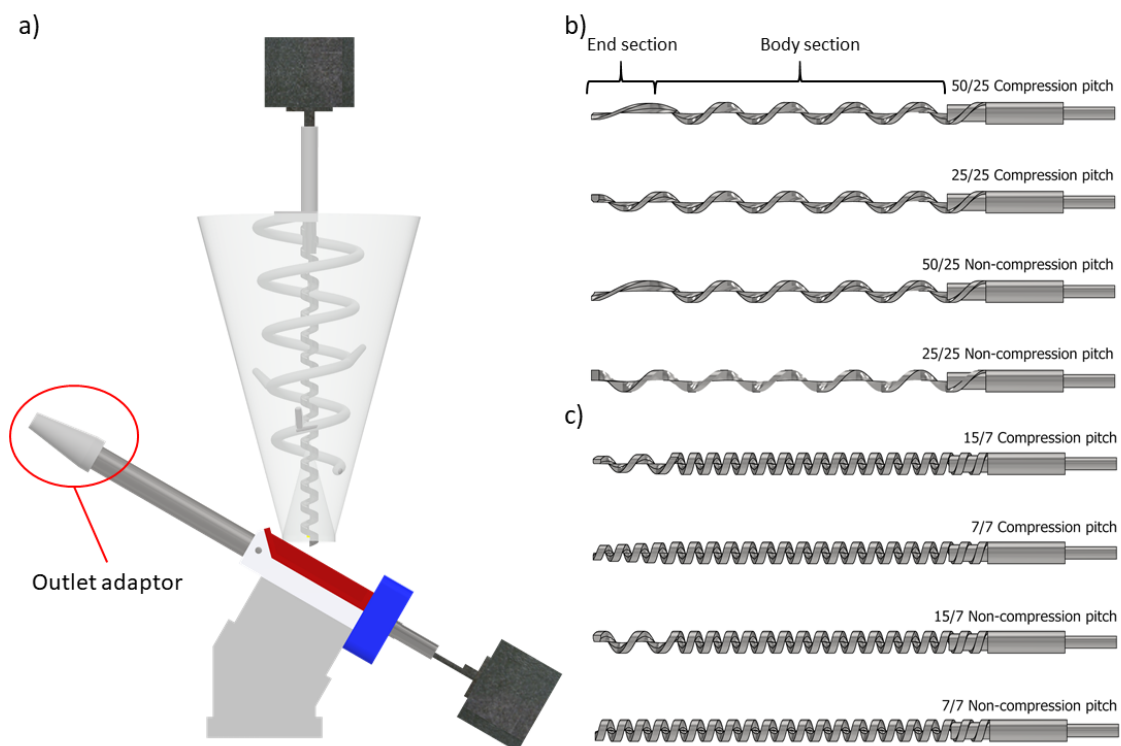


Figure 8-8: Enhanced feeding efficiency with modified micro-feeder outlet and feeding screw flight configurations: (a) shows the modified inclined micro-feeder fitted with an angled outlet adaptor, while (b) and (c) display high and low pitch ends for non-flowing material and cohesive material, respectively. The compression ends of both designs help enhance feeding efficiency.

This section investigates the effect of different feeding screw flight configurations in feeding screw speeds on cohesive and non-flowing materials at a constant agitator speed. The results for cohesive materials reveal a direct correlation between screw speeds and powder flow rate across all four feeding flight configurations (Figure 8-9). Interestingly, the powder flow rate

increases as the screw end pitch increases, regardless of whether it's a compression or non-compression screw. The analysis of the ratio of screw speed to agitator speed in Figure 8-9b highlights the 3:2.5 (Screw speed: Agitator speed) ratio as optimal for all feeding screw flight configurations. However, both 7/7 and 15/7 non-compression screw designs show superior performance in terms of the ratio. Furthermore, Figure 8-9c and Figure 8-9d show that for cohesive materials, the 15/7 non-compression screw has better repeatability and stability than other designs, although the 7/7 compression screw also exhibits inferior stability. Overall, these results provide insightful findings on the influence of feeding screw design for cohesive material on powder flow rate, stability, and repeatability, which are crucial factors in the design and optimisation of feeders.

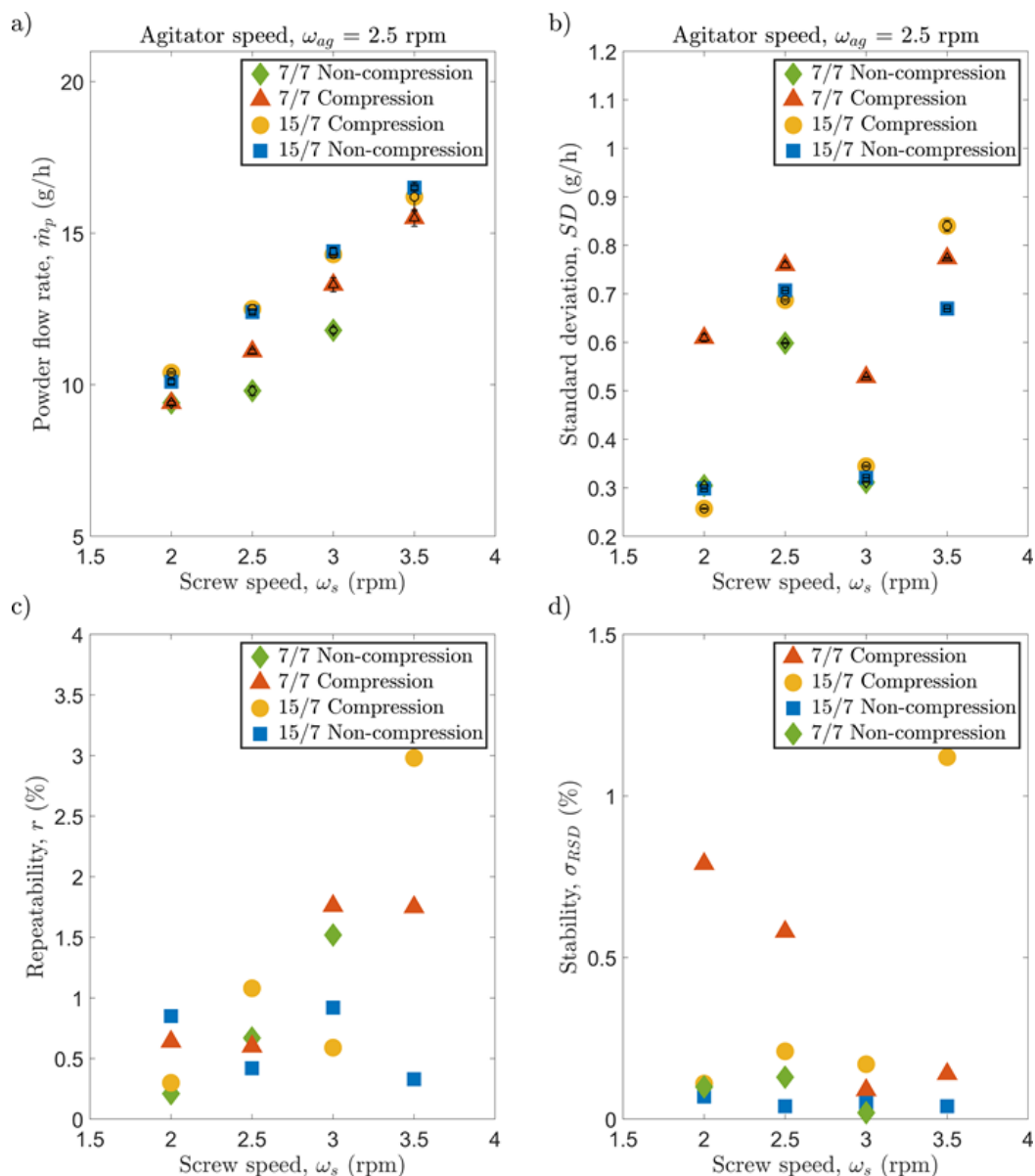


Figure 8-9: Influence of screw speed on CCS powder flow rate, standard deviation, repeatability, and Stability at a fixed agitator speed of 2.5 rpm. a) shows the powder flow rate as a function of screw speed, while b) illustrates the SD. c) and d) display the repeatability and stability, respectively, as a function of screw speed. All measurements were taken at a fixed agitator speed of 2.5 rpm.

Figure 8-10a indicates that the powder flow rate remains relatively constant for non-flowing material, despite changes in feeding screw speed. Notably, the 25/25 compression feeding screw consistently maintains a steady powder flow rate, regardless of changes in the screw speed. The statement suggests that in the context of non-flowing powder feeding, an equal pitch combined with a compression end may offer greater stability in the feeding process. Figure 8-10b demonstrates that the 25/25 compression feeding screw has the lowest SD of 0.38 g/h at a screw speed of 4 rpm and exhibits good repeatability at 0.18% and stability at 0.1%, as shown in Figure 8-10c and Figure 8-10d, respectively.

Based on the results presented in this section, 15/7 non-compression feeding and 25/25 compression feeding screw appear to be promising improvements for CCS and APAP, respectively.

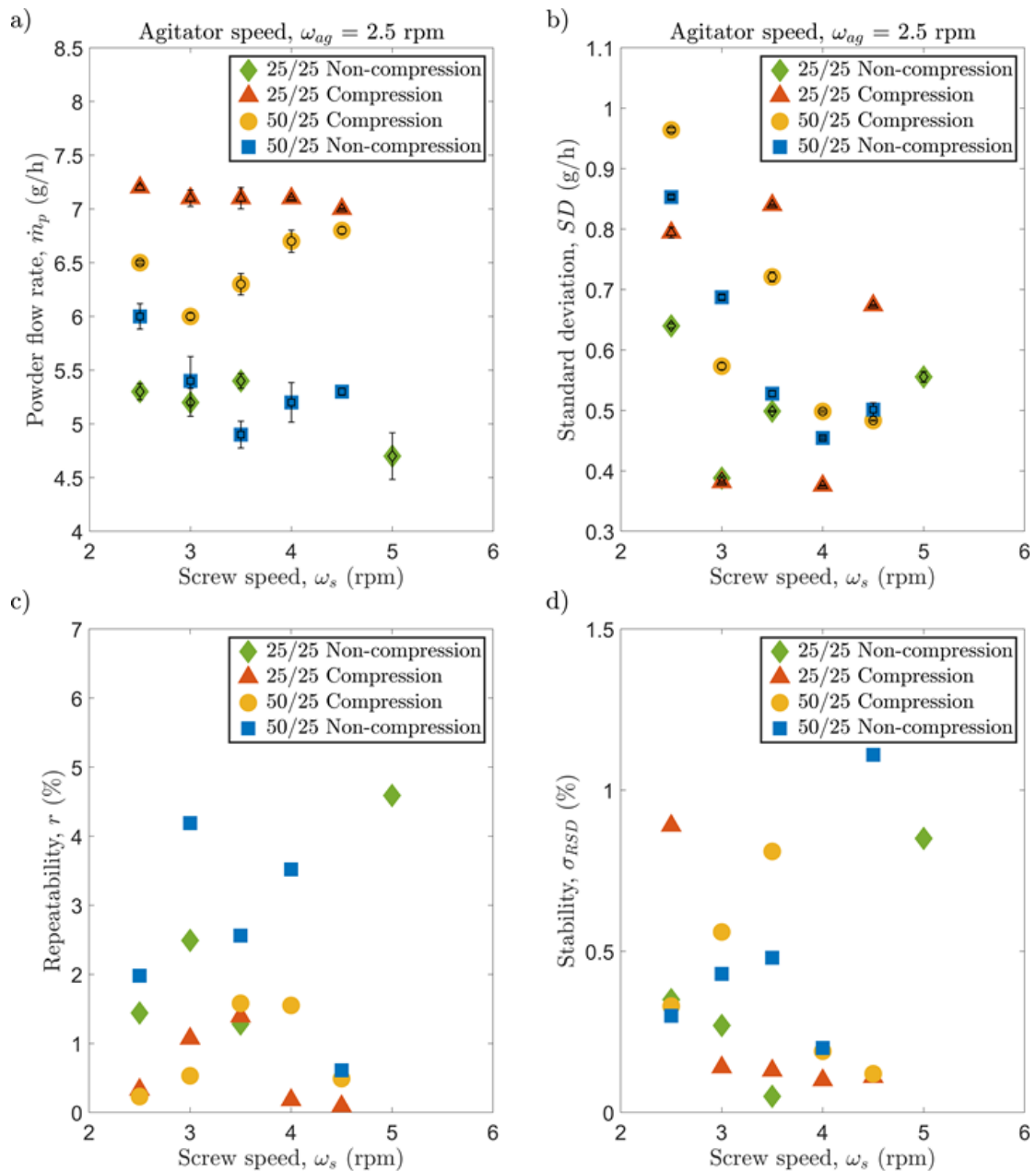


Figure 8-10: Influence of screw speed on APAP powder flow rate, SD, repeatability, and Stability at a fixed agitator speed of 2.5 rpm. a) shows the powder flow rate as a function of screw speed, while b) illustrates the SD. c) and d) display the repeatability and stability, respectively, as a function of screw speed. All measurements were taken at a fixed agitator speed of 2.5 rpm.

Through an exploration of the feed factor, Figure 8-11 depicts how the feed factor changes with screw speed at a constant agitator speed of 2.5 rpm for CCS and APAP. In both cases, there is a notable decrease in the feed factor as the screw speed increases under a consistent agitator speed. This observation underscores the significant influence of the agitator in regulating uniform material feeding to the screw. The heightened screw speed correlates with a reduction in powder fill, revealing the agitator's role in maintaining stability.

Moreover, the figure highlights the stability of 15-7 non-compression and compression ends. At a constant agitator speed, the study indicates that the 15-7 non-compression end tends to

be flat. It demonstrates that variations in screw speed have minimal impact on the feed factor, particularly with the use of the 15-7 compression end. Therefore, it shows that there is better control by the use of the 15-7 compression as it is more stable. Both 15-7 non-compression and 15-7 compression ends exhibit higher feed factors, suggesting superior screw fill efficiency. Therefore, this subtle design adjustment effectively controls the powder flow rate.

For APAP, the 25-25 compression end showcases a well-defined linear or slightly curved relationship between feed factor and screw speed, demonstrating the effective control of screw speed can be used to minimise the powder flow rate variation. Overall, the 25-25 compression end consistently outperforms other ends in terms of feed factor, indicating its accurate control efficacy in feeding material in the system.

In summary, the examination of different screw geometries and designs in this study validates that modifications to screw geometries indeed influence bulk density rearrangement to a certain extent. Furthermore, the study identifies a more suitable screw for the specific material being fed, leading to enhanced material conveyance and greater overall efficiency in the feeding process.

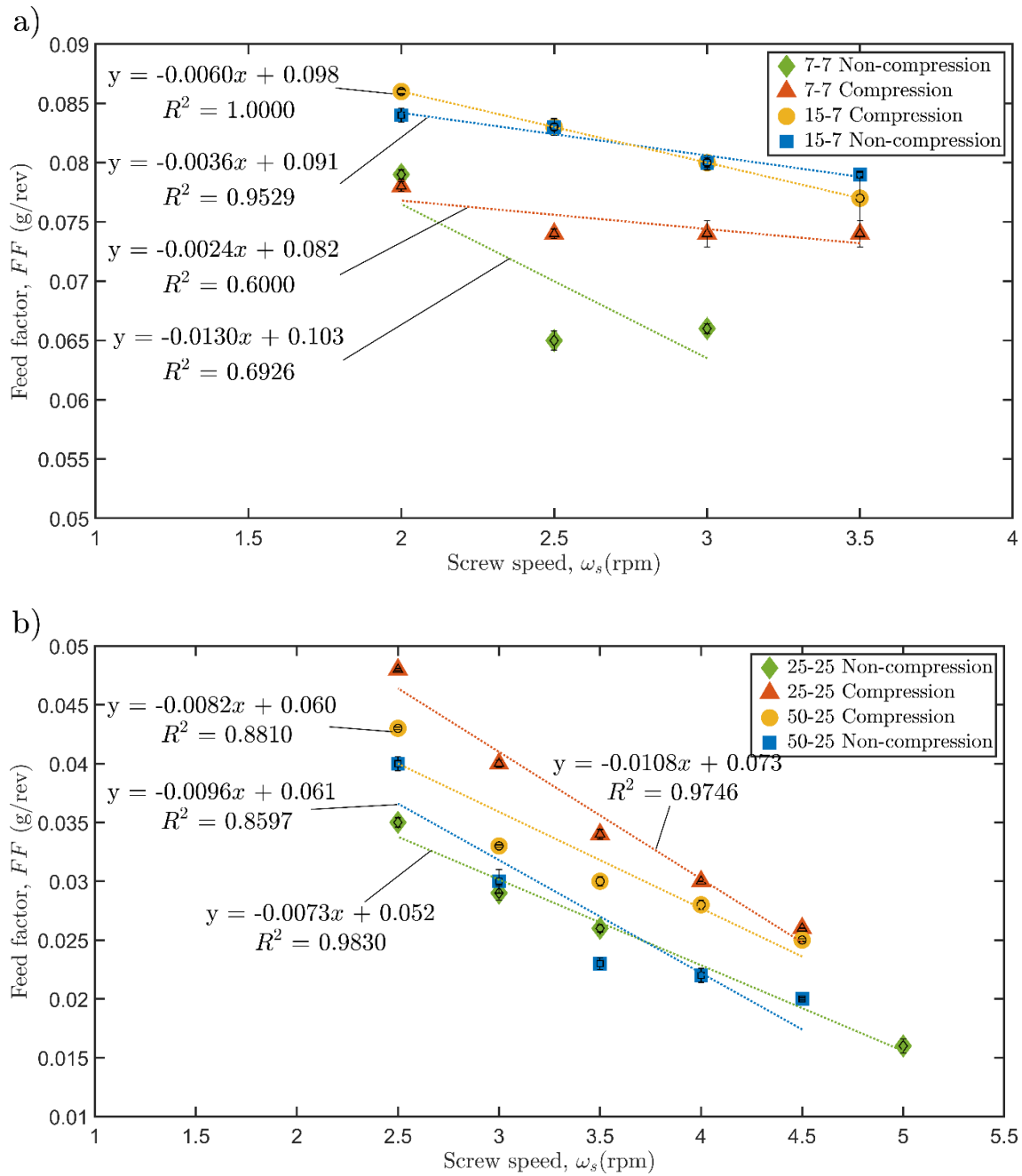


Figure 8-11: Variation of feed factor with screw speed at a constant agitator speed of 2.5 rpm in the powder feeding process for a) CCS and b) APAP, showcasing the influence of various screw flight configurations.

8.3.3 Optimising powder feeding performance: A study on feeding screw flight configurations at various feed rates

The preceding section examined the effect of different feeding screw flight configurations on powder flow rate under varying screw speeds and a constant agitator speed. In this section, we explore the effect of feeding screw design on powder feeding performance at optimal points.

For CCS, the results shown in Figure 8-12a reveal that the application of a 15/7 non-compression screw raises the powder flow rate of approximately 2.6 g/h to 4 g/h, compared to a 7/7 non-compression screw at the same parameter setting. In the compression flight configurations, 15/7 leads to an increase in the powder flow rate of approximately 0.7 to 2.2 g/h across the range of powder flow rates compared to a 7/7 screw. The non-compression end has a lower powder flow rate compared to the compression end for the 7/7 pitch end. However, there is not much difference in the SD between 7/7 non-compression, 15/7 non-compression, and 15/7 compression when considering the change in SD. Their values are very close to each other across various powder flow rates. On the other hand, 7/7 compression exhibits a poor SD above 0.4 g/h across various powder flow rates. While 7/7 non-compression has a lower SD at low powder flow rate feeding than others, it has a wider range of SD across the powder flow rates. Although 15/7 non-compression has a higher SD than 7/7 non-compression, its range is more consistent than that of 7/7 non-compression.

For APAP, the results shown in Figure 8-12b illustrate that the powder flow rate increases in the following order: 25/25 compression > 50/25 compression > 50/25 non-compression > 25/25 non-compression. This reveals that the powder flow rate of 25/25 compression ranges from approximately 1.9 g/h to 3.3 g/h higher than that of the 25/25 non-compression end screw across varying powder flow rates. The difference between 50/25 compression and non-compression ends is minor, around 0.2 g/h to 1.6 g/h. The 50/25 non-compression end has a powder flow rate of about 0.6 g/h to 2.5 g/h higher than the 25/25 non-compression end. The 25/25 compression end is 0.3 to 0.7 g/h higher than the 50/25 compression end. From the SD viewpoint, the figure shows that a 25/25 end has a low SD, particularly the 25/25 compression end, as some other cases exhibit a high SD above 4 g/h in a high powder flow rate.

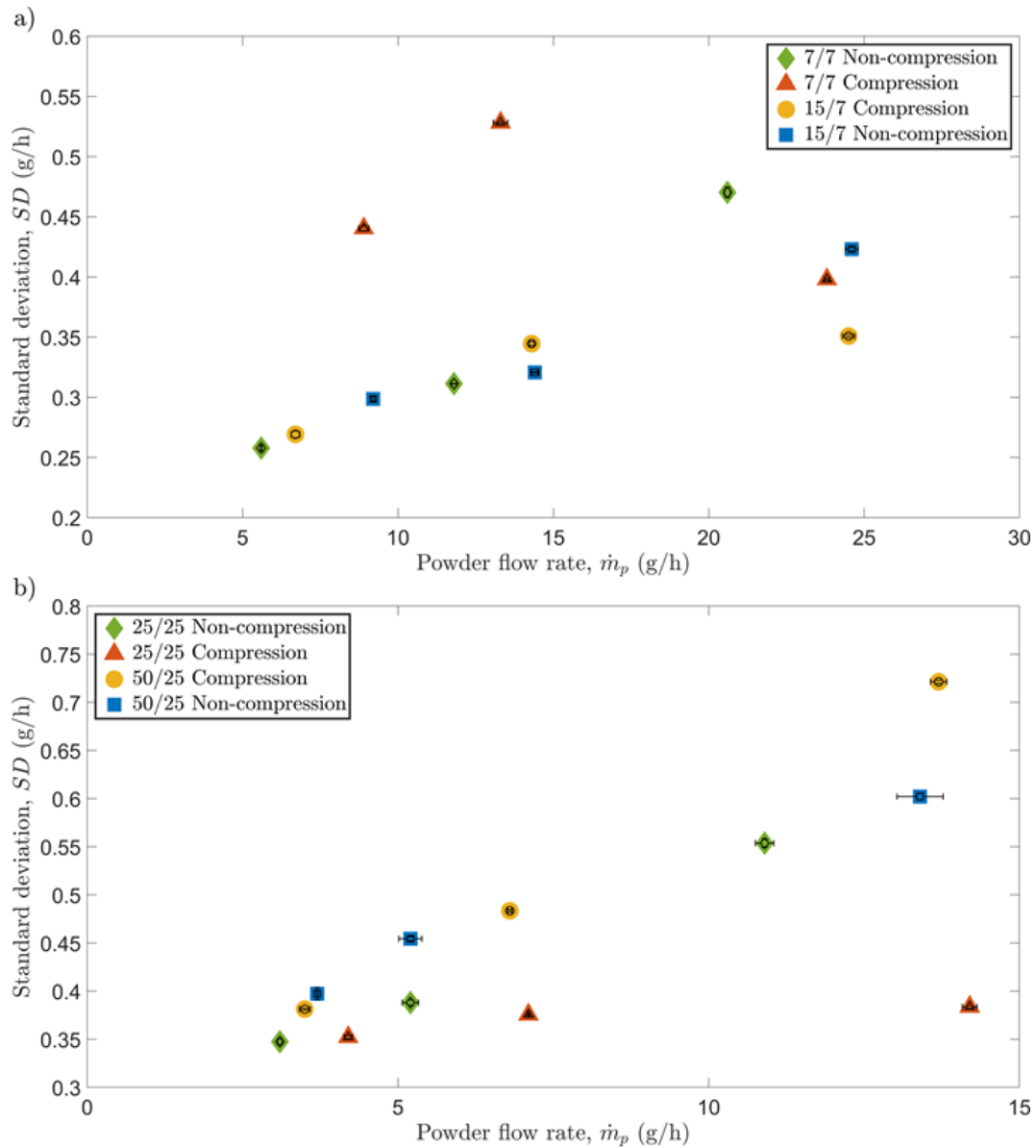


Figure 8-12: SD of powder flow rate across different feeding screw flight configurations for a) CCS and b) APAP. It shows that equal-pitch compression ends generally have a low SD, while the 25/25 compression screw exhibits a minor SD for APAP. For CCS, 7/7 non-compression and 15/7 non-compression exhibit a minor SD.

This investigation also examines the influence of four different feeding screw flight configurations on the repeatability of consistent powder feeding. The results demonstrate that 25/7 and 7/7 non-compression-end feeding screws outperform 25/7 and 7/7 compression-end counterparts for cohesive materials in terms of repeatability (Figure 8-13). In contrast, the 25/25 compression-end feeding screw exhibits remarkable repeatability for non-flowing materials.

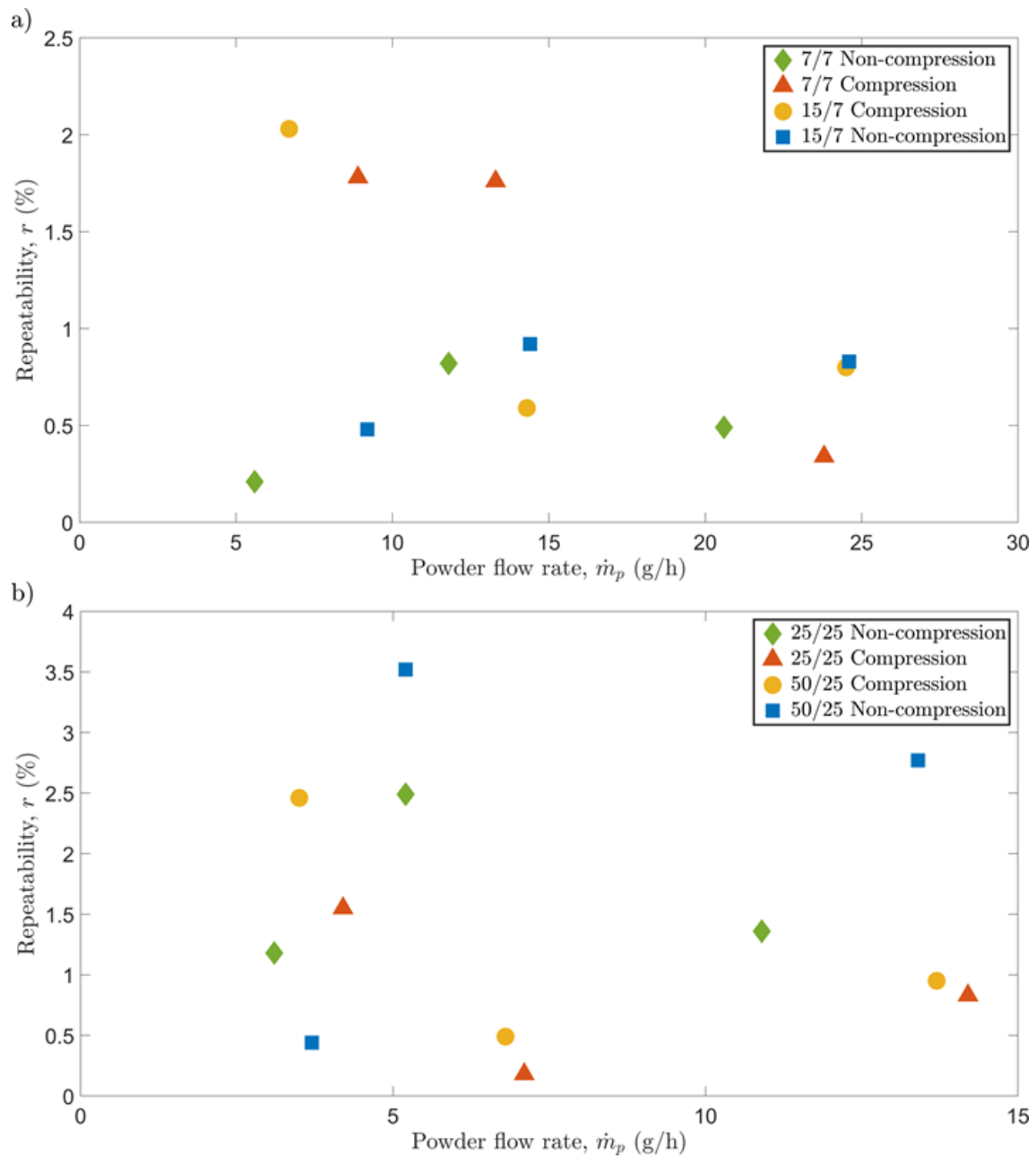


Figure 8-13: Repeatability as a function of powder flow rate: a) CCS b) APAP for four different feeding screw flight configurations.

The results illustrated in Figure 8-14a suggest that no definitive trend can be observed regarding the stability of the different feeding screw flight configurations. However, it does indicate that the 15/7 non-compression feeding screw and 7/7 compression feeding screw exhibit more consistent stability with $<0.2\%$ for cohesive material compared to the other designs. Conversely, Figure 8-14b demonstrates that both 50/25 and 25/25 compression-end feeding screw flight configurations exhibit favourable stability compared to the other flight configurations for non-flowing materials. This indicates that the compression flight configuration is a suitable approach for non-flowing materials. These observations underscore the significance of selecting an appropriate feeding screw design that aligns with the

characteristics of the powder being utilised to achieve the desired feeding repeatability and stability.

Based on the results presented in this section, 15/7 non-compression feeding should be chosen for CCS as they exhibit a minor SD, good repeatability and stability, and a 25/25 compression feeding screw is chosen for APAP. These feeding screw flight configurations will be used for the subsequent experiments to investigate the effects of various inner screw pitch configurations of a double-screw agitator.

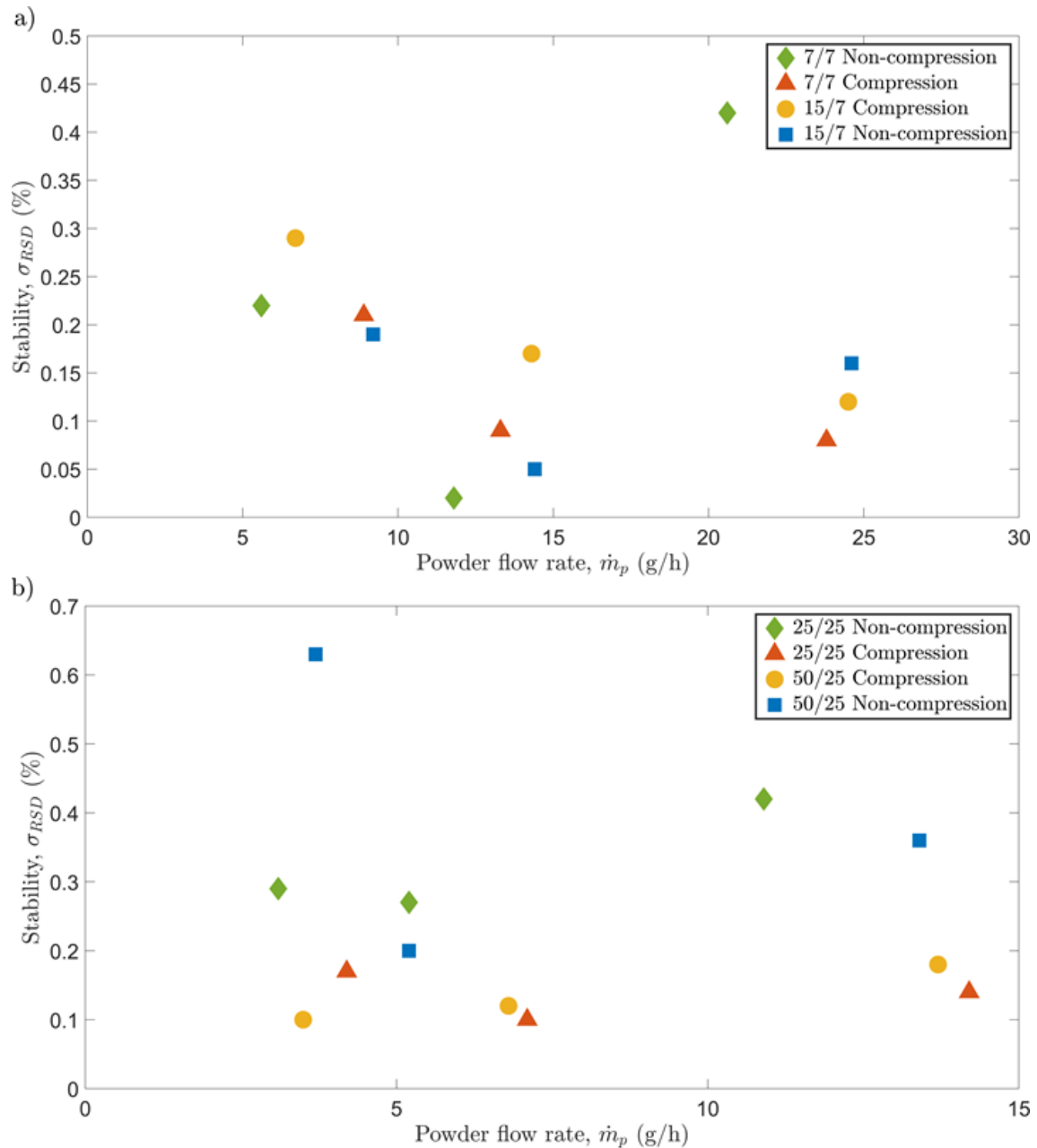


Figure 8-14: Influence of four different feeding screw flight configurations on powder feeding stability for a) CCS and b) APAP.

Figure 8-15 illuminates the effect of diverse screw flight configurations on the feed factor as agitator speed increases. As elucidated in Section 8.3.2, the agitator serves as a pivotal factor in controlling powder flow rates. This study aims to scrutinise the influence of screw flight configurations on the feed factor at optimal points.

Within the CCS feeding context, both the 15-7 non-compression and 7-7 compression screw flight configurations display consistent and stable linear increases in contrast to other configurations. Nevertheless, findings in Section 8.3.2 favour the stability provided by the 15-7 non-compression flight configuration. In summary, based on these observations, the 15-7 non-compression option is recommended.

Regarding APAP feeding, the feed factor demonstrates an upward trend with increasing agitator speed across four screw flight configurations. The 25-25 non-compression end screw demonstrates stable control, while the analysis and discussion in Section 8.3.2 highlight commendable performance from the 25-25 compression end screw flight configuration.

In summary, Figure 8-15 and Figure 8-11 sheds light on the influence of screw flight configurations, emphasising their divergent effects on the feed factor in both CCS and APAP feeding scenarios. Specifically, the 15-7 non-compression end screw exhibits favourable stability for CCS, while the 25-25 compression end screw performs well for APAP.

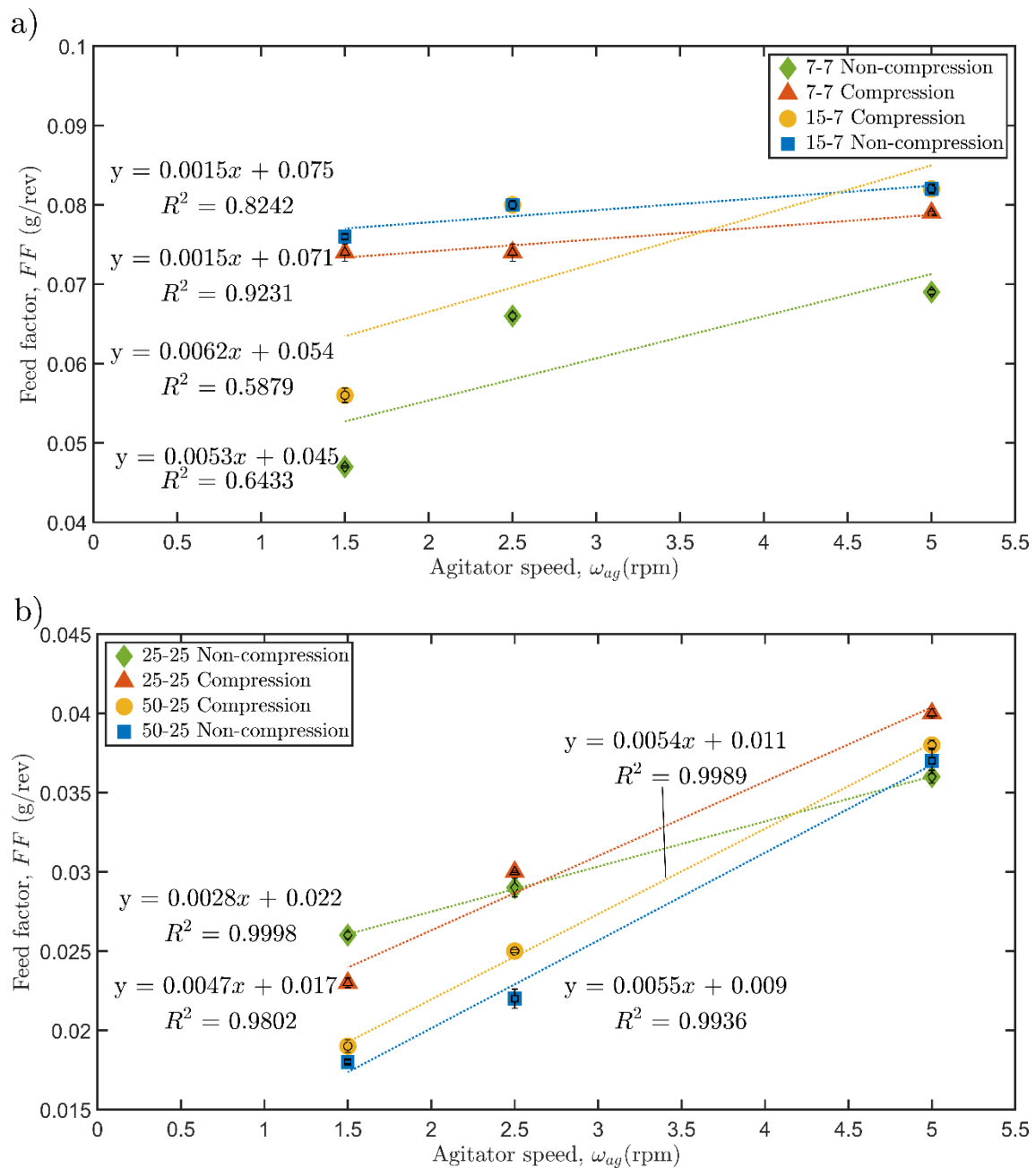


Figure 8-15: Variation of feed factor at an optimal point across the agitator speed in the powder feeding process for a) CCS and b) APAP.

8.3.4 The effect of on inner screw pitch of a double-screw agitator at various feeding screw speeds

The previous sections investigated the optimisation of feeding screw angles and feeding screw flight configurations. Building on this work, this section aims to evaluate the effect of different pitches of the inner screw of the double-screw agitator on powder flow rate and feeding consistency using identical feeding screws and angles. To achieve this, three pitches of inner screws, namely 7 mm, 10 mm, and 15 mm, were studied (Figure 8-16). The experimental setup was configured to match the optimal settings in sections 8.3.1 and 8.3.3, including a 30° inclined feeding screw angle, a 15/7 non-compression screw for cohesive material, and a

25/25 compression screw for non-flowing material. The findings from this investigation intended to provide valuable insights into the inner screw pitch of double-screw agitators and their potential applications in handling cohesive and non-flowing materials.

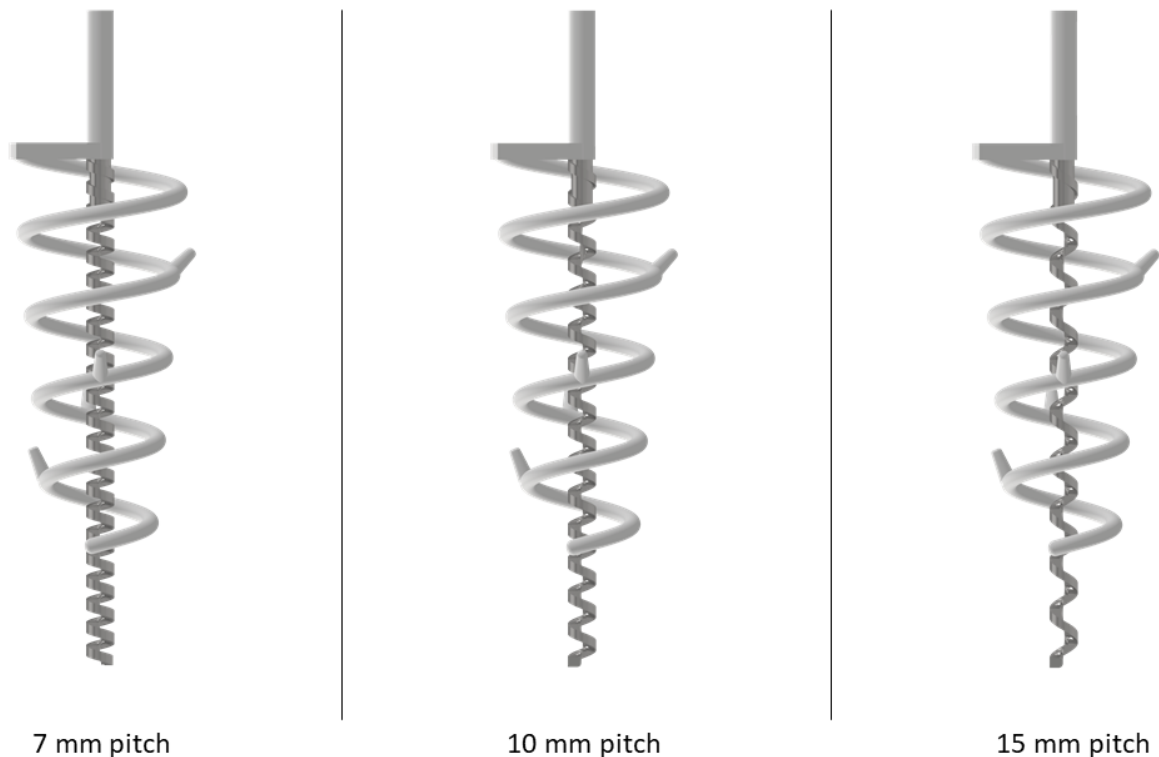


Figure 8-16: Three inner screw double-screw agitators, each featuring a unique screw pitch of 7 mm, 10 mm, and 15 mm, respectively, while maintaining a uniform outer screw configuration. It studies the effect of different inner screw pitches of the double-screw agitator on cohesive powder feeding performance under different feeding screw speeds.

Figure 8-17a demonstrates a positive correlation between powder flow rate and feeding screw speed for CCS, consistent with the findings of section 8.3.2. Interestingly, an increase in the inner screw pitch only resulted in a slight increase in the powder flow rate. Figure 8-17b reveals that a ratio of 3:2.5 offers the lowest SD among the three pitches studied, consistent with the findings of section 8.3.2. This implies that the change of the inner screw pitch seems not to influence the optimal ratio between the feeding screw speed and double-screw agitator speed for cohesive material. Figure 8-17c indicates that the ratio of 2.5:2.5 is favourable for a 15 mm pitch, whereas a ratio of 3:2.5 is optimal for a 7 mm pitch in terms of good repeatability. However, Figure 8-17d shows that the 7 mm pitch provides more consistent stability across various feeding screw speeds. In summary, the 7 mm pitch offers the most significant improvement.

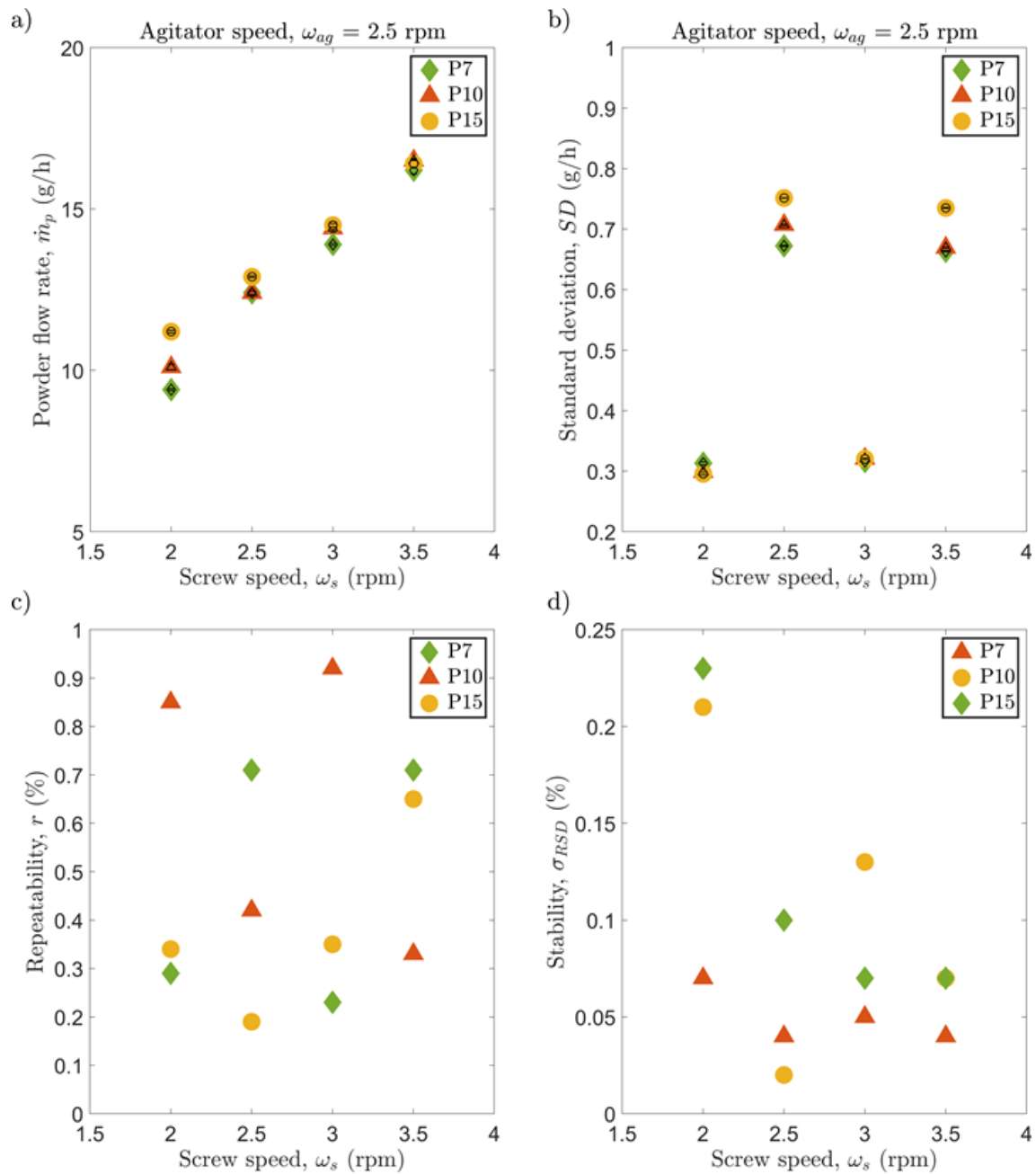


Figure 8-17: The effect of different inner screw pitches of the double-screw agitator on cohesive powder feeding performance under different feeding screw speeds: a) the effect of inner screw pitch on CCS powder flow rate at different screw speeds, with a fixed agitator speed of 2.5 rpm. b) the variation in SD with screw speed at a fixed agitator speed of 2.5 rpm. c) the relationship between repeatability and screw speed, with a fixed agitator speed of 2.5 rpm. d) the effect of screw speed on stability at a fixed agitator speed of 2.5 rpm.

Figure 8-18a reveals that the powder flow rate for APAP is largely influenced by the pitch of the inner screw of the double-screw agitator rather than the feeding screw speeds. Specifically, as depicted in Figure 8-18a, an increase in pitch leads to an increase in powder flow rate. In terms of minimising variation, Figure 8-18b and Figure 8-18c indicate that the 10 mm and 15 mm pitches have the lowest SD and good repeatability, respectively. However, Figure 8-18d reveals that the 10 mm pitch offers the best stability for feeding non-flowing

powder. Therefore, for optimal feeding of non-flowing material, the results recommend using a 30° inclined feeding screw with a 25/25 compression feeding screw and a double-screw agitator with a 10 mm inner screw pitch.

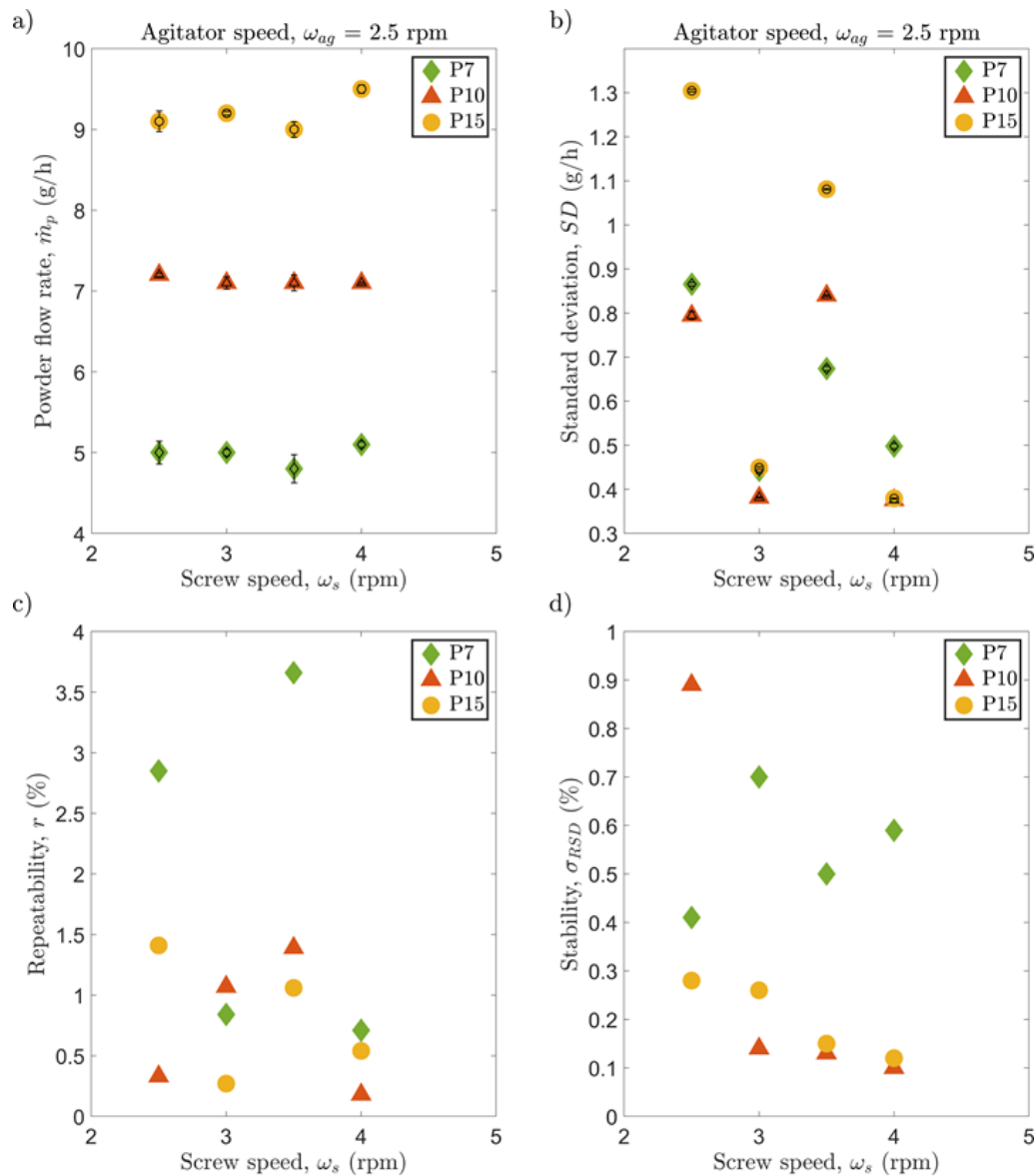


Figure 8-18: The effect of different inner screw pitches of the double-screw agitator on non-flowing powder feeding performance under different feeding screw speeds: a) the effect of inner screw pitch on APAP powder flow rate at different screw speeds, with a fixed agitator speed of 2.5 rpm. b) the variation in SD with screw speed at a fixed agitator speed of 2.5 rpm. c) the relationship between repeatability and screw speed, with a fixed agitator speed of 2.5 rpm. d) the effect of screw speed on stability at a fixed agitator speed of 2.5 rpm.

Figure 8-19 presents an analysis of the feed factor as a function of screw speed under a consistent agitator speed of 2.5 rpm, exploring various agitator inner screw pitches.

In Figure 8-19a, the 7 mm pitch is associated with inadequate control and a low feed factor for CCS. Conversely, pitches of 10 mm and 15 mm exhibit effective control over screw fill at the constant agitator speed of 2.5 rpm. Notably, the 15 mm pitch displays a steep slope, indicating

that even slight increases could significantly amplify the powder flow rate. The 10 mm pitch would provide a better powder flow rate control. For APAP, the feed factor experiences a linear decrease with increasing screw speed at a constant agitator speed (Figure 8-19b). Additionally, an increase in the agitator's inner pitch contributes to higher feed factors and powder flow rates.

In summary, Figure 8-19 emphasises how varying agitator inner screw pitches influence the feed factor, yielding unique responses in CCS and APAP feeding scenarios. Notably, the 10 mm pitch proves more effective in controlling powder flow rates for CCS. In the case of APAP, adjusting the agitator inner pitch allows for modulation of feeding throughput range, offering a means to increase or decrease it. Collectively, these findings underscore the necessity for careful consideration in selecting the agitator inner screw pitch to ensure optimal control of the feeding process.

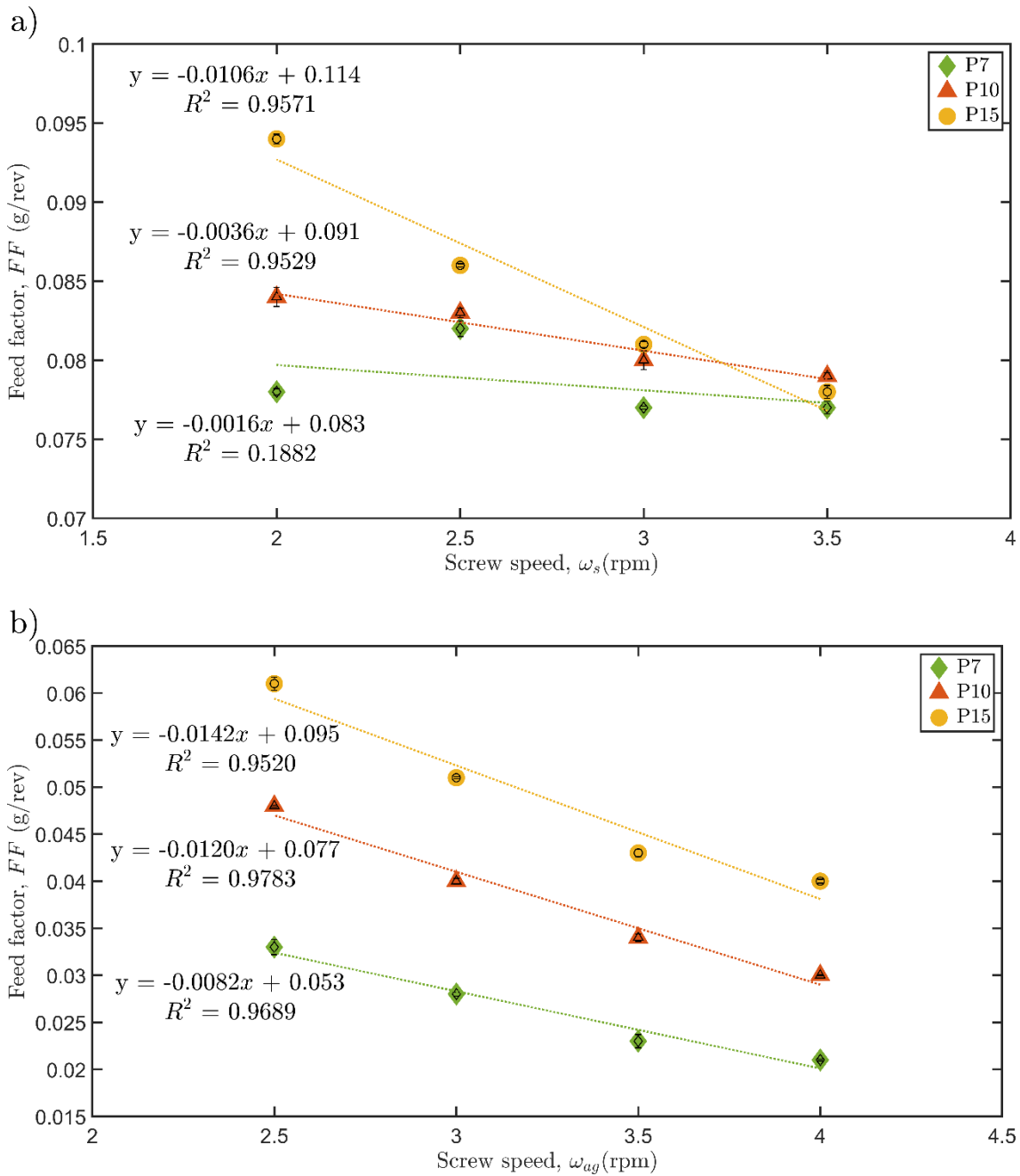


Figure 8-19: The feed factor as a function of screw speed at a constant agitator speed of 2.5 rpm, featuring various agitator inner screw pitches in its configuration.

8.3.5 Optimising powder feeding performance: A study on inner screw pitch of double-screw agitator at various feed rates

This section provides an in-depth investigation into the effect of the inner screw pitch of the double-screw agitator on the performance of powder feeding. The results show that the changes in the inner screw pitch of the double-screw agitator significantly influence the powder flow rate and SD for both cohesive and non-flowing materials. Figure 8-20 reveals that the powder flow rate gradually increases with the increase of the inner screw pitch, particularly in non-flowing powder feeding. Interestingly, Figure 8-20 reveals that the SD does not

significantly increase with the increase of inner screw pitch in cohesive powder feeding and non-flowing material. The findings suggest that the 15 mm pitch exhibits a lower SD than others for cohesive materials at a feed rate under 10 g/h, while the 7 mm pitch shows potential at a feed rate above 10 g/h. In non-flowing material, the implementation of a 10 mm pitch has demonstrated the capability of achieving an SD below 0.4 g/h across varying feed rates.

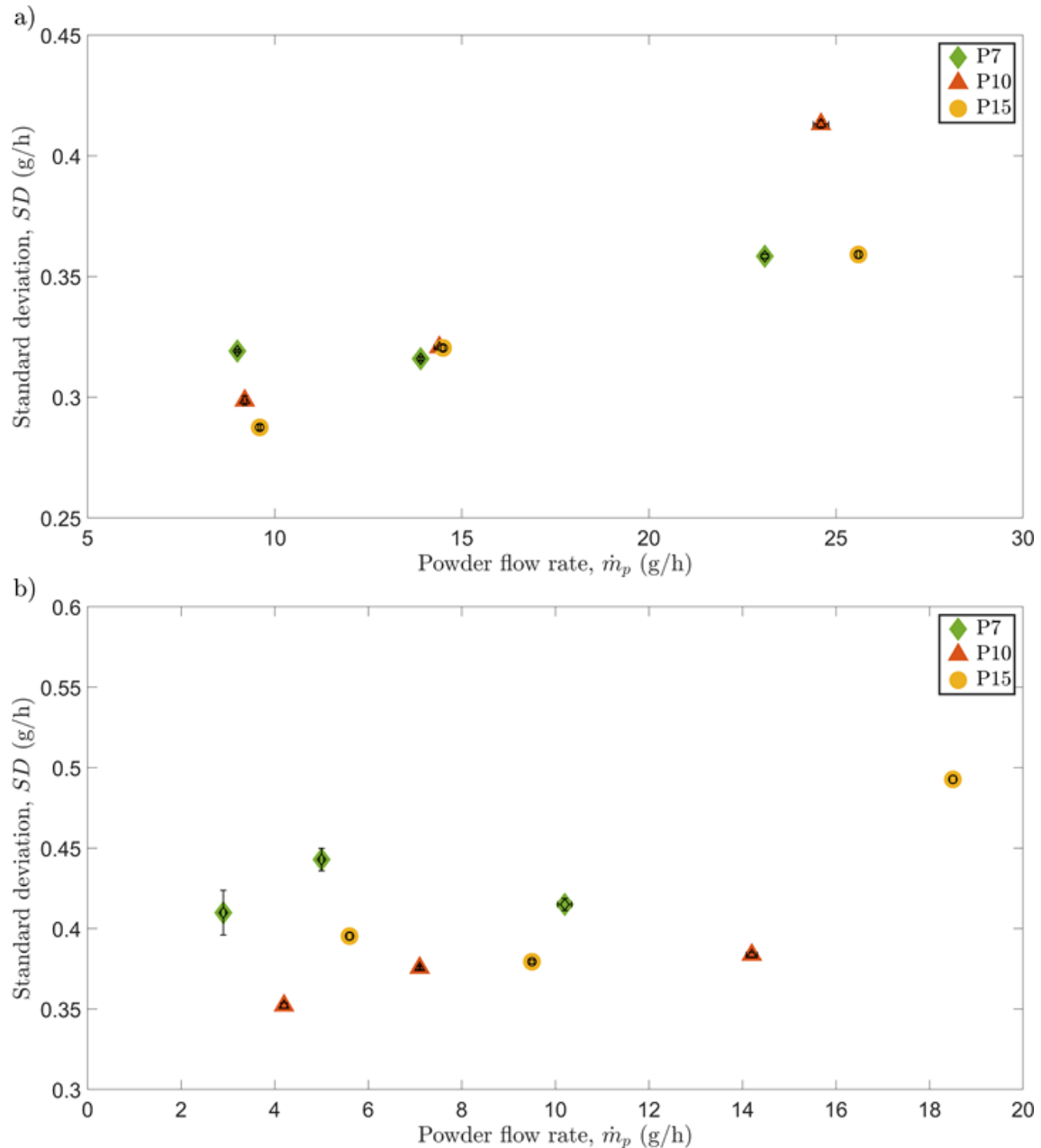


Figure 8-20: Relationship between powder flow rate and SD for a) CCS and b) APAP, using a double-screw agitator with varying inner screw pitches. Results show that the changes in the inner screw pitch of the double-screw agitator have a significant influence on powder flow rate and SD.

The results demonstrate that, for cohesive material, the 7 mm and 15 mm pitches yield low and consistent repeatability, ranging from 0.2% to 0.4% and from 0.2% to 0.35%, respectively (Figure 8-21a). Conversely, Figure 8-21b reveals no distinct pattern in the repeatability of non-

flowing powder feeding. Notably, the 10 mm pitch for non-flowing material presents a wide range of repeatability, varying from 0.2% to 1.6% across the feed rates. Nevertheless, the findings still indicate that the system has excellent repeatability (<2%) across different inner screw pitches.

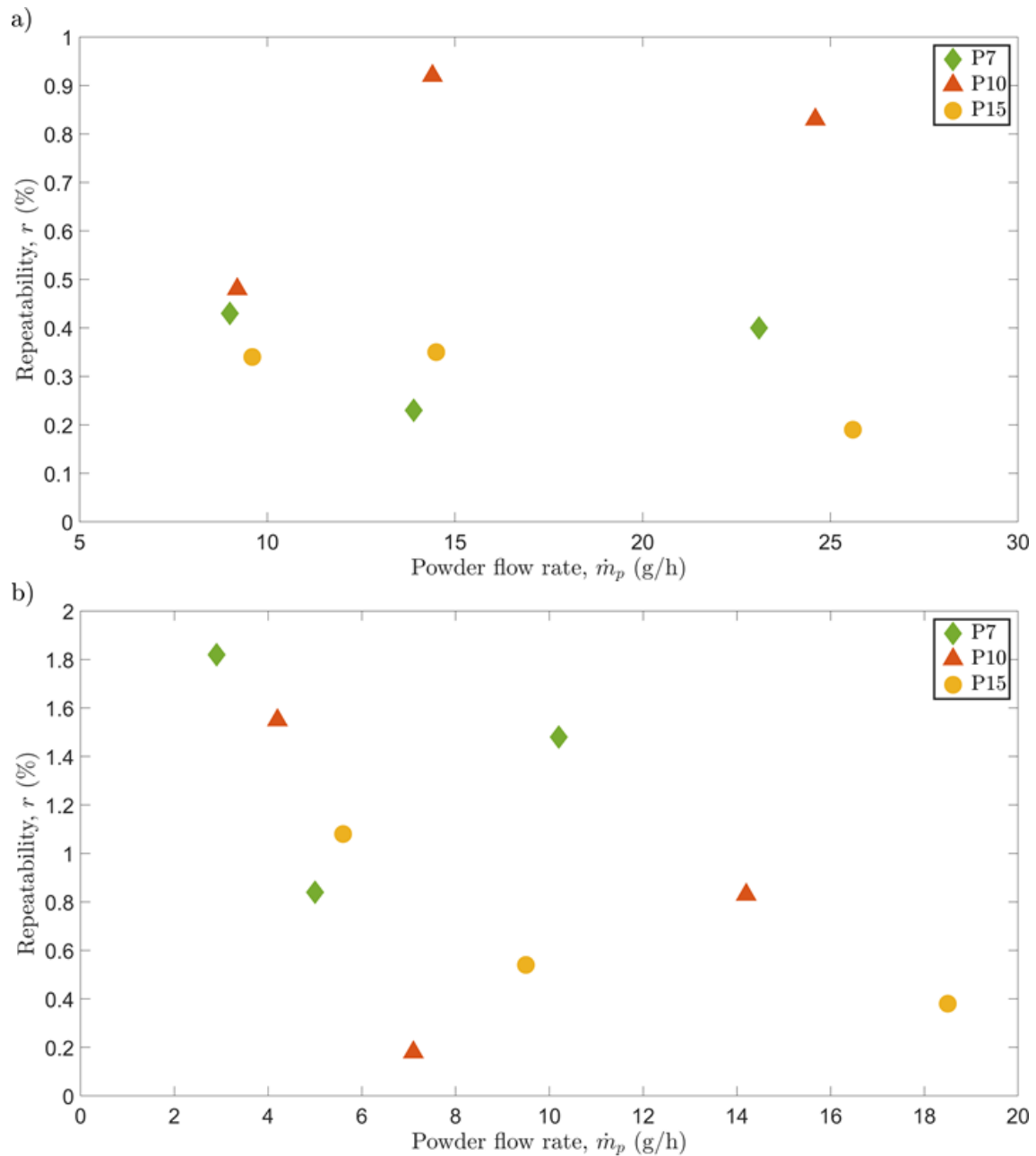


Figure 8-21: The effect of different inner screw pitches of a double-screw agitator on the repeatability of powder feeding as a function of powder flow rate for (a) CCS and (b) APAP, demonstrating the effect of varying inner screw pitch on the repeatability of consistent powder feeding for the two different materials.

Figure 8-22a reveals that the 7 mm pitch exhibits the best stability for cohesive material. However, Figure 8-22b demonstrates that the 10 mm pitch provides excellent and consistent stability. Based on the findings from this section and previous ones, a 7 mm pitch inner screw

is suggested for cohesive powder feeding, while a 10 mm pitch is recommended for non-flowing powder feeding applications. This also implies that materials with better flowability should utilise a narrower pitch inner screw, whereas those with poorer flowability should opt for a higher pitch inner screw.

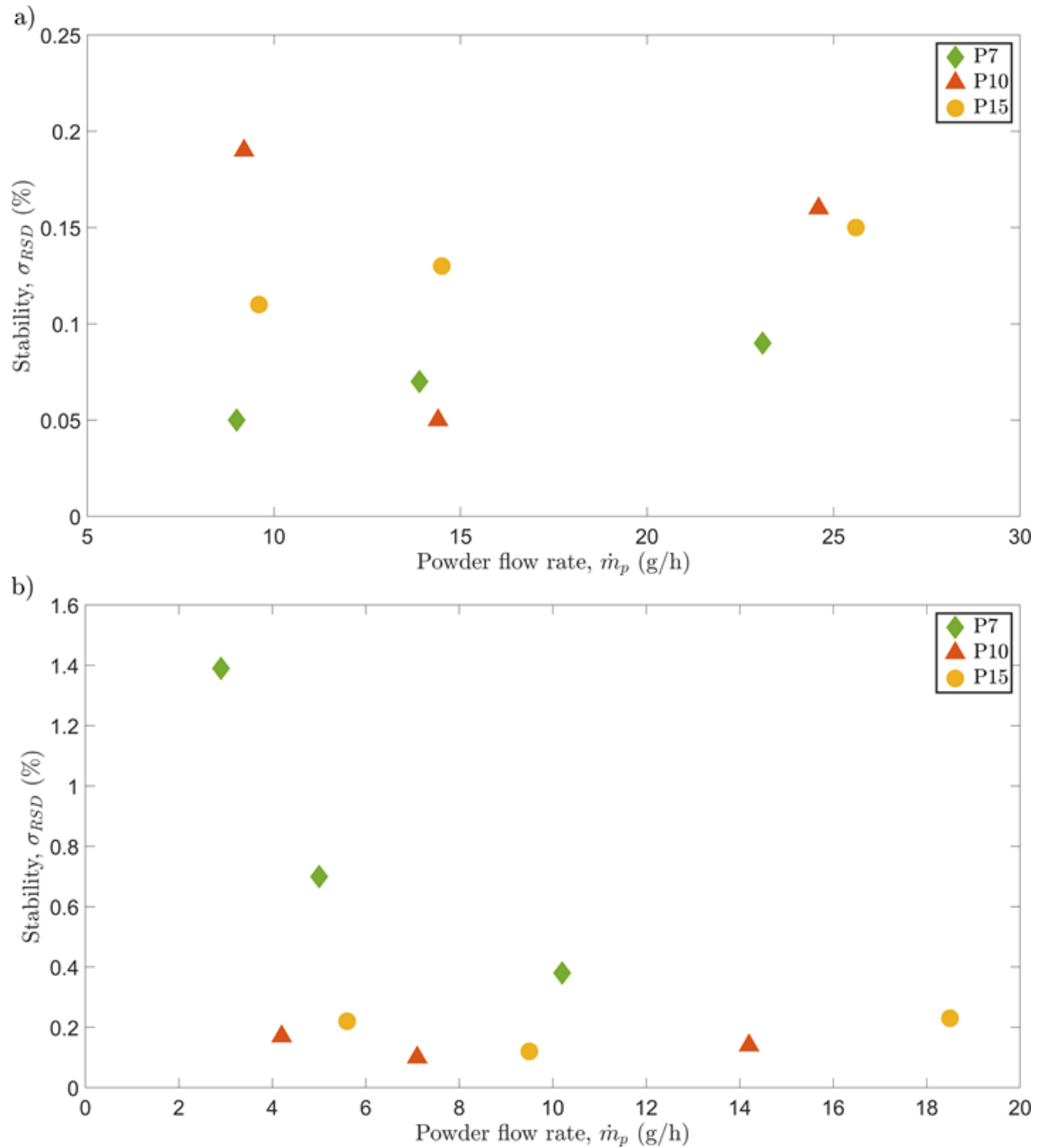


Figure 8-22: The effect of inner screw pitch on feeding stability for (a) CCS and (b) APAP as a function of powder flow rate, demonstrating the relationship between flow rate and the stability of powder feeding while varying the inner screw pitch for both cohesive and non-flowing materials.

An experiment is conducted to visualise the effect of the agitator screw inner pitch on both the feed factor and powder flow rate across varying agitator speeds at the optimal powder feeding points (Figure 8-23).

At the identified optimal points, the feed factor analysis figure demonstrates that a 15 mm pitch provides robust stability for CCS, while a 10 mm pitch achieves similar stability for APAP. In both cases, an increase in agitator screw pitch corresponds to an increase in both the feed factor and powder flow rate. Conversely, a 7 mm pitch demonstrates poor control. This consistent observation across both CCS and APAP emphasises the crucial role played by the agitator screw inner pitch and agitator speed in controlling the powder flow rate within this design.

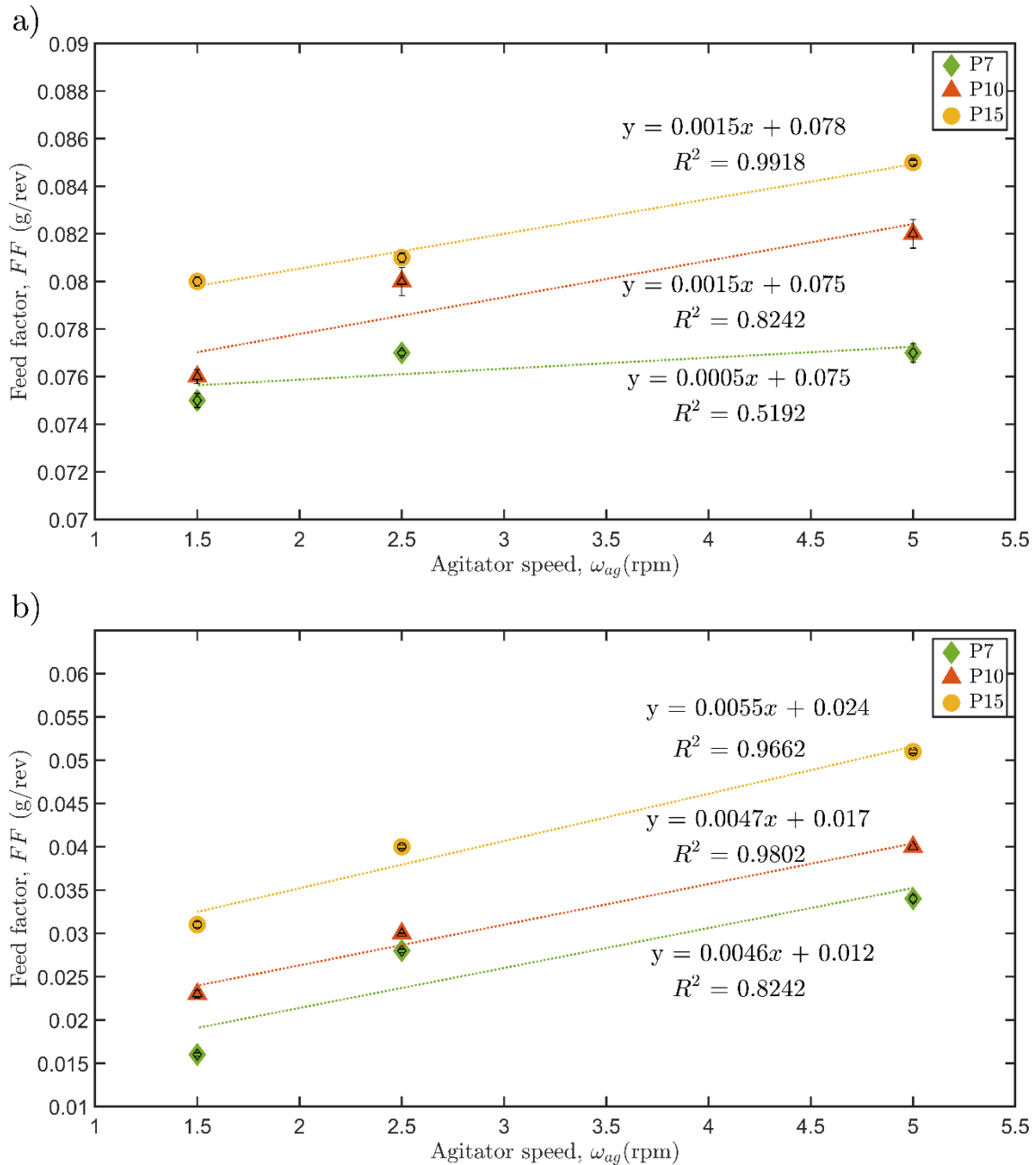


Figure 8-23: Effect of agitator screw inner pitch on feed factors with respect to agitator speed at the optimal powder feeding point.

8.3.6 Analysis of improvement between the original design and the optimal design

The extent of improvement is investigated by comparing the previously established design in Chapter 7 with the optimal design proposed in this chapter. The former feeding system employed a 30° inclination, 10 mm pitch inner screw double-screw agitator, 7/7 non-compression feeding screw for cohesive material and 25/25 non-compression feeding screw for non-flowing materials. On the other hand, the suggested optimal design in this chapter employs a 30° inclination, 7 mm pitch inner screw double-screw agitator and 15/7 non-compression feeding screw for cohesive material, whereas a 30° inclination, 10 mm pitch inner screw double-screw agitator and 25/25 compression feeding screw for non-flowing material.

Due to variations in powder flow rates caused by different system designs and in order to fairly compare the data, reliability (ν_f) is defined in this chapter as the ratio of the difference between the highest and lowest SDs of each design in Figure 8-24, divided by the average SDs across the powder flow rates in the exact figure. It can be expressed as

$$\nu_f = \frac{\sigma_{highest} - \sigma_{lowest}}{\bar{\sigma}} \times 100\%, \quad \text{Equation 8-1}$$

where $\sigma_{highest}$ represents the highest point of the SD, σ_{lowest} denotes the lowest point of the SD, and $\bar{\sigma}$ signifies the average of the SDs across the powder flow rates. This value serves as an indicator of the design's feeding variability, where a higher ν_f value indicates an unreliable equipment setting and a lower ν_f value indicates a reliable design.

Figure 8-24 compares the two designs for CCS and APAP, revealing that the optimal design yields a narrow SD range across the feed rates for both materials. From the figure, we observe an ν_f value of 61% for the previous design and 22% for the optimal design in CCS. It indicates that the optimal design has a 39% improvement over the previous design. Similarly, for APAP, we obtain ν_f values of 48% and 8.5% for the previous and optimal designs, respectively. The results for both cohesive and non-flowing material indicate that the optimal design has around 39% improvement over the previous design. These results indicate a significant improvement in both materials with the optimal design.

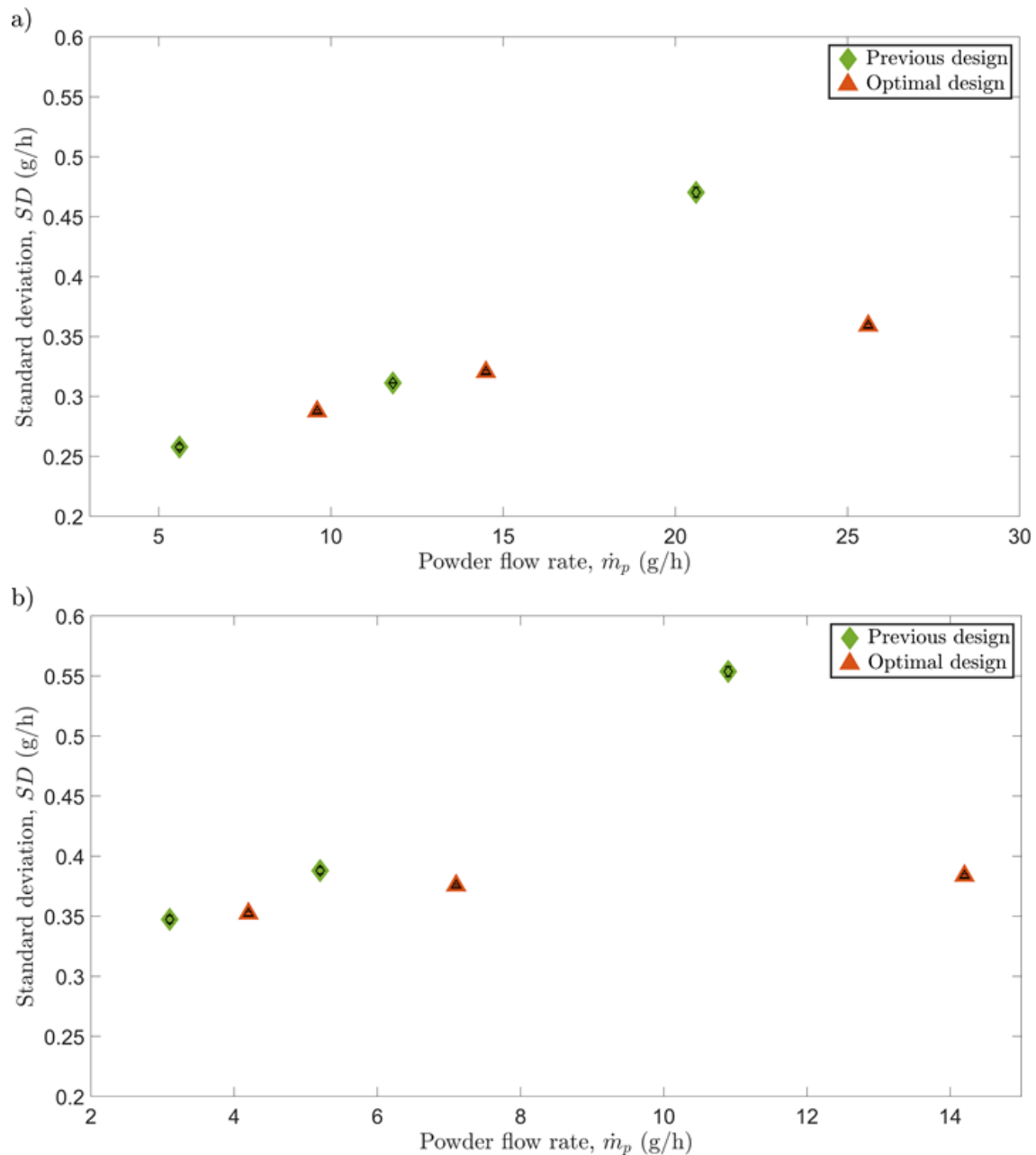


Figure 8-24: A comparative analysis between the equipment designs presented in Chapter 6 and the optimal designs proposed in this study for a) CCS and b) APAP. The SDs are plotted in relation to the powder flow rates for each design.

8.3.7 An observational feeding performance between the commercial and inclined micro-feeders


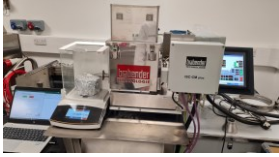

An observational assessment of feeding performance was conducted, comparing the inclined micro-feeder and two commercially available feeders in CMAC laboratory: Brabender MiniTwin Feeder (Model: DDW-M-MT-S) and FlexWall Feeder (Model: DDW-M-FW20). Table 8-1 outlines the setup and two configurations for the Brabender feeders.

The Brabender FlexWall (single screw) employs massage agitation to facilitate powder movement from the hopper to the screw fill, enabling it to handle cohesive or non-flowing

materials effectively. In contrast, the Brabender MiniTwin utilises twin concave screws with hopper agitation for powder feeding. This twin-screw mechanism enhances precision in controlling the powder flow rate but may pose challenges when dealing with cohesive materials, leading to compression (Santos et al., 2018).

To ensure a standardised evaluation, the experiment adopted a volumetric principle, equipping all feeders, including the inclined micro-feeder, with the same catch balance for performance assessment. The hopper was filled to around 80% of its capacity and remained without refilling throughout the process to reduce any influence of powder filling on powder conveying.

Table 8-1: A comparison of the inclined micro-feeder versus two Brabender feeders.

Feature	Brabender MiniTwin DDW-M-MT-S	Brabender FlexWall DDW_M-FW20	Inclined micro-feeder
Type	Twin-Screw feeder	Flexible Wall feeder	Single-screw feeder with an agitator
Application	Laboratory and small scale	Versatile material handling	Continuous small material feeding
Configuration	Twin concave screws design	Flexible wall design – single spiral screw	Single-screw design fitted with an agitator
Screw diameter	12 mm	12 mm	9.5 mm
Screw pitch	6 mm	10 mm	7 mm for CCS 25 mm for APAP
Material handling	Various materials	Ideal for challenging flows	Cohesive materials
Capacity	0.5 – 37.5 kg/h ^{*a}	0.5 – 2.5 kg/h ^{*a}	0.02 – 0.001 kg/h
Feeder used in the experiments			

*Based on Brabender product datasheet.

^aGravimetric throughput assumes a bulk density of 0.5 kg/dm³.

While the experimental approach may not ensure a completely equitable comparison, given the less-than-optimal setup conditions for the commercial feeder operating at rates below its specified minimum feed rate, it nevertheless provides insights into our feeder's performance in relation to commercially available alternatives. It's essential to recognise that commercial feeders are meticulously designed for gravimetric powder feeding to optimise their overall functionality. However, the adjustment of feeder settings, contingent upon the properties of the powder material may be necessary for consistent feeding performance – aspects that were

not thoroughly explored in this thesis. Refer to Table 8-1 for detailed equipment settings. It's crucial to acknowledge that this study does not contain a direct head-to-head comparison. In the described commercial feeder setting, the study's results, depicted in Figure 8-25, reveal that the Brabender MiniTwin feeder achieves a minimum flow rate of 115.9 g/h with a variation of 2.4% for CCS, while the FlexWall feeder achieves 63.1 g/h with a variation of 5.2%. In terms of APAP feeding, the Brabender MiniTwin exhibits unstable feeding. MiniTwin shows a slight decrease in powder flow rate over time for both CCS and APAP, suggesting an influence of hopper level on feeding for both materials. In contrast, the FlexWall and the inclined feeder demonstrate more stable powder feeding for APAP. The FlexWall feeder exhibits performance comparable to the inclined micro-feeder, achieving 16.8 g/h with a variation of 8.4%. The results indicate that the MiniTwin's performance is affected by the rat role and bridge, particularly for APAP. Unlike the FlexWall feeder, which doesn't encounter this problem, however, it experiences higher powder flow rate variation due to inconsistent powder drag into the screw. The inclined micro-feeder with its double-screw agitator consistently fills the screw, resulting in consistent feeding.

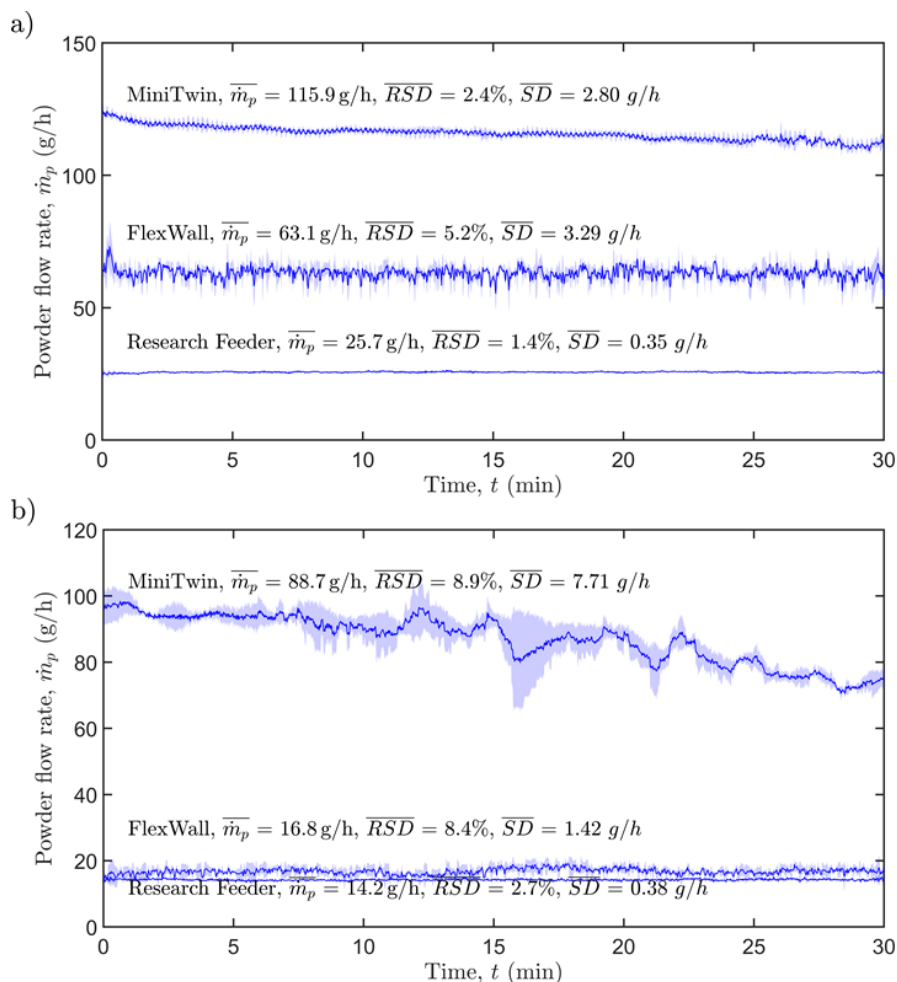


Figure 8-25: A comparative assessment of the performance of an inclined micro-feeder and two commercial feeders in volumetric feeding: a) CCS, b) APAP. The motor speeds were pre-determined and remained unchanged throughout the feeding process.

Furthermore, a comparative analysis between the research data and literature was conducted (Figure 8-26). The comparison reveals that when feeding CCS at micro flow rates, the powder pump with and without control exhibits variations exceeding 5%. In contrast, the inclined micro-feeder demonstrates variations below 5%, albeit slightly higher when feeding at 2.8 g/h. The results of this study highlight the potential of the proposed inclined micro-feeder system, emphasising that it is worthy of further optimisation to enhance its suitability for industrial applications.

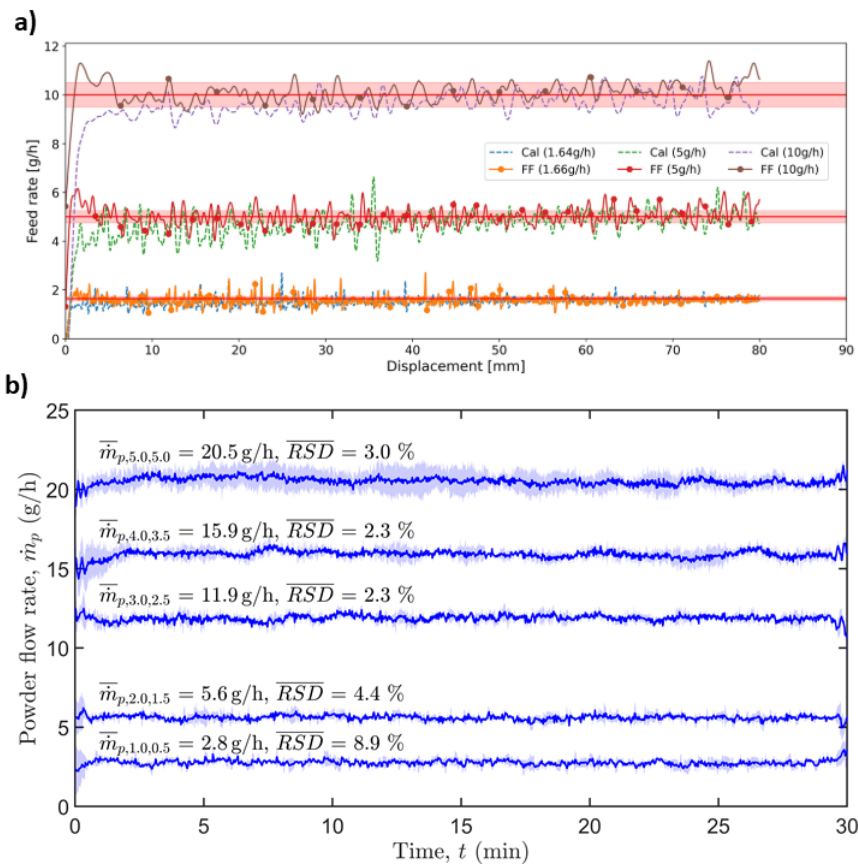


Figure 8-26: A comparative analysis of experimental data and literature findings, showcasing feeding CCS at varying feed rates using a powder pump, both without control (Cal) and with control (FF). The red band indicates a $\pm 5\%$ variation, as observed in a study by Fathollahi et al. (2021). Additionally, our experimental data is presented for further examination (b).

8.4 Conclusions

In summary, this study aimed to improve the inclined micro-feeding system introduced in Chapter 7 and evaluate its performance, specifically focusing on consistent powder feeding. Through meticulous exploration of feeding screw angles, feeding screw flight configurations, and variations in the inner screw pitch of the double-screw agitator using cohesive (CCS) and non-flowing (APAP) powders, the study generated insights into optimising the micro-feeder.

The results underscored the pivotal role of inclining the micro-feeder, demonstrating a significant enhancement in powder feeding consistency for both CCS and APAP materials.

Notably, specific feeding screw angles were identified as optimal for each material: minus 30 and 0 degree inclinations for CCS, and a 30 degree inclination attributed to gravity ensuring a consistent bed and axial velocity. The study also revealed that distinct feeding screw flight configurations rearranged the bulk density and influenced feed rates and feed rate variations, with 15-7 non-compression and compression end feeding screws exhibiting stable powder feeding for CCS, and 25-25 compression end providing superior consistency for APAP.

Additionally, the findings highlighted the substantial impact of the agitator's inner screw pitch on powder feeding performance. The inner screw pitch of 7 mm resulted in poor stability for both materials, while 10 mm pitch exhibited stable powder feeding. Moreover, an increase in the inner screw pitch demonstrated a linear correlation with higher powder fill to the feeding screw and an increased powder flow rate.

Compared to the previous design, the optimised settings resulted in an impressive 39% improvement. A comparative analyse with two commercial feeders and literature indicates the inclined micro-feeder's consistent and stable cohesive powder feeding in micro flow rate, suggesting its potential in industrial applications.

In conclusion, this study provides clear advancements in the optimised inclined micro-feeding system.

9 Conclusions and future works

9.1 Conclusions

Feeding in pharmaceutical drug manufacturing requires mass flow rates as low as 10 g/h with an accuracy of less than $\pm 5\%$. Through the course of this research, two micro-feeder technologies were developed for feeding pharmaceutical materials to meet these requirements: 1) batch pneumatic micro-feeder, and 2) a continuous inclined micro-feeder with a feeding screw and agitator. This work advanced the understanding of micro-feeder technologies, in particular the mechanisms, material attributes and process conditions influencing the performance of the pneumatic feeder and screw feeder.

For the pneumatic micro-feeder, key findings include

- Adjustable cross-sectional areas in the air inlet and process line enable the system to fine-tune entrainment energy to consistently pick up particles and achieve the desired powder flow rate.
- The current configuration of the pneumatic feeder accommodates solely powder type A (aeratable powder, fine particles between 50 and 100 μm), while excluding powder C (cohesive powders, particles size of less than 50 μm) because of its very fine particles (<50 μm), high bulk density and high cohesion, causing particles to agglomerate (Figure 5-4).
- The operational flow pattern observed in this investigation displays a dilute phase flow for all examined materials, as indicated by solid loading analysis (Table 5-1).
- As the powder flow rates increase, there is a logarithmic rise in entrainment energy observed (Figure 6-6).
- The correlation between entrainment energy requirements for the materials investigated and the Hausner ratio is non-linear. However, when contrasting APAP and MCC, it becomes apparent that APAP necessitates higher entrainment energy due to cohesion (Figure 6-6). Hence, cohesion is identified as the primary factor influencing entrainment energy requirements, with particle weight assuming a secondary role.

For the continuous micro-feeder, key findings include

- The design of the double screw agitator in the inclined micro-feeder enables continuous vertical circulation of the powder in the hopper. It eliminates rat-holes and bridging that often occurs when feeding cohesive or non-flowing powder. It also minimises powder flow rate variations caused by powder compression during hopper refilling and stabilising continuous powder feeding without interruption from refilling.

- Beyond a 30-degree inclination, gravity flattens the particle bed, reduces void spaces, and establishes a uniform bed. This specific inclination, when set at 30 degrees and combined with a low screw speed, reduces swirl velocity and promotes a more uniform axial velocity, leading to a stable powder flow rate (Owen and Cleary, 2009). The feeder's inclined position induces shear flow within a consistently deep bed, driven by gravity and evenly distributed across the screw surface. This design is implemented to mitigate variations in powder flow rates and ensure a more consistent flow, especially when handling non-flowing materials such as APAP (Figure 8-7).
- The conventional screw feeder operates on the principle of having a flooded inlet, resulting in nearly 100% fill. However, the volumetric efficiency in our feeder configuration measures below 25%, signifying that the screw is not fully flooded when compared to a conventional screw feeder (Figure 7-11). The reason behind this discrepancy lies in the control exerted by the inner screw of the double screw agitator and inclination.
- The predicted volumetric efficiency significantly surpasses the actual volumetric efficiency, as the prediction model neglects internal shear within the bulk solid. However, it is essential to take into account internal shear, especially as the inclination increases, leading to higher friction in this study.
- Equation 2-31 provides a more accurate prediction of the powder flow rate when compared to Equation 2-32. This improvement is attributed to the inclusion of the inclination correction factor and loading ratio in Equation 2-31. According to Owen and Cleary (2009), the DEM predictions for screws inclined at 30 to 60 degrees tend to underestimate mass flow rates by 16% to 24%. In this work, the inclination correction factor was determined to be 0.55 for a 30 degree inclination across all tested materials. Furthermore, the loading ratios are found for CCS is 45%, while it is 14% for MgSt and 12% for APAP in this design.
- Regarding the feed factor, minimal changes are observed across various sizes of screw pitch, attributed to the low feed rate (Figure 7-12). In this study, the screw fill is predominantly influenced by the agitator.
- It is observed that the feed factor increases when the agitator speed increase, which emphasises the role of agitator in governing the powder flow rate. Additionally, the feed factor demonstrates an increase corresponding to the decrease in Hausner ratio (Figure 7-23).

In summary, both pneumatic and inclined micro-feeders have the potential to meet industry needs. Additionally, the inclined micro-feeder has the potential to bridge the gap in continuous high-precision feeding of cohesive materials in the low range of few grams per hour in the

pharmaceutical sector as well as in industries as diverse as nutrition, cosmetics, food, and catalyst production, etc.

9.2 Future works

This section will present a range of opportunities for optimising, transforming, and applying the two novel technologies. These opportunities are not limited to the pharmaceutical industry but can also be extended to other fields. Subsequent work will focus on:

- Conduct further research and optimise their technologies (Section 9.2.1).
- Investigate integrating the pneumatic micro-feeder with the inclined micro-feeder to enable continuous feeding functionality. This will be considered an alternative option for industrial applications (Section 9.2.2).
- Incorporate pressure sensors to address pressure drops in pneumatic micro-feeders and convert them into a mass flow sensor (Section 9.2.3).
- Search for a suitable mass flow sensor, such as a capacitance sensor, to replace the current catch balance and develop a gravimetric feeding system that can self-calibrate to enhance accuracy and operational efficiency (Section 9.2.3).
- Convert the inclined and pneumatic micro-feeders into blenders and examine their performance in terms of blend uniformity (Section 9.2.4).

9.2.1 The optimisation of the inclined micro-feeder

Despite demonstrating high levels of consistency, repeatability, and stability in the powder feeding system, there is still room for improvement to enhance its potential for wider industrial applications. The study and optimisation of the next step have been outlined below:

- Evaluate the efficiency of the inclined micro-feeder when handling more challenging materials such as silicon dioxide (SiO_2) and micronised paracetamol (μAPAP).
- Analyse the influence of refilling and determine if the system can effectively minimise disturbances caused by refilling to the extent that algorithmic control is no longer necessary in industrial processes.
- Investigate the ability of the technology to scale and meet varying feeding rate requirements.
- Utilise DEM simulation to optimise the system design and enhance performance.
- Determine the maximum capacity of the current inclined micro-feeder.
- Integrate the newly invented agitator from this study into commercial feeders to improve their powder-feeding efficiency.
- Redesign the system to comply with cGMP standards.
- Examine the effectiveness of the multi-screw agitator (Section 9.2.1.1).

- Investigate the performance of a vertical micro-feeder (Section 9.2.1.2).

9.2.1.1 Multi-screw agitator

The utilisation of the granulation process presents promising benefits in producing agglomerated materials by enhancing particle flow and mitigating segregation issues commonly encountered during blending. A reliable feeder is characterised by its accurate and consistent feeding performance without segregation problems. Such reliability translates to reduced dependence on binding chemicals, minimised waste generation, decreased investment and maintenance costs associated with granulation equipment, and improved efficiency in drug manufacturing through the potential elimination of one or more steps in the process via direct capsulising or tableting methods (Byrn et al., 2015).

Figure 9-1 presents the multi-screw agitator, which consists of a centrally located feeding screw and multiple outer spiral screws. This distinctive design facilitates the powder's more efficient circulation within the hopper, promotes homogenisation of the bulk density, and eradicates common problems such as rat holes, bridging, and segregation often encountered in traditional LIW feeders. The taper angle and pitch of both the central and outer screws are adjustable, providing flexibility to accommodate a broader spectrum of powder properties.

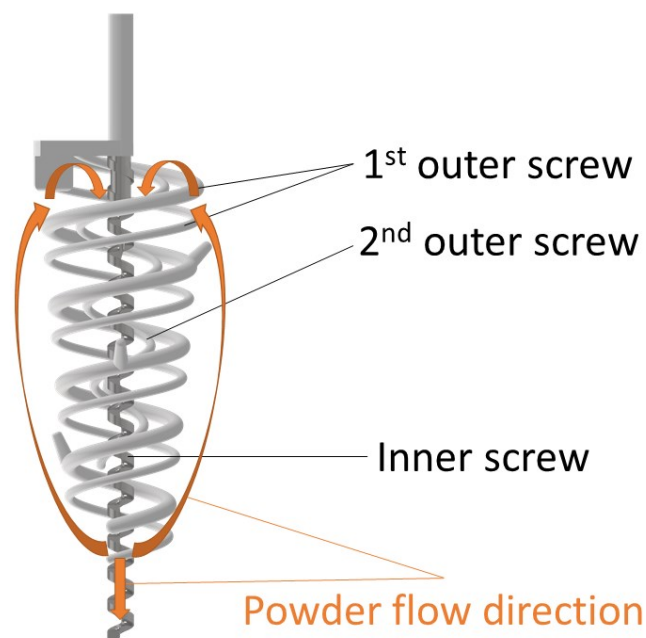


Figure 9-1: The multi-screw agitator to homogenise the powder density to minimise the powder flow rate variation.

9.2.1.2 Vertical micro-feeder

To enhance its versatility and simplify the control mechanism, the inclined micro-feeder can be modified to operate in a vertical orientation (Figure 9-2). Additionally, the design of the inner screw can be customised by replacing it with a compression screw or any other type of screw.

This modification expands the range of powder properties that the micro-feeder system can accommodate. The modification of the micro-feeder to operate in a vertical orientation is particularly useful in applications where space is limited or where the process requires the feeding of powders in a vertical direction. The adaptation of the inner screw also offers advantages by using different types of screws that can cater to the specific properties of the powder being fed. The versatility of the modified micro-feeder system makes it suitable for a wide range of applications, including pharmaceuticals, food processing, and chemical industries. The ability to adapt the system to varying powder properties and process requirements is a significant advantage that enhances its efficiency and effectiveness.

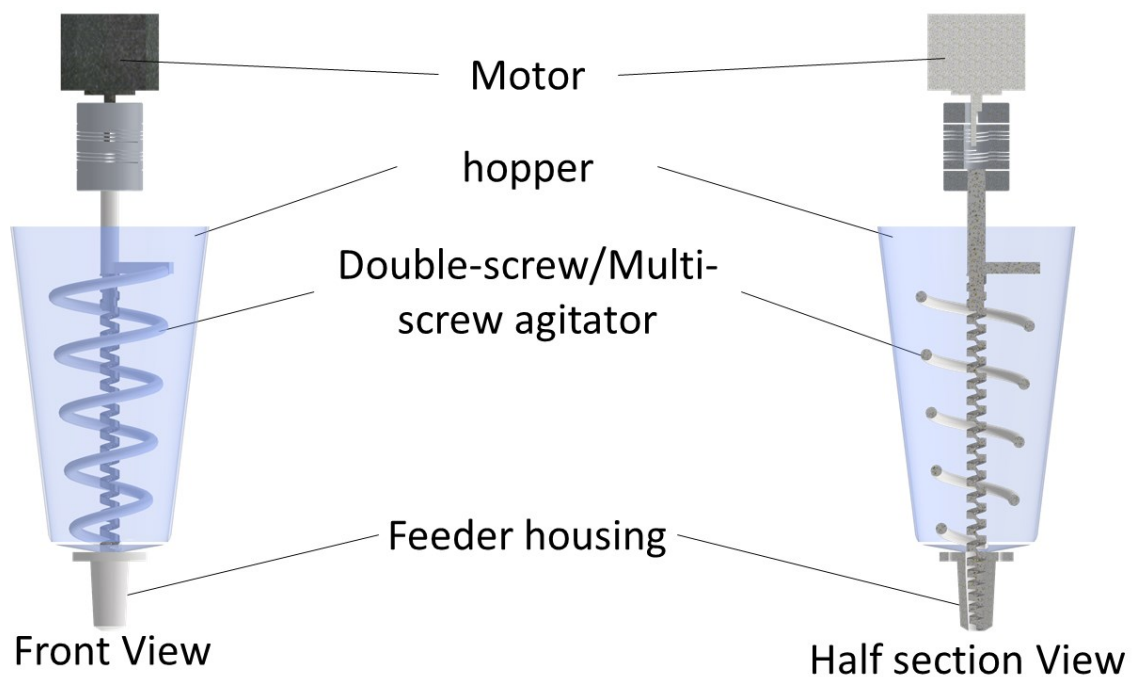


Figure 9-2: The schematic drawing of a vertical micro-feeder.

9.2.2 Integration of pneumatic micro-feeder and inclined micro-feeder feeder

Figure 9-3 depicts the integration of a pneumatic micro-feeder and an inclined micro-feeder. This integration provides benefits such as enabling continuous feeding of the pneumatic micro-feeder and broad applicability in industrial settings, particularly where pressure presence can affect consistent powder feeding into the process. In drug manufacturing, the seeding process necessitates precise and small quantity powder feeding into a vessel that exhibits a vapour appearance. The presence of vapour can create pressure in the vessel, restricting the powder feeding, and it can also cause moisture in the powder by entering the screw, influencing the consistency of powder feeding. This design overcomes this challenge. Furthermore, the modular design removes the separator in this case. The powder-air stream can be directly fed into the vessel or through a dip pipe into the liquid. However, further research is required to validate this concept.

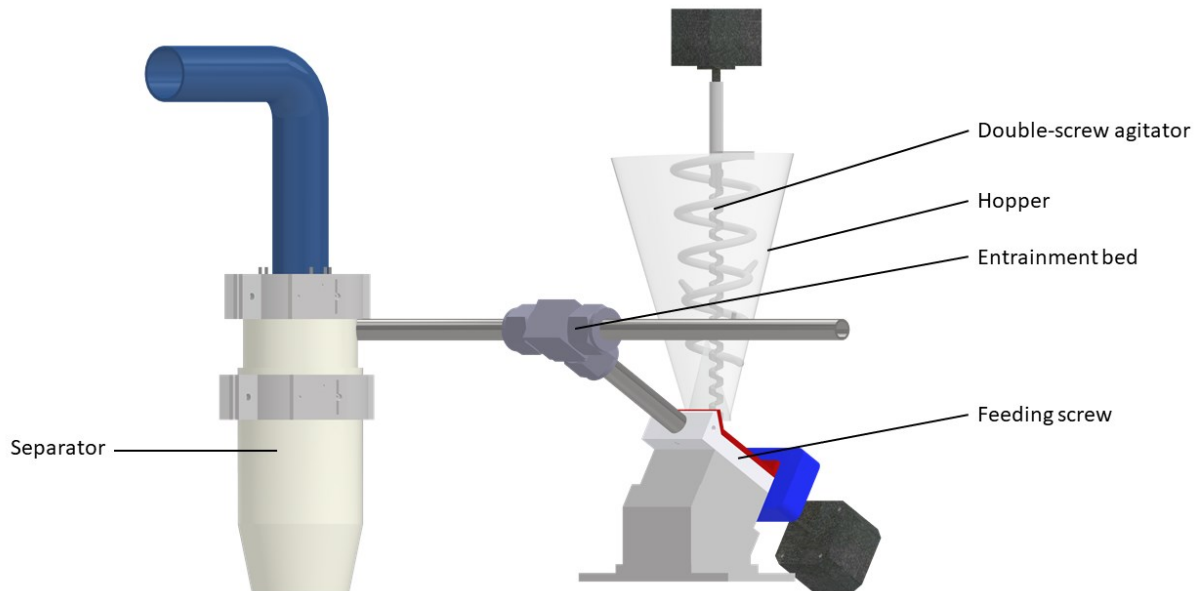


Figure 9-3: A schematic of the integration of the pneumatic micro-feeder with the inclined micro-feeder.

9.2.3 Automation & sensors

To enhance its industrial application and improve feeding accuracy and consistency, a micro-feeding system will be integrated with a feedback control loop. Various mass measurements can be chosen and incorporated into the system, including Gain-In-Weight (GIW) control loop, Loss-In-Weight (LIW) control loop, and a mass flow rate sensor control loop.

9.2.3.1 Gain-In-Weight (GIW) control loop

Figure 9-4 depicts the control loop for both the batch and continuous modes. First, the system will be fitted with two proximity sensors (low and high) in the powder pump to monitor and control the start and stop of the powder pump motor in batch mode (Figure 9-4a). A level transmitter is fitted on the hopper to monitor and control the material level in the hopper for the continuous process (Figure 9-4b). The hopper can be refilled regularly for the continuous process. Due to the advantage of using the double-screw agitator, the refilling does not affect the consistent feeding, compared to current commercial feeders. The weight measurement from the subsequent step will send the reading back to the controller. The reading is converted to a corresponding air flow rate in the controller and compared with the setpoint to regulate the air control valve and adjust the air flow rate.

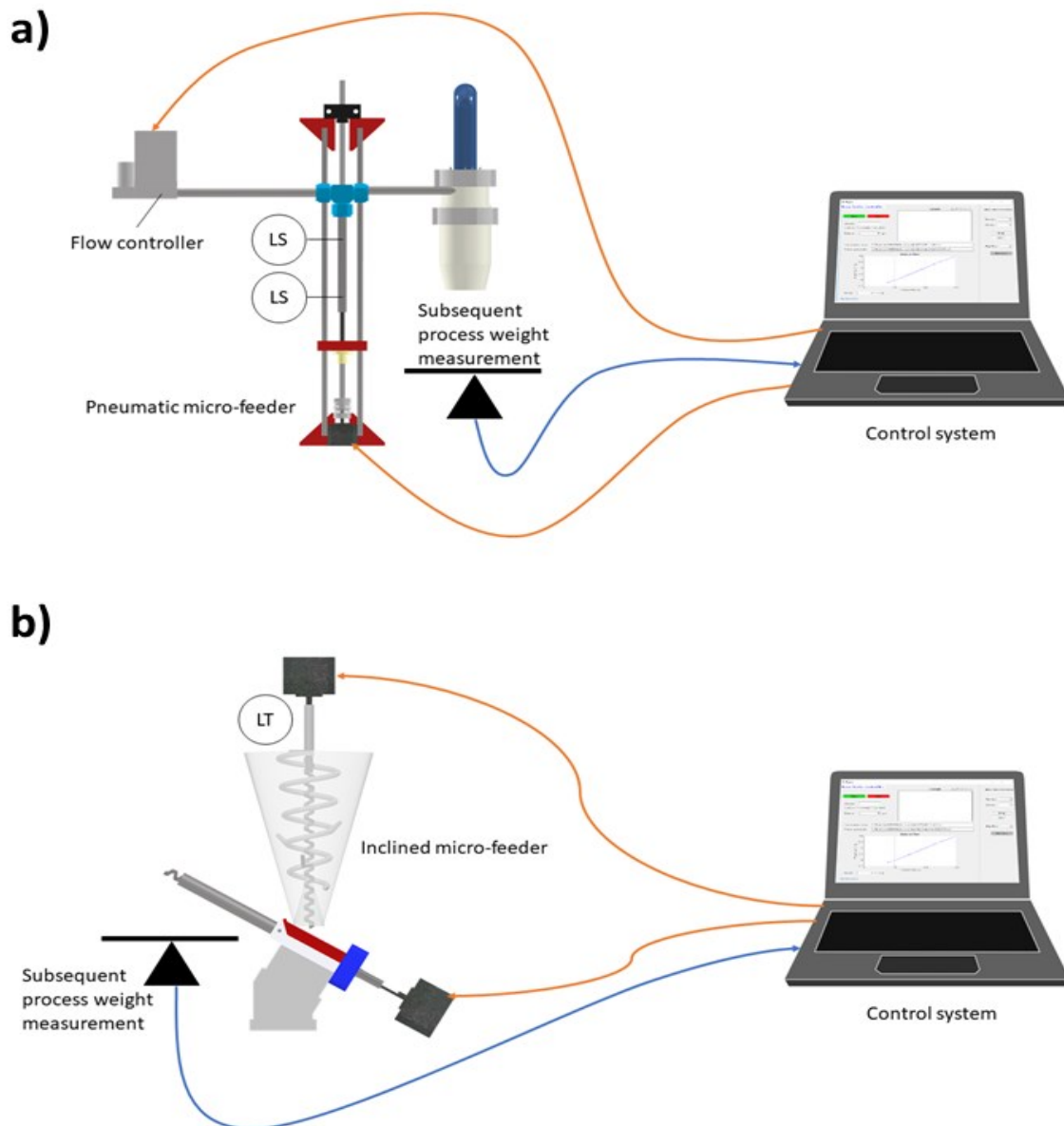


Figure 9-4: GIW control loop using weight scale a) batch process; b) continuous process.

9.2.3.2 Loss-In-Weight (LIW) control loop

The proposed system employs the loss-in-weight (LIW) principle to regulate the feed rate by incorporating load cells into the entire unit. In this control loop, the micro-feeder is placed on load cells (Figure 9-5). These load cells measure the weight loss and transmit this information to the control system. Upon receipt, the control system compares the measurement with a predetermined set-point and determines whether to regulate the speed of both the feeding screw and agitator based on the difference. This approach guarantees precise and efficient regulation of the feed rate, leading to enhanced system performance. Furthermore, due to its dependable and accurate control capabilities, the LIW principle is extensively used in various industries, such as pharmaceuticals, chemicals, and food processing.

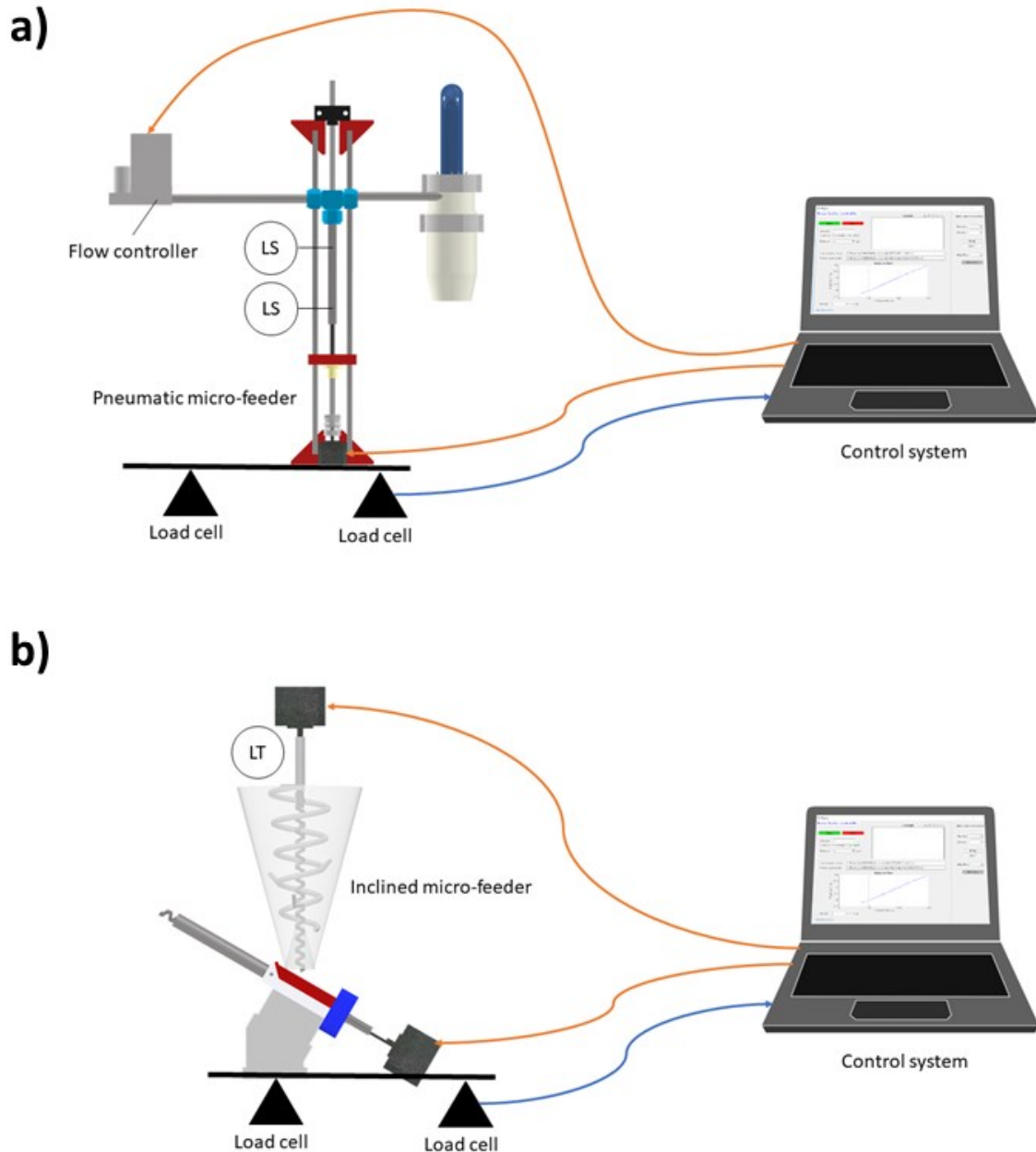


Figure 9-5: LIW feedback loop

9.2.3.3 Mass flow sensor control loop

The present control system deviates from the conventional loss-in-weight (LIW) feedback loop by incorporating a mass flow sensor, such as a capacitance or NIR sensor, to monitor the powder mass flow rate. The mass flow sensor generates a signal proportional to the mass flow rate, which is then transmitted to the control system for further analysis. The control system subsequently compares this signal with a predetermined set-point and adjusts the speed of both the feeding screw and double-screw agitator for inclined micro-feeders based on the difference. In the case of a pneumatic micro-feeder, the system converts the measurement and compares it to the set point to regulate the air flow rate. This approach offers several advantages over the traditional LIW system. By integrating a mass flow sensor,

the system enables continuous and real-time feeding while mitigating the influence of refilling. Figure 9-6 illustrates the control loop utilising a mass flow sensor for both batch and continuous operations.

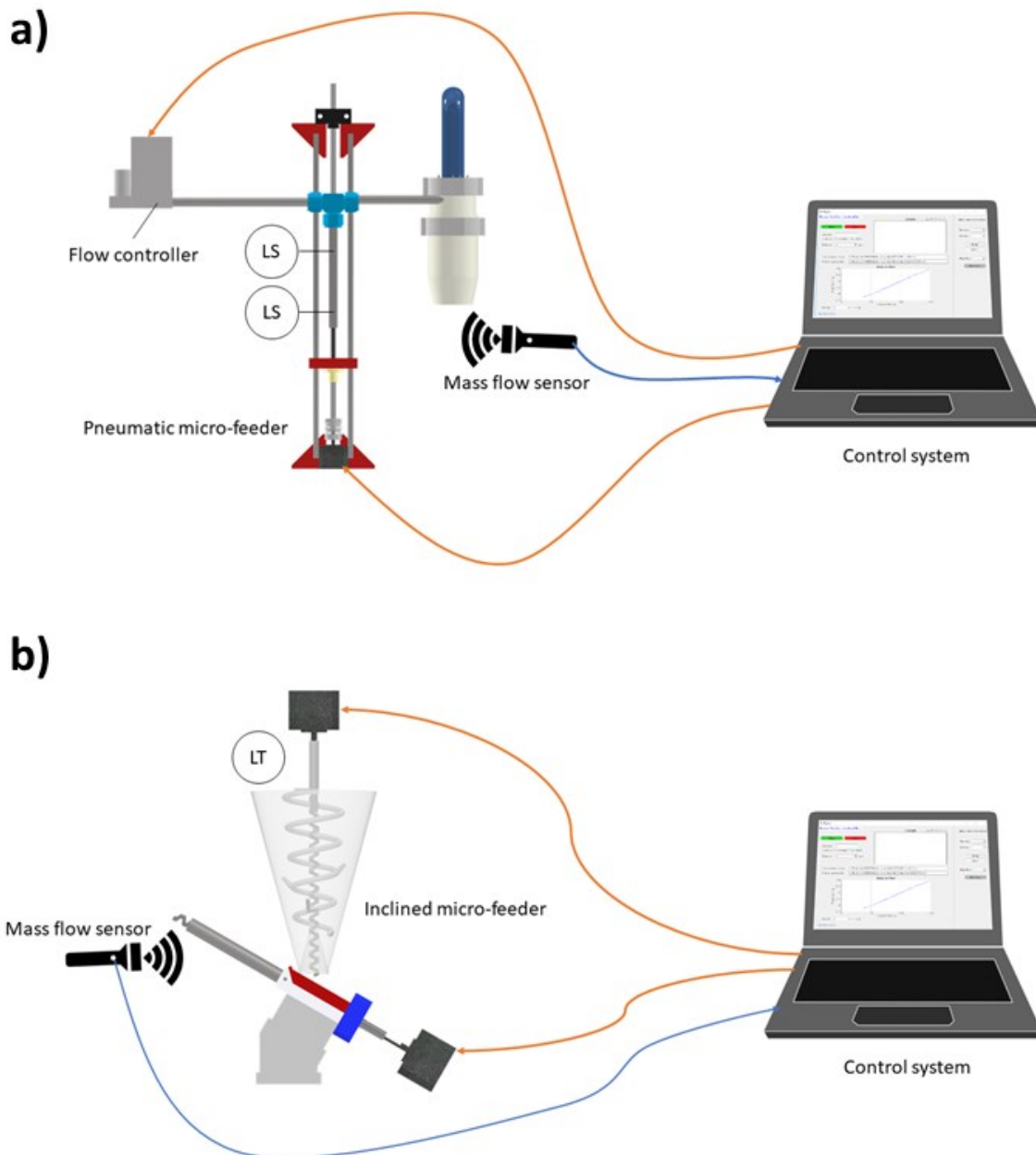


Figure 9-6: The mass flow sensor control loop. a) batch process; b) continuous process.

9.2.3.4 Pressure drop sensor control loop

The pressure drop feedback loop control system only works for the pneumatic micro-feeder and the integration system when the inclined micro-feeder acts as a powder supply unit. Figure 9-7 depicts the differential pressure control loop. This control loop uses three pressure sensors to control the process. The controller relates the three signals from the pressure sensors to a powder flow rate. The controller then compares the powder flow rate to the setpoint. This

powder flow rate variation is then converted to the required air flow rate. The controller compares this required air flow rate to the actual air flow rate. The air control valve then regulates the variation to the required point.

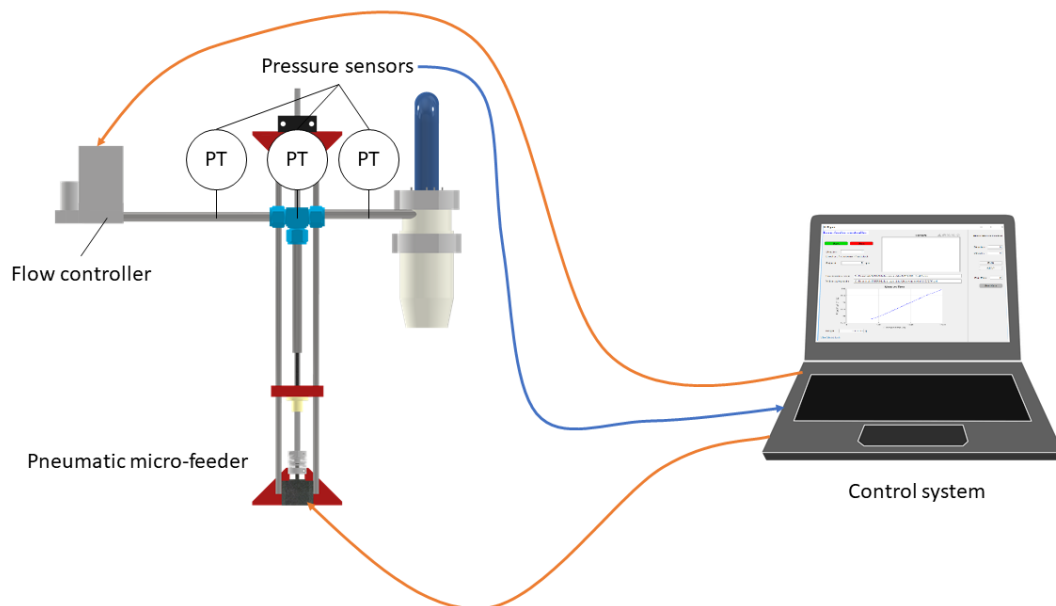


Figure 9-7: Differential pressure sensor control loop for batch (a) and continuous (b) processes, which uses three pressure sensors to regulate the powder flow rate and maintain consistency in feeding.

9.2.4 Blender

It is also found that integrating multiple pneumatic micro-feeders may offer a blending feeder that offers the uniform blending necessary for pharmaceutical manufacturing. This type of blender is particularly critical in drug production. Figure 9-8 provides a conceptual representation of this blending system. However, further studies are necessary to validate the performance and effectiveness of this blending approach.

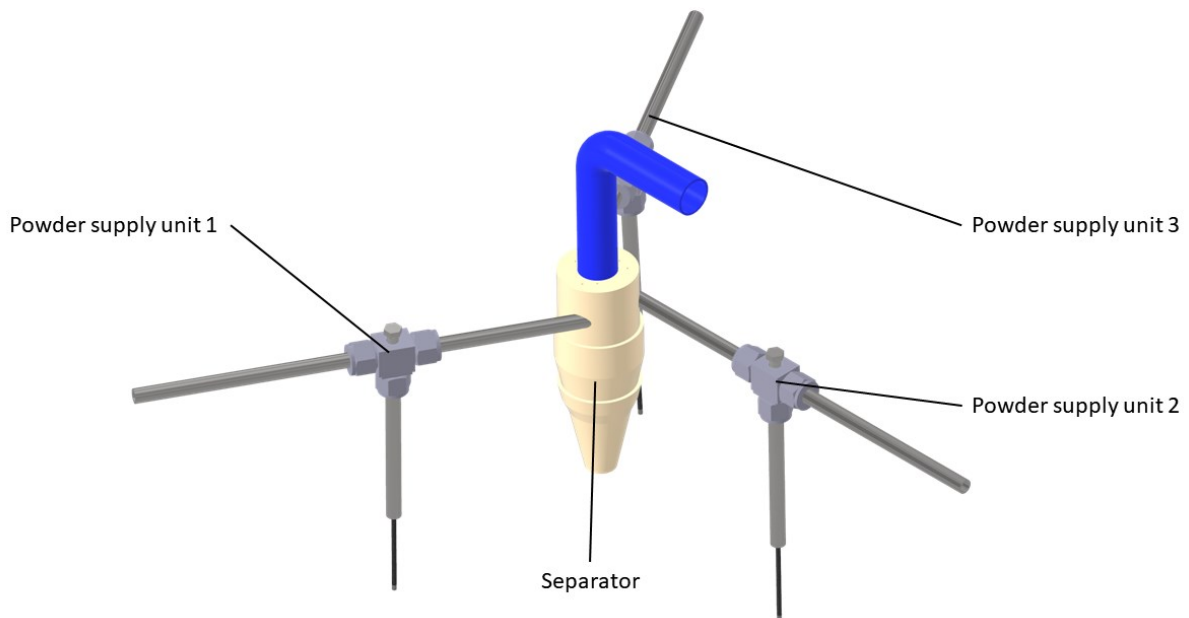


Figure 9-8: Conversion of pneumatic micro-feeders into a blender through integration: A novel approach for uniform blending in pharmaceutical manufacturing.

The inclined micro-feeder, with its unique design and precise feeding capabilities, is suitable for a wide range of industrial applications. One innovative application is the adaptation of this inventive micro-feeder as a blender and feeder, which combines two functions into one system. This is achieved using two or multiple inclined micro-feeders to feed the active pharmaceutical ingredient (API) and excipients to a blending feeder (Figure 9-9).

Combining the inclined micro-feeder and the blending feeder may result in an efficient and uniform blending of powders in the hopper. Furthermore, the blender feeder also serves as a continuous and consistent powder feeder, offering cost-saving and space-saving benefits. The use of a single system for both blending and feeding operations also reduces the need for additional equipment, saving both capital and operational costs.

The flexibility of the micro-feeder system is enhanced by the easy adaptation of the agitator and feeding screw, which enables the system to accommodate a wider range of powder properties. This adaptability is particularly useful in the pharmaceutical and chemical industries, where powders with varying properties are common. The system's ability to blend and feed powders continuously and consistently while accommodating different powders makes it an attractive option for various industrial applications.

In summary, the inclined micro-feeder system can be adapted as a blender and feeder, providing a cost-saving and space-saving solution. The system's ability to blend powders uniformly and feed them continuously and consistently, as well as its flexibility to accommodate different powder properties, make it an innovative and valuable solution for a wide range of industrial applications.

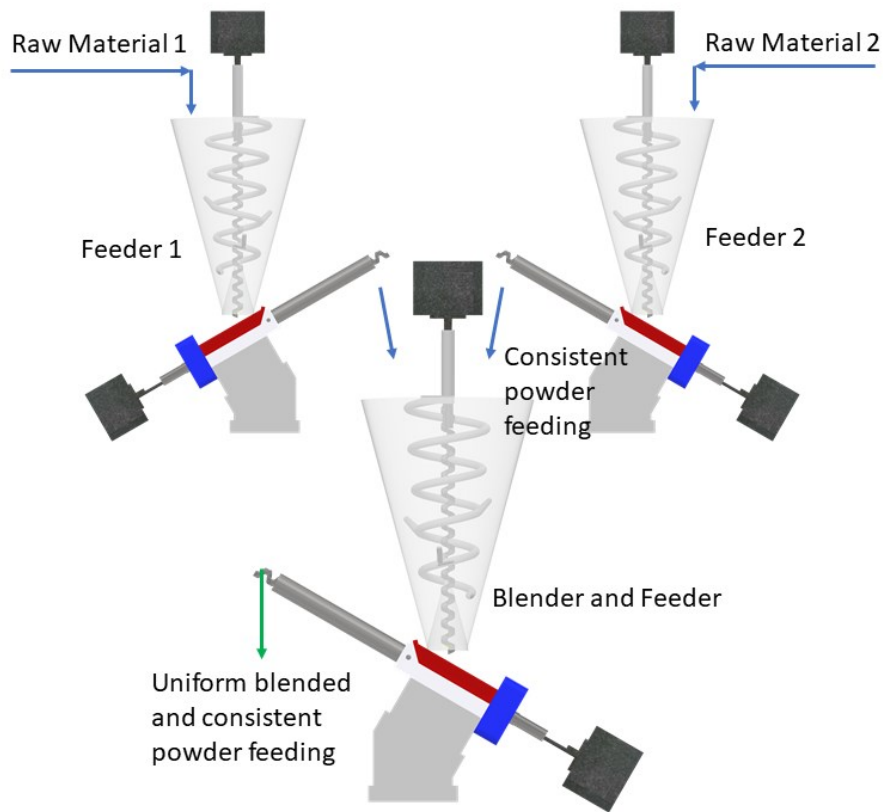


Figure 9-9: Schematic illustration of the inclined micro-feeder used as a blending feeder. This novel 2-in-1 application offers the potential for improved efficiency and reduced equipment costs in various industries, including pharmaceutical and food manufacturing.

Future work could involve the demonstration of these technologies in real-world industrial settings. Additionally, the integration of cGMP standards in the design and fabrication of the system would facilitate its use in the pharmaceutical and food industries by ensuring compliance with regulatory requirements for quality control and assurance. In conclusion, future research could focus on integrating these technologies into existing manufacturing processes to enhance efficiency, accuracy, and safety. The technologies developed in this study have a number of potential futures.

10 Appendix

10.1 Appendix for Chapter 5

10.1.1 Detail design of pneumatic micro-feeder

10.1.1.1 Photograph of the pneumatic micro-feeder

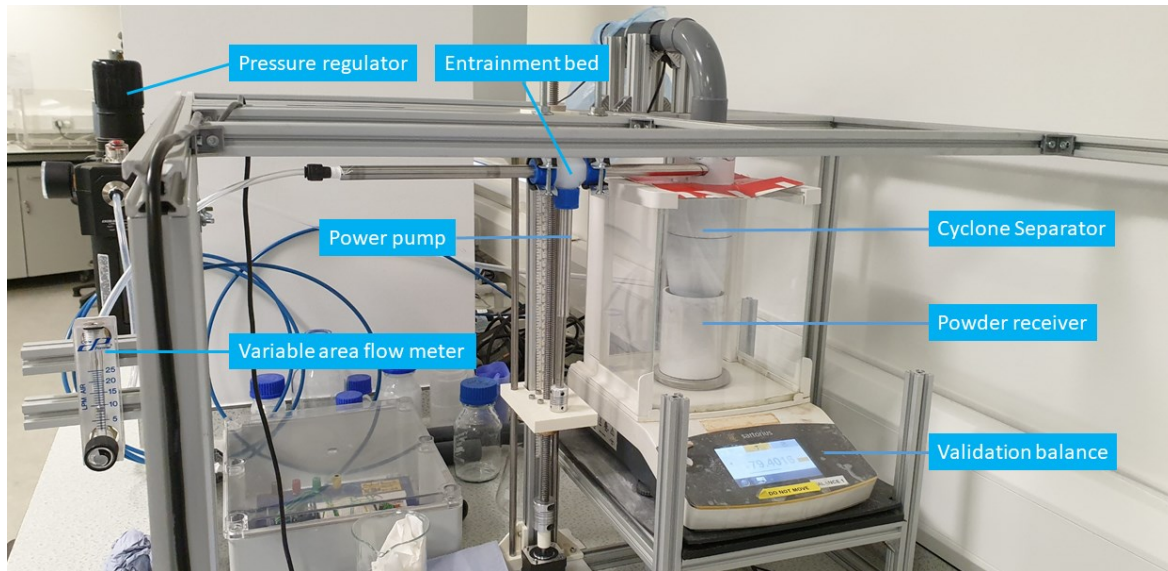


Figure 10-1: Photograph of the pneumatic micro-feeder system with a validation balance.

10.1.1.2 Powder pump and entrainment bed

A ½ inch PFA Swagelok union tee with tube fitting (Part No: PFA-820-3) was selected as the entrainment bed. ½ inch stainless steel tube with an internal diameter of 9.52 mm was selected as an air inlet tube, a process line and a powder pump barrel. The internal surface finish of stainless steel is milling finish. The piston was made from acrylonitrile butadiene styrene (ABS) filament using a CEL Robox 3D printer and assembled with a 150 mm long 8 mm stainless steel rod. Figure 10-2 shows the assembly of the powder pump with the entrainment bed.

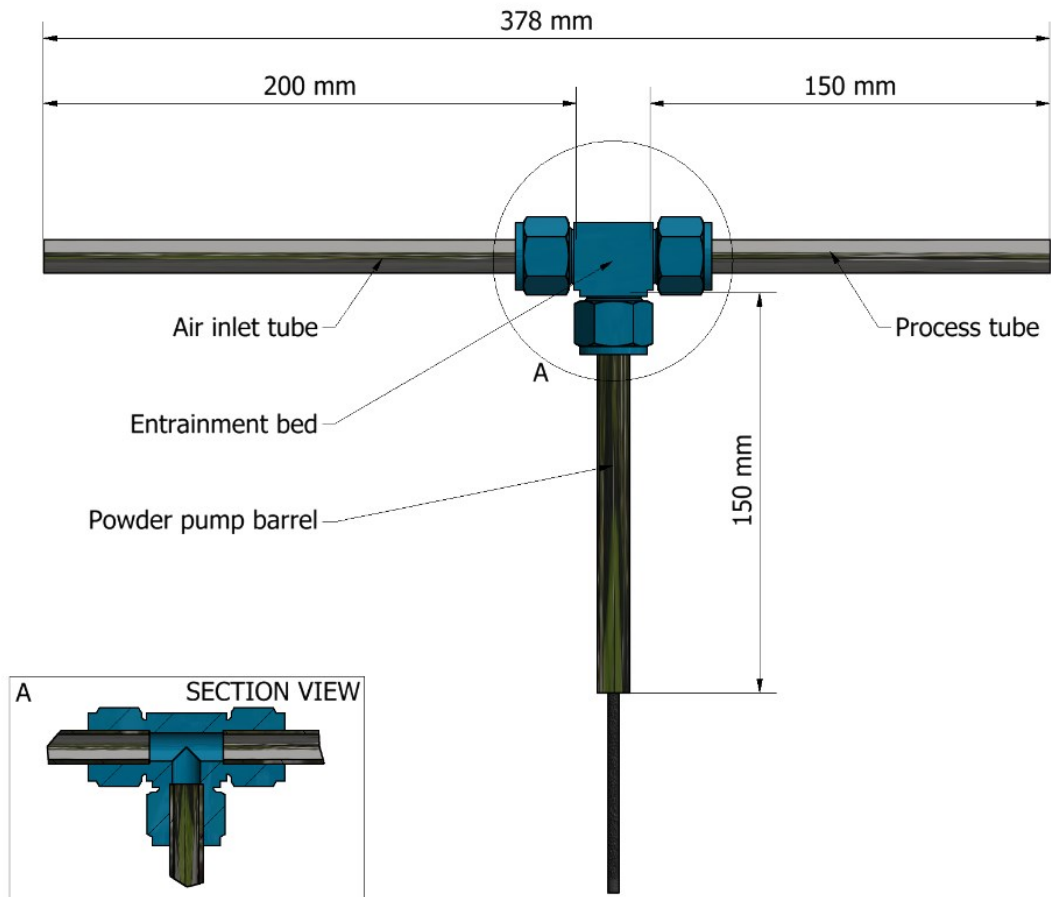


Figure 10-2: Overall dimension of powder pump and entrainment bed.

10.1.1.3 Air supply line

An air supply line is used to provide the air flow to the entrainment bed. Because the powder flow rate is sensitive to the air supply conditions, a pressure regulator fitted with a dehumidifier and a filter (Norgren-E74H-4GK-QD1-NFG-QPB, Norgren), and a variable area flowmeter (WZ-32460-48, Masterflex, Cole-Parmer) are used to stabilise the air flow (Hamor and Smith, 1971). The items are connected using a ½" 316 stainless steel tube and fluoropolymer air hose with tube fittings supplied by Swagelok. The assembly is shown in Figure 10-3. A dehumidifier is used to remove the moisture in the supply air to avoid solid agglomeration. A 40 µm polypropylene filter is used to remove dust from the air supply system. A pressure regulator completed with a gauge will be set at a fixed supply pressure in order to control the air supply volumetric flow rate. A variable area flow transmitter is used to control the air inlet flow rate. The measurement range of this flow meter is 0-5 l/min at 0.3 barg, 25 C.

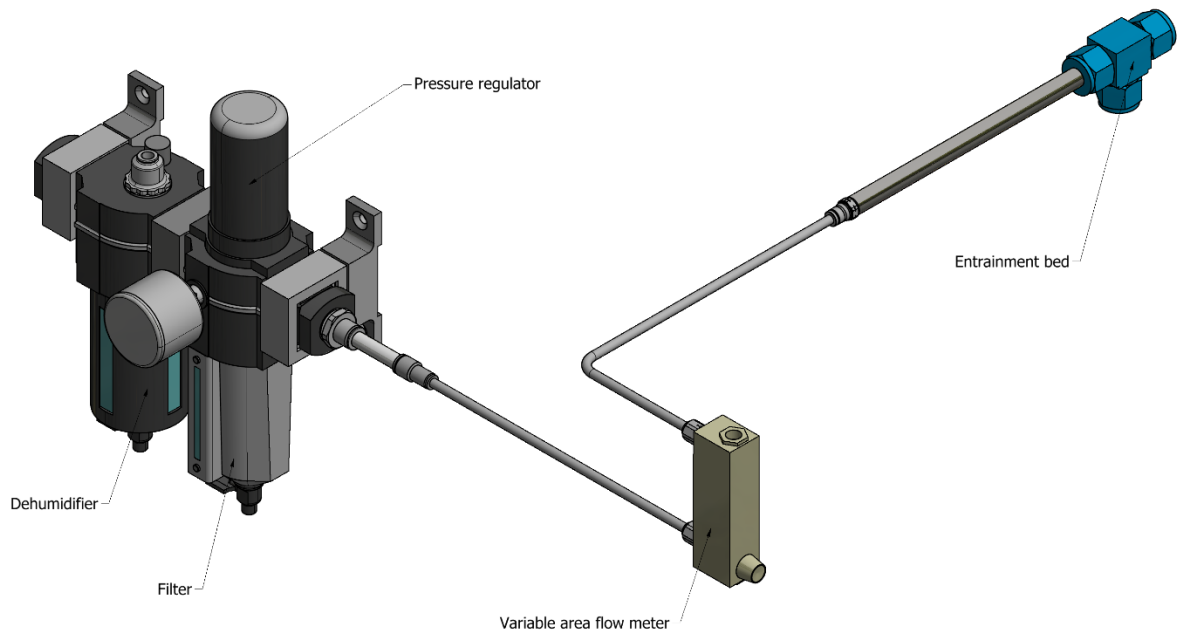
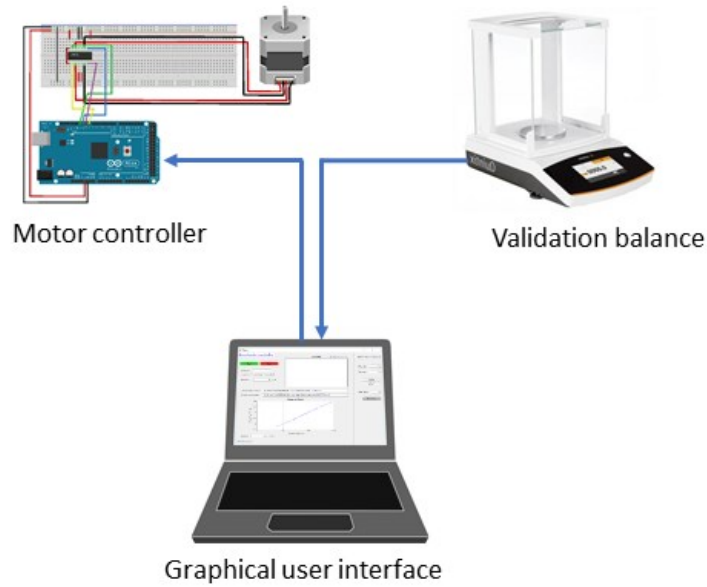


Figure 10-3: Air supply line assembled with a fluidised section.

10.1.1.4 Hardware control unit

In this study, the control unit includes hardware and software. Arduino Mega 2560 microcontroller board is used to control the motor used to motorise the piston. All the communication to the laptop use COM connections via USB cables (Figure 10-4). The control sequences are programmed by using the open-source Arduino software and MATLAB app designer.

a)



b)

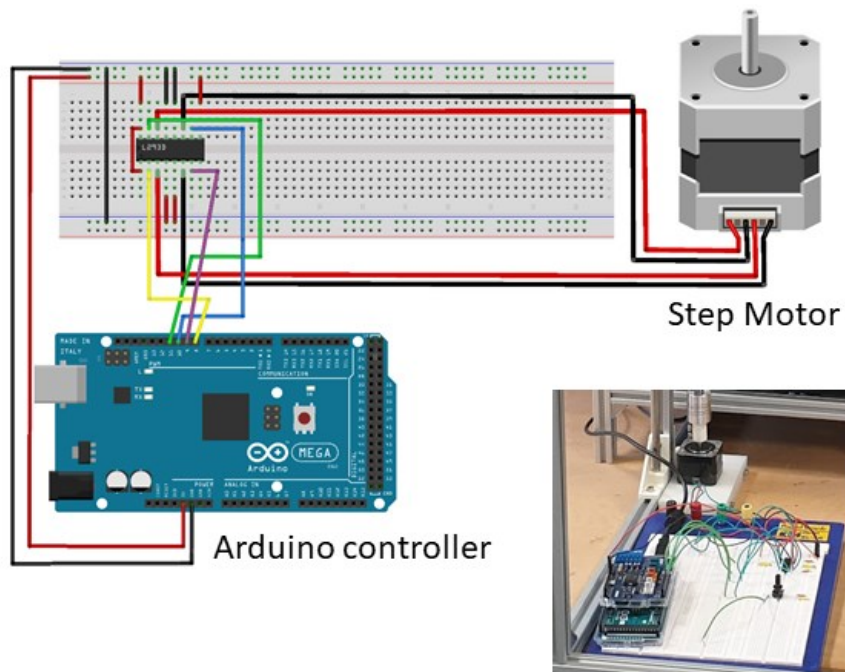


Figure 10-4: (a) the electrical wiring between the stepper motor and the Arduino Mega micro-controller, (b) Network architecture of the pneumatic micro-feeder.

10.1.2 Piston speed calibration

A scale ruler was attached to the structure. The motor speed is set at 1, 5, 10, and 100 rpm for 1 minute, and the displacement height is recorded. Each motor speed is tested in triplicate. The result shows that 1 rpm motor speed is equivalent to 1 mm/min piston speed (Figure 10-5).

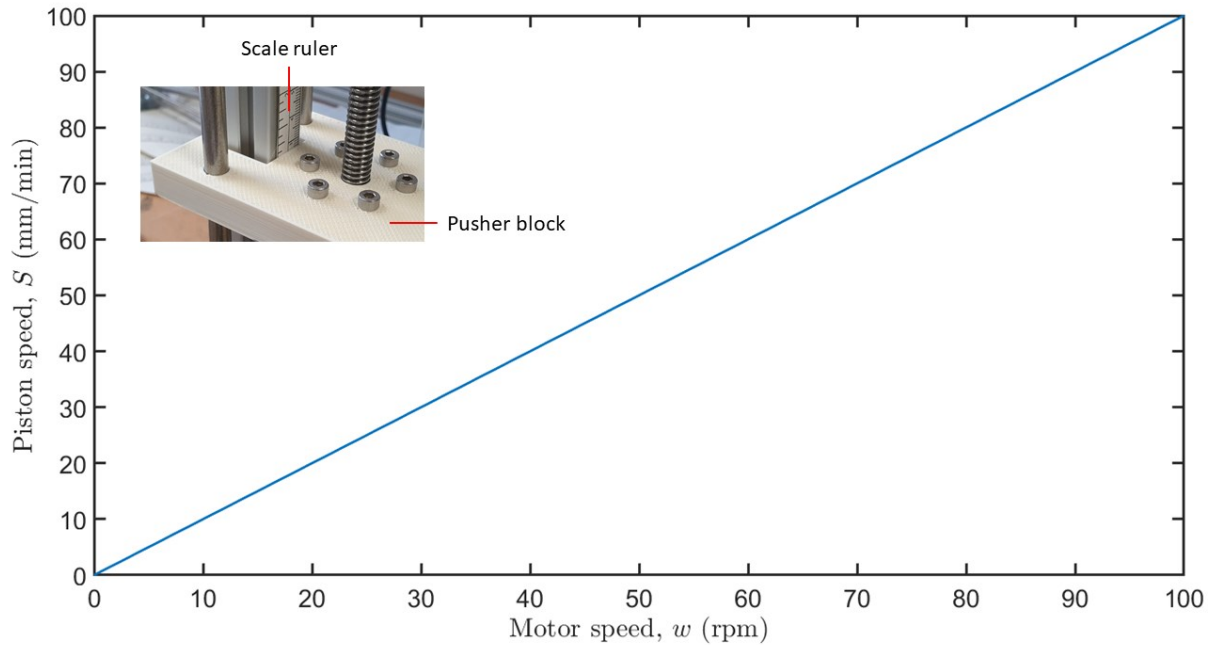


Figure 10-5: The piston speed change over motor speeds with a picture of the pusher block and scale ruler.

10.1.3 Pre-run

Phase I can be reduced significantly by applying a pre-run that moves the piston at a constant high speed until the powder reaches the entrainment bed. The benefit of eliminating phase I is to reduce the overall process time and make the device more efficient for its industrial application. Figure 10-6 reveals the MCC feedings with and without pre-run at the same parameter setpoints (piston speed (S) of 2 mm/min, air pressure (P) of 25 kPa and air flow rate (Q) of 4 l/min). The pre-run, in this case, was operating the piston speed at 88 mm/min for 11 seconds before starting the feeding process. This analysis demonstrates that the piston speed does not influence the compression length for the same material in the same system. The compression length can be calculated by

$$L_C = S \cdot t_{\text{Phase I}}, \quad \text{Equation 10-1}$$

where $t_{\text{Phase I}}$ is the duration of phase I. The compression length was $L_C = 16.4$ mm considering a phase I of about 8.2 min and a 2 mm/min piston speed. Conversely, it can be estimated from this equation that to eliminate phase I of the MCC at a piston speed of 88 mm/min, the timer should be set to 11 – 12 s.

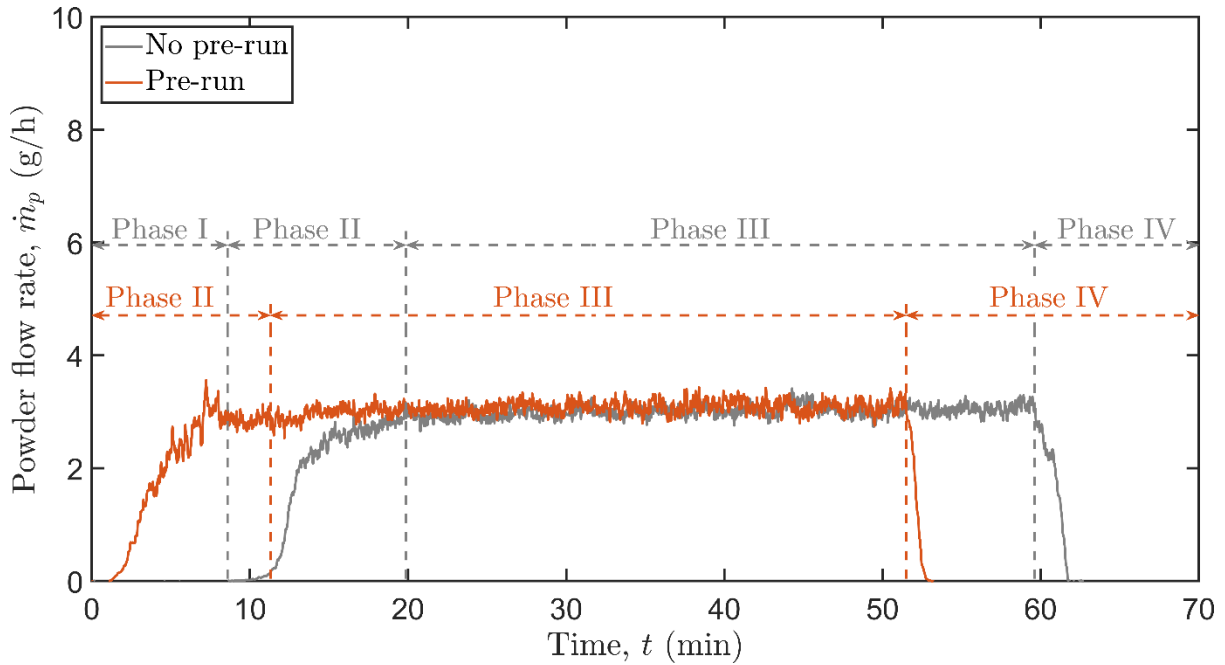


Figure 10-6: MCC powder feeding process at a feed rate of 3 g/h with no pre-run (grey line) compared to the powder feeding with pre-run (red line). Process parameters: piston speed of 2 mm/min; air pressure of 25 kPa; air flow rate of 4 l/min.

10.1.4 Piston speed estimation

In order to predict the piston speed setting, the piston speed (S) and the powder mass flow rate (\dot{m}_p) was estimated following the equation derived below. The powder volumetric (Q_p) flow rate is given as

$$Q_p = \frac{\dot{m}_{p,b}}{\rho_{b,actual}}, \quad \text{Equation 10-2}$$

where $\dot{m}_{p,b}$ is the powder flow rate from the powder pump, and $\rho_{b,actual}$ is the actual bulk density of the powder in the powder pump. The relationship between the piston speed (S) and powder volumetric flow rate ($Q_{p,b}$) is given by

$$S = \frac{Q_{p,b}}{A_b}. \quad \text{Equation 10-3}$$

Combining Equation 10-2 and Equation 10-3 yields

$$\dot{m}_{p,b} = S \rho_{b,actual} A_b, \quad \text{Equation 10-4}$$

where the cross-section area of the powder pump (A_b) is 71.18 mm². After the piston moves upward, the actual bulk density needs to be corrected by the compressibility (C) of the material. The actual bulk density is the bulk density divided by the fraction of actual powder that was compressed in the powder pump:

$$\rho_{b,actual} = \frac{\rho_b}{(1-C)}. \quad \text{Equation 10-5}$$

Substituting Equation 10-5 into Equation 10-4 yields

$$\dot{m}_p = S\rho_b A_b / (1 - C) , \quad \text{Equation 10-6}$$

where ρ_b is the powder bulk density. Equation 5-18 helps estimate the piston speed setting when the desired powder flow rate is known. In this study, the current motor can only set integer values. In future work, a wider range of motor speed settings will provide a more accurate powder flow rate.

10.1.5 Disturbances and limitations

10.1.5.1 Disturbance from compression

The influence of powder compression on the stability of the powder flow rate was studied. The compressed powder was prepared by filling the powder into the powder pump and using the piston to push the powder against a blind on the outlet of the powder pump. It simulates the state of the powder after being compressed. Figure 10-7 shows that the free filling experiment was very stable, whereas the compressed powder experienced severe fluctuations. The fluctuations are attributed to increased cohesion caused by compression. The increase in cohesion raises the demand for entrainment energy. However, the current system is a constant air supply unit, and therefore it cannot provide a sufficiently high entrainment energy (air velocity and air flow rate) to overcome high cohesion. In summary, the stability of the powder flow rate depends on the air entrainment, and compression should be avoided.

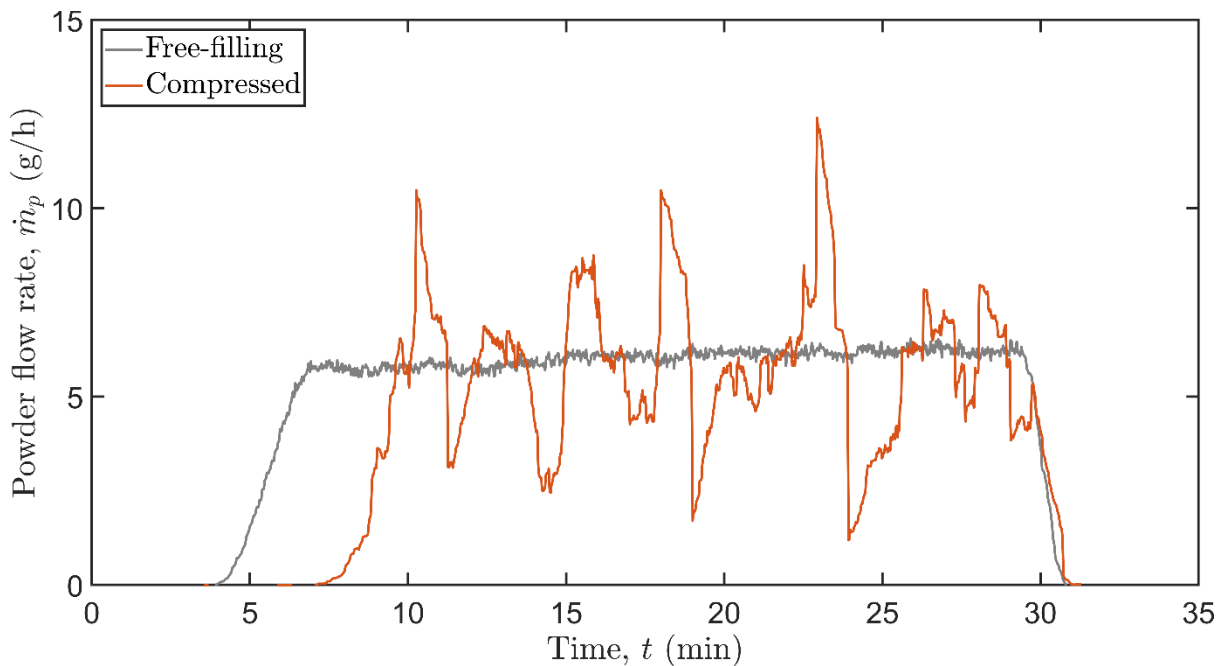


Figure 10-7: Comparison between free-filling experiment and powder compressed experiments for MCC at the same parameter settings.

10.1.5.2 Limitation from the separator

Although cyclone separators can separate various materials, fouling is a problem when dealing with cohesive materials. This study investigated three different separator materials

such as acrylonitrile butadiene styrene (ABS), polylactic acid (PLA), and stainless steel (SS). It is known that a lower friction coefficient and less static electricity can reduce the amount of powder adhering to the separator interior wall. Therefore, 3D printed separators (ABS and PLA) were polished with abrasive, starting with 120-grit and gradually increasing to 3500-grit. Then an anti-static coating (Techspray Licron ESD-Safe aerosol coating) was applied to minimise electrostatics and stabilise the powder flow rate. The stainless steel separator was mechanically polished and left uncoated. However, there was still fouling observed for all separator materials tested (Figure 10-8). Adhesion forces such as static electricity and mechanical locking are still the main causes of fouling.

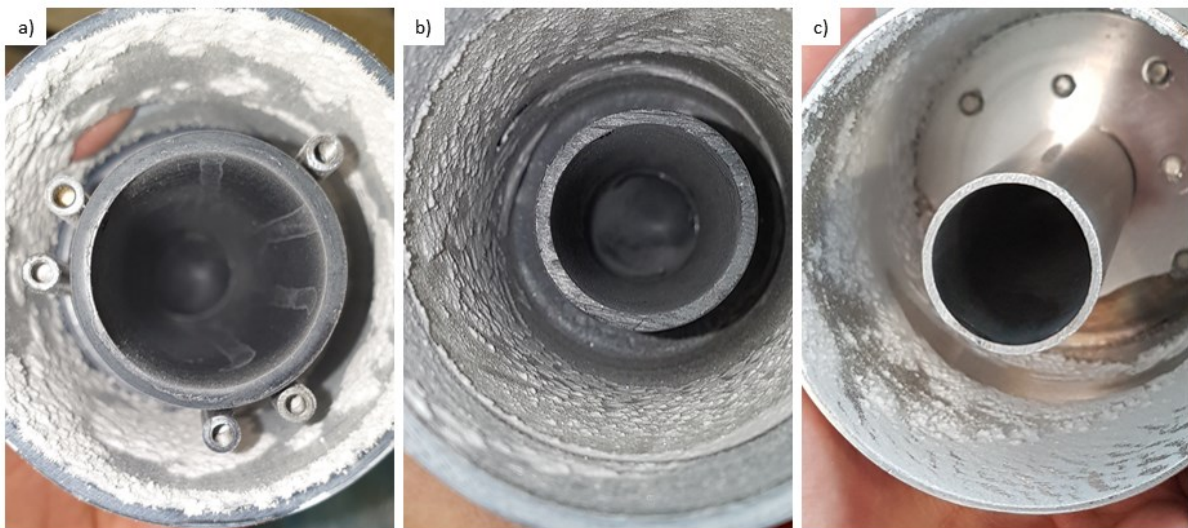


Figure 10-8: The APAP separation in different separator materials: a) acrylonitrile butadiene styrene (ABS); b) polylactic acid (PLA); and c) stainless steel (SS).

Furthermore, it was observed that particles tend to accumulate at the edge of the separator outlet, causing fouling and ultimately affecting the powder flow rate. Therefore, three cone-shaped separators were compared: a cone with a flat edge, a cone with a radiused edge, and a flared cone with a radiused edge (Figure 10-9). Experiments revealed that the flared cone with a radiused edge resulted in considerable stability improvement, followed by the radiused edge cone. Even though the flared cone with a radiused edge reduced fouling and provided good stability, it eliminated the backpressure in the separator and caused poor air/solid separation in the separator, resulting in the escape of small particles from the system.

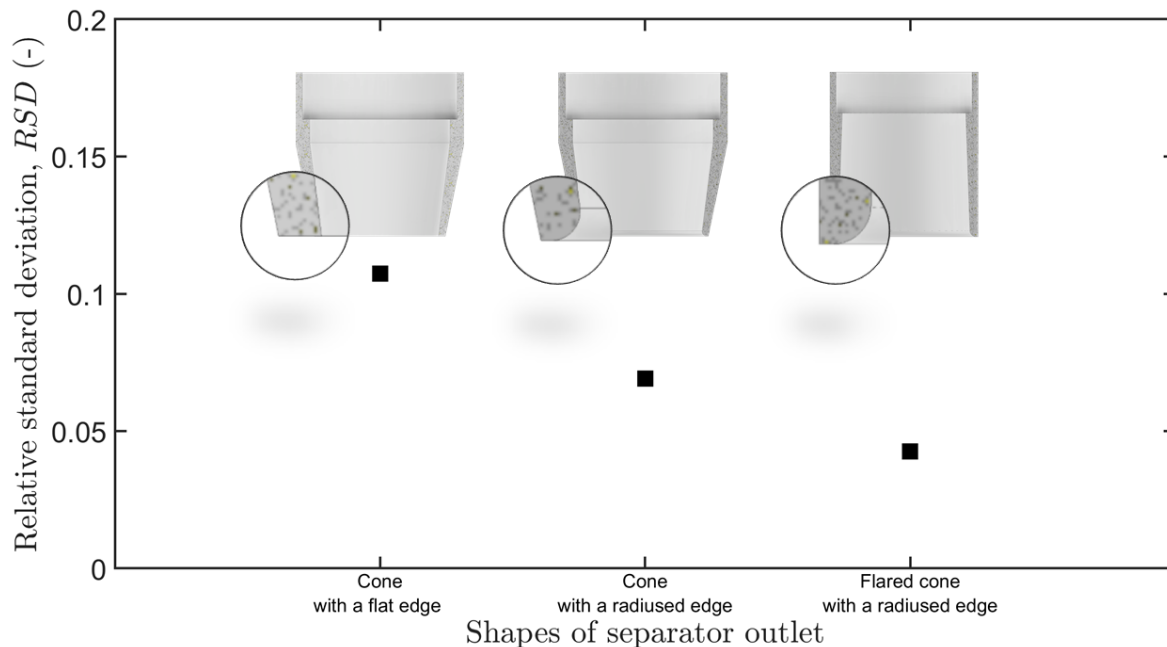


Figure 10-9: The design of the separator cone influences the stability of MCC powder flow rate: a) cone with a flat edge; b) cone with a radiused edge; c) flared cone with a radiused edge.

The use of rods increases the separation efficiency, especially on materials with low adhesion. However, adhesive materials such as APAP tend to clump on the rod (Figure 10-10). Lumps eventually become more pronounced, drop to the validation balance, and lead to remarkably high peaks. It was concluded that the rods should be used with caution for cohesive materials.

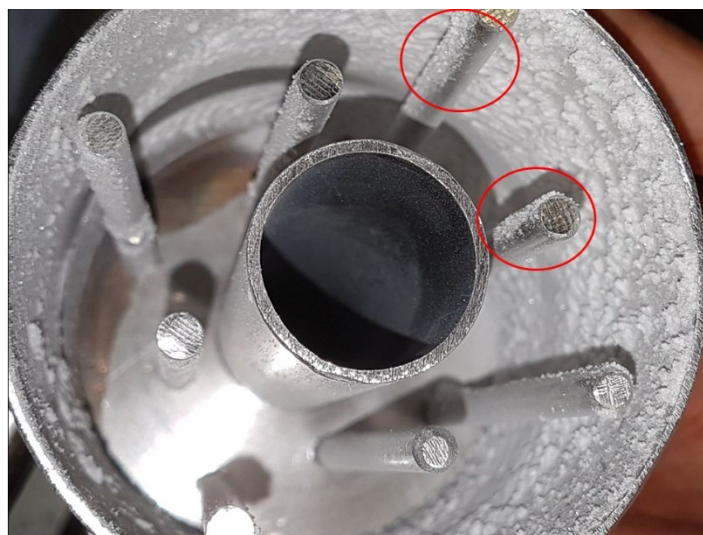


Figure 10-10: APAP adhered on the rods and the stainless steel separator wall.

In addition, the use of vibration motors was assessed to reduce fouling. The results (Figure 10-11) indicated that the use of vibration did not work efficiently, which was primarily attributed to 1) the vibration was not strong enough; 2) the vibration was not efficiently transferred to the separator as the material (plastic) absorbed the vibration.

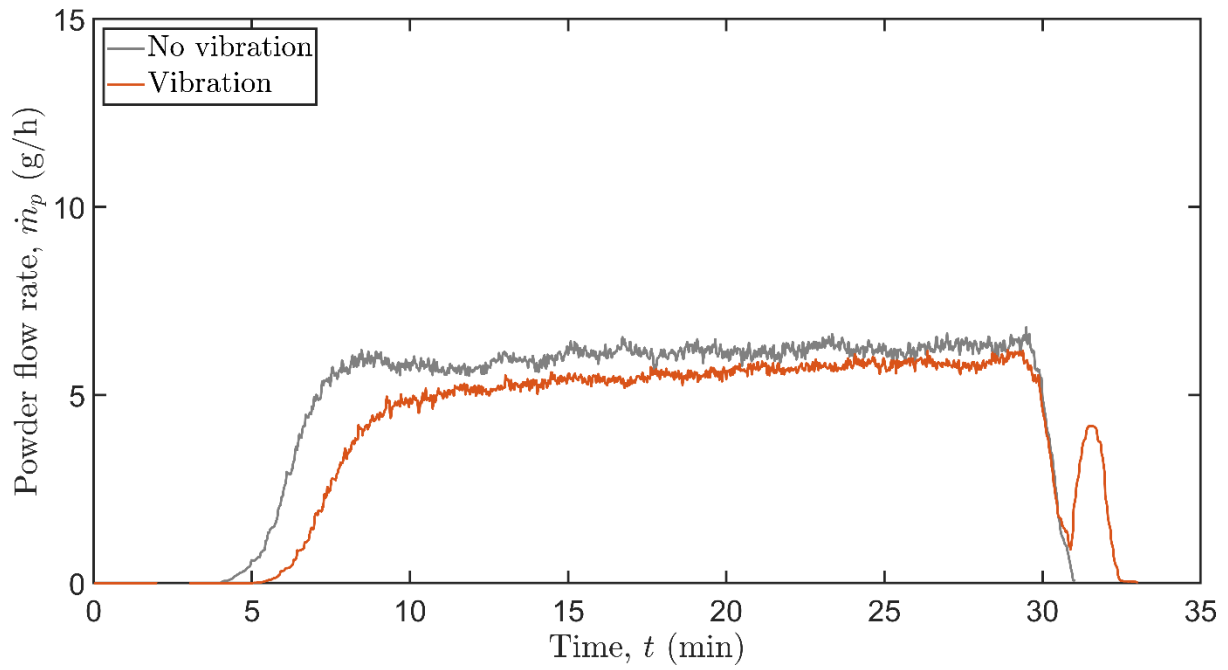


Figure 10-11: Comparison of vibration and no vibration on the separator for MCC feeding at the same parameter settings (4 mm/min of piston speed, 25 kPa of air pressure and 6 l/min of air flow rate).

10.2 Appendix for Chapter 7

10.2.1 Graphic user interface

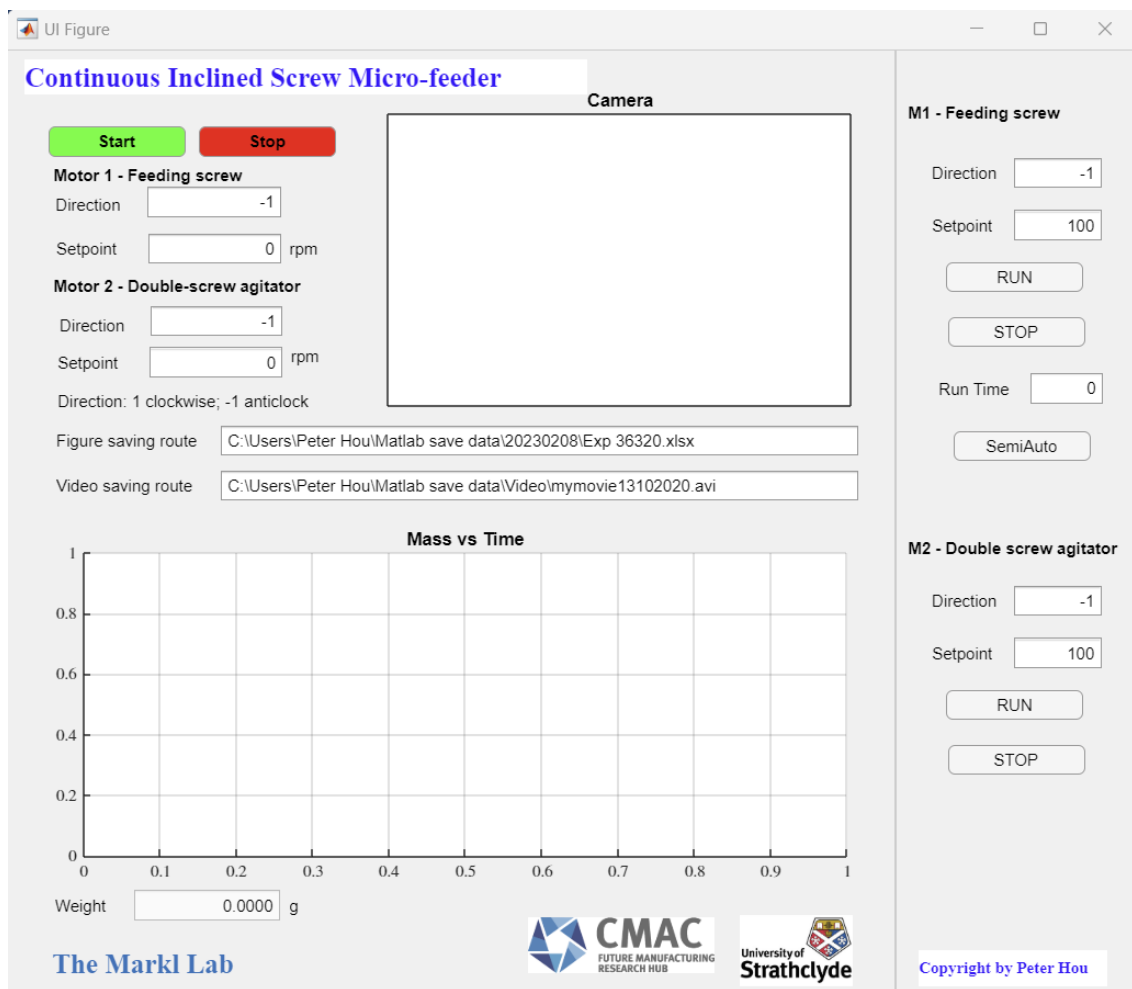


Figure 10-12: The MATLAB Design app GUI was utilised to regulate the motors and record the measurements from the lab-scale balance.

10.2.2 The effect of feed height on measurement noise

Figure 10-13 exhibits the effect of the feed outlet height on the measurement noise of the powder feeding. The results indicate that altering the height from 120 mm to 80 mm has a negligible effect on the standard deviation (SD) and relative standard deviation (RSD). Consequently, it may be inferred that minor modifications in the height setting do not significantly influence the powder feeding performance.

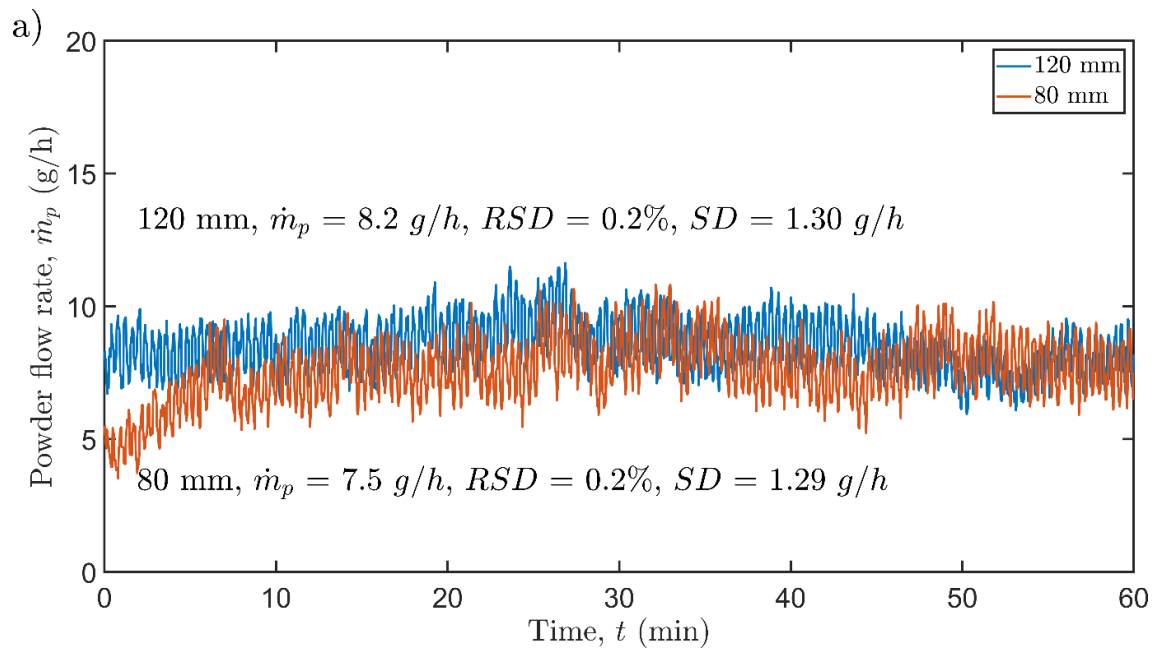


Figure 10-13: A comparison of two different configurations of the equipment, with the feed outlet to the balance pan set at two different heights: 120 mm and 80 mm. The parameters in the experiment were also set at equal speeds (2.5 rpm screw and agitator speeds), and a 10 mm pitch screw was used.

10.2.3 Comparison of moving mean filter and Savitzky-Golay derivative filter

The results demonstrate a high degree of similarity in the powder feeding patterns obtained from the analysis performed using both the moving mean filter and the Savitzky-Golay derivative filter, as depicted in Figure 10-14.

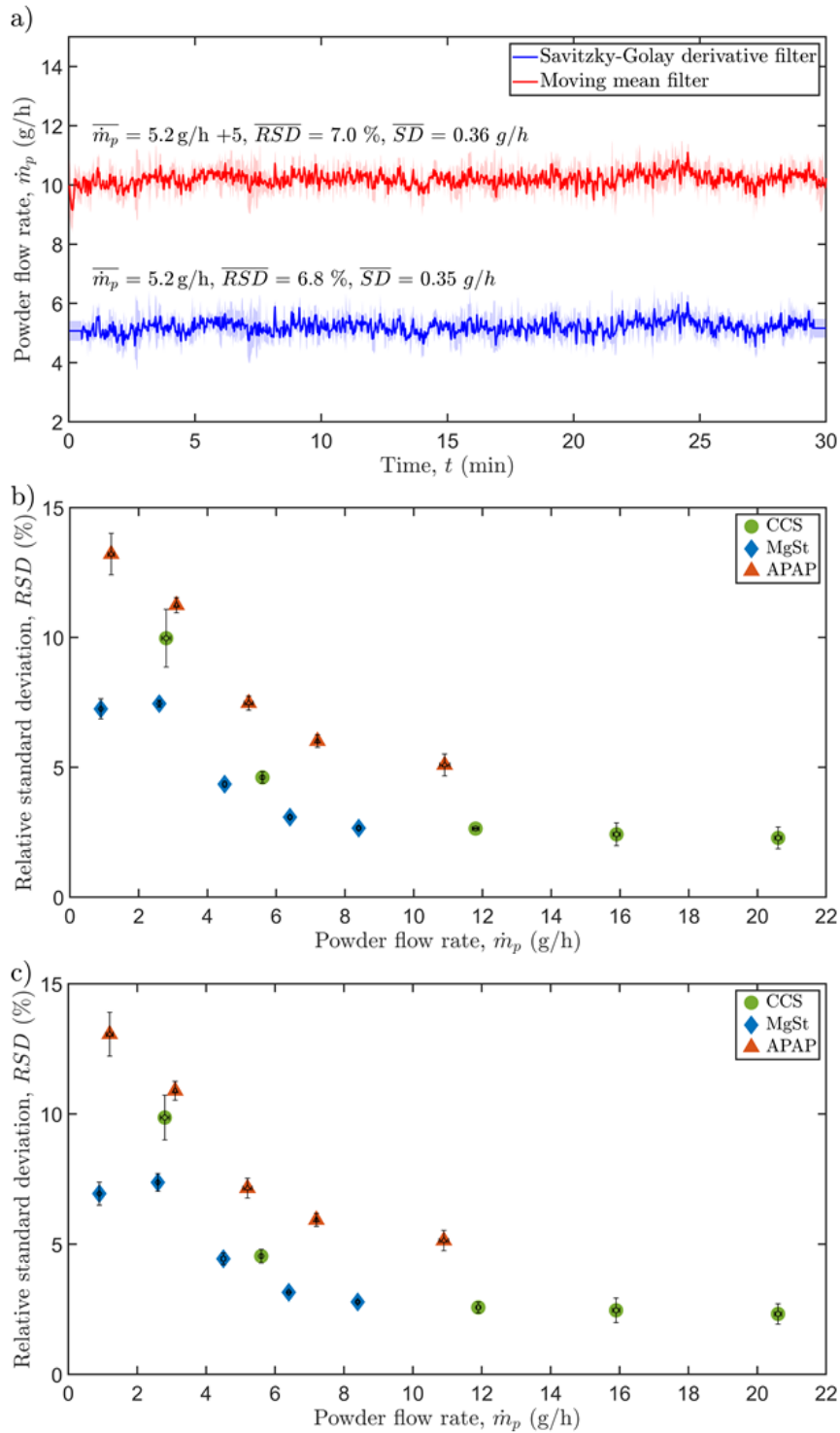


Figure 10-14: Comparison of moving mean filter and Savitzky-Golay derivative filter applications on powder flow rate. a) Analysis of APAP powder feeding using moving mean filter (red) and Savitzky-Golay derivative filter (blue). b) Analysis of data using a moving mean filter. c) Analysis of data using the Savitzky-Golay derivative filter.

10.2.4 Feeder performance summary

Table 10-1: Summary of the CCS feeding performance at two ratios between the screw and agitator speeds: equal and optimal ratios.

Material	Screw speed, ω_s (rpm)	Agitator speed, ω_{ag} (rpm)	Powder flow rate, \dot{m}_p (g/h)	SD (g/h)	RSD (%)	Average powder flow rate (g/h)	Average SD (g/h)	Average RSD (%)	Repeatability (%)	Stability (%)
CCS	5.0	5.0	20.5	0.3847	1.9	20.6	0.4703	2.3	0.49	0.42
			20.6	0.5612	2.7					
			20.7	0.4650	2.2					
	4.0	3.5	15.8	0.3276	2.1	15.9	0.3847	2.4	0.63	0.44
			16.0	0.3641	2.3					
			15.9	0.4625	2.9					
	3.5	3.5	13.7	0.7120	5.2	13.8	0.6860	5.0	0.51	0.21
			13.9	0.6604	4.8					
			13.8	0.6857	5.0					
	3.0	2.5	11.7	0.3082	2.6	11.8	0.3113	2.6	0.82	0.02
			11.9	0.3163	2.7					
			11.8	0.3095	2.6					
	2.5	2.5	9.7	0.5999	6.2	9.8	0.5983	6.1	1.52	0.13
			9.8	0.6011	6.1					
			10.0	0.5940	6.0					
	2.0	1.5	5.6	0.2691	4.8	5.6	0.2578	4.6	0.21	0.22
			5.6	0.2595	4.6					
			5.6	0.2448	4.4					
	1.5	1.5	5.5	0.6069	10.9	5.6	0.6007	10.8	0.61	0.23
			5.6	0.6080	10.8					
			5.6	0.5872	10.5					
	1.0	0.5	2.9	0.2628	9.0	2.8	0.2778	10.0	4.64	1.11
			2.8	0.2733	9.7					
			2.7	0.2973	11.2					
0.5	0.5	2.0	0.6928	35.0	2.0	0.6745	34.6	2.09	0.66	
		1.9	0.6661	35.0						
		2.0	0.6646	33.8						

Table 10-2: Summary of the MgSt feeding performance at two ratios between the screw and agitator speeds: equal and optimal ratios.

Material	Screw speed, ω_s (rpm)	Agitator speed, ω_{ag} (rpm)	Powder flow rate, \dot{m}_p (g/h)	SD (g/h)	RSD (%)	Average powder flow rate (g/h)	Average SD (g/h)	Average RSD (%)	Repeatability (%)	Stability (%)
MgSt	5.0	5.0	8.4	0.2238	2.7	8.4	0.2227	2.7	0.42	0.07
			8.4	0.2166	2.6					
			8.3	0.2278	2.7					
	6.0	3.5	6.4	0.1965	3.1	6.4	0.1960	3.1	0.63	0.06
			6.4	0.2007	3.1					
			6.3	0.1909	3.0					
	3.5	3.5	6.0	0.3981	6.6	6.0	0.3766	6.2	0.35	0.31
			6.1	0.3703	6.1					
			6.0	0.3615	6.0					
	5.0	2.5	4.5	0.1928	4.3	4.5	0.1964	4.3	0.85	0.10
			4.5	0.2027	4.5					
			4.5	0.1936	4.3					
	2.5	2.5	3.9	0.3928	10.0	4.0	0.3953	9.8	2.10	0.16
			4.1	0.3939	9.7					
			4.1	0.3991	9.8					
	2.0	1.5	2.6	0.1989	7.6	2.6	0.1952	7.5	0.34	0.13
			2.6	0.1956	7.4					
			2.6	0.1911	7.3					
	1.5	1.5	2.5	0.3737	14.8	2.5	0.3682	14.7	0.67	0.26
			2.5	0.3590	14.4					
			2.5	0.3717	14.8					
	1.5*	0.5	1.0	0.0661	6.9	0.9	0.0684	7.3	1.94	0.39
			0.9	0.0719	7.6					
			0.9	0.0674	7.3					
0.5*	0.5	0.8	0.0959	12.2	0.8	0.0958	11.8	2.62	0.32	
		0.8	0.0957	11.7						
		0.8	0.0959	11.6						

Table 10-3: Summary of the APAP feeding performance at two ratios between the screw and agitator speeds: equal and optimal ratios.

Material	Screw speed, ω_s (rpm)	Agitator speed, ω_{ag} (rpm)	Powder flow rate, \dot{m}_p (g/h)	SD (g/h)	RSD (%)	Average powder flow rate (g/h)	Average SD (g/h)	Average RSD (%)	Repeatability (%)	Stability (%)
APAP	5.0	5.0	10.9	0.5870	5.4	10.9	0.5537	5.1	1.36	3.91
			11.1	0.5106	4.6					
			10.8	0.5636	5.2					
	4.0	3.5	7.2	0.4409	6.2	7.2	0.4312	6.0	0.23	1.63
			7.2	0.4124	5.7					
			7.2	0.4403	6.1					
	3.5	3.5	7.3	0.6396	8.8	7.2	0.6223	8.6	0.87	1.80
			7.2	0.6236	8.7					
			7.3	0.6038	8.3					
	3.0	2.5	5.1	0.3633	7.2	5.2	0.3880	7.5	2.49	2.27
			5.3	0.4080	7.6					
			5.2	0.3926	7.6					
	2.5	2.5	5.3	0.6289	11.9	5.3	0.6400	12.1	1.44	1.18
			5.4	0.6387	11.9					
			5.2	0.6525	12.5					
	2.0	1.5	3.1	0.3508	11.5	3.1	0.3474	11.2	1.18	0.53
			3.1	0.3413	10.9					
			3.1	0.3502	11.3					
	1.5	1.5	3.1	0.6335	20.3	3.0	0.6129	20.5	3.97	1.79
			3.0	0.6035	20.4					
			2.9	0.6017	20.8					
1.0*	0.5	1.3	0.1571	12.3	1.2	0.1553	13.2	7.63	0.28	
		1.2	0.1568	13.5						
		1.1	0.1521	13.9						
0.5*	0.5	0.7	0.1756	26.4	0.8	0.1802	24.2	11.54	1.23	
		0.8	0.1942	25.7						
		0.8	0.1710	20.4						

10.2.5 The effect of different speed ratios between the agitator and feeding screw

According to the findings presented in Figure 10-15, an evaluation was conducted to investigate the repeatability of cohesive, very cohesive, and non-flowing materials in relation to their respective powder flow rates, whilst comparing the equal and optimal ratios. The results reveal that repeatability exhibits a stochastic nature, irrespective of the equal or optimal ratio employed, when observed across similar materials. Additionally, the study observed that the repeatability has a significant improvement when the powder flow rate is above 5 g/h for both the equal and optimal ratios for all tested materials.

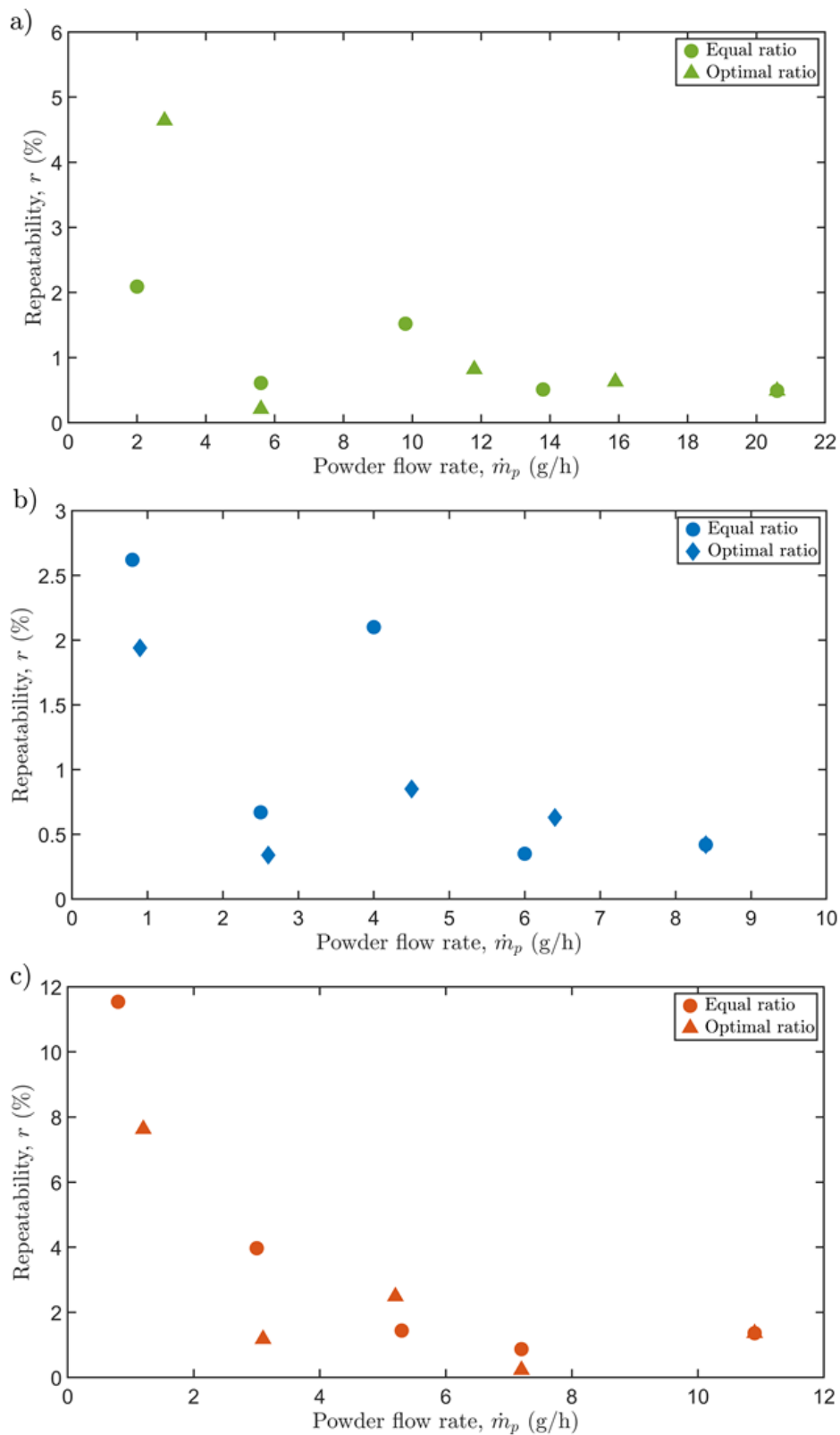


Figure 10-15: Comparison of repeatability for the equal and optimal ratios between screw speed and agitator speed as a function of powder flow rate for three different materials - a) CCS, b) MgSt, and c) APAP.

In Figure 10-16, the stability of cohesive, very cohesive, and non-flowing materials was examined in relation to the powder flow rate, whilst comparing the equal and optimal ratios.

The results reveal that the stability exhibits a random nature when observed across similar materials.

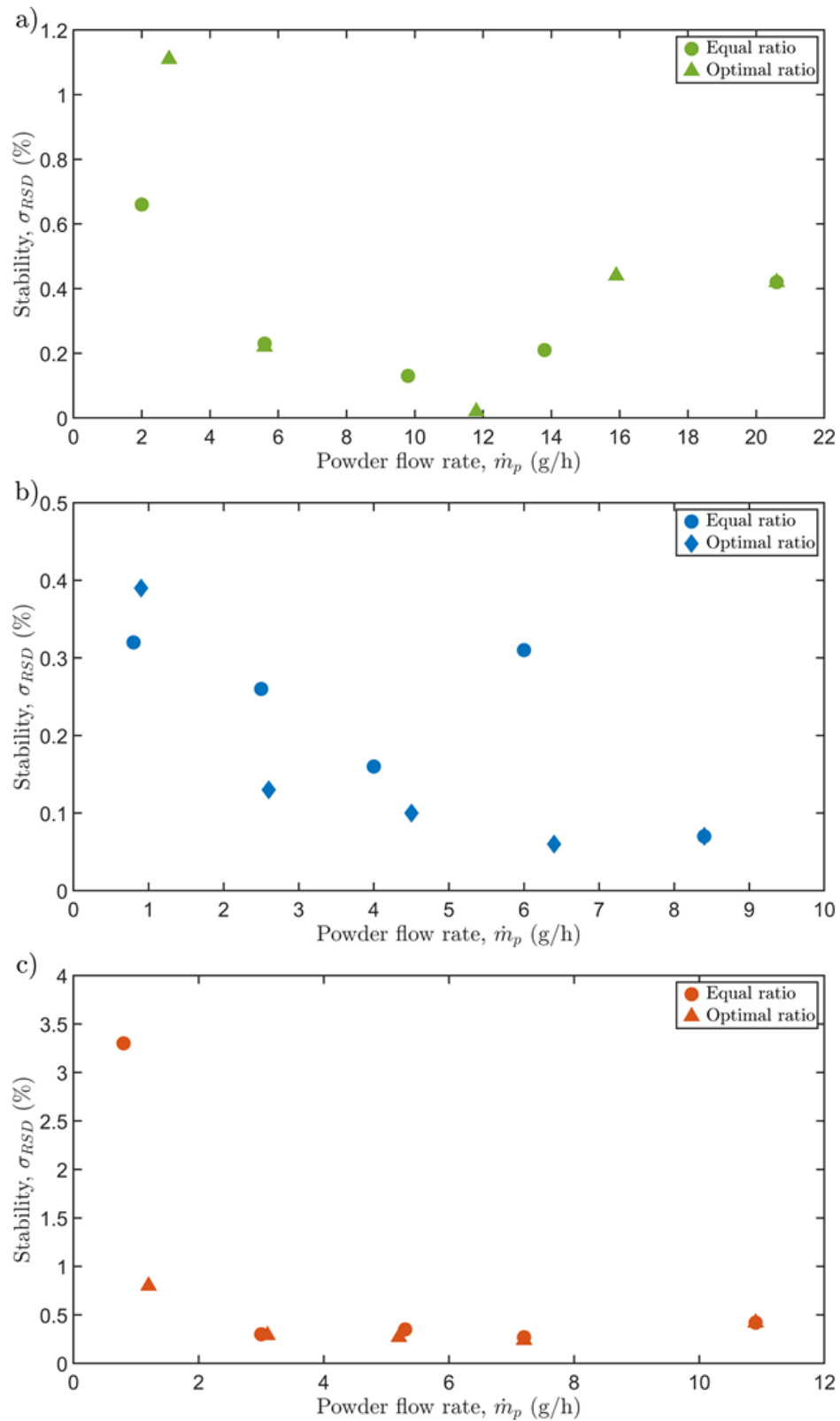


Figure 10-16: Comparison of stability as a function of powder flow rate for three different materials - a) CCS, b) MgSt, and c) APAP, while comparing the equal and optimal ratios.

10.3 Additional tasks and engagements during PhD period

Volunteering

- 1 NPL PGI communication ambassador, 2019 - 2021
- 2 Co-organiser of NPL PGI 2020 Conference, 2020
- 3 Chair of 2021 NPL PGI conference career section, 2020
- 4 Co-editor of PGI Gradpost, published two seasonal magazines, 2019 – 2021
- 5 CMAC Exploration - 3D Printing Medicines, 2022

Case Study

- 1 NPL 2021 annual report - Case study, Title: Developing a small and miniature feeder for pharmaceuticals, 2021.
- 2 Technology was listed in IN-PART: https://strath.portals.in-part.com/P8n78OnM0vV2?utm_source=technologies&utm_medium=portal&utm_term=search&utm_content=%7B%22opportunity%22%3A%5B%22%22%2C%22%22%2C%22%22%5D%7D
- 3 CMAC Meet the Team, 2023, <https://cmac.ac.uk/news-database/meet-our-team-peter-hou>

Other projects involved

- 1 DM² – To develop a powder transportation unit which is used to contain the powder for analysis and compression, suitable for a robot arm
- 2 Tablet dissolution – Developing a tablet holder to hold a tablet on the bottom of a dissolution vessel under agitation conditions.
- 3 Tablet moisture monitoring– Developing a control system with a GUI to long-term monitor and record the moisture loss from a tablet. Help to understand the analysed data and provide the idea of experimental design to understand the moisture loss mechanism from a tablet.
- 4 3D printing medicine – assist colleague to optimise a commercial 3D printer to 3D print medicine.
- 5 Converge KickStart – Business Case: Smart Feeding (August 2023).

11 References

- 3P Innovation, 2022. VF1, Vibratory Feeder [WWW Document]. <https://www.3pinnovation.com/pharma-equipment/discover-range/vibratory-feeder>.
- Abbas, F., Yan, Y., Wang, L., 2020. Mass flow measurement of pneumatically conveyed solids through multi-modal sensing and machine learning. I2MTC 2020 - Int. Instrum. Meas. Technol. Conf. Proc. 1–6. <https://doi.org/10.1109/I2MTC43012.2020.9128576>
- Abrar, U., Shi, L., Raza Jaffri, N., Kang, Y., Nawaz, M., Huixian, Z., 2020. Estimate Mass Flow Rate of Dense Phased Powder Solids. E3S Web Conf. 191, 04005. <https://doi.org/10.1051/e3sconf/202019104005>
- Adel, A., 2022. Future of industry 5.0 in society: human-centric solutions, challenges and prospective research areas. J. Cloud Comput. 11. <https://doi.org/10.1186/s13677-022-00314-5>
- Aleksandar I. Ribić & Željko V. Despotović, 2010. High-Performance Feedback Control of Electromagnetic Vibratory Feeder. IEEE Trans. Ind. Electron. <https://doi.org/10.1109/TIE.2009.2037677>
- Alvarado-Hernández, B.B., Sierra-Vega, N.O., Martínez-Cartagena, P., Hormaza, M., Méndez, R., Romañach, R.J., 2020. A sampling system for flowing powders based on the theory of sampling. Int. J. Pharm. 574, 118874. <https://doi.org/10.1016/J.IJPHARM.2019.118874>
- Amouzegar, K., Amant, G. St., Harrison, S., 2000. United States Patent (19) 11 Patent Number : BATTERY-49. United States Pat.
- Annamalai, K., Ruiz, M., Vo, N., Anand, V., 1992. Locally fluidizing feeder for powder transport. Powder Technol. 73, 181–190. [https://doi.org/10.1016/0032-5910\(92\)80079-C](https://doi.org/10.1016/0032-5910(92)80079-C)
- APBI, 2019. Clinical trials: How the UK is researching medicines of the future, APBI.
- Artega, P., Tüzün, U., 1990. Flow of binary mixtures of equal-density granules in hoppers-size segregation, flowing density and discharge rates. Chem. Eng. Sci. 45, 205–223. [https://doi.org/10.1016/0009-2509\(90\)87093-8](https://doi.org/10.1016/0009-2509(90)87093-8)
- Augsburger, L., Hoag, S., 2008. Pharmaceutical Dosage Forms - Tablets, Pharmaceutical Dosage Forms - Tablets. <https://doi.org/10.3109/9781420020281>
- Azzaro-Pantel, C., 2018. New Product Development and Supply Chains in the Pharmaceutical Industry, 1st ed, Computer Aided Chemical Engineering. Elsevier B.V. <https://doi.org/10.1016/B978-0-444-63963-9.00001-4>

- B417-22, A., 2022. Standard Test Method for Apparent Density of Non-Free-Flowing Metal Powders Using the Carney Funnel, ASTM Standard. <https://doi.org/10.1520/B0417-22.2>
- Baltrėnas, P., Chlebnikovas, A., 2019. Removal of fine solid particles in aggressive gas flows in a newly designed multi-channel cyclone. *Powder Technol.* 356, 480–492. <https://doi.org/10.1016/j.powtec.2019.08.018>
- Barati Dalenjan, M., Jamshidi, E., Ale Ebrahim, H., 2015. A screw-brush feeding system for uniform fine zinc oxide powder feeding and obtaining a homogeneous gas-particle flow. *Adv. Powder Technol.* 26, 303–308. <https://doi.org/10.1016/j.appt.2014.10.010>
- Barletta, D., Donsi, G., Ferrari, G., Poletto, M., Russo, P., 2007. PVAm–PIP/PS composite membrane with high performance for CO₂/N₂ separation. *AIChE J.* 53, 2240–2253. <https://doi.org/10.1002/aic>
- Baserinia, R., Sinka, I.C., 2019. Powder die filling under gravity and suction fill mechanisms. *Int. J. Pharm.* 563, 135–155. <https://doi.org/10.1016/j.ijpharm.2019.01.068>
- Baserinia, R., Sinka, I.C., 2018. Mass flow rate of fine and cohesive powders under differential air pressure. *Powder Technol.* 334, 173–182. <https://doi.org/10.1016/j.powtec.2018.04.041>
- Baserinia, R., Sinka, I.C., Rajniak, P., 2016a. Vacuum assisted flow initiation in arching powders. *Powder Technol.* 301, 493–502. <https://doi.org/10.1016/j.powtec.2016.03.051>
- Baserinia, R., Sinka, I.C., Rajniak, P., 2016b. Vacuum assisted flow initiation in arching powders. *Powder Technol.* 301, 493–502. <https://doi.org/10.1016/j.powtec.2016.03.051>
- Basu, P., Joglekar, G., Rai, S., Suresh, P., Vernon, J., 2008. Analysis of Manufacturing Costs in Pharmaceutical Companies. *J. Pharm. Innov.* 3, 30–40. <https://doi.org/10.1007/s12247-008-9024-4>
- Bates, L., 2000. Guide to the design, selection and application of screw feeders.
- Bates, L., 1986. Interfacing Hoppers with Screw Feeders. *Bulk Solids Handl.* 6, 65–78.
- Bates, L., 1969. Entrapment Patterns of Screw Hopper Dischargers. *J. Eng. Ind.* 91, 295. <https://doi.org/10.1115/1.3591561>
- Bekaert, B., Penne, L., Grymonpré, W., Van Snick, B., Dhondt, J., Boeckx, J., Vogeleer, J., De Beer, T., Vervaet, C., Vanhoorne, V., 2021. Determination of a quantitative relationship between material properties, process settings and screw feeding behavior via multivariate data-analysis. *Int. J. Pharm.* 602. <https://doi.org/10.1016/j.ijpharm.2021.120603>

- Bekaert, B., Van Snick, B., Pandelaere, K., Dhondt, J., Di Pretoro, G., De Beer, T., Vervaet, C., Vanhoorne, V., 2022. In-depth analysis of the long-term processability of materials during continuous feeding. *Int. J. Pharm.* 614, 121454. <https://doi.org/10.1016/J.IJPHARM.2022.121454>
- Bellon, C., Truffer, C., Steiner, A., Moreillon, A., Nicolay, L., 2013. Mixing effectiveness of a new pneumatic PTS-Batchmixer® with an in-line sampling device. *Adv. Powder Technol.* 24, 43–50. <https://doi.org/10.1016/j.appt.2012.01.008>
- Beretta, M., Kruisz, J., Hörmann-Kincses, T.R., Magosi, V., Guo, M., Naderi, M., Heupl, S., Kastner, J., Spoerk, M., Paudel, A., 2023. Assessment of Tribo-charging and Continuous Feeding Performance of Direct Compression Grades of Isomalt and Mannitol Powders. *AAPS PharmSciTech* 24, 91. <https://doi.org/10.1208/s12249-023-02552-5>
- Besenhard, M.O., Fathollahi, S., Siegmann, E., Slama, E., Faulhammer, E., Khinast, J.G., 2017. Micro-feeding and dosing of powders via a small-scale powder pump. *Int. J. Pharm.* 519, 314–322. <https://doi.org/10.1016/j.ijpharm.2016.12.029>
- Besenhard, M O, Faulhammer, E., Fathollahi, S., Reif, G., Calzolari, V., Biserni, S., Ferrari, A., Lawrence, S.M., Llusa, M., Khinast, J.G., 2015. Accuracy of micro powder dosing via a vibratory sieve – chute system. *Eur. J. Pharm. Biopharm.* 94, 264–272. <https://doi.org/10.1016/j.ejpb.2015.04.037>
- Besenhard, M.O., Karkala, S.K., Faulhammer, E., Fathollahi, S., Ramachandran, R., Khinast, J.G., 2016. Continuous feeding of low-dose APIs via periodic micro dosing. *Int. J. Pharm.* 509, 123–134. <https://doi.org/10.1016/j.ijpharm.2016.05.033>
- Besenhard, Maximilian O, Neugebauer, P., Ho, C., Khinast, J.G., 2015. Crystal Size Control in a Continuous Tubular Crystallizer. *Cryst. Growth Des.* 15, 1683–1691. <https://doi.org/10.1021/cg501637m>
- Bettega, J., Richiedei, D., Tamellin, I., Trevisani, A., 2023. Integrated Inverse Dynamics and Optimized Mechanical Design in Underactuated Linear Vibratory Feeders Under Periodic Excitation. *J. Vib. Eng. Technol.* <https://doi.org/10.1007/s42417-023-00950-4>
- Beverloo, W.A., Leniger, H.A., van de Velde, J., 1961. The flow of granular solids through orifices. *Chem. Eng. Sci.* 15, 260269. <https://doi.org/10.1111/j.2042-7158.1966.tb07903.x>
- Blackshields, C.A., Crean, A.M., 2018. Continuous powder feeding for pharmaceutical solid dosage form manufacture: a short review. *Pharm. Dev. Technol.* 23, 554–560. <https://doi.org/10.1080/10837450.2017.1339197>

- Bornett, D., 2008. High-Potency APIs: Containment and Handling Issues. *Pharm. Technol.* 2008.
- Bostijn, N., Dhondt, J., Ryckaert, A., Szabó, E., Dhondt, W., Van Snick, B., Vanhoorne, V., Vervaet, C., De Beer, T., 2019. A multivariate approach to predict the volumetric and gravimetric feeding behavior of a low feed rate feeder based on raw material properties. *Int. J. Pharm.* 557, 342–353. <https://doi.org/10.1016/j.ijpharm.2018.12.066>
- Brabender, 2023a. FlexWall ® FW20/0.
- Brabender, 2023b. Twin screw feeder MiniTwin 2.0.
- Brown, C.J., Mcglone, T., Yerdelen, S., Srirambhatla, V., Mabbott, F., Gurung, R., Briuglia, M.L., Ahmed, B., Polyzois, H., McGinty, J., Perciballi, F., Fysikopoulos, D., Macfhionnghaile, P., Siddique, H., Raval, V., Harrington, T.S., Vassileiou, A.D., Robertson, M., Prasad, E., Johnston, A., Johnston, B., Nordon, A., Srai, J.S., Halbert, G., Ter Horst, J.H., Price, C.J., Rielly, C.D., Sefcik, J., Florence, A.J., 2018. Enabling precision manufacturing of active pharmaceutical ingredients: workflow for seeded cooling continuous crystallisations. *Mol. Syst. Des. Eng.* 3, 518–549. <https://doi.org/10.1039/c7me00096k>
- Bruni, G., Lettieri, P., Newton, D., Barletta, D., 2007. An investigation of the effect of the interparticle forces on the fluidization behaviour of fine powders linked with rheological studies. *Chem. Eng. Sci.* 62, 387–396. <https://doi.org/10.1016/J.CES.2006.08.059>
- Bulsara, P.U., Zenz, F.A., Eckert, R.A., 1964. Pressure and Additive Effects on Flow of Bulk Solids. *Ind. Eng. Chem. Process Des. Dev.* 3, 348–355.
- Burch, T.E., Conway, R.B., Chen, W.Y., 1991. A practical pulverized coal feeder for bench-scale combustion requiring low feed rates. *Rev. Sci. Instrum.* 62, 480–483. <https://doi.org/10.1063/1.1142091>
- Burcham, C.L., Florence, A.J., Johnson, M.D., 2018. Continuous Manufacturing in Pharmaceutical Process Development and Manufacturing. *Annu. Rev. Chem. Biomol. Eng.* 9, 253–281. <https://doi.org/10.1146/annurev-chembioeng-060817-084355>
- Burstein, S.H., Lin, Y., Wu, W., Ge, Q., 2020. Review of sensing technologies for measuring powder density variations during pharmaceutical solid dosage form manufacturing. *TrAC Trends Anal. Chem.* 95, 106408. <https://doi.org/10.1016/j.trac.2020.116147>
- Byrn, S., Futran, M., Thomas, H., Jayjock, E., Maron, N., Meyer, R.F., Myerson, A.S., Thien, M.P., Trout, B.L., 2015. Achieving continuous manufacturing for final dosage formation:

- Challenges and how to meet them May 20-21, 2014 continuous manufacturing symposium. *J. Pharm. Sci.* 104, 792–802. <https://doi.org/10.1002/jps.24247>
- Carleton, A.J., 1972. The effect of fluid-drag forces on the discharge of free-flowing solids from hoppers. *Powder Technol.* 6, 91–96. [https://doi.org/10.1016/0032-5910\(72\)80062-7](https://doi.org/10.1016/0032-5910(72)80062-7)
- Carleton, A.J., Miles, J.E.P., Valentin, F.H.H., 1969. A Study of Factors Affecting the Performance of Screw Conveyers and Feeders. *J. Eng. Ind.* 329–333.
- Carman, P.C., 1937. Fluid Flow through Granular Beds. *Trans. Inst. Chem. Eng.* 15, 150–166.
- Carr, R.L., 1965. Evaluating flow properties of solids. *Chem. Eng.* 72, 163–168.
- Carrigy, M.A., 1970. EXPERIMENTS ON THE ANGLES OF REPOSE OF GRANULAR MATERIALS1. *Sedimentology* 14, 147–158. <https://doi.org/https://doi.org/10.1111/j.1365-3091.1970.tb00189.x>
- Cartwright, J.J., Robertson, J., D'Haene, D., Burke, M.D., Hennenkamp, J.R., 2013. Twin screw wet granulation: Loss in weight feeding of a poorly flowing active pharmaceutical ingredient. *Powder Technol.* 238, 116–121. <https://doi.org/10.1016/J.POWTEC.2012.04.034>
- Chamberlain, R., Windolf, H., Geissler, S., Quodbach, J., Breitzkreutz, J., 2022. Precise Dosing of Pramipexole for Low-Dosed Filament Production by Hot Melt Extrusion Applying Various Feeding Methods. *Pharm. Technol.* 46, 16–20. <https://doi.org/10.3390/pharmaceutics14010216>
- Chandravanshi, M.L., Mukhopadhyay, A.K., 2017. Dynamic analysis of vibratory feeder and their effect on feed particle speed on conveying surface. *Measurement* 101, 145–156. <https://doi.org/10.1016/j.measurement.2017.01.031>
- Chandravanshi, M.L., Mukhopadhyay, A.K., 2015. Experimental modal analysis of the vibratory feeder and its structural elements. *Int. J. Appl. Eng. Res.* 10, 33303–33310.
- Chen, X., Seyfang, K., Steckel, H., 2012. Development of a micro dosing system for fine powder using a vibrating capillary . Part 1 : The investigation of factors influencing on the dosing performance. *Int. J. Pharm.* 433, 34–41. <https://doi.org/10.1016/j.ijpharm.2012.04.068>
- Chourasia, S., Tyagi, A., Murtaza, Q., Walia, R.S., Sharma, P., 2023. A Critical Review on Industry 5.0 and Its Medical Applications, in: *Advances in Modelling and Optimization of Manufacturing and Industrial Systems*. Springer Nature Singapore, pp. 251–261. https://doi.org/10.1007/978-981-19-6107-6_18

- Clayton, J., 2019. An Introduction to Powder Characterization, Handbook of Pharmaceutical Wet Granulation. Elsevier Inc. <https://doi.org/10.1016/b978-0-12-810460-6.00021-x>
- CMAC, 2019. Annual review 2019.
- Conveyors Incorporated, 2023. Screw Conveyor Engineering Guide.
- Coperion, 2013. Coperion K-Tron Product Specification Twin Screw Loss-in-Weight Feeder K-CLSFS-MT12.
- Copot, D., 2022. A Systematic Framework for Design and Evaluation of Control Strategies for Continuous Manufacturing of Tablets, in: 2022 IEEE International Conference on Automation, Quality and Testing, Robotics (AQTR). IEEE. <https://doi.org/10.1109/aqtr55203.2022.9801916>
- Couillaud, B.M., Espeau, P., Mignet, N., Corvis, Y., 2019. State of the Art of Pharmaceutical Solid Forms: from Crystal Property Issues to Nanocrystals Formulation. *ChemMedChem* 14, 8–23. <https://doi.org/10.1002/cmdc.201800612>
- Crewdson, B.J., Ormond, A.L., Nedderman, R.M., 1977. Air-impeded discharge of fine particles from a hopper. *Powder Technol.* 16, 197–207. [https://doi.org/10.1016/0032-5910\(77\)87007-1](https://doi.org/10.1016/0032-5910(77)87007-1)
- Cundall, P.A., Strack, O.D.L., 1979. A discrete numerical model for granular assemblies. *Geotechnique* 29, 47–65. <https://doi.org/10.1680/geot.1980.30.3.331>
- Cunningham, C., Hansell, J., Nuneviller III, F., Rajabi-Siahboomi, A.R., 2010. Evaluation of recent advances in continuous film coating processes. *Drug Dev. Ind. Pharm.* 36, 227–233. <https://doi.org/10.3109/03639040903410326>
- Dai, J., Grace, J.R., 2008. A model for biomass screw feeding. *Powder Technol.* 186, 40–55. <https://doi.org/10.1016/j.powtec.2007.10.032>
- Datta, A., Mishra, B.K., Das, S.P., Sahu, A., Datta, A., Mishra, B.K., Das, S.P., Sahu, A., 2008. A DEM Analysis of Flow Characteristics of Noncohesive Particles in Hopper A DEM Analysis of Flow Characteristics of Noncohesive Particles in Hopper 6914. <https://doi.org/10.1080/10426910701774742>
- David J Smith, 2020. The Chemical Engineer Issue 944. *ICHEME* 40–43.
- De Souter, L., Waeytens, R., Van Hauwermeiren, D., Grymonpré, W., Bekaert, B., Nopens, I., De Beer, T., 2023. Elucidation of the powder flow pattern in a twin-screw LIW-feeder for various refill regimes. *Int. J. Pharm.* 631, 122534. <https://doi.org/10.1016/J.IJPHARM.2022.122534>

- de Vasconcelos, P.D.S., Amarante Mesquit, A.L., 2011. Gas-Solid Flow Applications for Powder Handling in Industrial Furnaces Operations. *Heat Anal. Thermodyn. Eff.* <https://doi.org/10.5772/22393>
- DEC Group, 2023. Microdosing [WWW Document]. <https://www.dec-group.net/microdosing-products>.
- Demming, W.E., Mehring, A.A., 1929. The Gravitational Flow of Fertilizers and Other Comminuted Solids. *Ind. Eng. Chem.* 21, 661–665. <https://doi.org/10.1021/ie50235a013>
- Deshmukh, O.S., Dhital, S., Olarte Mantilla, S.M., Smyth, H.E., Boehm, M.W., Baier, S.K., Stokes, J.R., 2019. Ring Shear Tester as an in-vitro testing tool to study oral processing of comminuted potato chips. *Food Res. Int.* 123, 208–216. <https://doi.org/10.1016/j.foodres.2019.04.037>
- Dhenge, R.M., Cartwright, J.J., Doughty, D.G., Hounslow, M.J., Salman, A.D., 2011. Twin screw wet granulation: Effect of powder feed rate. *Adv. Powder Technol.* 22, 162–166. <https://doi.org/10.1016/j.appt.2010.09.004>
- DiMasi, J.A., 2002. The value of improving the productivity of the drug development process: Faster Times and Better Decisions. *Pharmacoeconomics* 20, 1–10. <https://doi.org/10.2165/00019053-200220003-00001>
- Donsì, G., Ferrari, G., Poletto, M., Russo, P., 2004. Gas pressure measurements inside an aerated hopper. *Chem. Eng. Res. Des.* 82, 72–84. <https://doi.org/10.1205/026387604772803089>
- Enabling Technologies Consortium, 2020. POWDER FEEDING SYSTEM [WWW Document]. [etconsortium.org](https://www.etconsortium.org/powderfeedingsystem). URL <https://www.etconsortium.org/powderfeedingsystem>
- Engisch, W.E., Muzzio, F.J., 2015. Feedrate deviations caused by hopper refill of loss-in-weight feeders. *Powder Technol.* 283, 389–400. <https://doi.org/10.1016/j.powtec.2015.06.001>
- Engisch, W.E., Muzzio, F.J., 2014. Loss-in-Weight Feeding Trials Case Study: Pharmaceutical Formulation. *J. Pharm. Innov.* 10, 56–75. <https://doi.org/10.1007/s12247-014-9206-1>
- Erdim, E., Akgiray, Ö., Demir, I., 2015. A revisit of pressure drop-flow rate correlations for packed beds of spheres. *Powder Technol.* 283, 488–504. <https://doi.org/10.1016/j.powtec.2015.06.017>
- Evaluate Ltd., 2022. WORLD PREVIEW 2022 Outlook to 2028: Patents and Pricing.

EvaluatePharma.

- Farid, S.S., Baron, M., Stamatis, C., Nie, W., Coffman, J., 2020. Benchmarking biopharmaceutical process development and manufacturing cost contributions to R&D. *MABs* 12, 1754999. <https://doi.org/10.1080/19420862.2020.1754999>
- Fathollahi, S., Kruisz, J., Sacher, S., Rehrl, J., Escotet-Espinoza, M.S., DiNunzio, J., Glasser, B.J., Khinast, J.G., 2021. Development of a Controlled Continuous Low-Dose Feeding Process. *AAPS PharmSciTech* 22, 1–14. <https://doi.org/10.1208/s12249-021-02104-9>
- Fathollahi, S., Sacher, S., Escotet-Espinoza, M.S., Dinunzio, J., Khinast, J.G., 2020. Performance Evaluation of a High-Precision Low-Dose Powder Feeder. *AAPS PharmSciTech* 21. <https://doi.org/10.1208/s12249-020-01835-5>
- FDA USP 788, 2009. Guidance for Industry Q4B Evaluation and Recommendation of Pharmacopoeial Texts for Use in the Guidance for Industry. Evaluation.
- Fernandez, J.W., Cleary, P.W., McBride, W., 2011. Effect of screw design on hopper drawdown of spherical particles in a horizontal screw feeder. *Chem. Eng. Sci.* 66, 5585–5601. <https://doi.org/10.1016/j.ces.2011.07.043>
- Francis, T.M., Gump, C.J., Weimer, A.W., 2006. Spinning wheel powder feeding device - fundamentals and applications. *Powder Technol.* 170, 36–44. <https://doi.org/10.1016/j.powtec.2006.08.012>
- Freeman Technology Ltd, 2016. Freeman Technology _ FT4 powder rheometer [WWW Document]. <https://www.freemantech.co.uk/powder-testing/ft4-powder-rheometer-powder-flow-tester>. URL <https://www.freemantech.co.uk/powder-testing/ft4-powder-rheometer-powder-flow-tester>
- Gad, S.C., 2007. Pharmaceutical Manufacturing Handbook: Regulations and Quality, *Pharmaceutical Manufacturing Handbook: Regulations and Quality*. <https://doi.org/10.1002/9780470259832>
- Geldart, D., 1973. Types of Gas Fluidization. *Powder Technol.* 7, 285–292.
- Geldart, D., Abdullah, E.C., Hassanpour, A., Nwoke, L.C., Wouters, I., 2006. Characterization of powder flowability using measurement of angle of repose. *China Particuology* 4, 104–107. [https://doi.org/10.1016/s1672-2515\(07\)60247-4](https://doi.org/10.1016/s1672-2515(07)60247-4)
- Genck, W.J., Joye, I.J., McClements, D.J., O'Grady, D., Barrett, M., Casey, E., Glennon, B., Thiering, R., Dehghani, F., Foster, N.R., Grady, D.O., Dycus, E., Autochem, M., Ingredient, F., Smith, B., Sullivan, B.O., Autochem, M., O'Grady, D., Redman, T.P.,

- Smith, B., Autochem, Mettler-toledo, Toledo, M., Index, R.B., Understanding, I.P., Crystallization, I., Designing, S., Process, O., Evidence, B., Step, S., Rbi, B., Barrett, P., Glennon, B., Barrett, M., O'Grady, D., Casey, E., Glennon, B., Sullivan, B.O., Smith, B., Baramidze, G., 2002. Recent Advances for Seeding a Crystallization Process: A Review of Modern Techniques. *Chem. Eng. Res. Des.* 80, 799–805. <https://doi.org/http://dx.doi.org/10.1205/026387602320776876>
- Gericke, 2023. Website: Gerickegroup. [WWW Document]. Gericke. URL <https://www.gerickegroup.com/rotary-valves>
- Gericke, 2022. Gericke FEEDOS S.
- GLOBE NEWSWIRE, 2022. Personalized Medicine Market Size to Reach US\$ 5.7 Trillion by 2030 [WWW Document]. GLOBE NEWSWIRE. URL <https://www.globenewswire.com/news-release/2022/1/25/2372822/0/en/Personalized-Medicine-Market-Size-to-Reach-US-5-7-Trillion-by-2030.html>
- Goossens, W.R.A., 1998. Classification of fluidized particles by archimedes number. *Powder Technol.* 98, 48–53. [https://doi.org/10.1016/S0032-5910\(98\)00027-8](https://doi.org/10.1016/S0032-5910(98)00027-8)
- Grace, J.R., 1986. Gas-Solid and Other Two-Phase Suspemmm 64.
- GVR, 2023. Clinical Trials Market Size, Share & Trends Analysis Report By Phase (Phase I, Phase II, Phase III, Phase IV), By Study Design, By Indication (Pain Management, Oncology, CNS Condition, Diabetes, Obesity), By Region, And Segment Forecasts, 2023 - 2030.
- Haaker, G., van Poppelen, M.P., Jongejan, M., Bekhuis, J., 1994. A method to optimize screw feeder geometry for equable draw-down performance.
- Haaker, G., van Poppelen, M.P., Jongejan, M.P., Stokkers, G.J., 1993. Improvement of screw feeder geometry for better draw-down performance, in: *International Symposium Reliable Flow of Particulate Solids II*. Oslo, Norway. pp. 551–552.
- Haleem, A., Javaid, M., 2019. Industry 5.0 and its expected applications in medical field. *Curr. Med. Res. Pract.* 9, 167–169. <https://doi.org/10.1016/j.cmrp.2019.07.002>
- Hamor, R.J., Smith, I.W., 1971. Fluidizing feeders for providing fine particles at low, stable flows. *Fuel* 50, 394–404. [https://doi.org/10.1016/0016-2361\(71\)90028-7](https://doi.org/10.1016/0016-2361(71)90028-7)
- Hanson, J., 2018. Control of a system of loss-in-weight feeders for drug product continuous manufacturing. *Powder Technol.* 331, 236–243. <https://doi.org/10.1016/j.powtec.2018.03.027>

- Hartman, M., Phořelý, M., Trnka, O., 2006. Transport velocities of different particulate materials in pneumatic conveying. *Chem. Pap. Slovak Acad. Sci.* 60, 74–77. <https://doi.org/10.2478/s11696-006-0015-y>
- Hassanpour, A., Ghadiri, M., 2007. Characterisation of flowability of loosely compacted cohesive powders by indentation. *Part. Part. Syst. Charact.* 24, 117–123. <https://doi.org/10.1002/ppsc.200601111>
- Hausner, H.H., 1967. FRICTION CONDITIONS IN A MASS OF METAL POWDER. *Int. J. Powder Metall.* 3, 7–13.
- Heinrici, H., Toerner, L., Biebe, J., 1998. Apparatus for the metered discharge of bulk material from a flexible supply.
- Hemph, R., Wachem, B. Van, Almstedt, A., 2019. DEM Modeling of Hopper Flows : Comparison and Validation of Models and DEM Modeling of Hopper Flows : Comparison and Validation of Models and Parameters.
- Hickey, A.J., 2001. *Pharmaceutical Process Engineering, Pharmaceutical Process Engineering.* <https://doi.org/10.1201/9781420002324>
- Higashitani, K., Makino, H., Matsusaka, S., 2020. *Powder Technology Handbook, 4th Edition.*
- Horio, T., Yasuda, M., Matsusaka, S., 2014. Effect of particle shape on powder flowability of microcrystalline cellulose as determined using the vibration shear tube method. *Int. J. Pharm.* 473, 572–578. <https://doi.org/10.1016/j.ijpharm.2014.07.040>
- Hörmann-Kincses, T.R., Beretta, M., Kruisz, J., Stauffer, F., Birk, G., Piccione, P.M., Holman, J., Khinast, J.G., 2022. Predicting powder feedability: A workflow for assessing the risk of flow stagnation and defining the operating space for different powder-feeder combinations. *Int. J. Pharm.* 629. <https://doi.org/10.1016/j.ijpharm.2022.122364>
- Hou, P., Besenhard, M.O., Halbert, G., Naftaly, M., Markl, D., 2023. Development and implementation of a pneumatic micro-feeder for poorly-flowing solid pharmaceutical materials. *Int. J. Pharm.* 635, 122691. <https://doi.org/10.1016/J.IJPHARM.2023.122691>
- Hou, Q.F., Dong, K.J., Yu, A.B., 2014. DEM study of the flow of cohesive particles in a screw feeder 256, 529–539. <https://doi.org/10.1016/j.powtec.2014.01.062>
- Huang, X., Zheng, Q., Liu, D., Yu, A., Yan, W., 2022. A design method of hopper shape optimization with improved mass flow pattern and reduced particle segregation. *Chem. Eng. Sci.* 253, 117579. <https://doi.org/10.1016/j.ces.2022.117579>
- Huang, Y.-S., Medina-González, S., Straiton, B., Keller, J., Marashdeh, Q., Gonzalez, M.,

- Nagy, Z., Reklaitis, G. V., 2021. Real-time Monitoring of Powder Mass Flowrates for Plant-wide Control of a Continuous Direct Compaction Tablet Manufacturing Process. *J. Pharm. Sci.* <https://doi.org/10.1016/j.xphs.2021.06.005>
- Huang, Y.S., Medina-González, S., Straiton, B., Keller, J., Marashdeh, Q., Gonzalez, M., Nagy, Z., Reklaitis, G. V., 2022. Real-Time Monitoring of Powder Mass Flowrates for Plant-Wide Control of a Continuous Direct Compaction Tablet Manufacturing Process. *J. Pharm. Sci.* 111, 69–81. <https://doi.org/10.1016/j.xphs.2021.06.005>
- Ikumi, S., Wakayama, H., Masuda, H., 1986. Particle Reentrainment by an Air Stream from Deposited Layer. *KAGAKU KOGAKU RONBUNSHU* 12, 589–594.
- IPharmachine, 2023. Type of table compression machines: A complete guide [WWW Document]. <https://www.ipharmachine.com/type-of-tablet-presses>.
- Irani, R.R., Callis, C.F., Liu, T., 1959. How to select flow conditioning and anticaking agents. *Ind. Eng. Chem.* 51, 1285–1288.
- Janssen, P.H.M., Kulkarni, S.S., Torrecillas, C.M., Tegel, F., Weinekötter, R., Meir, B., Dickhoff, B.H.J., 2022. Effect of batch-to-batch variation of spray dried lactose on the performance of feeders. *Powder Technol.* 409, 117776. <https://doi.org/10.1016/J.POWTEC.2022.117776>
- Jaspers, M., de Wit, M.T.W., Kulkarni, S.S., Meir, B., Janssen, P.H.M., van Haandel, M.M.W., Dickhoff, B.H.J., 2021. Impact of excipients on batch and continuous powder blending. *Powder Technol.* 384, 195–199. <https://doi.org/10.1016/j.powtec.2021.02.014>
- Jenike, A.W., 1964. Storage and Flow of Solids. Bull. No. 123, Utah State Univ.
- Jiang, Y., Matsusaka, S., Masuda, H., Qian, Y., 2009. Development of measurement system for powder flowability based on vibrating capillary method. *Powder Technol.* 188, 242–247. <https://doi.org/10.1016/j.powtec.2008.05.003>
- Johanson, J.R., 1965. A Rolling Theory for Granular Solids. *J. Appl. Mech.* 32, 842–848. <https://doi.org/10.1115/1.3627325>
- Johnson, B.J., Sen, M., Hanson, J., García-Muñoz, S., Sahinidis, N. V., 2022. Stochastic analysis and modeling of pharmaceutical screw feeder mass flow rates. *Int. J. Pharm.* 621. <https://doi.org/10.1016/j.ijpharm.2022.121776>
- Jones-Salkey, O., Chu, Z., Ingram, A., Windows-Yule, C.R.K., 2023. Reviewing the Impact of Powder Cohesion on Continuous Direct Compression (CDC) Performance. *Pharmaceutics* 15, 1–48. <https://doi.org/10.3390/pharmaceutics15061587>

- K-Tron International, 2009. Continuous Pharmaceutical Dry Granulation and Direct Compression Tableting Processes. K-Tron Process Gr. 1, 1–4.
- K-Tron Technologies Inc, 2012. Metered Dry Powder Addition for Continuous and Batch Coating Processes Metered Dry Powder Addition for Continuous and Batch Coating Processes Volumetric versus Gravimetric Feeding K-Tron Advantage. K-Tron Technol. Inc 1–2.
- Kashan Bashir, 2015. Design and fabrication of cyclone separator. ResearchGate. <https://doi.org/10.13140/RG.2.2.20727.83368>
- Kaur, B., Mittal, A., Wypych, P., Mallick, S.S., Jana, S., 2017. On developing improved modelling and scale-up procedures for pneumatic conveying of fine powders. Powder Technol. 305, 270–278. <https://doi.org/10.1016/j.powtec.2016.09.080>
- Kerins, B.M., O'Mahony, M., Crean, A.M., 2023. Study of the feeding performance of mesoporous silica in a loss-in-weight feeder. Powder Technol. 424, 118529. <https://doi.org/10.1016/j.powtec.2023.118529>
- Ketterhagen, W.R., Hancock, B.C., 2010. Optimizing the design of eccentric feed hoppers for tablet presses using DEM. Comput. Chem. Eng. 34, 1072–1081. <https://doi.org/10.1016/j.compchemeng.2010.04.016>
- Kharitonov, Y., Vasilyev, P., Bebikhov, Y., Egorov, A., Semenov, A., 2022. Justifying the actuator type selection for the flow-line conveyor system with vibration-assisted transportation of bulk material. Transp. Res. Procedia 63, 2670–2677. <https://doi.org/10.1016/J.TRPRO.2022.06.308>
- Kousaka, Y., Okuyama, K., Endo, Y., 1980. Re-entrainment of small aggregate particles from a plane surface by air stream. J. Chem. Eng. JAPAN 13, 143–147. <https://doi.org/10.1252/jcej.13.143>
- Kozeny, J., 1927. Ueber kapillare Leitung des Wassers im Boden. Akad. Wiss.Wien 136, 271–306.
- Kruisz, J., Rehr, J., Hörmann-Kincses, T.R., Khinast, J.G., 2021. Effects of signal processing on the relative standard deviation in powder feeding characterization for continuous manufacturing. Powder Technol. 389, 536–548. <https://doi.org/10.1016/j.powtec.2021.05.068>
- Kuang, S., Zhou, M., Yu, A., 2019. CFD-DEM modelling and simulation of pneumatic conveying: A review. Powder Technol. 2–23.

<https://doi.org/10.1016/j.powtec.2019.02.011>

Kumar, N., 2023. Fundamentals of conveyors, Transporting Operations of Food Materials within Food Factories. Elsevier Inc. <https://doi.org/10.1016/B978-0-12-818585-8.00003-9>

KWS Manufacturing Company Ltd., 2015. Screw Conveyors. KWS Manuf. Co. Ltd.

LCI Corporation, 2020. Circle Feeder™ A unique table feeder TECHNICAL Circle Feeder Specifications [WWW Document]. <https://www.lcicorp.com/en/powder-handling-equipment/circle-feeder>.

Lee, Y.S.L., Poynter, R., Podczek, F., Newton, J.M., 2000. Development of a dual approach to assess powder flow from avalanching behavior. *AAPS PharmSciTech* 1. <https://doi.org/10.1208/pt010321>

Leung, L.Y., Mao, C., Srivastava, I., Du, P., Yang, C.Y., 2017. Flow Function of Pharmaceutical Powders Is Predominantly Governed by Cohesion, Not by Friction Coefficients. *J. Pharm. Sci.* 106, 1865–1873. <https://doi.org/10.1016/j.xphs.2017.04.012>

Li, M., Luo, J., Wu, B., Hua, J., 2018. Experimental research of the mechanism and particle flow in screw conveyer. *Int. J. Heat Technol.* 36, 173–181. <https://doi.org/10.18280/ijht.360123>

Li, X., Hou, Q., Dong, K., Zou, R., Yu, A., 2020. Promote cohesive solid flow in a screw feeder with new screw designs. *Powder Technol.* 361, 248–257. <https://doi.org/10.1016/j.powtec.2019.08.045>

Lim, E., Yao, J., 2009. Modeling and simulation of the polymeric nanocapsule formation process. *IFAC Proc. Vol. 7*, 405–410. <https://doi.org/10.1002/aic>

Liu, M., Wang, N., Chen, X., Shan, Y., Li, J., 2020. Design of feed screw conveyor. *J. Phys. Conf. Ser.* 1601. <https://doi.org/10.1088/1742-6596/1601/6/062005>

Llusa, M., 2014. Continuous low-dose capsule filling of pharmaceutical inhalation powders.

Lopes Neto, J.P., Meira, A.S., Do Nascimento, J.W.B., 2017. Flow properties and pattern flow prediction of food industrial powders. *Eng. Agric.* 37, 627–636. <https://doi.org/10.1590/1809-4430-Eng.Agric.v37n4p627-636/2017>

López, A., Vivacqua, V., Hammond, R., Ghadiri, M., 2020. Analysis of screw feeding of faceted particles by discrete element method. *Powder Technol.* 367, 474–486. <https://doi.org/10.1016/j.powtec.2020.03.064>

- M. Bortolamasi and J. Fottner, 2001. Design and sizing of screw feeders. *Int. Congr. Part. Technol.* 27–29.
- Mahajan, N.P., Deshpande, S.B., Kadwane, S.G., 2018. Design and implementation of an advanced controller in plant distributed control system for improving control of non-linear belt weigh feeder. *J. Process Control* 62, 55–65. <https://doi.org/10.1016/J.JPROCONT.2017.12.010>
- Mahajan, N.P., Deshpande, S.B., Kadwane, S.G., 2016. Optimizing weigh feeder performance using modeling and simulation, in: *International Conference & Workshop on Electronics & Telecommunication Engineering (ICWET 2016)*. pp. 8–14. <https://doi.org/10.1049/cp.2016.1115>
- Markarian, J., 2022. Breaking Through Barriers to Continuous Manufacturing. *Pharm. Technol.* 46, 16–20.
- Market Data Forecast, 2023. Global HPAPI Market Size, Share, Trends, COVID-19 Impact & Growth Analysis Report – Segmented By Type (Innovative HPAPI's & Generic HPAPI's), Synthesis (Biotech HPAPI's & Synthetic HPAPI's), Therapeutic Application & Region – Industry Forecast (2023 to 20).
- Martínez-Cartagena, P.A., Sierra-Vega, N.O., Alvarado-Hernández, B.B., Méndez, R., Romañach, R.J., 2021. An innovative sampling interface for monitoring flowing pharmaceutical powder mixtures. *J. Pharm. Biomed. Anal.* 194, 113785. <https://doi.org/10.1016/J.JPBA.2020.113785>
- Matsumoto, S., 1977. Effect of Particle Size on the Minimum Transport Velocity for Horizontal pneumatic conveying of solids. *J. Chem. Eng. Jpn.*; 10, 273–279.
- Matusaka, S., Masuda, H., 1996. Particle Reentrainment from a Fine Powder Layer in a Turbulent Air Flow. *Aerosol Sci. Technol.* 6826, 69–84. <https://doi.org/10.1080/02786829608965353>
- Mazor, A., Orefice, L., Michrafy, A., Ryck, A. De, Johannes, G., 2018. A combined DEM & FEM approach for modelling roll compaction process. *Powder Technol.* 337, 3–16. <https://doi.org/10.1016/j.powtec.2017.04.053>
- McDougall, I.R., Knowles, G.H., 1969. Flow of particles through orifices. *Trans. Inst. Chem. Engrs.* 47, T73.
- McGlinchey, D., 2009. Bulk Solids Handling: Equipment Selection and Operation, Bulk Solids Handling: Equipment Selection and Operation. <https://doi.org/10.1002/9781444305449>

- Mehos, G., 2023. Maximum solids discharge rates from hoppers.pdf. Chem. Eng. Res. Des. 191, 564–567.
- Mehos, G., 2020. PBE Hopper Design.pdf. Powder Bulk Eng.
- Mehos, G., 2018. STORAGE AND HANDLING OF BULK SOLIDS, www.mehos.net.
- Mehrabi, M., Gardy, J., Talebi, F.A., Farshchi, A., Hassanpour, A., Bayly, A.E., 2023. An investigation of the effect of powder flowability on the powder spreading in additive manufacturing. Powder Technol. 413. <https://doi.org/10.1016/j.powtec.2022.117997>
- Mendez, R., Muzzio, F., Velazquez, C., 2010. Study of the effects of feed frames on powder blend properties during the filling of tablet press dies. Powder Technol. 200, 105–116. <https://doi.org/10.1016/j.powtec.2010.02.010>
- Mendez, R., Velazquez, C., Muzzio, F.J., 2012. Effect of feed frame design and operating parameters on powder attrition, particle breakage, and powder properties. Powder Technol. 229, 253–260. <https://doi.org/10.1016/j.powtec.2012.06.045>
- Messmer, T., 2013. Choosing a feeder: It's all about your. Powder Bulk Eng.
- Metcalf, J.R., 1965. The Mechanics of the Screw Feeder. Proc. Inst. Mech. Eng. 180, 131–146. https://doi.org/10.1243/PIME_PROC_1965_180_015_02
- MG2, 2023. FlexaLAB: MG2 innovative solution for manufacturing a variety of dosages and capsule sizes [WWW Document]. <https://www.mg2.it/2023/04/17/quotient-sciences-flexalab-microdose/>.
- Mi, C.Q., McLean, A.G., Arnold, P.C., 1991. Optimal mechanical design of single span screw feeders. Powder Handl. Process. J. 3, 227–239.
- Mikulic, M., 2022. Global pharmaceutical industry - statistics & facts [WWW Document]. <https://www.statista.com/topics/1764/global-pharmaceutical-industry/>. URL https://www.statista.com/topics/1764/global-pharmaceutical-industry/#topicHeader__wrapper
- Mills, D., 2016a. Pipeline Feeding Devices, Pneumatic Conveying Design Guide. Butterworth-Heinemann. <https://doi.org/10.1016/B978-0-08-100649-8.00005-6>
- Mills, D., 2016b. Pneumatic Conveying Design Guide, Pneumatic Conveying Design Guide. Elsevier Ltd. <https://doi.org/10.1016/b978-0-08-100649-8.01001-5>
- Mills, L.A., Sinka, I.C., 2013. Effect of particle size and density on the die fill of powders. Eur. J. Pharm. Biopharm. 84, 642–652. <https://doi.org/10.1016/j.ejpb.2013.01.012>

- Minglani, D., Sharma, A., Pandey, H., Dayal, R., Joshi, J.B., 2021. Analysis of flow behavior of size distributed spherical particles in screw feeder. *Powder Technol.* 382, 1–22. <https://doi.org/10.1016/j.powtec.2020.12.041>
- Minglani, D., Sharma, A., Pandey, H., Dayal, R., Joshi, J.B., Subramaniam, S., 2020. A review of granular flow in screw feeders and conveyors. *Powder Technol.* 366, 369–381. <https://doi.org/10.1016/j.powtec.2020.02.066>
- Mišljen, P., Mitrović, R., Despotović, Ž. V., Matijević, M., 2015. SCADA application for control and monitoring of vibratory feeder, in: 3rd International Conference & Workshop Mechatronics in Practice and Education (MECHEDU). pp. 14–16.
- Moghtadernejad, S., Escotet-Espinoza, M.S., Oka, S., Singh, R., Liu, Z., Román-Ospino, A.D., Li, T., Razavi, S., Panikar, S., Scicolone, J., Callegari, G., Hausner, D., Muzzio, F., 2018. A Training on: Continuous Manufacturing (Direct Compaction) of Solid Dose Pharmaceutical Products. *J. Pharm. Innov.* 13, 155–187. <https://doi.org/10.1007/s12247-018-9313-5>
- Molerus, O., 1996. Overview: Pneumatic transport of solids. *Powder Technol.* 88, 309–321. [https://doi.org/10.1016/s0032-5910\(96\)03136-1](https://doi.org/10.1016/s0032-5910(96)03136-1)
- Molerus, O., 1982. Interpretation of Geldart's type A, B, C and D powders by taking into account interparticle cohesion forces. *Powder Technol.* 33, 81–87.
- Moysey, P.A., Thompson, M.R., 2005. Modelling the solids inflow and solids conveying of single-screw extruders using the discrete element method. *Powder Technol.* 153, 95–107. <https://doi.org/10.1016/j.powtec.2005.03.001>
- Nagy, Z.K., Braatz, R.D., 2012. Advances and New Directions in Crystallization Control. *Annu. Rev. Chem. Biomol. Eng.* 3, 55–75. <https://doi.org/10.1146/annurev-chembioeng-062011-081043>
- Nagy, Z.K., Hagrasy, A. El, Litster, J., 2020. *Book of Continuous Pharmaceutical Processing*.
- Narang, A.S., Badawy, S.I.F.B.T.-H. of P.W.G. (Eds.), 2019. *HANDBOOK OF PHARMACEUTICAL WET GRANULATION*. Academic Press. <https://doi.org/https://doi.org/10.1016/B978-0-12-810460-6.09991-7>
- Nedderman, R.M., Tüzün, U., Savage, S.B., Houlsby, G.T., 1982. The flow of granular materials—I: Discharge rates from hoppers. *Chem. Eng. Sci.* 37, 1597–1609.
- Novartis, 2023. Novartis lung cancer drug Zykadia® gains EU approval, providing new therapy for certain patients with ALK+ NSCLC [WWW Document]. Novartis. URL

<https://www.novartis.com/news/media-releases/novartis-lung-cancer-drug-zykadia-gains-eu-approval-providing-new-therapy-certain-patients-alk-nscl>

Nowak, S., 2016. Three ways to improve continuous loss-in-weight feeding accuracy. *Powder Bulk Eng.*

Nowak, S., 2015. Optimizing feeding accuracy for your batch or continuous process. *Powder Bulk Eng.*

Nowak, S., 2013. Using a gravimetric feeder to dose pharmaceutical bulk solids: Loss-in-weight feeders provide high accuracy for batch or continuous processes. *Pharm. Technol. Eur.* 25, 50–52.

O Oyewumi, M., 2015. 3D Printing Technology in Pharmaceutical Drug Delivery: Prospects and Challenges. *J. Biomol. Res. Ther.* 04. <https://doi.org/10.4172/2167-7956.1000e141>

Orefice, L., Khinast, J.G., 2017. DEM study of granular transport in partially filled horizontal screw conveyors. *Powder Technol.* 305, 347–356. <https://doi.org/10.1016/j.powtec.2016.09.067>

Orehek, J., Teslić, D., Likozar, B., 2021. Continuous Crystallization Processes in Pharmaceutical Manufacturing: A Review. *Org. Process Res. Dev.* 25, 16–42. <https://doi.org/10.1021/acs.oprd.0c00398>

Owen, P.J., Cleary, P.W., 2009. Prediction of screw conveyor performance using the Discrete Element Method (DEM). *Powder Technol.* 193, 274–288. <https://doi.org/10.1016/j.powtec.2009.03.012>

Papazoglou, C.S., Pyle, D.L., 1970. Air-Assisted Flow from a Bed of Particles The flow of solid particles from beds and hoppers is a subject of considerable practical and theoretical interest- The work reported here originated in a study of the flow of fluidised solids through an orifice : *Powder Technol.* 4, 9–18.

Parambil, J. V., Heng, J.Y.Y., 2017. Seeding in crystallisation. *NATO Sci. Peace Secur. Ser. A Chem. Biol. PartF1*, 235–245. https://doi.org/10.1007/978-94-024-1117-1_13

Park, D., 2020. Design of Cyclone Separator Critical Diameter Model Based on Machine Learning and CFD 1–13.

Pasha, M., Hare, C., Hassanpour, A., Ghadiri, M., 2015. Numerical analysis of strain rate sensitivity in ball indentation on cohesive powder Beds. *Chem. Eng. Sci.* 123, 92–98. <https://doi.org/10.1016/j.ces.2014.10.026>

Pauli, V., Kleinebudde, P., Krumme, M., 2020. From powder to tablets: Investigation of

- residence time distributions in a continuous manufacturing process train as basis for continuous process verification. *Eur. J. Pharm. Biopharm.* 153, 200–210. <https://doi.org/10.1016/j.ejpb.2020.05.030>
- Peddapatla, R.V.G., Caroline, B., Cronin, M., Crean, A.M., 2016. Behaviour of magnesium stearate in continuous feeding, in: *AIChE Annual Meeting*.
- Peterwitz, M., Gerling, S., Schembecker, G., 2022. Challenges in tracing material flow passing a loss-in-weight feeder in continuous manufacturing processes. *Int. J. Pharm.* 612, 121304. <https://doi.org/10.1016/J.IJPHARM.2021.121304>
- Pingali, K.C., Shinbrot, T., Hammond, S. V., Muzzio, F.J., 2009. An observed correlation between flow and electrical properties of pharmaceutical blends. *Powder Technol.* 192, 157–165. <https://doi.org/10.1016/J.POWTEC.2008.12.012>
- Plumb, K., 2005. Continuous processing in the pharmaceutical industry: Changing the mind set. *Chem. Eng. Res. Des.* 83, 730–738. <https://doi.org/10.1205/cherd.04359>
- Pohořelý, M., Svoboda, K., Hartman, M., 2004. Feeding small quantities of particulate solids. *Powder Technol.* 142, 1–6. <https://doi.org/10.1016/j.powtec.2004.03.005>
- PowderProcess.net, 2022. Equipment Handbook _ Screw Conveyor Design [WWW Document]. https://powderprocess.net/Equipments%20html/Screw_Conveyor_Design.html.
- Qi, L., Zeng, X., Zhou, J., Luo, J., Chao, Y., 2011. Stable micro-feeding of fine powders using a capillary with ultrasonic vibration. *Powder Technol.* 214, 237–242. <https://doi.org/10.1016/j.powtec.2011.08.015>
- Raijada, D., Wac, K., Greisen, E., Rantanen, J., Genina, N., 2021. Integration of personalized drug delivery systems into digital health. *Adv. Drug Deliv. Rev.* 113857. <https://doi.org/10.1016/j.addr.2021.113857>
- Ramachandran, V., Halfpenny, P.J., Roberts, K.J., 2017. *Crystal science fundamentals*, NATO Science for Peace and Security Series A: Chemistry and Biology. https://doi.org/10.1007/978-94-024-1117-1_1
- Rhodes, M., 2008a. *Introduction to Particle Technology: Second Edition*, Introduction to Particle Technology: Second Edition. <https://doi.org/10.1002/9780470727102>
- Rhodes, M., 2008b. *Introduction to particle technology*, 2nd ed.. ed. Hoboken, NJ : Wiley, Hoboken, NJ.
- Richardson, J.F., Harker, J.H., Backhurst, J.R., 2002. *Coulson and Richardson's CHEMICAL*

ENGINEERING - Volume 2 - Particle Technology and Separation Processes.

- Rietema, K., 1984. Powders, what are they? *Powder Technol.* 37, 5–23. [https://doi.org/10.1016/0032-5910\(84\)80002-9](https://doi.org/10.1016/0032-5910(84)80002-9)
- Roberts, A.W., 1999. The influence of granular vortex motion on the volumetric performance of enclosed screw conveyors. *Powder Technol.* 104, 56–67. [https://doi.org/10.1016/S0032-5910\(99\)00039-X](https://doi.org/10.1016/S0032-5910(99)00039-X)
- Roberts, A.W., 1996. Predicting the Volumetric and Torque Characteristics of Screw Feeders. *Bulk Solids Handl.* 16, 233–244.
- Roberts, A.W., Manjunath, K.S., McBride, W., 1992. The Mechanics of Screw Feeder Performance for Bulk Solids Flow Control. 4th Int. Conf. Bulk Mater. Storage, Handl. Transp. 7th Int. Symp. Freight Pipelines; Prepr. Pap.
- Roberts, A.W., Wiche, S.J., 1993. Prediction of lining wear life of bins and chutes in bulk solids handling operations. *Tribol. Int.* 26, 345–351. [https://doi.org/10.1016/0301-679X\(93\)90071-8](https://doi.org/10.1016/0301-679X(93)90071-8)
- Rogers, A.J., Hashemi, A., Ierapetritou, M.G., 2013. Modeling of particulate processes for the continuous manufacture of solid-based pharmaceutical dosage forms. *Processes* 1, 67–127. <https://doi.org/10.3390/pr1020067>
- Rotolok UK, 2023. Website: Rotolok [WWW Document]. Rotolok UK. URL https://www.rotolok.co.uk/products/rotary-valves-airlocks?utm_medium=cpc&gclid=CjwKCAjwitShBhA6EiwAq3RqA7_7xZ9HDaQQxV5tK67zZV9xInbCuV7EKkLiVtcMkna7bDh3dM9BBxoCi8EQAvD_BwE
- Ruiz-Carcel, C., Starr, A., Nsugbe, E., 2018. Estimation of powder mass flow rate in a screw feeder using acoustic emissions. *Powder Technol.* 336, 122–130. <https://doi.org/10.1016/j.powtec.2018.05.029>
- Sacher, S., Fathollahi, S., Khinast, J.G., 2021. Comparative Study of a Novel Micro-feeder and Loss-in-weight Feeders. *J. Pharm. Innov.* <https://doi.org/10.1007/s12247-021-09599-6>
- Sacher, S., Heindl, N., Alberto Afonso Urich, J., Krusz, J., Khinast, J.G., 2020. A solution for low-dose feeding in continuous pharmaceutical processes. *Int. J. Pharm.* 591, 119969. <https://doi.org/10.1016/j.ijpharm.2020.119969>
- Santos, B., Carmo, F., Schlindwein, W., Muirhead, G., Rodrigues, C., Cabral, L., Westrup, J., Pitt, K., 2018. Pharmaceutical excipients properties and screw feeder performance in

- continuous processing lines: a Quality by Design (QbD) approach. *Drug Dev. Ind. Pharm.* 44, 2089–2097. <https://doi.org/10.1080/03639045.2018.1513024>
- Scheibelhofer, O., Balak, N., Wahl, P.R., Koller, D.M., Glasser, B.J., Khinast, J.G., 2013. Monitoring Blending of Pharmaceutical Powders with Multipoint NIR Spectroscopy. *AAPS PharmSciTech* 14, 234–244. <https://doi.org/10.1208/s12249-012-9910-4>
- Schneider, L.C.R., Sinka, I.C., Cocks, A.C.F., 2007. Characterisation of the flow behaviour of pharmaceutical powders using a model die-shoe filling system. *Powder Technol.* 173, 59–71. <https://doi.org/10.1016/j.powtec.2006.11.015>
- Schomberg, A.K., Kwade, A., Finke, J.H., 2020. The challenge of die filling in rotary presses— a systematic study of material properties and process parameters. *Pharmaceutics* 12. <https://doi.org/10.3390/pharmaceutics12030248>
- Schulze, D., 2011. Round robin test on ring shear testers. *Adv. Powder Technol.* 22, 197–202. <https://doi.org/10.1016/j.apt.2010.10.015>
- Schulze, D., 2008. *Powders and bulk solids*.
- Schulze, D., 2007. *Powders and bulk solids : behavior, characterization, storage and flow / [internet resource]*, 1st ed. 20. ed. Berlin , Berlin .
- Semenov, A., Semenova, M., Bebikhov, Y., Egorov, A., Vasilyev, P., Kharitonov, Y., 2021. Vibrating Feeder Electromagnetic Drive Model Implemented in MatLab/Simulink, in: 2021 International Conference on Electrotechnical Complexes and Systems (ICOECS). pp. 88–92. <https://doi.org/10.1109/ICOECS52783.2021.9657343>
- Seppälä, K., Heinämäki, J., Hatara, J., Seppälä, L., Yliruusi, J., 2010. Development of a new method to get a reliable powder flow characteristics using only 1 to 2 g of powder. *AAPS PharmSciTech* 11, 402–408. <https://doi.org/10.1208/s12249-010-9397-9>
- Shah, D.S., Moravkar, K.K., Jha, D.K., Lonkar, V., Amin, P.D., Chalikwar, S.S., 2023. A concise summary of powder processing methodologies for flow enhancement. *Heliyon* 9, e16498. <https://doi.org/10.1016/j.heliyon.2023.e16498>
- Shaikh, R., O'Brien, D.P., Croker, D.M., Walker, G.M., 2018. The development of a pharmaceutical oral solid dosage forms, *Computer Aided Chemical Engineering*. <https://doi.org/10.1016/B978-0-444-63963-9.00002-6>
- Shier, A.P., Kumar, A., Mercer, A., Majeed, N., Doshi, P., Blackwood, D.O., Verrier, H.M., 2022. Development of a predictive model for gravimetric powder feeding from an API-rich materials properties library. *Int. J. Pharm.* 625, 122071.

<https://doi.org/10.1016/J.IJPHARM.2022.122071>

- SI, S., CAI, L., CHEN, H., BAO, C., LIU, X., 2022. Theoretical model and testing method for ball indentation based on the proportional superposition of energy in pure elasticity and pure plasticity. *Chinese J. Aeronaut.* 35, 141–153. <https://doi.org/10.1016/j.cja.2021.06.014>
- Sierra-Vega, N.O., Romañach, R.J., Méndez, R., 2019. Feed frame: The last processing step before the tablet compaction in pharmaceutical manufacturing. *Int. J. Pharm.* 572, 118728. <https://doi.org/10.1016/j.ijpharm.2019.118728>
- Simonaho, S.P., Ketolainen, J., Ervasti, T., Toiviainen, M., Korhonen, O., 2016. Continuous manufacturing of tablets with PROMIS-line - Introduction and case studies from continuous feeding, blending and tableting. *Eur. J. Pharm. Sci.* 90, 38–46. <https://doi.org/10.1016/j.ejps.2016.02.006>
- Singh, C., Chandravanshi, M.L., 2022. Dynamic analysis and performance assessment of a vibratory feeder for different motor positions on trough. *Mech. Based Des. Struct. Mach.* 1–18. <https://doi.org/10.1080/15397734.2022.2047720>
- Singh, R., Román-Ospino, A.D., Romañach, R.J., Ierapetritou, M., Ramachandran, R., 2015. Real time monitoring of powder blend bulk density for coupled feed-forward/feed-back control of a continuous direct compaction tablet manufacturing process. *Int. J. Pharm.* 495, 612–625. <https://doi.org/10.1016/j.ijpharm.2015.09.029>
- Sinka, I.C., Cocks, A.C.F., 2009. Evaluating the flow behaviour of powders for die fill performance. *Powder Metall.* 52, 8–11. <https://doi.org/10.1179/174329009X441736>
- Snick, B. Van, Dhondt, J., Pandelaere, K., Bertels, J., Mertens, R., Klingeleers, D., Di, G., Paul, J., Vervaet, C., Beer, T. De, 2018. A multivariate raw material property database to facilitate drug product development and enable in-silico design of pharmaceutical dry powder processes. *Int. J. Pharm.* 549, 415–435. <https://doi.org/10.1016/j.ijpharm.2018.08.014>
- Stauffer, F., Vanhoorne, V., Pilcer, G., Chavez, P., Schubert, M.A., Vervaet, C., 2019. *European Journal of Pharmaceutics and Biopharmaceutics* Managing active pharmaceutical ingredient raw material variability during twin-screw blend feeding 135, 49–60. <https://doi.org/10.1016/j.ejpb.2018.12.012>
- Stauffer, F., Vanhoorne, V., Pilcer, G., Chavez, P.F., Vervaet, C., De Beer, T., 2019. Managing API raw material variability during continuous twin-screw wet granulation. *Int. J. Pharm.* 561, 265–273. <https://doi.org/10.1016/j.ijpharm.2019.03.012>

- Stranzinger, S., 2018. Novel stand-alone test tool for scientific qualification of a dosator capsule filling process.
- Stranzinger, S., Faulhammer, E., Biserni, S., Ferrari, A., D'Elpidio, G., Cicognani, S., Khinast, J.G., 2023. Micro-dosing of powders into capsules using a new automated micro-dosing system: effect of powder characteristics and operating conditions on the filling of 0.5 mg–100 mg weights. *Drug Dev. Ind. Pharm.* 1–8. <https://doi.org/10.1080/03639045.2023.2226213>
- Suri, A., Horio, M., 2009. A novel cartridge type powder feeder. *Powder Technol.* 189, 497–507. <https://doi.org/10.1016/j.powtec.2008.08.001>
- Tahir, F., Palmer, J., Khoo, J., Holman, J., Yadav, I.K., Reynolds, G., Meehan, E., Mitchell, A., Bajwa, G., 2020. Development of feed factor prediction models for loss-in-weight powder feeders. *Powder Technol.* 364, 1025–1038. <https://doi.org/10.1016/j.powtec.2019.09.071>
- Taiwo, M.I., Namadi, M.A., Mokwa, B., 2016. Design and analysis of cyclone dust separator 1130–134.
- Tang, L., Chen, W.Y., 1999. Improvements on a particle feeder for experiments requiring low feed rates. *Rev. Sci. Instrum.* 70, 3143–3144. <https://doi.org/10.1063/1.1149876>
- Tanida, K., Honda, K., Kawano, N., Kawaguchi, T., Tanaka, T., Tsuji, Y., 1998. Particle Motion in Screw Feeder Simulated by Discrete Element Method. *NIP Digit. Fabr. Conf.* 14, 429–431.
- Tardos, G.I., Lu, Q., 1996. Precision dosing of powders by vibratory and screw feeders: An experimental study. *Adv. Powder Technol.* 7, 51–58. [https://doi.org/10.1016/S0921-8831\(08\)60891-2](https://doi.org/10.1016/S0921-8831(08)60891-2)
- Taylor, D., 1948. A simple theory of static and dynamic hardness. *Proc. R. Soc. London. Ser. A. Math. Phys. Sci.* 192, 247–274. <https://doi.org/10.1098/rspa.1948.0008>
- Teżyk, M., Milanowski, B., Ernst, A., Lulek, J., Teżyk, M., Milanowski, B., Ernst, A., Lulek, J., 2016. Recent progress in continuous and semi-continuous processing of solid oral dosage forms: a review. *Drug Dev. Ind. Pharm.* 42, 1195–1214. <https://doi.org/10.3109/03639045.2015.1122607>
- Tirapelle, M., Santomaso, A.C., Hare, C., 2020. Dynamic ball indentation for powder flow characterization. *Powder Technol.* 360, 1047–1054. <https://doi.org/10.1016/j.powtec.2019.11.009>

- U.S. Pharmacopoeial Convention, 2011. (905) Uniformity of Dosage Units. Stage 6 Harmonization. 3, 4–6. <https://doi.org/10.1128/AEM.02374-10>
- US Pharmacopoeial Convention, n.d. USP29-NF24 (2006) General Information Chapter '<1174> Powder Flow'. US Pharmacopoeial Convention, Rockville, MD, USA, p. 3017.
- Van Snick, B., Holman, J., Cunningham, C., Kumar, A., Vercruyssen, J., De Beer, T., Remon, J.P., Vervaet, C., 2017. Continuous direct compression as manufacturing platform for sustained release tablets. *Int. J. Pharm.* 519, 390–407. <https://doi.org/10.1016/j.ijpharm.2017.01.010>
- Vanarase, A.U., Muzzio, F.J., 2011. Effect of operating conditions and design parameters in a continuous powder mixer. *Powder Technol.* 208, 26–36. <https://doi.org/10.1016/j.powtec.2010.11.038>
- Vemavarapu, C., Surapaneni, M., Hussain, M., Badawy, S., 2009. Role of drug substance material properties in the processability and performance of a wet granulated product. *Int. J. Pharm.* 374, 96–105. <https://doi.org/10.1016/j.ijpharm.2009.03.014>
- Verghese, T.M., Nedderman, R.M., 1995. The discharge of fine sands from conical hoppers. *Chem. Eng. Sci.* 50, 3143–3153. [https://doi.org/10.1016/0009-2509\(95\)00165-2](https://doi.org/10.1016/0009-2509(95)00165-2)
- Vlachos, N., Chang, I.T.H., 2011. Investigation of flow properties of metal powders from narrow particle size distribution to polydisperse mixtures through an improved Hall-flowmeter. *Powder Technol.* 205, 71–80. <https://doi.org/10.1016/j.powtec.2010.08.067>
- Vujovic, M., Despotovic, D.Z., 2015. Dynamic Stress Distribution in Composite Leaf Springs for Electromagnetic Vibratory Feeder, in: 3rd International Conference & Workshop Mechatronics in Practice and Education (MECHEDU). pp. 14–16.
- Wada, K., Fujimoto, Y., Hayano, N., Haniya, K., 1990. The mechanism of transportation inside the screw feeder. *Trans. Japan Soc. Mech. Eng.* 56, 935–940.
- Wagner, J.R., Mount, E.M., Giles, H.F., 2014. Feed Systems. *Extrusion* 377–397. <https://doi.org/10.1016/b978-1-4377-3481-2.00033-8>
- Wang, H., Wu, L., Zhang, T., Chen, R., Zhang, L., 2018a. Continuous micro-feeding of fine cohesive powders actuated by pulse inertia force and acoustic radiation force in ultrasonic standing wave field. *Int. J. Pharm.* 545, 153–162. <https://doi.org/10.1016/j.ijpharm.2018.05.006>
- Wang, H., Zhang, T., Zhao, M., Chen, R., Wu, L., 2018b. Micro-dosing of fine cohesive powders actuated by pulse inertia force. *Micromachines* 9.

<https://doi.org/10.3390/mi9020073>

- Wang, S., Li, H., Tian, R., Wang, R., Wang, X., Sun, Q., Fan, J., 2019. Particuology Numerical simulation of particle flow behavior in a screw conveyor using the discrete element method. *Particuology* 43, 137–148. <https://doi.org/10.1016/j.partic.2018.01.016>
- Wang, Y., Li, T., Muzzio, F.J., Glasser, B.J., 2017a. Predicting feeder performance based on material flow properties. *Powder Technol.* 308, 135–148. <https://doi.org/10.1016/j.powtec.2016.12.010>
- Wang, Y., Li, T., Muzzio, F.J., Glasser, B.J., 2017b. Predicting feeder performance based on material flow properties. *Powder Technol.* 308, 135–148. <https://doi.org/10.1016/j.powtec.2016.12.010>
- Welsch, R., 2003. Using loss-in-weight feeders in compounding. *Plast. Addit. Compd.* 5, 40–45.
- Wen, C.-Y., Simons, H.P., 1959. Flow characteristics in horizontal fluidized solids transport. *AIChE J.* 5, 263–267. <https://doi.org/https://doi.org/10.1002/aic.690050225>
- Wibberley, L.J., Phong-Anant, D., 1986. A Simple Laboratory Feeder for Fine Particles. *Combust. Sci. Technol.* 49, 93–97. <https://doi.org/10.1080/00102208608923904>
- Wouters, I.M.F., Geldart, D., 1996. Characterising Semi-Cohesive Powders using angle of repose. *Part. Part. Syst. Charact.* 13, 254–259. <https://doi.org/https://doi.org/10.1002/ppsc.19960130408>
- Yang, S., Evans, J.R.G., 2007. Metering and dispensing of powder; the quest for new solid freeforming techniques. *Powder Technol.* 178, 56–72. <https://doi.org/10.1016/j.powtec.2007.04.004>
- Yang, W.C., 2007. Modification and re-interpretation of Geldart's classification of powders. *Powder Technol.* 171, 69–74. <https://doi.org/10.1016/j.powtec.2006.08.024>
- Yoon, S., Galbraith, S., Cha, B., Liu, H., 2018. Flowsheet modeling of a continuous direct compression process, 1st ed, *Computer Aided Chemical Engineering*. Elsevier B.V. <https://doi.org/10.1016/B978-0-444-63963-9.00005-1>
- Yu, Y., 1997. Theoretical modelling and experimental investigation of the performance of screw feeders.
- Yu, Y., Arnold, P.C., 1997. Theoretical modelling of torque requirements for single screw feeders. *Powder Technol.* 93, 151–162.

- Zafar, U., Hare, C., Hassanpour, A., Ghadiri, M., 2017. Ball indentation on powder beds for assessing powder flowability: Analysis of operation window. *Powder Technol.* 310, 300–306. <https://doi.org/10.1016/j.powtec.2017.01.047>
- Zainuddin, I.M., Yasuda, M., Horio, T., Matsusaka, S., 2012. Experimental Study on Powder Flowability Using Vibration Shear Tube Method 29, 8–15. <https://doi.org/10.1002/ppsc.201100052>
- Zakhvatayeva, A., Zhong, W., Makroo, H.A., Hare, C., Wu, C.Y., 2018. An experimental study of die filling of pharmaceutical powders using a rotary die filling system. *Int. J. Pharm.* 553, 84–96. <https://doi.org/10.1016/j.ijpharm.2018.09.067>
- Zhang, F., Shan, B., Wang, Y., Zhu, Z., Yu, Z., Y. Ma, C., 2021. Progress and Opportunities of Seeding Technique in Crystallization Processes. *Org. Process Res. Dev.* 25, 1496–1511.
- Zhang, H., Liu, M., Li, T., Huang, Z., Bo, H., Dong, Y., 2016. Experimental study on plug formation characteristics of a novel draft tube type feeder for vertical pneumatic conveying of coarse particles. *Powder Technol.* 301, 730–736. <https://doi.org/10.1016/j.powtec.2016.06.049>
- Zhang, J., He, X.Y., Wei, X.L., 2010. An automatic shake mechanism for the biomass pyrolysis feeding. *Adv. Mater. Res.* 97–101, 2314–2317. <https://doi.org/10.4028/www.scientific.net/AMR.97-101.2314>
- Zhao, Y., Collins, E.G., 2003. Fuzzy PI control design for an industrial weigh belt feeder. *IEEE Trans. Fuzzy Syst.* 11, 311–319. <https://doi.org/10.1109/TFUZZ.2003.812686>
- Zhong, H., Chan, G., Hu, Y., Hu, H., Ouyang, D., 2018. A comprehensive map of FDA-approved pharmaceutical products. *Pharmaceutics* 10, 1–19. <https://doi.org/10.3390/pharmaceutics10040263>
- Zhou, H., Hu, Z., Zhang, Q., Wang, Q., Lv, X., 2019. Numerical study on gas-solid flow characteristics of ultra-light particles in a cyclone separator. *Powder Technol.* 344, 784–796. <https://doi.org/10.1016/j.powtec.2018.12.054>
- Zhou, Y., Wang, T., Zhu, J., 2023. Investigation on minimum fluidization velocity in a modified Geldart's diagram. *Chem. Eng. J.* 453, 139984. <https://doi.org/10.1016/j.cej.2022.139984>